CANADIAN THESES ON MICROFICHE

I.S.B.N.

THESES CANADIENNES SUR MICROFICHE

## NOTICE

The quality of this microfiche is heavily dependent upon the quality of the original thesis submitted for microfilming. Every effort has been made to ensure the highest quality of reproduction possible.

If pages are missing, contact the university which granted the degree.

Some pages may have indistinct print especially if the original pages were typed with a poor typewriter ribbon or if the university sent us a poor photocopy.

Previously copyrighted materials (journal articles, published tests, etc.) are not filmed.

Reproduction in full or in part of this film is governed by the Canadian Copyright Act, R.S.C. 1970, c. C-30. Please read the authorization forms which accompany this thesis.

## AVIS

La qualité de cette microfiche dépend grandement de la qualité de la thèse soumise au microfilmage. Nous avons tout fait pour assurer une qualité supérieure de reproduction.

S'il manque des pages, veuillez communiquer avec l'université qui a conféré le grade.

La qualité d'impression de certaines pages peut laisser à désirer, surtout si les pages originales ont été dactylographiées à l'aide d'un ruban usé ou si l'université nous a fait parvenir une photocopie de mauvaise qualité.

Les documents qui font déjà l'objet d'un droit d'auteur (articles de revue, examens publiés, etc.) ne sont pas microfilmés.

La reproduction, même partielle, de ce microfilm est soumise à la Loi canadienne sur le droit d'auteur, SRC 1970, c. C-30. Veuillez prendre connaissance des formules d'autorisation qui accompagnent cette thèse.

### THIS DISSERTATION HAS BEEN MICROFILMED EXACTLY AS RECEIVED

### LA THÈSE A ÉTÉ MICROFILMÉE TELLE QUE NOUS L'AVONS REÇUE

Canada

O-315-19391-3

# PERMISSION TO MICROFILM — AUTORISATION DE MICROFILMER

● Please print or type — Écrire en lettres moulées ou dactylographier

Full Name of Author — Nom complet de l'auteur

SOO BENG KHOO

| Date of Birth — Date de naissance | Country of Birth — Lieu de naissance |
|---|---|
| 3-3-1952 | MALAYSIA |

Permanent Address — Résidence fixe

31, JALAN SELENDANG, EAST GARDEN, PENANG, MALAYSIA

Title of Thesis — Titre de la thèse

INTERACTIONS OF ORGANIC NEGATIVE IONS WITH CATIONS

University — Université

UNIVERSITY OF ALBERTA EDMONTON, ALBERTA, CANADA.

Degree for which thesis was presented — Grade pour lequel cette thèse fut présentée

P.h.D.

| Year this degree conferred — Année d'obtention de ce grade. | Name of Supervisor — Nom du directeur de thèse |
|---|---|
| 1984 | PROF. STANLEY PONS |

| Date | Signature |
|---|---|
| 20/7/84 | |

THE UNIVERSITY OF ALBERTA


INTERACTIONS OF ORGANIC NEGATIVE IONS WITH CATIONS


by

© S. B. KHOO


A THESIS

SUBMITTED TO THE FACULTY OF GRADUATE STUDIES AND RESEARCH

IN PARTIAL FULFILMENT OF THE REQUIREMENTS FOR THE DEGREE

DOCTOR OF PHILOSOPHY


DEPARTMENT OF CHEMISTRY


EDMONTON, ALBERTA

FALL, 1984

# THE UNIVERSITY OF ALBERTA

## RELEASE FORM

NAME OF AUTHOR    S. B. KHOO

TITLE OF THESIS    INTERACTIONS OF ORGANIC NEGATIVE

IONS WITH CATIONS.

DEGREE FOR WHICH THESIS WAS PRESENTED    PH.D.

YEAR THIS DEGREE GRANTED    1984

(SIGNED)_____

PERMANENT ADDRESS:

31, Jalan Selendang,
East Garden
Penang, Malaysia

DATED _17th JULY_ 1984

THE UNIVERSITY OF ALBERTA

FACULTY OF GRADUATE STUDIES AND RESEARCH
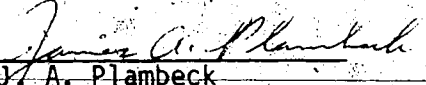
The undersigned certify that they have read, and recommend
to the Faculty of Graduate Studies and Research, for
acceptance, a thesis entitled

INTERACTIONS OF ORGANIC NEGATIVE IONS WITH CATIONS

submitted by S. B. KHOO

in partial fulfilment of the requirements for the degree of

DOCTOR OF PHILOSOPHY.

_____
S. Pons, Supervisor

_____
J. A. Plambeck

_____
G. Horlick

_____
S. Fraga

_____
S. Wanke

_____
J. Janata, External
             Examiner

DATE _17th July_ 1984.

To my wife, Judy

## ABSTRACT

The electroreduction of the polycyclic aromatic hydro-
carbons anthracene, fluoranthene, and the π-acids tetracyano-
ethylene and 7,7,8,8-tetracyanoquinodimethane in non-aqueous
aprotic media was examined. In particular, the interactions
between the electrogenerated organic negative ions with
countercations were investigated. It was found that in
general, the dianions formed ion pairs with alkali metal
cations but the dianion radicals did not.

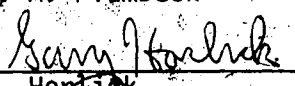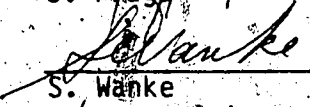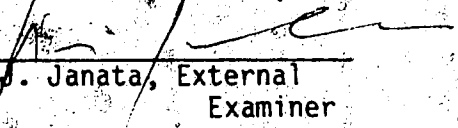Polarographic reduction waves for mixtures of aromatic
hydrocarbon-alkali metal cations showed unusual current depres-
sions. It was found that these current depressions were not
due to adsorption or film formation processes but to the effect
of the interactions between the organic dianions with metal
cations. A model was proposed to account for the current
depressions and the stoichiometries of the dianion-metal cation
complexes were determined. However, the formation constants
for the complexes could not be calculated due to the unstable
nature of the dianions. Kinetic studies showed that the rate
of ion-pair complex formation was very fast, close to the cal-
culated diffusion controlled-rate. The experimental rate
constants were determined based on the competition between
metal cations and water for the dianions.

In the case of the π-acids, cyclic voltammetric studies

showed that the electrochemical reduction of the anion radicals to the dianions was highly dependent on the countercations of the supporting electrolyte. The reduction of the tetracyano-ethylene anion radicals to the dianions was found to be either quasi-reversible or irreversible depending on the electrolyte used. Heterogeneous rate constants were determined from the variation of delE(p) values with scan rate. Large shifts in Eh values for the second reduction waves of tetracyanoethylene and 7,7,8,8-tetracyanoquinodimethane were found when different supporting electrolytes were used, pointing to the existence of strong ion pairing of the dianions. For tetracyanoethylene the use of mixed electrolytes gave rise to strong adsorption effects. Thus ion pairing constants could not be determined. However, for 7,7,8,8-tetracyanoquinodimethane, two types of ion pairs were found with stoichiometries of 1:1 and 1:2 (dianion: cation). The formation constants for these ion pair complexes were calculated. Further evidence for the existence of dianion--cation interactions was provided by the shifts in IR adsorption bands with different supporting electrolytes.

## ACKNOWLEDGEMENTS

# TABLE OF CONTENTS

Chapter 5.  ELECTROCHEMICAL STUDIES OF TETRACYANOETHYLENE
(TCNE) AND 7,7,8,8-TETRACYANOQUINODIMETHANE
(TCNQ).THE EFFECT OF COUNTERCATIONS.

# LIST OF TABLES

# LIST OF FIGURES

xiv

xvii

## Chapter 1  Introduction

### 1.1  Objective

The main goal of this thesis research is to investigate the interactions of the electrochemically generated negative ions of polycyclic aromatic hydrocarbons, and the $\pi$-acids tetracyanoethylene and 7,7,8,8-tetracyanoquinodimethane with cations present in solution. The electrochemistry is investigated in nonaqueous, aprotic media (N,N,dimethylformamide (DMF) and acetonitrile (ACN)). It is envisioned that through these studies the electrochemical behavior of the organic substrates could be established, as well as the dependence of this behavior on various counter-cations and also the role played by the solvent medium. In particular, the manner of interactions of electrogenerated organic negative ions with cations,

their stoichiometries and the mechanism of these

interactions are examined. Although many polycyclic

aromatic hydrocarbons are studied, a detailed report

is confined to two of them; namely, anthracene and

fluoranthene. The cations considered are alkali metal

and tetraalkylammonium. The justification for these

types of studies is well-established. Electrochemical

characteristics can give insight into the molecular

structure of reactants and products (1-3). Reduction

potentials can be correlated to electron affinities

and molecular orbital energy (4-8). Electrochemical

behavior can be dependent on the nature of electrolyte

cation (9-11). The anions of organic molecules are

known to be reactive species. The reactivity of these

species is greatly affected by the presence and type

of ionic interactions in solution (12-16). In some

cases the reaction pathway can be altered (17,18).

Solvation plays a major role in all these processes

and must be considered. It is intended that the

results of these investigations add to the knowledge

of these areas of chemistry.

## 1.2 Historical Background

In the following sections, a historical survey of

the areas pertaining to the present research will be

summarized.

### 1.2.1 Electrochemical Reduction of Aromatic Hydrocarbons In Non-aqueous Media

The earliest studies on the electroreduction of aro-

matic hydrocarbons were done by Laitinen and Wawzonek

(19-20), and Wawzonek and Fan (21). These investiga-

tions were not carried out in fully non-aqueous media

but rather in 75% dioxane-water mixture. Polycyclic

aromatic hydrocarbons e.g. anthracene were found to

give a two-electron polarographic wave.  Anthracene

gave a small second wave in this medium but it was

ignored.  A mechanism involving the transfer of one

electron from the electrode to the organic molecule to

form an anion radical was postulated.  This was an

important step at this time and Austen et al (31)

later proved that the intermediate in the first

reduction step was indeed a free radical ion by

electron spin resonance (esr) studies.  Chopard-

dit-Jean and Heilbronner (22), from their studies

of reduction of azulenes, deduced the general rule

that alternant hydrocarbons always give a two-

electron polarographic wave whereas non-alternant

hydrocarbons may give either a one- or two-electron

wave.  Hoijtink et al (23) recognized that the

mechanism proposed earlier (19-20) was inconsistent

with the results; namely, the existence of the

second wave. They found that in 96% dioxane-water

mixture (a "more aprotic" solvent than 75% dioxane-

water), anthracene exhibited two successive one-

electron waves of approximately equal height. If

the water content was increased, the first wave

changed from a one-electron to an overall two-

electron wave with the disappearance of the second

wave. The same effect could be brought about by

the addition of hydrogen iodide as a proton source

instead of water. Thus, the general rule derived

by Chopard-dit-Jean and Heilbronner was shown to

be incorrect. Subsequently, the reduction of

aromatic hydrocarbons was carried out in acetoni-

trile and dimethylformamide (24) and similar results

were obtained. Hoijtink et al extended their studies

to dimethylformamide solvent and found that for all

the aromatic hydrocarbons studied, the rate constants

for the first electron transfer were practically the

same and had the value 0.1 cm/s. However, it is

now known that rate constants for electron transfer

to aromatic hydrocarbons are very much faster (28).

Aten et al (29) determined a value of 5 cm/s

for the first electron transfer and about one order

lower for the second step. Kojima and Bard (30)

found a value of 5 cm/s for the first electron

transfer of anthracene and perylene in DMF. Further,

it was found that addition of water up to 5% did

not affect the processes in the first wave.

The mechanism currently accepted for the electro-

reduction of aromatic hydrocarbons, as was established by

Hoijtink et al and later confirmed by Given and Peover

(26,27), is discussed below. In a totally aprotic

environment, the reduction of the aromatic hydrocarbon R

occurs in two successive one-electron steps

$$R + e = R: \qquad E1$$

$$R: + e = R= \qquad E2$$
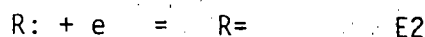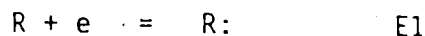
where $E2$ is more negative than $E1$.

Since the rate constants for electron transfer of both

processes are large, the Nernst equation will be obeyed

and the processes are reversible. However, a totally

aprotic environment is difficult to achieve for even the

most carefully purified solvent contains traces of water.

The dinegative ion is more reactive than the anion

radical, and while small amounts of proton donors may not

react with the anion radical, they could cause the pro-

tonation of the dianion.

Then $R= + HX = RH- + X-$ , and

$$RH- + HX = RH_2 + X-$$
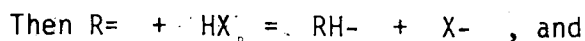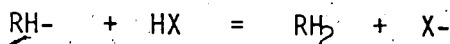
The rate of protonation is dependent on the proton affinity of the dianion and on the strength and amount of the proton donor. The product of protonation, $RH_2$, could further be reduced to give rise to additional wave(s) at more negative potentials. It has been reported that dianion protonation could be prevented by adding neutral alumina to the solution to remove the last traces of proton donors (32).

If sufficient proton donors are present, the stability of the anion radical could be affected:

$$R^- + HX = RH\cdot + X^-$$

$$RH\cdot + e = RH^-$$

$$RH^- + HX = RH_2 + X^-$$
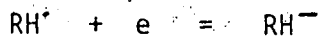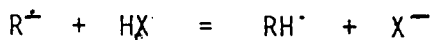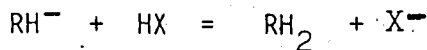
In the case of alternant hydrocarbons, the radical

$RH^{\cdot}$ is always reduced at a potential less negative than

the parent R, and therefore will be reduced as soon as it

is formed (23). In this case only one wave will be

observed involving the overall transfer of two electrons.

In the intermediate case where the rate of protonation of

$R=$ is not too fast, two waves will be observed, the first

of which (involving more than one electron) will be

greater in height than the second. Detailed discussions

regarding this mechanism are discussed in the references

cited. A review was given by Hoijtink in 1970 (4).

1.2.2   Electrochemical Reduction of Alkali Metal Cations
        in Nonaqueous Media.

The first reported electrodeposition of alkali

metal in nonaqueous solvent was in 1895 by Laszczynski

(33). Up to the 1920's a number of studies on the electro-

chemistry of alkali metal cations had been made, most of

which were rather qualitative in nature. A review was

made by Brenner in 1967 (34). Observations of the

electrochemical reduction of alkali metal cations in

nonaqueous solvents are important in the understanding

of solute-solvent and solute-solute interaction in

solution. Also they have a direct impact on the field of

high energy density batteries (35,36).

The electrochemical deposition of alkali metals on

electrodes of the same metal or on inert materials such

as vitreous carbon or pyrolitic graphite (37), platinum,

etc. in nonaqueous solvents is complicated by the extreme

reactivity of these metals. The deposited metal could

react with the solvent or with trace impurities (water,

oxygen) present. Such reactions lead to highly irrepro-

ducible results (38-40) and possibly, in the extreme

case, to the passivation of the electrode towards further

electrolysis. Further, where the electrode material is

different from the deposited metal, implantation of the

deposited metal into the electrode often occurs (41-43).

Such problems are essentially absent where mercury

is the electrode material since the alkali metal is

dissolved in mercury and forms an amalgam which greatly

lowers the reactivity of the metal. Thus, at the

mercury cathode, reduction of the alkali metal cations

can conveniently be performed even in aqueous media (44-

48). The d.c. polarographic behavior of alkali metal

cations has been studied in such nonaqueous solvents as

acetic acid anhydride (49), propionitrile, benzonitrile,

phenylacetonitrile (50), isobutyronitrile (51), dimethyl-

sulfoxide (52,53) and a host of other solvents (54-57).

Alkali metal cations, in general, give well-defined,

diffusion-controlled polarographic waves in nonaqueous

solvents. In acetonitrile (58) the reduction of sodium,

potassium and rubidium iodides, with tetraalkylammonium

salts as supporting electrolyte, show reversible char-

acter. Similar behavior was obtained in dimethylform-

amide (59). However, the nature of the reduction of

lithium cation is somewhat more contradictory, as can be

seen from literature results. For example, Brown and

Urfali (59) found lithium reduction to be d.c. reversible

in dimethylformamide whereas McMasters et al (60)

observed irreversible behavior in the same solvent.

Diggle et al (61) pointed out the results obtained by

the above workers are not comparable because Brown and

Urfali used iodide salts whereas McMasters et al used

perchlorate salts. They determined values of standard

heterogeneous rate constants ks for the cations at the

hanging mercury drop electrode, in dimethylformamide, by

cyclic voltammetry. It was found that ks increased in

the order Li+ (1.2 e-3 cm/s) < K+ (4.3 e-3 cm/s)

< Na+ (7.2 e-3 cm/s) < Cs+ (9.4 e-3 cm/s) .

Although the authors found that lithium reduction was d.c.

reversible, they reported that in general, lithium reduction

is less reversible than the other alkali metal cations.

The ease of alkali cation reduction has been

correlated to their solvation energies, where more nega-

tive values of solvation energies are associated with

smaller values of ks. The trend above is in agreement

with this since lithium is the most strongly solvated

and caesium the least. This type of argument has

frequently been used to explain trends in ks values for

alkali metal cations (61,62).

In dimethylacetamide, d.c. polarographic and

oscillopolarographic studies again showed that sodium,

potassium, rubidium and caesium cations are reduced

reversibly (63). However, lithium was not reduced in

strictly anhydrous dimethylacetamide in the potential

range available. With the addition of water, a wave

appeared which shifted more positive with increasing

water content. Also, the wave height increased with

increasing water content up to 3% water, then remaining

constant up to 7% water. Logarithmic analysis showed that

the wave (3% water) was partially irreversible with a

66 mV slope. However, oscillopolarographic results

indicated that the reduction was reversible. The above

results were explained in terms of strong solvation of the

lithium ions forming a stable symmetrical complex with a

high polarographic overvoltage. Addition of water

distorted the symmetry of the complex and decreased this

overvoltage. Also, the d.c. irreversibility was attributed

to slow deactivation of the primary reduction product which

under oscillopolarographic conditions was not given enough

time to occur, thus explaining the reversibility under

these conditions. Besette and Harwood (64) studied

the same system using cyclic voltammetry. They found

agreement with the above results. A series of periodic

oxidation waves was obtained on the reverse scan in cyclic

voltammetry. These oscillations were attributed to

reaction of the lithium amalgam with water, giving rise

to a film of lithium hydroxide and hydrogen gas evolution..

More recently, Fawcett and co-workers, in a series of

studies (65-67), investigated the effect of solvents,

solution composition and electrode composition on the

electroreduction of alkali metal cations. They found that

the kinetic parameters, namely, ks and α, the apparent

transfer coefficient, depend strongly on the above factors.

Changes in solvation of reactants and products and the

electrostatic environment were considered to be the main

contributing factors.


1.2.3. The Interaction between Aromatic Hydrocarbon
       Negative Ions and Alkali Metal Cations

       No account of the interactions between aromatic

hydrocarbon negative ions and alkali metal cations is

complete without mentioning the early attempts in trying

to react hydrocarbons with alkali metals. Berthelot (68),

in 1867, reacted potassium directly with naphthalene at

elevated temperature and obtained the dipotassium product.

More intensive studies were made by Schlenk et al in

diethyl ether as solvent (69,70). The reaction of sodium

with anthracene was observed and lithium reacted with

naphthalene to give the dilithium product, though only to

a limited extent. A solution of sodium in liquid ammonia

was reported to bring about the addition of sodium to

naphthalene (71), a 4:1 ratio of sodium to naphthalene

being observed. However, ether was not a very successful

solvent for these reactions because only a limited number

of aromatic hydrocarbons could be coaxed to react and even

then reaction rate was often slow. Liquid ammonia was not

satisfactory because rapid ammonolysis of the reaction

product occurred (72). Significant progress was made when

Scott et al (72) discovered than certain ethers like

methyl ether and 1,2-dimethoxyethane could promote the

reaction of alkali metals with aromatic hydrocarbons.

Jeannes and Adams (73) investigated the addition of

sodium with phenanthrene and proposed a mechanism as

given below
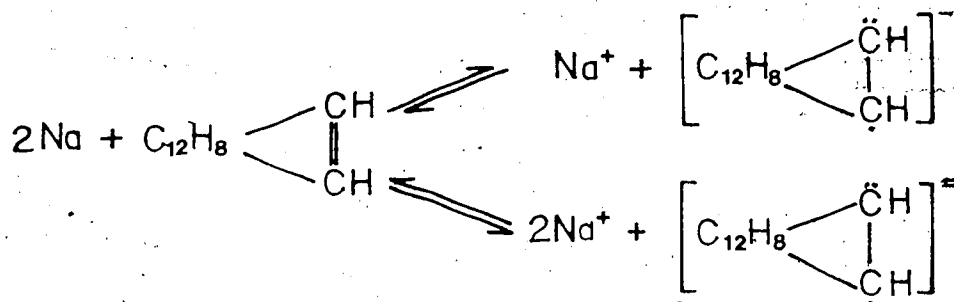
It appears that this is the first instance where

some sort of anion radical intermediate was proposed.

However, the authors erroneously thought that the green

color of the solution was due to the dianion which was

also thought to be the major product. From these

pioneering studies, it was realized that the soluble

alkali metal-hydrocarbon complexes are highly colored,

very reactive and ionic in nature (as evidenced by the

electrical conductivity of the solutions (74)).

However, the mechanism of the reactions and the type of

products formed was not well understood. For example,

it was thought that the reaction of naphthalene with sodium

involved the transfer of one or two electrons from sodium

atoms to one naphthalene molecule and a complex of the

form $NaC_{10}H_8Na$ was proposed (74). Also, stoichiometries

such as 1:1, 2:1, 4:1 for alkali metal-hydrocarbon

complexes have been proposed (see previous references).

The next important step was made by Lipkin et al (75)

who first established the free radical nature of the

product of these reactions. They reacted sodium with

naphthalene, anthracene, phenanthrene etc. in 1,2-dimeth-

oxyethane and tetrahydrofuran and found that the product

exhibited intense paramagnetic absorptions and all

products were found to have a free electron value of one.

They deduced that the reactions involved the transfer of

one electron from sodium to the hydrocarbons to form free

radical ions. However, it was not thought that dianions

could be formed as well. The equilibrium nature of alkali

metal-hydrocarbon reactions was known (72) and these

authors suggested that the principal factor which determines

the ability of high oxygen content ethers such as dimethyl

ether and 1,2-dimethoxyethane to promote reaction was due

to the favorable energy of solvation of the metal ion

(and possibly the hydrocarbon anion) thus shifting the

equilibrium to the anion side. They also suggested that

the solvation of the metal ion involves chelate structures

with unhindered ethers as was proposed earlier (37). At

about the same time, Weissman et al (89) reported the

first published hyperfine splittings in the paramagnetic

resonance spectrum of the naphthalene anion radical in

tetrahydrofuran which exhibited nineteen components. Chu

and Yu (76) studied the magnetic susceptibilities of

sodium with anthracene, biphenyl, naphthalene, phenanthrene,

and m-terphenyl in tetrahydrofuran. They reported that

in the case of anthracene and phenanthrene, dianions are

formed as well as anion radicals.

Further studies in this area were made by Hoijtink

(77,78, 81-87) and co-workers. Comparison was made

between chemical and electrochemical reductions, both of

which yielded the same products, namely, the anion radicals

and dianions. However, in the case of chemical reduction,

whether or not the dianions are formed depends on the

electron affinities of the hydrocarbons. Potentiometric

(77,78) and spectrophotometric (80) techniques were used

to establish a relative electron affinity scale for the

hydrocarbons. In the potentiometric studies, standard

reduction potentials referenced to the reduction potential

of biphenyl were in good agreement with polarographic

values. However the results obtained from the two

techniques did not agree. Jagur-Gradzinski et al (88)

made careful studies in tetrahydrofuran using both

techniques in order to resolve the differences obtained

in the two studies above. They assumed that the ions

are mainly undissociated in tetrahydrofuran, and compared

the two techniques. Their results were in qualitative

agreement with those of Hoijtink et al (78).

In most of these studies, it was implicitly assumed

that the hydrocarbon negative ions exist as free ions in

solution. The role played by the counterions in solvent

was not well understood. However, the pioneering work of

Winstein et al (90) and Grunwald (91) has established the

existence of different types of ion associates. Szwarc

and his school established the presence of an equilibrium

between contact and solvent-separated ion pairs (92).

There has been tremendous interest in the reactivities of

organic anions since they take part in numerous important

processes. For example, radical anions act as initiators

in anionic polymerization (93). These reativities are

greatly affected by counter cations, solvent, and tempera-

ture. It is interesting to note that early interest in

alkali metal-hydrocarbon reactions led naturally to later

studies of ionic interactions and discovery that these

reactions occur so well in solvents of low dielectric

constant such as tetrahydrofuran, 2-methyltetrahydrofuran,

1,2-dimethoxyethane and dioxane. It follows that chemical

reduction is the predominant method of generation of

hydrocarbon anions in later studies. More attention has

been paid to anion radicals than dianions. There are

several reasons for this. First, chemical reductions do

not produce dianions in all aromatic hydrocarbons. Second,

the dianions, even if they are produced, are much more

reactive than anions, and require special techniques for

their preservation. Third, one of the most powerful

methods for studying ion associates is electron spin

resonance which can only be applied to free radical ions.

Electrochemical generation of anions has been employed in

numerous such studies (31, 94, 95).

Many techniques have been used in the study of ion

pairing. Conductance methods were used to detect the

presence of ion pairs of polycyclic aromatic hydrocarbon

anions with alkali metal cations (96). Spectroscopic

methods include UV-VIS (93,96-98), and infrared (99-101).

However, by far the most powerful and popular techniques employed are magnetic resonance, both nuclear and electron spin. These methods yield detailed information about the structural and dynamic properties of the various ion pairs. Several reviews have been written concerning the development of the concept of ion pairing and its importance in different fields of chemical research (14,15,102).

1.2.4. Tetracyanoethylene (TCNE)

There is tremendous interest in tetracyano-ethylene and its related family members due to their unusual properties. TCNE was the first of a new class of compounds (known as percyano olefins) to be synthesized (103). Prior to this, the only known cyanocarbons were dicyanoacetylene and dicyanobutadiene (104). TCNE is exceptionally reactive and undergoes addition and substitution readily. These reactions have been

discussed (105-109).

The physical and electronic properties of TCNE have been extensively studied. Relative electron affinities were obtained from studies of molecular charge transfer complexes (110-112). The absolute electron affinity was found to be 2.3(±0.3) eV by the technique of photo-detachment of electrons from negative ions (113) which is about 0.5 eV less than the value obtained by the magnetron surface ionization technique (114). The theoretically calculated value is 3.06 eV (115).

Vibrational spectra of TCNE has been studied in detail. Raman and iR spectra, both in the solid state and in solution have been published (116-122). Electronic absorption spectra in solvents such as 2-methyltetra-hydrofuran (123) and acetonitrile (124) are available. Theoretical absorption energies (125) and simulated spectra (126) have been calculated.

The most widely-studied property of TCNE results

from the presence of its four cyano groups. These four

electron withdrawing groups make TCNE a very strong π-

acid. It forms molecular π-complexes with π-bases such

as aromatic hydrocarbons. The formation constants of

these complexes have been obtained from spectroscopic

(127) and polarographic studies (128,129). Molecular

orbital calculations of these complexes have been made

(130).

TCNE can be easily reduced in a number of different

ways. Chemically, it can be reduced by iodides, thiols,

mercaptans and hydrogen on palladium (106), and even

cyanide ion (124). TCNE is found to react with metals

such as K, Na, Al, Mg, Cu, Pb etc. at room temperature

to give the corresponding metal salts (124,131). The

existence of these metal tetracyanoethylenides was first

recognized by Weissman (132). These metal salts are

very stable in the solid state. For example, K+TCNE=

has been known to remain unchanged even after heating for

three hours at 150°C in an inert atmosphere, and also

after exposure to the atmosphere for one month (124).

The anion radical of TCNE (TCNE$^-$) can also be pro-

duced by irradiation with a light pulse from an Argon flash

lamp (133). In solution, the anion radical, in contrast

to the solid salt, is sensitive to oxygen and less so,

to water (124). It has been reported that TCNE$^-$ is produced

spontaneously in solvents such as dimethylsulfoxide,

dimethylformamide and dimethylacetamide, the rate of

production being accelerated in the presence of light.

The anion radical production was explained in terms of the

thermal ionic dissociation of the electron donor-acceptor

complexes (EDA) formed with these solvents (134-137).

However, Butler et al studied the dimethylsulfoxide-TCNE

system and came to the conclusion that the presence of TCNE$^-$

was the result of complex chemical reactions taking place

between the components of the system and not due to thermal

dissociation of the EDA complex (137).

TCNE$^-$ has been studied by IR and Raman spectroscopy

(121,138-141) and UV-VIS spectroscopy (123,142).

Electron spin resonance studies were undertaken (143-145)

to study the effect of counterions on the reactions of

TCNE$^-$. Theoretical studies on the electron spin distri-

bution of TCNE$^-$ have also been made (146).

The anion radical and dianion of TCNE can also be

prepared by electrochemical methods. Peover studied the

polarographic reduction of TCNE to TCNE$^-$ in acetonitrile,

dimethylformamide, chloroform and methylene chloride.

In acetonitrile and dimethylformamide using tetra-

ethylammonium perchlorate, the reduction was found to be

reversible and involved the transfer of one electron.

Further reduction was not carried out. In chloroform,

using tetrabutylammonium perchlorate (0.5M), similar

results were obtained. However, in methylene chloride,

reduction to the dianion was carried out (0.5M tetra-

butylammonium perchlorate). Both waves involved one

electron transfer and were reversible. Van Duyne et al

(138) reduced TCNE at platinum electrode in acetonitrile

using tetrabutylammonium perchlorate as solvent.

Employing cyclic voltammetry they found the first wave to

be a reversible one-electron wave and the anion radical

was found to be stable over at least 40 minutes. However

the second wave was irreversible. The irreversibility of

the second reduction was attributed to the change in

geometry in going from $TCNE^-$ to $TCNE^=$. Pons et al (139)

obtained similar results, but showed that the irrever-

sibility was due to other causes. Kaplan et al plotted the

reduction potentials against the calculated energy of the

lowest unoccupied molecular orbitals for a series of

cyanocarbons but could find no correlation (147). Hetero-

geneous rate constants for the first electron transfer

have been determined by cyclic voltammetry at different

electrode materials and in different solvents. The

diffusion coefficients were also obtained (148,149).

1.2.5   7,7,8,8-Tetracyanoquinodimethane (TCNQ)

Since the discovery of TCNE, and the demonstra-

tion of its exceptional properties, there was increased

effort to explore new members of the percyano class of

compounds.  Particular interest was paid to structures

where the ethylene bond was replaced by a conjugated

system.  One outstanding member which surfaced was

7,7,8,8-tetracyanoquinodimethane (TCNQ).

TCNQ was prepared for the first time in 1961 (150)

but details of its preparation were only published in

1962 (151).  Although many properties of TCNQ parallel

those of TCNE, there are also some important differences.

For example, TCNQ undergoes displacement of it's cyano
group on the same carbon atom as does TCNE. However,
TCNQ does not form the Diels-Alder adduct with dienes and
addition occurs at the 1,6-positions in contrast to the
1,4-positions for TCNE.

TCNQ, like TCNE, is a strong π-acid. It has been
reported (152), based on polarographic half-wave potentials,
that TCNE has the stronger acidity of the two. The Eh
values, obtained in acetonitrile, are TCNQ = +0.127 V
(vs SCE) and TCNE = +0.152 V (vs SCE). However,
experimental (115) and theoretical (113) determinations
both showed that TCNQ has ~~slightly higher~~ absolute
electron affinity. The experimental values were 2.4 and
2.3 eV for TCNQ and TCNE respectively and the theoretical
values were 3.42 and 3.06 eV respectively.

Like TCNE, TCNQ forms 1:1 π-complexes with many

organic donors. These complexes can be isolated in the

solid form. Many of them are electrically conductive and

have been the subject of intensive research. The electrical

properties of the most famous of them, the tetrathiofulva-

lene-tetracyanoquinodimethane (TTF-TCNQ) complex was

first discovered by Heeger et al (153). It was found that,

at room temperature, TTF-TCNQ has an electrical conduc-

tivity comparable to that of graphite (about $1000/\Omega$ cm).

The conductivity increased dramatically at lower tempera-

tures, reaching a maximum value of slightly over $11000/\Omega$

cm at 60 K before decreasing again. Due to this high

conductivity and its chain-like structure, it has been

referred to as a quasi-one-dimensional metal (154,155).

The duPont group, who discovered TCNQ (as well as

TCNE) (147), has published an extensive series of studies

of the chemical and physical properties of TCNQ and its

derivatives (151,152,156). TCNQ can be easily reduced to

its anion radical by iodides and metals such as copper,

silver, etc. to form simple salts. With tetraalkyl-

ammonium cations, complex salts of formula $M+:(TCNQ^-)TCNQ$

are obtained. Peover (128,129) has studied TCNQ-aromatic

hydrocarbon complexes polarographically and has

determined their stability constants. Heats of formation

and electron affinities have also been derived from

thermochemical studies. As for TCNE, relative electron

affinities have been determined (110-112) and absolute

electron affinities obtained both experimentally and

theoretically (113-115). Various spectroscopic methods

have been employed to study TCNQ and its anions.

Jeanmaire and Van Duyne obtained the electronic and

Raman resonance spectra of TCNQ and its anion radical in

acetonitrile. The anion radical, $TCNQ^-$, was generated

electrochemically (157). Infrared spectroscopy has been

applied to the study of its anion radical in solution

(158,159) and in the solid state (160,161). Khatkale

and Devlin studied the vibrational and electronic

spectra of the mono-, di-, and trianion salts of TCNQ

using a vapor deposition method (162). The resonance

Raman spectroelectrochemistry of the dianion and its

oxygen decay product was studied by Suchanski and Van

Duyne (163). Theoretical calculations of the spectro-

scopic properties of TCNQ, $TCNQ^-$, and TCNQ= have been

performed. The ionization and reduction potentials and

dipole moment has also been calculated theoretically

(126). Electron spin resonance has been applied to the

study of $TCNQ^-$ and its reactions (165-167). Theoretical

spin density distribution calculatons have also been

made (146,147).

Electrochemical studies have shown that the reduc-

tion of TCNQ in homogeneous solvents involve two well-

defined one-electron steps, with the formation of the

anion radical and then the dianion. Peover found that

both steps were polarographically reversible in chloroform

and methylene chloride. In acetonitrile and DMF, where

only the first reduction step was studied, the same

result was obtained (128,129). Suchanski and Van Duyne

also found reversibility for both electron transfers in

acetonitrile on a voltammetric time scale (0.2 to 2.0s

(163). Sharp obtained the heterogeneous rate

constants for the first reduction steps in various

dipolar aprotic solvents and at different electrode

materials. Diffusion coefficient values were also

obtained (148,149).

Due to its additional conjugation, the anions of TCNQ

are expected to be more stable than those of TCNE (148).

However the stability of the anion radical and dianion are

still affected by oxygen and water. In deaerated aceto-

nitrile, TCNQ$^{\bar{}}$ is reported to be stable for 3 hours whereas

TCNQ= at least for 40 m. The oxygen decay of TCNQ=

has also been studied (163). The rate of protonation of

$TCNQ^-$ in methanol, ethanol, acetonitrile and water has also

been determined (169,170). $TCNQ^-$ is known also to dimerize

in water (171).

Chapter 2    Electrochemical Techniques


2.1   Introduction

In this chapter the electrochemical techniques

employed in this reasearch are described.  As far as

possible, detailed mathematical derivations are avoided.

Since most of them are established techniques, the

details are presented in most textbooks and review

series (172-176).  However, pertinent equations will be

given here.



2.2  General Considerations

The modern electrochemical experiment employs a

three electrode system.  This consists of the working

electrode, where the electrode reaction of interest is

monitored, the counter electrode which completes the

current path through the solution, and the reference electrode. The reference electrode draws extremely small currents and its potential remains essentially constant. The applied potential is controlled with respect to the reference electrode by a potentiostat. Also, depending upon the technique used, a potential program (e.g. ramp, pulse etc.) can be applied from some source such as a waveform generator.

In earlier two electrode systems, problems of voltage loss (iR loss) due to high solution resistance (especially in nonaqueous media) arose. However, with the use of the potentiostat employing operational amplifier circuitry in a three electrode configuration, the iR loss can be reduced to very small values by employing a positive feedback circuitry and proper place-ment of the reference electrode close to the working

electrode.

Consider the electrode reduction process

$$O + ne \underset{k(-1)}{\overset{k(1)}{=}} R \qquad\qquad (2.1)$$

where n is the number of electrons transferred, O and R

are the oxidized and reduced species of the redox couple,

and k(1) and k(-1) are the forward and reverse heterogeneous

rate constants respectively. At equilibrium where no net

current is flowing the Nernst equation applies

$$E(eq) = E(0) + RT/nF \ln(a(0)/a(R)) \qquad\qquad (2.2)$$

where E(eq) is the equlibrium potential, E(0) is the standard

potential, a(0) is the bulk activity of O, a(R) is the

bulk activity of R. All the activity coefficients can

be incorporated into E(0) to give the formal potential E(0)'

$$E(eq) = E(0)' + RT/nF \ln(C(0)/C(R)) \quad . \quad (2.3)$$

where the C's refer to concentration. Also, if the

electrode kinetics are very fast (i.e. the standard

heterogeneous rate constant ks (is large), equation (2.3) can

be applied to concentrations at the surface of the electrode

and the reaction is said to be electrochemically reversible

$$E = E(0)' + RT/nF \ln(C(0)'/C(R)') \quad (2.4)$$

where C(0)' and C(R)' are concentrations of 0 and R

respectively at the surface of the electrode.

The total current i, which flows in the electro-

chemical experiment comes primarily from two sources

$$i = i(c) + i(f) \quad (2.5)$$

The charging current i(c), is the current

required to charge the electrical double layer at the

electrode-solution interphase. The faradaic current i(f),

is the current which flows as a result of the system's

response to an applied potential, in order that equation

(2.4) could be obeyed. If the response of the system is

slow with respect to a changing potential (i.e. small ks)

then equation (2.3) cannot be established at the electrode

surface and the reaction is said to be electrochemically

irreversible. (It is assumed that species O and R are

otherwise stable so that homogeneous kinetics do not have

to be considered.) If the electrode kinetics are fast,

the current is only governed by the rate at which O can

be transported to the electrode. The electrode reaction

is then said to be mass-transfer controlled.

There are three methods of mass transport, namely,

convection, migration and diffusion. Therefore

$$i(f) = i(conv) + i(m) + i(d) \qquad (2.6)$$

where i(conv) is the convection current, i(m) the migration

and i(d) the diffusion current. In electrochemical

experiments, the migration current is suppressed by using

a large excess (ca 100 times substrate) of the supporting

electrolyte which conducts the current through the bulk

solution as well. Then, depending upon the electrochemical

technique, either convection or diffusion could be the

method of choice for mass transport. In the case of

diffusion control, Fick's laws of diffusion apply and for

linear diffusion to a plane electrode

$$-J(0)(x,t) = i/nFA = D(0)(\delta C(0)(x,t)/\delta x) \qquad (2.7)$$

$$\Delta C(0)(x,t)/\delta t = D(0)\Delta^2 C(0)(x,t)/\delta x^2 \qquad (2.8)$$

At this point, one or two words should be said about

"electrochemical reversibility or irreversibility." Any

process is said to be thermodynamically reversible if an

infinitesimal change in the direction of the driving force

changes the direction of the process. However, all

electrode processes occur at a finite rate and therefore

cannot be thermodynamically reversible. The definition

of electrochemical reversibility is thus one of practical

value rather than thermodynamic rigor. In the practical

sense, therefore, an electrochemical process is reversible

if the deviations from the Nernst equation are too small

to be measured. Also, reversibility would depend on the

technique used. If the time scale of the experiment is

short, and the kinetics of electron transfer are not fast

enough so that the Nernst equation cannot be established

at the electrode surface, the process will be irreversible.

## 2.3  Chronoamperometry

Chronoamperometry, as the name implies, is a technique whereby the current is monitored as a function of time. In common practice, the potential of the working electrode, which is initially set at a value where no electrode reaction is occurring, is stepped to a value large enough so that the electrode process is limited only by the diffusive transport of material to the electrode surface. Since the experiment is carried out in a conductive quiescent solution, this is the only mode of mass transport. Therefore, assuming semi-infinite linear diffusion to a plane, Fick's laws can be applied (equations (2.7) and 2.8)) together with some initial and boundary conditions:

$$C(0)(x,0) = C* \qquad\qquad (2.9)$$

$$C(0)(\text{large } x,t) = C* \qquad\qquad (2.10)$$

$$C(O)(0,t) = 0 \qquad\qquad (2.11)$$

Equations (2.7) and (2.8) together with the conditions above, can be solved by making use of the Laplace transformation. The current time function is given by

$$i = nFA\, D(O)^{\frac{1}{2}} C*/(\pi t)^{\frac{1}{2}} \qquad (2.12)$$

where i = current (uA)

D = diffusion coefficient $cm^2/s$)

C* = bulk concentration (mM)

A = area of electrode ,$cm^2$

n = number of electrons transferred

t = time (s)

F = 96487 coulombs.

Equation (2.12) is known as the Cottrell equation (177),

It should be noted that in the Cottrell equation the

current is independent of potential since the potential

is stepped to a value large enough so that the rate of

the electrode process is essentially infinite. Therefore,

if there are no coupled chemical reactions, the Cottrell

equation will hold whether or not the electrochemical

process is reversible or irreversible.


2.4 Cyclic Voltammetry

Linear sweep cyclic voltammetry is one of the most

popular electrochemical techniques used today. It has

been employed in many applications such as determination

of reversibility and standard heterogeneous rate constants,

elucidation of reaction mechanisms, determination of

homogeneous kinetic parameters, etc. It is almost always

used in initial investigations of new systems. For the

electrode process without coupled chemical reactions, the

theories for the reversible (178-183), quasi-reversible

(180,183,184) and the irreversible cases (186) have been

given. Many cases of charge transfer coupled with chemi-

cal reactions have also been studied (187-190). Later,

Nicholson and Shain (191), in a classic paper, reported

the analytical derivations for the theory for various

cases, both with and without coupled chemical reactions.

Although spherical, cylindrical and planar electrodes

have all been used in cyclic voltammetry, the following

discussion assumes planar diffusion. In the cyclic voltam-

metric experiment, if we consider the reduction process

as given by equation (2.1), the potential of the working

electrode is varied linearly in time from an initial

value where no electrode reaction is occurring to a more

negative value where the electrode reaction is governed by

diffusion. On reaching this value, known as the switching

potential, the linear potential sweep is reversed. The

sweep rate is usually the same for the forward and reverse

scans but need not be so. It can vary widely from a few

mV/s to over 1000 V/s. To describe the process

occurring at the electrode we consider the forward scan. As

the potential is scanned negative from the initial

potential, faradaic current will begin to flow as

prescribed by the Butler-Volmer equation. The surface

concentration of the substrate 0 will thus begin to

decrease. The current increases exponentially with the

potential, and the concentration of 0 is inevitably

driven to zero at the surface. At this point it is

impossible for the flux to continue increasing at such a

rate. As a result, the concentration of 0 near the

electrode continues to fall causing a decrease in the

gradient of 0 in the vicinity of the electrode. Since the

current is simply related to this gradient by Fick's

first law, it is observed that the current begins to fall,

causing a peak to appear in the current-voltage

characteristic. At more negative potentials, the current

is still diffusion limited, and the characteristic is

the same as that of a chronoamperogram, i.e. the current

falls as root t. Simultaneously, the concentration

profile of the electrogenerated species R has been

increasing near the surface of the electrode. It is found,

that if the potential sweep is now reversed, a similar

inverted response is observed. A peak in the opposite

signed direction is formed which corresponds to the

oxidation of R. Similar arguments are in effect for the

observed behavior.

For the reversible case the current is given by

$$i = nFAC(O)*(\pi a D(O))^{\frac{1}{2}} X(at) \qquad (2.13)$$

where $\quad a = (nFv/RT) \qquad (2.14)$

$\quad v = $ scan rate (V/s)

and X(at) is the current function which can be numerically

calculated (191). The peak current is given by

(X(at) = 0.4463).

$$i(p) = 0.4463 \; nFAC(0)*(nFvD(0)/RT)^{\frac{1}{2}} \qquad (2.15)$$

At 25°C

$$i(p) = (269000)n^{3/2} A (D(0)v)^{\frac{1}{2}}C(0)* \qquad (2.16)$$

where $i(p)$ = amperes, A = $cm^2$, D(0)= $cm^2/s$,

C(0)*=mol/$cm^3$ and v = V/s. Equation (2.16) is known as the

Randles- Sevcik equation.

For the reversible case the peak potential E(p) is

related to the polarographic half-wave potential Eh by

$$E(p)- Eh = -1.109(RT/nF) \qquad (2.17)$$

Also the potential at 1/2 i(p), E(p/2) is

$$E(p/2) - Eh = 1.09 \ (RT/nF) = (28.0/n) \ mV \qquad (2.18)$$

at 25°C

and $\qquad E(p) - E(p/2) = 2.20 \ (RT/nF) = (56.5/n)mV \ \ (2.19)$

at 25°C.

Considering both the forward and reverse waves

(cyclic voltammogram), for a Nernstian wave with stable R

$$(i(pa)/i(pc)) = 1 \ \text{if the switching potential} \qquad (2.20)$$

Eλ is at least 35/n mV past

the peak

where $\qquad$ i(pa) = peak anodic current measured from the

asymptotic limit of the decaying cathodic

current as baseline

i(pc) = peak cathodic current.

Also    $delE(p) = |E(p)(ox) - E(red)| = (59/n)mV$ at 25°C    (2.21)

For the totally irreversible case

$$i = nFAC(0)^* (\alpha n'FD(0)v\pi/RT)  X(bt)$$    (2.22)

where    $b = (\alpha n'vF/RT)$

and n' is the number of electrons transferred up to and including the rate determining step.

$$i(p) = (299000) n(\alpha n') AC(0)^* (D(0)v)$$    (2.23)

where n is the total number of electrons transferred.

When the current is at its peak

$$E(p) = E(0)' - (RT/\alpha n'F)[0.780 + ln(D(0) /ks) + ln(\alpha n'Fv/RT)]$$

(2.24)

and $\left|E(p)-E(p/2)\right| = (1.857RT/\alpha n'F) = (47.7/\alpha n')$ mV $\qquad$ (2.25)

at 25°C.

Thus, for the reversible case, E(p) is independent of scan

rate whereas for the irreversible case E(p) shifts

$(1.15 \, RT/\alpha n'F) = (30/\alpha n')$mV more negative at 25°C for each

decade increase in scan rate. Also it is noticed that

for the Nernstian case, no kinetic information can be

obtained, whereas the kinetic parameters, namely the

transfer coefficient $\alpha$ and the standard heterogeneous

rate constant ks, appear in the equations describing the

irreversible electron transfer.

Nicholson (184), has also derived the cyclic

voltammetric behavior for the quasi-reversible case. It was

found that, if $E(\lambda)$ is at least (90/n)mV past

the cathodic peak, the current-potential curves are

dependent on the dimensionless parameter $\alpha$ and $\Delta$ where

$$\Delta = ((D(O)/D(R))^{\frac{1}{2}} ks)/[(D(O)\pi v(nF/RT)]^{\frac{1}{2}} \qquad (2.26)$$

Also for $0.3 < \alpha < 0.7$, delE(p) values are essentially

independent of $\alpha$ and depend only on $\Delta$. DelE(p) values

together with their corresponding $\Delta$ values have been

calculated (assuming $\alpha = 0.5$). From these values, a

working curve can be plotted from which ks values for

quasi-reversible electrode reactions can be obtained by

observing the variation of delE(p) with sweep rate v.

For more details concerning the equations introduced

in this section references (172, 191) should be consulted.

2.5 Normal Pulse Polarography

The dropping mercury electrode (dme) was initially

introduced by Heyrovsky (206). The technique which its

use generated is called polarography, and has since

gained widespread use. (The term polarography used

here is distinguished from voltammetry in that the former

applies solely to the use of the dropping mercury

electrode.) Over the years, the polarographic technique

has undergone so much transformation and improvement that

the classical method commonly called d.c. polarography is

nowadays seldom used. This is because related techniques

which arose such as a.c. polarography, normal pulse

polarography, differential pulse polarography, current-

sampled polarography, etc. offer large advantages in terms

of diagnostics, sensitivity, resolution, recording etc.

Although normal pulse polarography is the method of

choice in this work, the general polarographic theory

must be briefly described with reference to the closely

related d.c. polarography. In the polarographic experi-

ment, the mercury issues from a capillary and grows

as spherical drops until the weight exceeds the surface

tension, when it drops. A new drop then emerges. Mean-

while the potential applied to the electrode is linearly

varied (slowly) so that the potential change per drop is

not more than 5 mV (174). This is required to satisfy the

condition of essentially constant potential and thus

electrochemical equilibrium. During the growth of each

drop, a current flows and the electroactive species in

the vicinity of the drop will be depleted. As the drop

falls, it stirs the solution and carries most of the

diffusion layer away so that each new drop is again born

into an essentially (not completely) fresh solution. The

periodic growth and fall of the mercury drops is

reflected in d.c. polarograms (current vs voltage plots)

which exhibit current oscillations.

For the reversible d.c. polarographic process as

given by equation (2.1), equations (2.3) and (2.4) hold.

The instantaneous current at the diffusion limit has

been derived by Ilkovic (207,208)

$$i(d) = 708 \ n \ C(0)^* \ (D(0))^{\frac{1}{2}} m^{2/3} \ t^{1/6} \qquad (2.27)$$

where $\quad$ m = mass flow rate of mercury in mg/sec

All the other terms have their usual meaning.

At the end of drop life $\quad t = t(max)$, and

$$i(d \ max) = 708 \ n \ C(0)^* D(0)^{\frac{1}{2}} \ (t \ max)^{1/6} \ m^{2/3} \qquad (2.28)$$

Also, it can be easily shown that the current-potential

curve is given by (174)

$$E = E(0)' + (RT/nF) \ ln((i(d) - i)/i)(D(R)/D(0))^{\frac{1}{2}} \qquad (2.29)$$

$$E = E(0)' + (RT/nF) \ ln \ (D(R)/D(0))^{\frac{1}{2}} +$$

$$(RT/nF) ln \ (i(d)-i)/i \qquad (2.30)$$

In the pulse polarographic experiment, the potential

program is different from the continuous linear change

of d.c. polarography.  Here, the potential is always

kept at an initial value where the reduction process does

not occur.  Towards the end of each drop life, a potential

pulse is applied, the amplitude of which increases

monotonically with each application. This program is illus-

trated in Figure 1. Thus, if the potential is at the diffusion

controlled limit the current is given by the Cottrell equation

$$i = (nFA(D(0))^{\frac{1}{2}} C(0)\star)/(\pi(t(2)-t(1))^{\frac{1}{2}} \qquad (2.31)$$

Equation (2.31) is based on the same assumptions of

linear diffusion as the Ilkovic equation (equation (2.27))

except that in the latter, the expansion of the mercury

drop is taken into account.  Since in pulse polarography

the potential pulse is applied at the end of drop life,

POTENTIAL

$T_1$

$T_2$

$T_{MAX}$

INITIAL
POTENTIAL
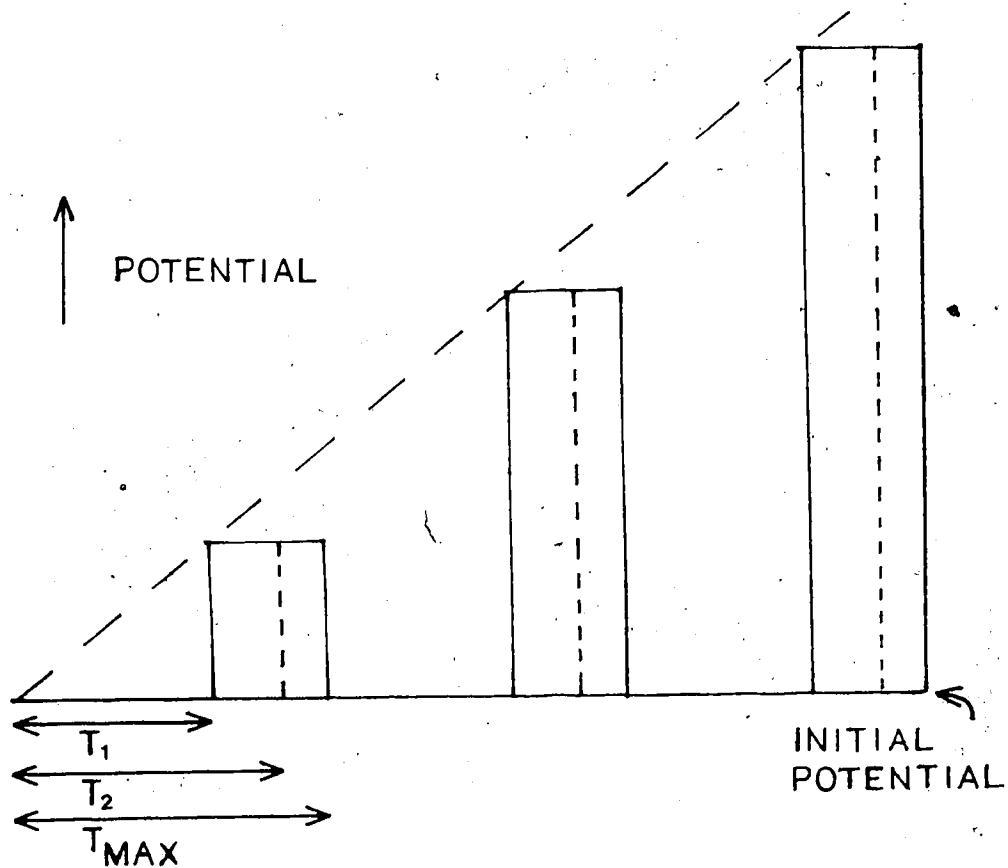
AT $T_1$ PULSE APPLIED

AT $T_2$ CURRENT MEASURED

$T_{MAX} =$ DROP LIFE, 0.5S

$T_{MAX} - T_1 = 57$ MS

$T_{MAX} - T_2 = 16.7$ MS

Figure 1. Normal pulse polarographic potential program.

the drop area is not changing very much. Thus the form

of the pulse polarogram consists of steps rather than

the current oscillations encountered in d.c. polarograms.

The current potential curve can also be shown to

have the same form as equation (2.30) i.e.

$$E = E(0)' + (RT/nF)\ln (D(R)/D(0))^{\frac{1}{2}} + (RT/nF)\ln((i(d)-i)/i)$$

$$(2.32)$$

At  $i = i(d)/2$

$$Eh = E(0)' + (RT/nF)\ln (D(R)/D(0))^{\frac{1}{2}} \qquad (2.33)$$

where Eh is the half-wave potential. In many cases D(R) =

D(0) so that Eh is usually taken to be the same as E(0)'.

Therefore for a reversible reaction, a plot of E vs

log (i(d)-i/i) should give an intercept equal to Eh and a

slope equal to (2.303 RT)/(nF) which has the value 59/n

mV at 25°C. The above equations apply equally well to d.c.

polarography. Also, it can be shown that under the usual

operating conditions, normal pulse polarography is about

6 to 7 times more sensitive than d.c. polarography (see

reference (174), p. 244).

## 2.6 Modulated Specular Reflectance Spectroscopy (MSRS)

Spectroscopy was successfully combined to electro-

chemistry in the 1960's (192,193). With this combination,

an extra selectivity dimension was added to the electro-

chemical experiment. Thus wavelength and potential became

the controllable experimental variables. This new

addition to the electrochemical arsenal is aptly called

spectroelectrochemistry.

Spectroelectrochemistry has been applied to the

studies of adsorption (194,195), double layer structure

(196,197), identification of intermediates and elucidation

of reaction mechanisms (198-200). The spectral regions

used have included IR and Raman (139,157,201), and UV-

VIS (198,202). Recently, the spectroscopic response to

the a.c. voltammetric experiment has been studied (203).

It has been noted that the spectroelectrochemical

techniques have the advantage in that the deleterious

effects of charging current which affect current measuring

methods have been eliminated.

In the spectroelectrochemical experiment both trans

mission (192,203,204) and reflectance (198,202,205)

methods have been used. However, reflectance has some

advantages over transmission in that due to its setup,

the counter electrode in the transmission method cannot

be positioned in such a way that every point in the

working electrode is equidistant from it. Thus uneven

current distribution arises. Also, the fact that the

optically transparent electrode is a thin conductive film

deposited on a transparent insulating material gives rise

to high resistance. Further discussion will be restricted

to the modulated specular reflectance technique (MSRS)

although the equations which arise are, in principle,

applicable to the transmission technique.

As used in the author's laboratory, the UV-VIS MSRS

experiment can be attained in two ways. For the electrode

process given in equation (2.1), the potential is modu-

lated such that, periodically, either O or R is present

in the diffusion layer. Meanwhile, the wavelength of the

incident radiation is scanned. Light passing through

the solution hits the electrode at an angle and is

reflected. In doing so, it passes twice through the layer

where the absorbing species are present with the periodic

formation and removal of R in the diffusion layer. The

resulting light signal is a difference spectrum of R since

the background condition is that with O initially present.

The light signal is detected by a photomultiplier and '

extracted out of background noise using a lock-in amplifier

referenced to the same frequency as the modulation.

In obtaining the spectrum, the signal is fed into

a lock-in amplifier. In doing so, time information is com-

plicated. To obtain kinetic information after obtaining the

spectrum, the wavelength of the incident radiation is

fixed, usually at the absorption maximum. This time,

the modulated light signal after detection at the photo-

multiplier is processed by a signal averager. Here, the

signals for the formation and disappearance of R for a

single cycle are signal averaged over a chosen number

of cycles to increase the signal-to-noise ratio. The

result is a reflectance-time transient from which kinetic

information is available.

In the single beam MSRS experiments discussed above,

the parameter which is actually measured is the nor-

malized reflectance

$$(delR/R) = [R(t)-R(0)]/R(0) \qquad (2.34)$$

where R(0) = reflectance at time t=0

R(t) = reflectance at time t

$$delR/R = [R(t)/R(0)]-1 \qquad (2.35)$$

$$R(t)/R(0) = 1+[delR/R] \qquad (2.36)$$

It has been shown that for any electrode process where only

R may absorb, the time-dependent absorbance for the

optical transmission electrode (OTE) experiment is given

by. (199)

$$A(t) = (\ell(R)/nFA) \int_0^t i(t)dt \qquad (2.37)$$

where $\ell(R)$ is the absorptivity of R and all the other

symbols have the usual meaning. The integral of the

current with respect to time is related to the number of

absorbing species in the light path length. For the

MSRS experiment, as mentioned earlier, light passes

through the path length twice at an angle $\theta$ as shown in

Figure 2. In the figure,

$$q/2 = x/\cos(\theta)$$

$$q = 2x/\cos(\theta)$$

Therefore, the path length in the MSRS experiment is

enhanced by $2/\cos(\theta)$ times that in the transmission experi-

ment.

$$A(t) = (2\ell(R)/nFA\cos(\theta)) \int_0^t i(t)dt \qquad (2.38)$$

But the absorbance

$$q = \frac{2X}{\cos \theta}$$

**Incident Radiation**

**Reflected Radiation**

$\theta$

X

q/2

**Electrode Interface**
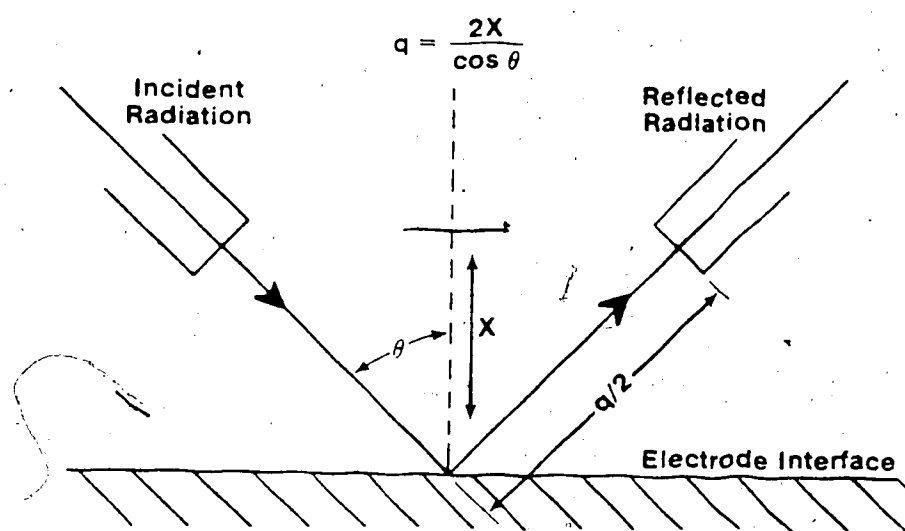
Figure 2. The coordinate system used in modulated
specular reflectance spectroscopy.
q is the pathlength of light beam
θ is the angle of incidence
x is the solution layer containing absorbing
species of interest

$$A(t) = \log(I(0)/I(t)) \tag{2.39}$$

$$A(t) = \log(R(0)/R(t)) \text{ or}$$

$$A(t) = -\log(R(t)/R(0)) \tag{2.40}$$

Thus

$$\log(R(t)/R(0)) = \log(1 + \text{delR/R}) \tag{2.41}$$

$$\log(1 + (\text{delR/R})) = (-2\ell(R)/nFA \cos(\theta)) \int_0^t i(t)dt \tag{2.42}$$

and $\ln(1 + (\text{delR/R})) = (-4.606\ell(R)/nFA \cos(\theta)) \int_0^t i(t)dt \tag{2.43}$

For small delR/R (experimental values of delR/R are seldom

greater than 1.0e-3 equation (2.43) can be approximated by

$$-\text{delR/R} = 4.6\ell(R)/nFA\cos(\theta) \int_0^t i(t)dt \tag{2.44}$$

Chapter 3   The Electrochemical Reduction of Alkali Metal
          Cations, Anthracene and Fluoranthene in
          Acetonitrile and Dimethylformamide.

3.1  Introduction

In this thesis research, I have undertaken to observe

the electrochemical behavior of alkali metal cations,

anthracene (An), and fluoranthene (Fa) in aprotic solvents

acetonitrile and dimethylformamide at the mercury elec-

trode.  The electroreduction of anthracene and fluoran-

thene was also carried out in the presence of alkali metal

cations.  Observations were focussed on the effect of the

cations on the anion radicals and dianions of the poly-

cyclic aromatic hydrocarbons.

As was mentioned in Chapter 1, in most of the previous

studies of aromatic hydrocarbon negative ions-alkali metal

cation interactions, the reaction was a chemical

reduction with alkali metals in ethereal solvents of low

dielectric constants. The powerful esr technique has been

frequently applied to the study of the anion radicals. The

fact that the dianions are very reactive means that these

species are difficult to study without extreme experimental

precautions. Buschow et al (96) measured the electrical

conductance of solutions of alkali-aromatic hydrocarbon

salts in 2-methyltetrahydrofuran, tetrahydrofuran and

1,2-dimethoxyethane. Information was obtained for condi-

tions under which the hydrocarbon negative ions are free

or associated with alkali counter ions. It was found that

at room temperature a 0.1 mM solution of the monolithium

salts of anthracene, tetracene, pentacene in 2-methyl-

tetrahydrofuran are completely dissociated whereas sodium

and potassium salts are associated. The dinegative ions

showed much stronger association and two countercations

were thought to be involved. The tendency of hydrocarbon

ion to associate with cations was found to increase with

(i) smaller size of the hydrocarbon ion, (ii) larger

radius of the cation, and (iii) increasing temperature.

Solvation was thought to play a very important role.

Disproportionation of solution phase radical anions is

affected by countercations as well as solvents. The

presence of ion pairing substantially increased the

equilibrium constants for the disproportionation espec-

ially if contact ion pairs are formed between the dianions

and the cations.

$$2 R^{\bar{\cdot}}, Cat \rightleftharpoons R + R^= ,2 Cat \quad k(disp) \qquad (3.1)$$
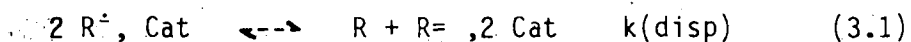
There have been many studies of the disproportionation

reactions of aromatic hydrocarbon anion radicals (223-225).

However, the k(disp) values have been found to be small,

ranging from 1.0e-7 to 1.0e-12.

Electrochemical techniques such as polarography and

cyclic voltammetry have been applied to the studies of ion

pairing of negative ions of organic molecules with alkali—

metal cations. In the cases where ion pairing occurs,

shifts in half-wave potentials or peak potentials toward

more positive values are observed. In the study of

polycyclic aromatic hydrocarbon dianion-alkali metal

cation interactions by electrochemical means, one problem

arises. This is because in most cases, the reductions

of the alkali cations are in the same potential region as

those of the aromatic hydrocarbon dianions. Therefore,

if solid electrodes of inert materials such as

platinum, carbon, gold etc. are used, deposition of

alkali metals occurs. Various complications could

then arise due to the reactivity of these alkali metals,

as mentioned in Chapter 1. Therefore, if solid electrodes

are to be used, the reduction potentials of the dianions

of the organic species under investigation have to be

positive to those of the alkali cations. However,

this problem could be easily solved, as noted earlier,

with the use of the mercury electrode. This material also

has the advantage of high surface reproducibility. Also

the use of electrochemical methods affords a very impor-

tant advantage over chemical reduction. The production of

the desired anions to be studied can be easily controlled

by controlling the potential. In chemical reduction,

species control is not easily accomplished.


## 3.2 Experimental


### 3.2.1. Instrumentation

The instrument used in the polarographic analyses

was the PAR 174A Polarographic Analyser which was operated in

the normal pulse mode. For this particular instrument in

the normal pulse mode, the duration of each pulse was

57 ms, the pulse being applied towards the end of drop

life. However, the current was only sampled during the

last 16.7 ms of the pulse length in order to minimize

the contribution of charging current to the total current.

Figure 1 illustrates the potential program and the current

sampling time interval. The scan rate used in all

experiments was 10 mV/s. Polarograms were recorded,

without smoothing, with a Houston Instruments Omnigraphic

2000 X-Y recorder. The capillary used for the dropping

mercury electrode was of length 18.4 cm and internal

diameter 0.03 mm. The mercury drop time was controlled by

an electromechanical drop timer set at 0.5 s. The use

of the drop timer avoids the problem of the variation of

surface tension and therefore drop time with potential. The

polarographic cell was a single compartment type with an

outer jacket for temperature control purposes. (Figure 3).

SILVER WIRE

FRIT

REFERENCE ELECTRODE

DME

PLATINUM
COUNTER
ELECTRODE
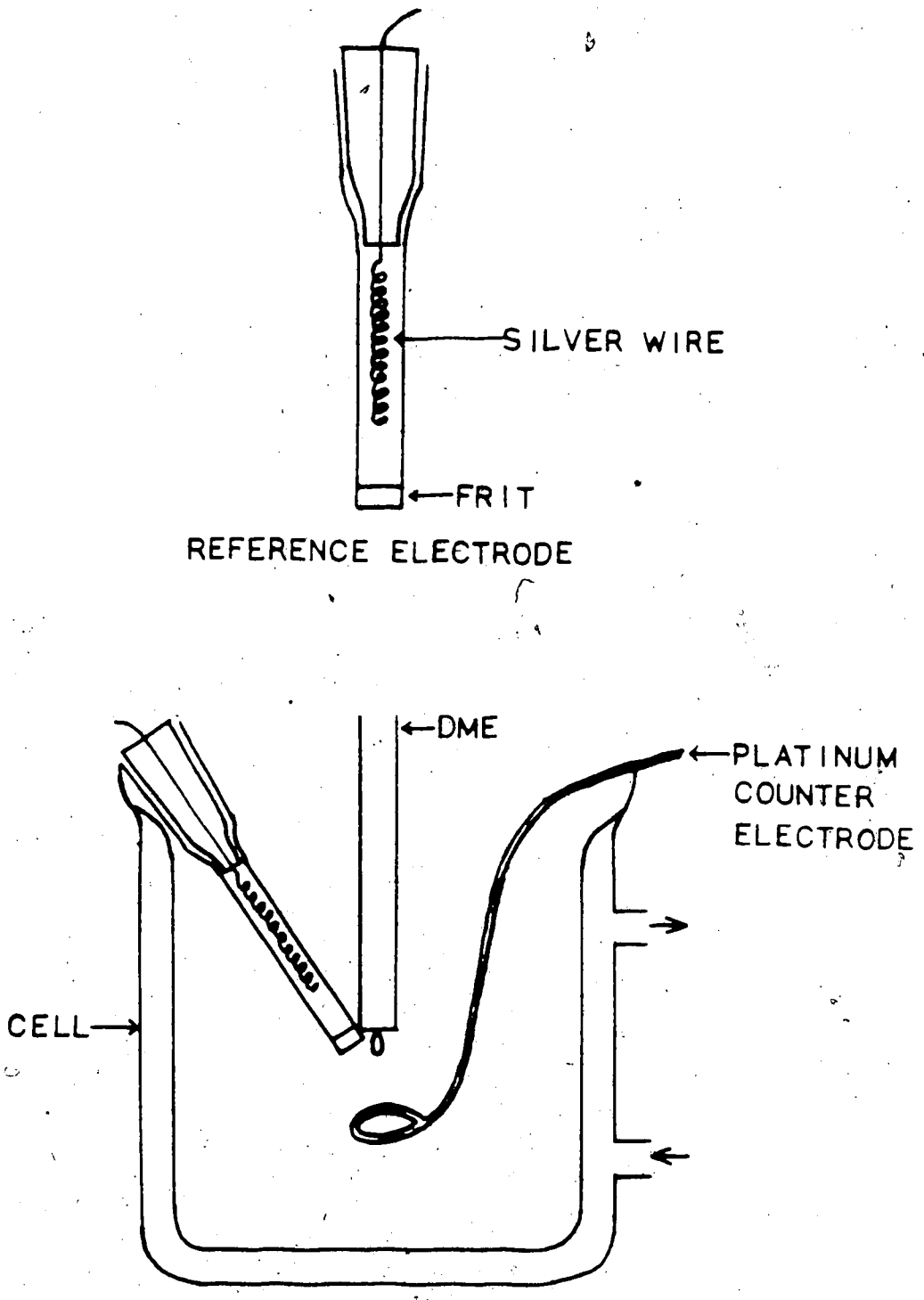
CELL

Figure 3. Polarographic cell arrangement.

### 3.2.2 Purification of Chemicals.

The mercury used was triply distilled and filtered

through a pin hole made in a filter paper to remove any

particulates or surface oxides. Reagent grade lithium,

sodium, potassium and rubidium perchlorates were re-

crystallized twice from triply distilled water. The

purified products were dried in vacuo at 110°C for a

minimum of 48 hours and stored in a vacuum dessicator

over calcium chloride. Anthracene (Aldrich Gold Label

99.9%) was used as received. Fluoranthene (Aldrich 98%)

was recrystallized once from ethanol. Tetra-n-butylammonium

tetrafluoroborate (TBAF) was prepared according to a

method similar to that of Lund and Iverson (213). This

was done as follows: equal numbers of moles of tetra-n-

butylammonium hydrogen sulfate and sodium tetrafluoro-

borate were dissolved separately in a minimum amount of

distilled water. The solutions were mixed in a separating

funnel whereby the TBAF precipitated out. Methylene

chloride was added to the separating funnel to dissolve

the TBAF. After shaking, the methylene chloride layer

was allowed to settle and drained out. It was then

added to ice-cooled anhydrous ether with stirring,

whereupon the TBAF crystallized and was recovered.

The product was redissolved in methylene chloride, mixed

with distilled water in the separating funnel and the

crystallization step repeated. The final product was

dried in vacuo at 80°C for a minimum of 48 hours and then

stored in a vacuum dessicator over calcium chloride.

Dimethylformamide (Fisher regent grade) was allowed to

stand over anhydrous barium oxide for 24 hours with

occasional shaking. It was then distilled from the

barium oxide under reduced pressure (trapped aspirator)

through a 1 m Vigreaux column (214). The freshly

distilled solvent was always used immediately since

dimethylformamide decomposes to form dimethylamine on

standing. Purification of acetonitrile has been des-

cribed elsewhere (202). However, it was found that

Caldeon HPLC grade acetonitrile (water content nominally

0.005%) after drying over Woelm neutral alumina (Super-

grade I) gave excellent results and was used in the

present work.


3.2.3. Procedure

In all experiments the supporting electrolyte

used was tetra-n-butylammonium tetrafluoroborate at a

concentration of 0.10 M. The counter electrode was a

large piece of platinum wire and the reference electrode

(see Figure 3) employed was Ag/Ag+(0.01 M Ag+, 0.10 M

TBAF, acetonitrile or dimethylformamide) dissolved in the

same solvent as that for the experiment. In the case of

dimethylformamide the reference solution was also always

prepared fresh for each experiment. The cell temperature

was controlled by circulating water through the outer

jacket from a temperature regulated bath controlled at

25.0 ± 0.1°C. The cell setup is shown in Figure 3. The

mercury head was set at either 57.0 cm or 40.0 cm from

the tip of the electrode. The mercury mass flow rate in

air at 57.0 cm was 1.29 mg/s and at 40.0 cm was 0.91

mg/s.

Calibration curves were set up for anthracene (An)

and fluoranthene (Fa) in dimethylformamide and aceto-

nitrile. This was also done for the alkali cations

lithium (Li+), sodium (Na+), potassium (K+) and rubidium

(Rb+) in dimethylformamide. However, in acetonitrile,

only Li+ and Na+ were studied due to low solubilities of

potassium and rubidium perchlorates in this solvent.

The calibration curves were obtained by employing the

method of standard addition. 25 ml of the background

solution (i.e. solvent containing only TBAF at 0.10 M)

which had been pre-equilibrated at 25°C was pipetted into

the polarographic cell. Portions of a stock solution

(usually about 9-13 mM, 0.10 M TBAF) of the electroactive

species of interest which also had been equilibrated at

25°C was then added to the cell using a micropipette. Solvent

saturated argon was bubbled through the cell solution. An

argon atmosphere was kept above the solution at all times.

This deaeration procedure was used in all experiments.

To investigate the effect of alkali metal cations on

the reduction of anthracene and fluoranthene, the standard

addition method was again used. 25 ml of a solution

containing 1.00 mM of the hydrocarbon (0.10 M TBAF) kept

at 25°C was pipetted into the cell. After each polaro-

graphic run, a known volume of a stock solution of the

alkali metal cation (10 mM, 0.10 M TBAF) which was also

1.00 mM in the hydrocarbon and which has been controlled

at 25°C was added to the cell with a micropipette.

For the anthracene:lithium and the anthracene:sodium systems in DMF, experiments were also performed where the metal cation concentration was kept constant and the hydrocarbon concentration varied. In the case of An:Li+, the Li+ concentration was fixed at 1.50 mM whereas for the An:Na+ system, the Na+ concentration was fixed at 2.00 mM. The procedure used in these instances was the same as that above, the only changes being that the additions involved the hydrocarbon and not the metal cations.

### 3.3 Results

The background solution containing only the solvent and supporting electrolyte was always obtained for a new batch of solvent or supporting electrolyte to check for purity. If the background breakdown occurred

more positive than -3.10V for ACN or -3.20 V (vs the

respective reference electrodes) for DMF, the solvent

was redistilled or the electrolyte recrystallized. Also,

the current should be less than 1 uA at these potentials

for the polarographic conditions used. Figure 4 shows

typical background polarograms for the two solvents.

It was mentioned earlier in the procedure section

that the mercury head used was either 57.0 cm or 40.0 cm.

In all experiments in DMF the mercury height used was 57.0

cm. However, it was found that, especially in aceto-

nitrile at high negative potentials, instability of

the mercury due to low surface tension at the electrode/

solution interface (66,67) gave rise to "missed drops."

This problem was largely alleviated by lowering the height

of mercury to increase the natural drop life of the dme.

Therefore in some experiments with ACN, the mercury head

was lowered to 40.0 cm.
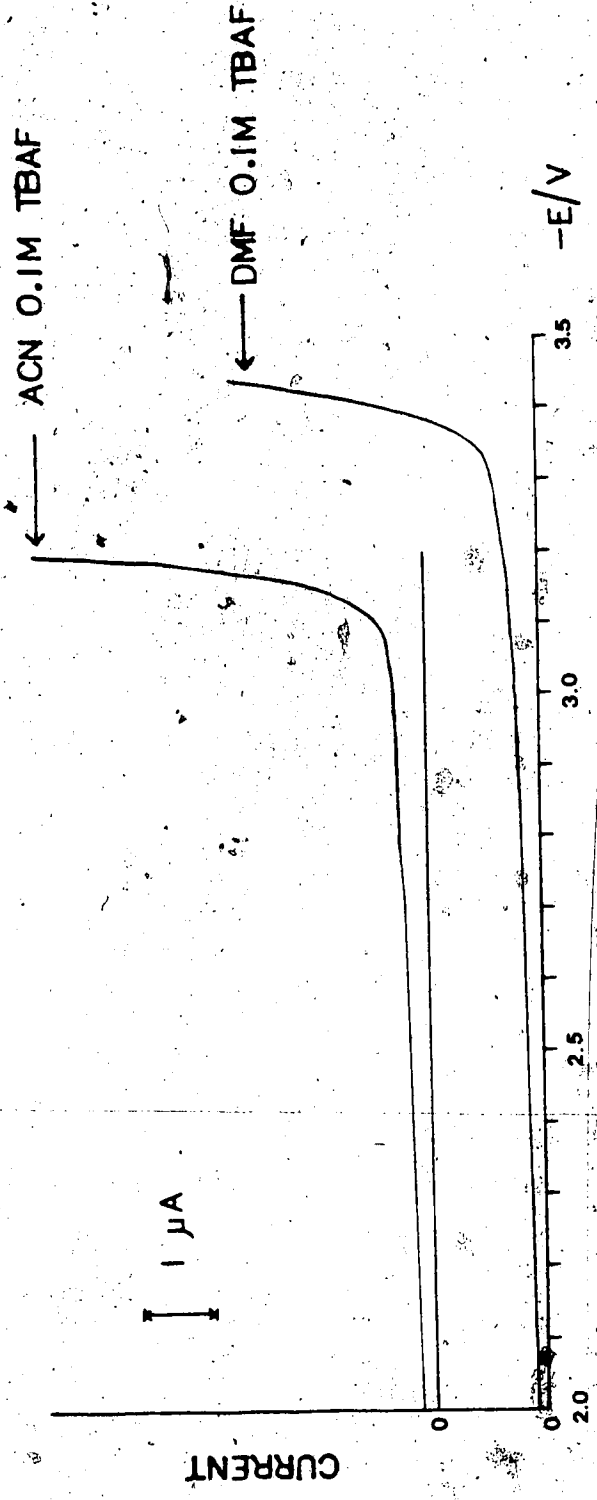
Figure 4. Polarographic background current.

The alkali metal cations showed single well-defined

polarographic waves in both solvents. Logarithmic

analysis revealed that, except for Li cation, all the

cations gave slopes for plots of E vs log ((i(d)-i)/i) of

59 mV (± 2 mV) for a one-electron reversible wave in

both solvents. However, in the case of Li+, slopes of

66 mV (± 2 mV) were obtained in both solvents, indicating

quasi-reversible behavior. Some examples of plots of E

vs log (i(d)-i)/i) are given in Figure 5a. In DMF, the Eh

value for Li+ was markedly more negative, by about 300 mV

than the others. The others were closely grouped, with only

about 30 mV separating them. The Eh value for Li+ in DMF

was 506 mV more negative than in ACN whereas for Na+, this

value was only 304 mV. Again, in ACN, Li+ has an Eh value

negative of Na+, this time only by 104 mV compared to 308

mV in DMF. These Eh values are tabulated in Table 1.

Linear calibration plots were obtained for the alkali

Table 1.  Polarographic Parameters **

DMF

| Reaction | Eh/-V vs Ag/Ag+ | i(d)/uA/mM h=57.0 cm | h=40.0 cm* |
|---|---|---|---|
| An ⇌ An: | 2.381 | 5.8 | – |
| An: ⇌ An= | 2.989 | 6.1 | – |
| Fa ⇌ Fa: | 2.193 | 5.4 | – |
| Fa: ⇌ Fa= | 2.819 | 5.7 | – |
| Li+ ⇌ Li(Hg) | 2.771 | 4.0 | – |
| Na+ ⇌ Na(Hg) | 2.463 | 4.9 | – |
| K+ ⇌ K(Hg) | 2.492 | 5.0 | – |
| Rb+ ⇌ Rb(Hg) | 2.481 | 5.2 | – |

*At high negative potentials, especially in ACN solutions,
the instability of the mercury drop gave rise to "missed"
drops.  After normal precautions were made, it was found
that increasing the natural drop time alleviated most of
the problem.
**Continued next page.

Table 1 · Continued

ACN

| Reaction | Eh/-V vs Ag/Ag+ | i(d)/uA/mM h=57.0 cm | h=40.0 cm* |
|---|---|---|---|
| An ⇌ An: | 2.319 | 8.8 | 6.7 |
| An: ⇌ An= | 2.904 | 8.9 | 7.2 |
| Fa ⇌ Fa: | 2.130 | – | 6.3 |
| Fa: ⇌ Fa= | 2.689 | – | 6.6 |
| Li+ ⇌ Li(Hg) | 2.265 | 7.1 | 5.4 |
| Na+ ⇌ Na(Hg) | 2.159 | 7.8 | 5.9 |
| K+ ⇌ K(Hg) | – | – | – |
| Rb+ ⇌ Rb(Hg) | – | – | – |

cations for concentrations up to about 4.00 mM in both

DMF and ACN. These plots are shown in Figures 5-7. It

can be seen that in DMF, the slope of the Li+ is signifi-

cantly smaller than the others having a value of 4.0 uA/mM.

In acetonitrile, where only Li+ and Na+ were studied, Li+

has a smaller slope than Na+. The values of these slopes

are given in Table 1. At concentrations about about 3.00

mM, it was observed that polarograms for the alkali metal

cations, especially Rb+, showed polarographic maxima.

These maxima were not reproducible and did not always

appear, even for the same conditions. They did not pose

any serious problems in these investigations.

Anthracene and fluoranthene both gave two well-

defined waves in ACN and DMF. The first wave in all

cases showed one-electron reversible behavior, giving

slopes of 59 mV (± 2mV) for E vs log ((i(d)-i)/i)) plots.

In DMF, both hydrocarbons gave second waves close to
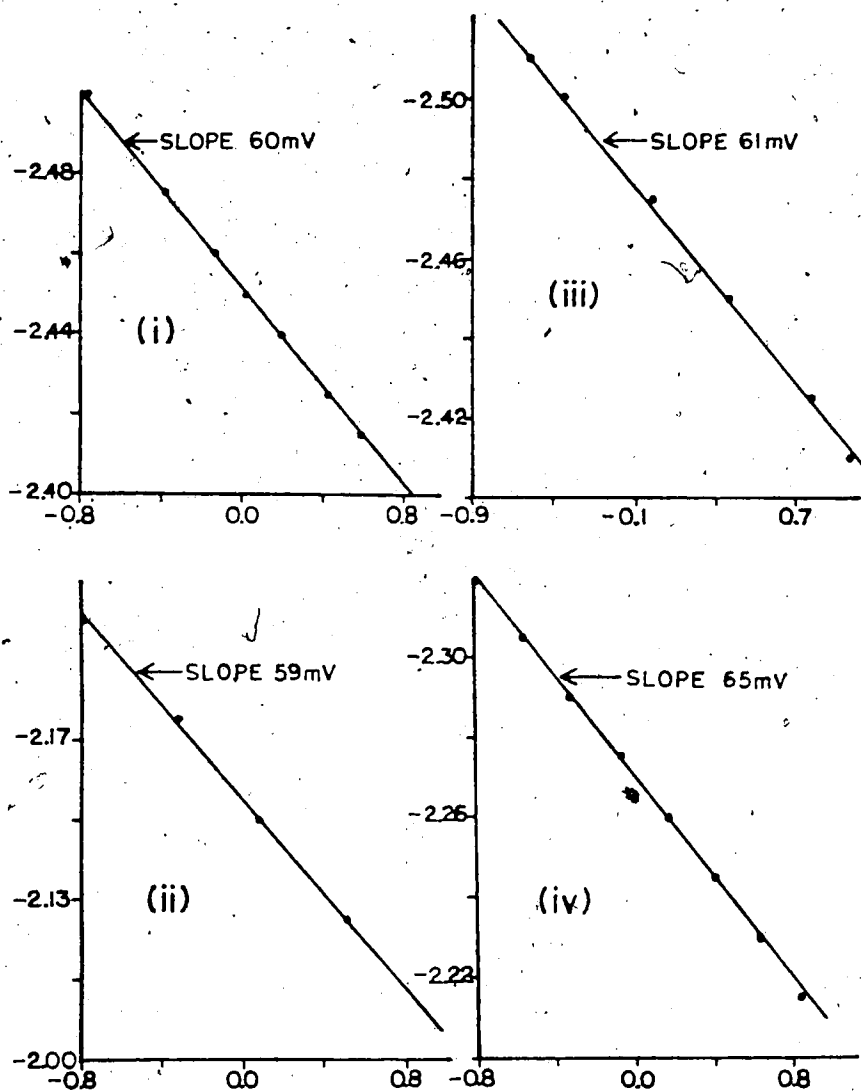
Figure 5a. Plots of E vs log $\dfrac{i_d - i}{i}$

(i)    $Na^+$ in DMF

(ii)   $Na^+$ in ACN

(iii)  $Li^+$ in DMF

(iv)   $Li^+$ in ACN

Mercury column 57.0 cm. 25 C.
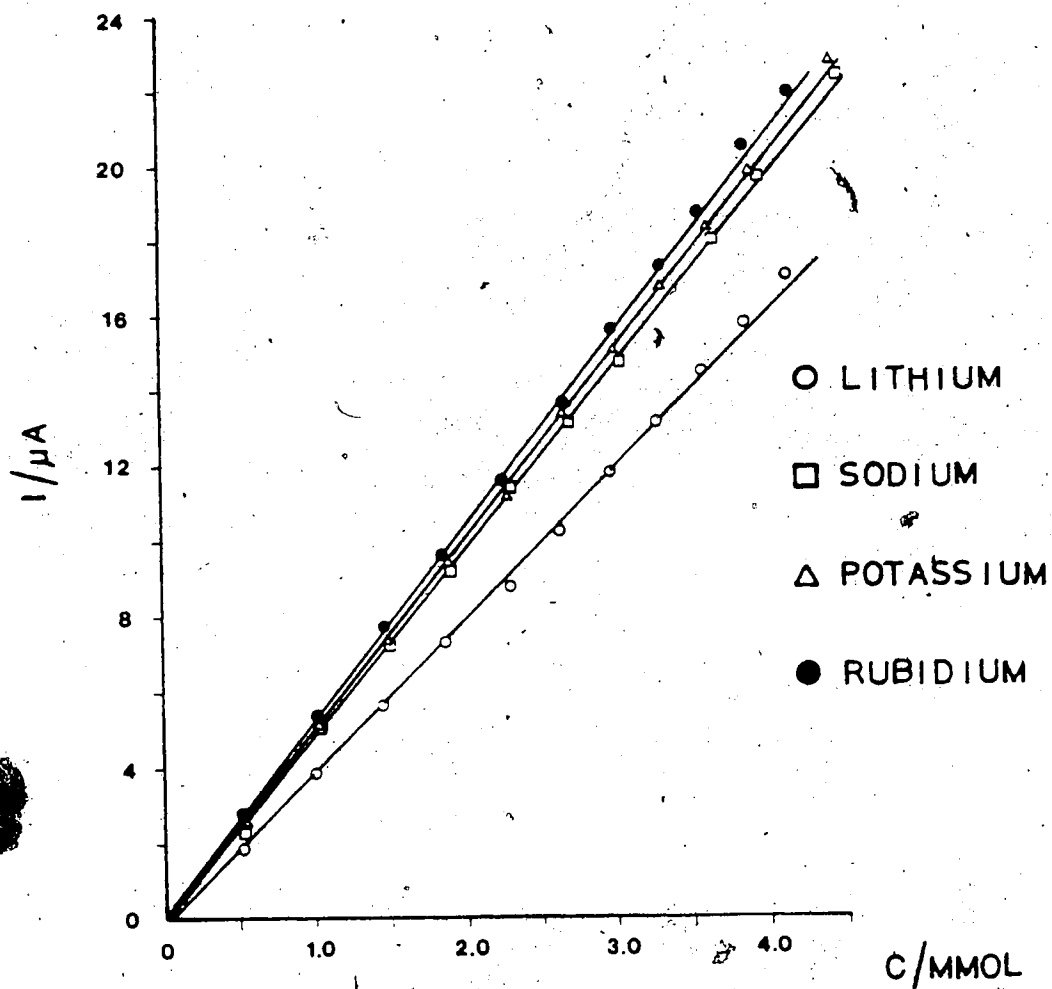
Figure 5. Alkali metal cations calibration plots in DMF at 25°C.
Mercury column 57.0 cm.
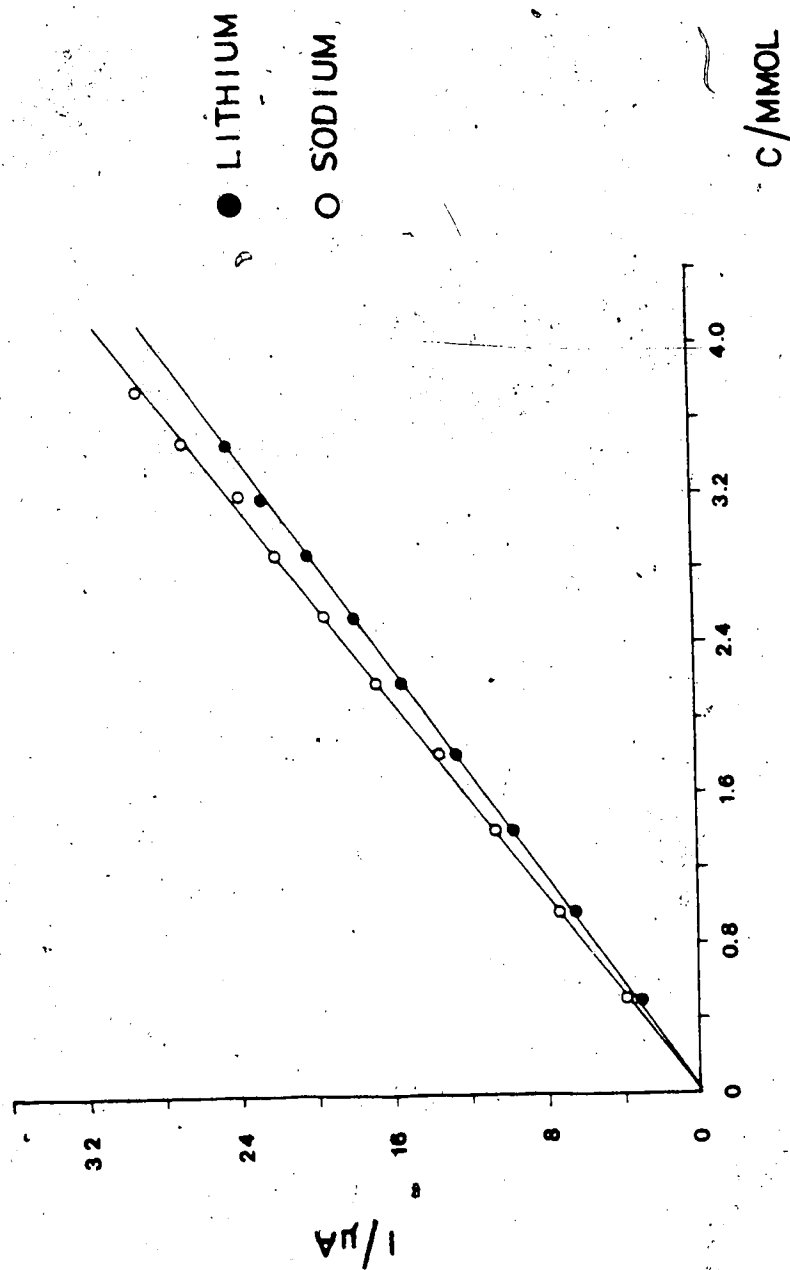
Figure 6. Alkali metal cation calibration plots in ACN at 25°C. Mercury column 57.0 cm.
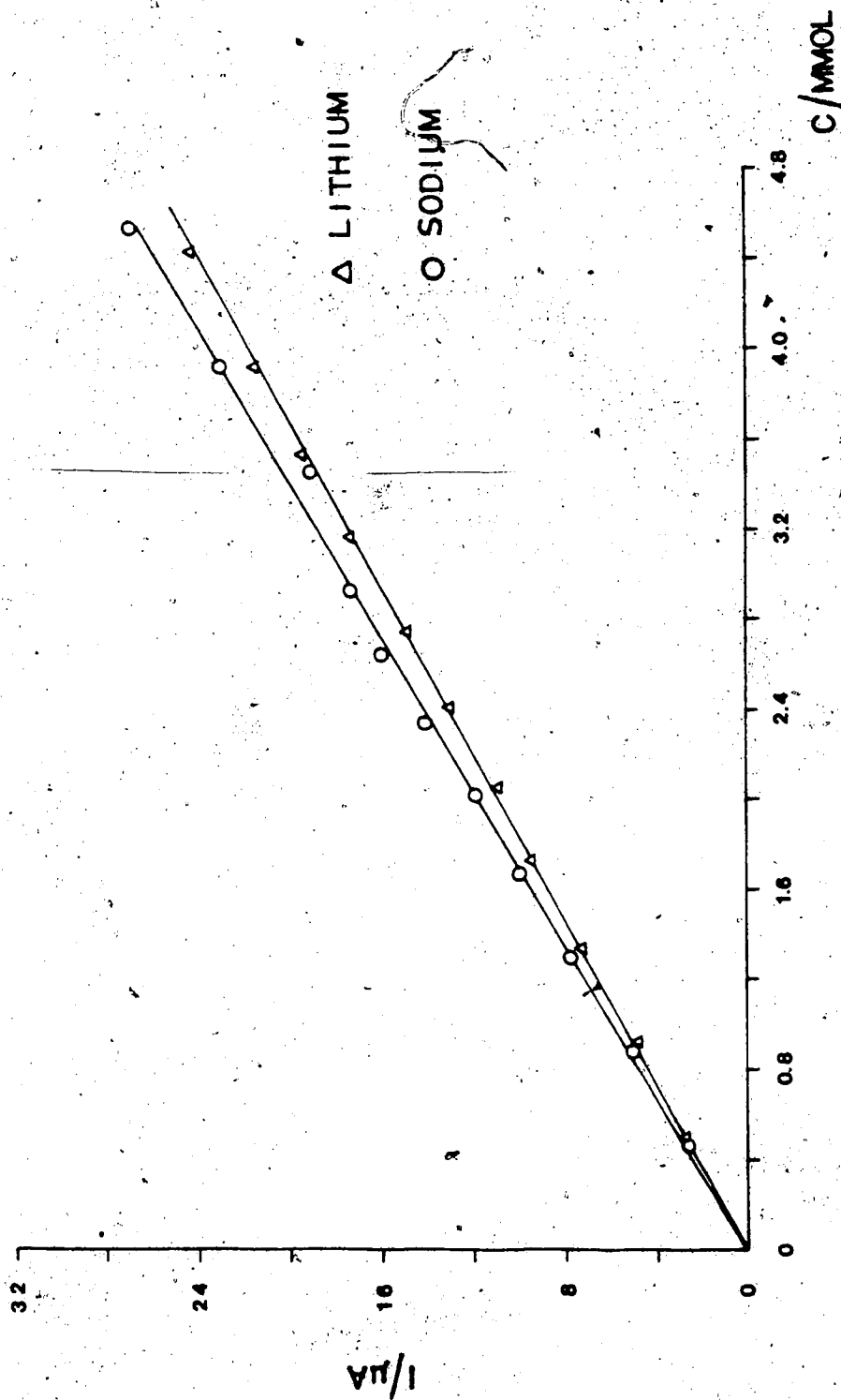
Figure 7. Alkali metal cation calibration plots in
ACN at 25°C.
Mercury column 40.0 cm.

reversible behavior. For example, from these determina-
tions, anthracene gave slopes of 63, 61 and 64 mV.

However, in ACN, these slopes have much larger values with
an average of 76 mV for anthracene and 67 mV for fluor-
anthene. Cyclic voltammetric data showed that the first
waves of anthracene and fluoranthene were reversible but
the second waves did not show any oxidation current on
the reverse scan for the second waves in both solvents.

The scan rate used was 100 mV/s. For both anthracene
and fluoranthene, the first and second polarographic
waves were approximately equal in height. Further,
linear calibration curves of approximately equal slopes
were obtained in both waves for concentrations up to
about 4.00 mM. The values of these slopes are given in
Table 1. It was observed that at concentrations greater
than about 2.00 mM, both anthracene and fluoranthene gave
polarographic maxima in their second wave. There were no

maxima in the first waves. The calibration plots are

given in Figures 8 and 9. For the second waves, currents

measured at the top of the maxima and also at the plateau

are given. The half-wave potentials are listed in Table 1.

These Eh 's are again more positive in acetonitrile than

in dimethylformamide and further, fluoranthene is reduced

more positive of anthracene by about 190 mV.

Figures 10-2I show polarograms of mixtures of An and

Fa with alkali metal cations. In DMF, An:Li+ (Figure 10)

exhibited three well-defined waves corresponding to

anthracene reduction, Li+ reduction and the anthracene

anion radical reduction respectively. On the other

hand, An:Na+, An:K+ and An:Rb+ solutions exhibited only

two waves (Figures 11-13) since the reduction of anthra-

cene and the alkali metal cations were not polarographi-

cally resolved. With fluoranthene, the converse is true:

Fa:Li+ solutions have two waves (Figure 14), this time
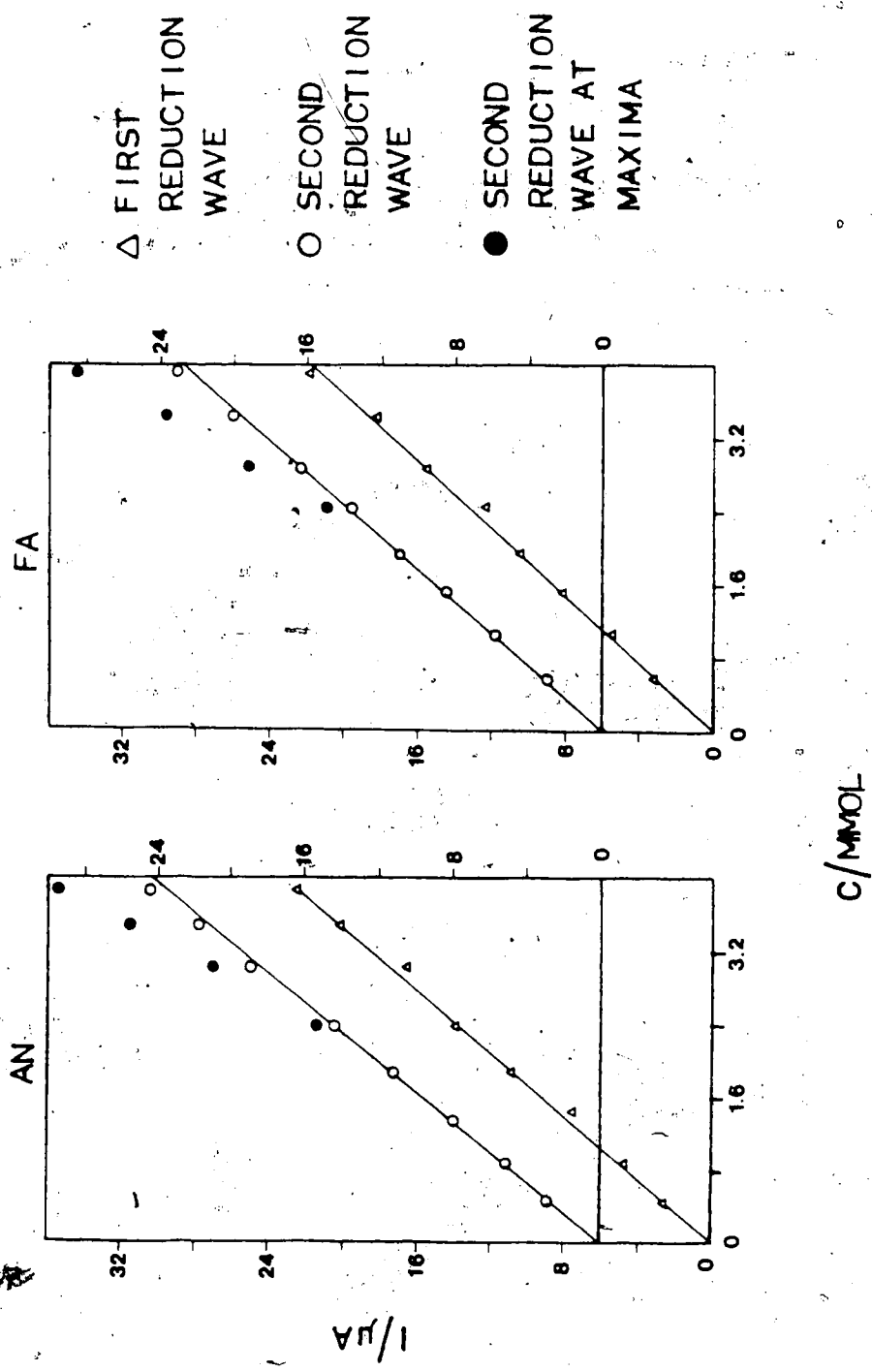
Figure 8. Anthracene and flouranthene calibration plots in DMF at 25°C. Mercury column 57.0 cm.
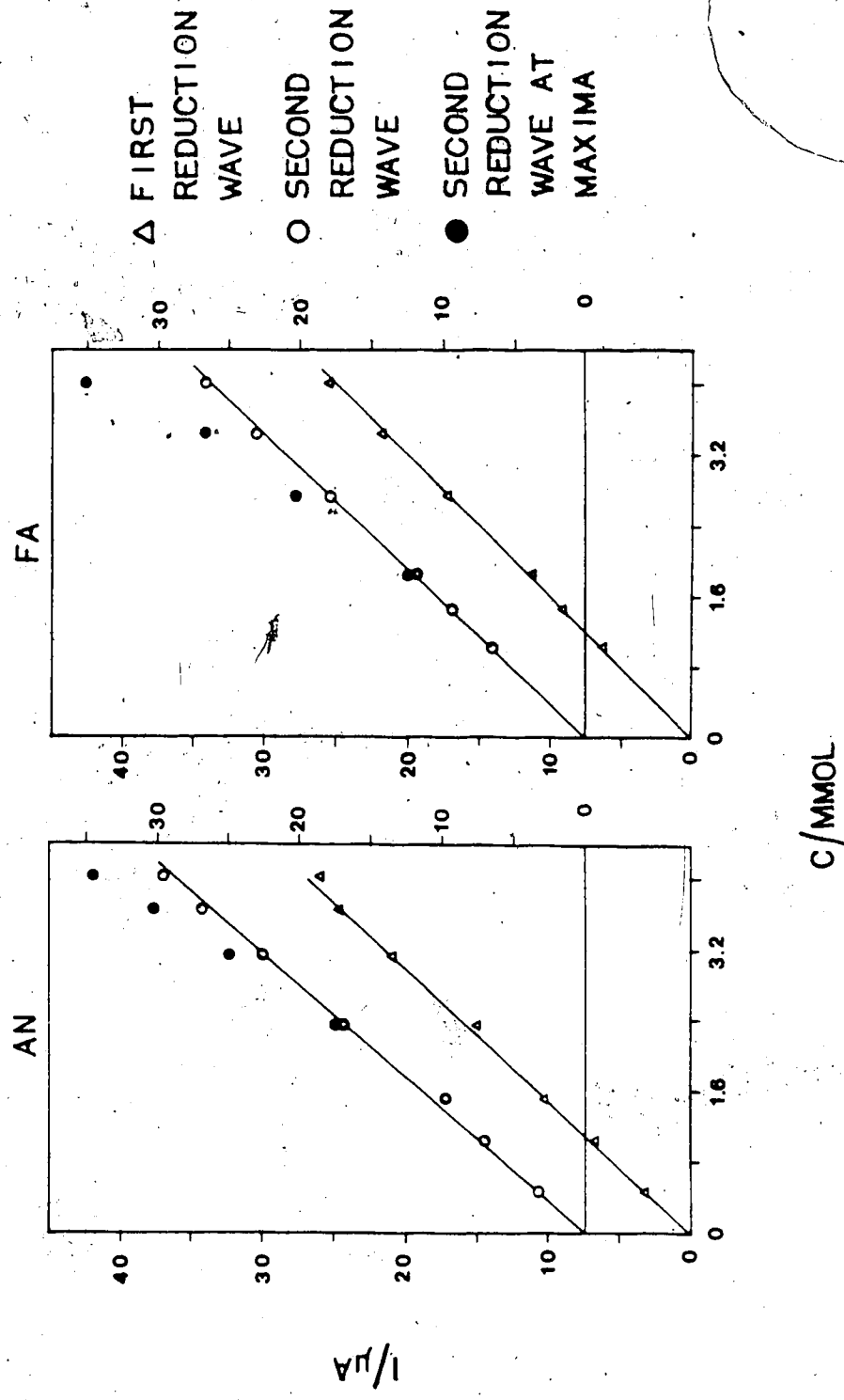
Figure 9. Anthracene and fluoranthene calibration plots in ACN at 25°C. Mercury column 40.0 cm.
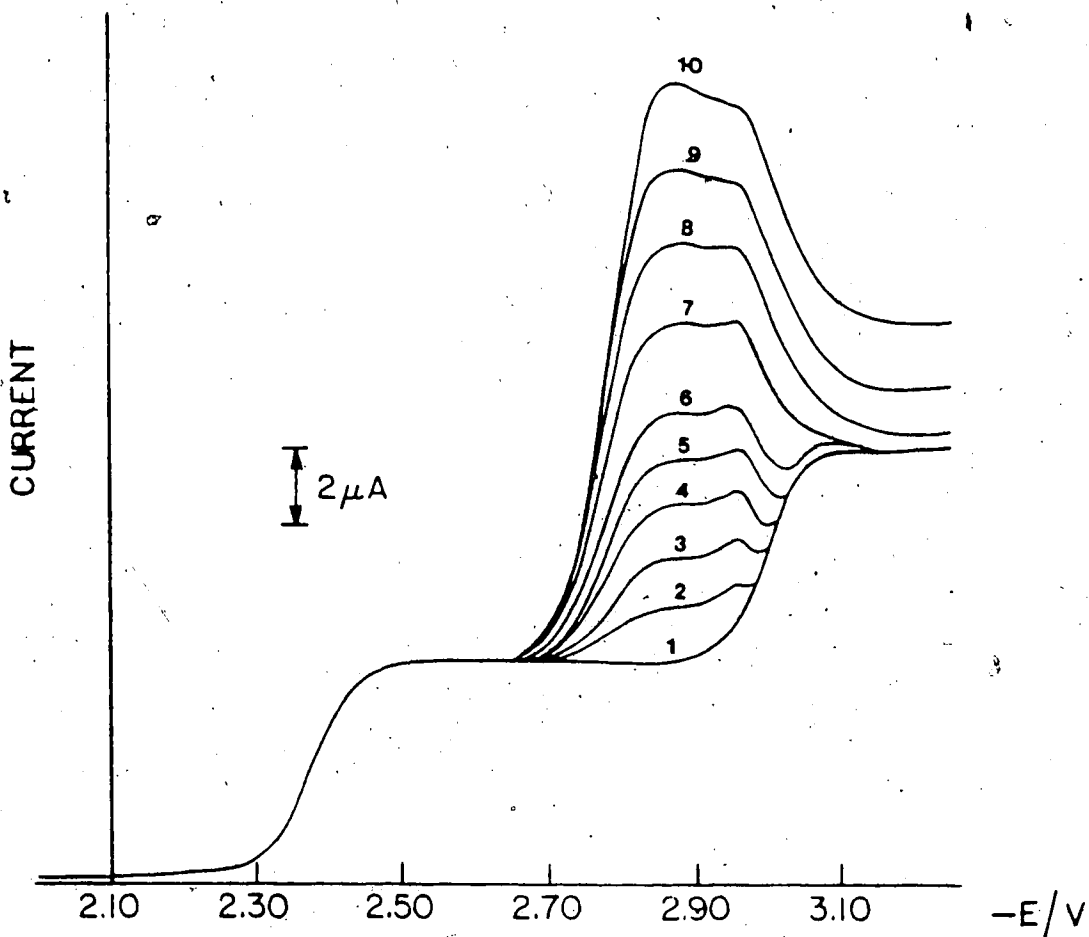
Figure 10.   Polarograms of anthracene-lithium cation
             mixtures in DMF at 25°C.
             Anthracene concentration is fixed at 1.00 mM.
             Lithium cation concentrations are (in mM):
             (1) 0.00, (2) 0.38, (3) 0.73, (4) 1.06,
             (5) 1.36, (6) 1.65, (7) 2.16, (8) 2.54,
             (9) 3.02, (10) 3.47.
             Mercury column 57.0 cm.
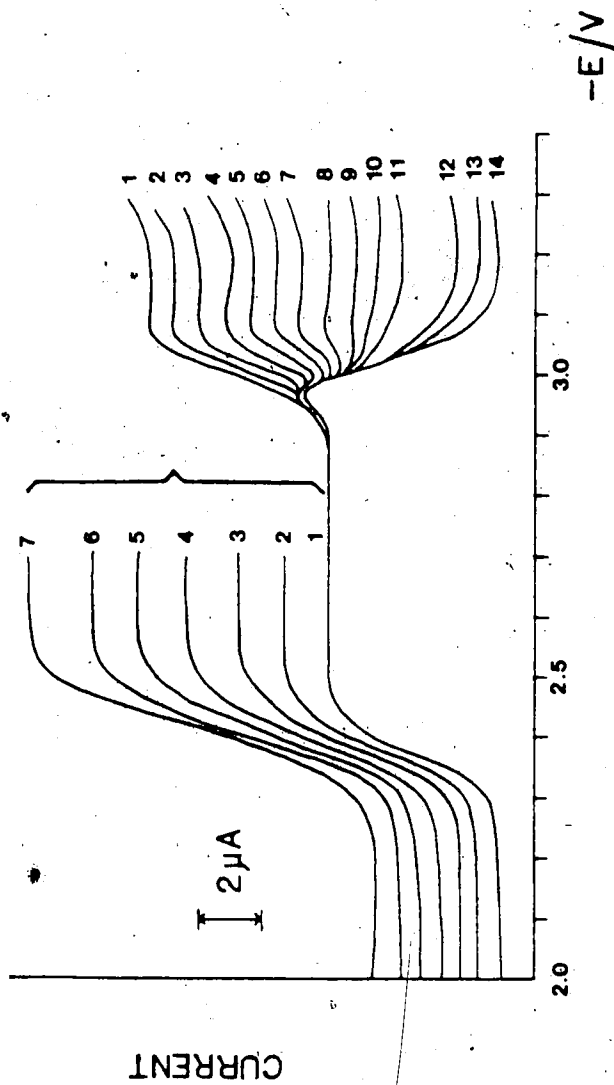
Figure 11. Polarograms of anthracene-sodium cation mixtures in DMF at 25°C.
Anthracene concentration is fixed at 1.00 mM.
Sodium cation concentrations are (in mM):
(1) 0.00, (2) 0.21, (3) 0.41, (4) 0.60,
(5) 0.79, (6) 0.97, (7) 1.14, (8) 1.31,
(9) 1.47, (10) 1.62, (11) 1.78, (12) 2.32,
(13) 3.04, (14) 3.82.
Mercury column 57.0 cm.
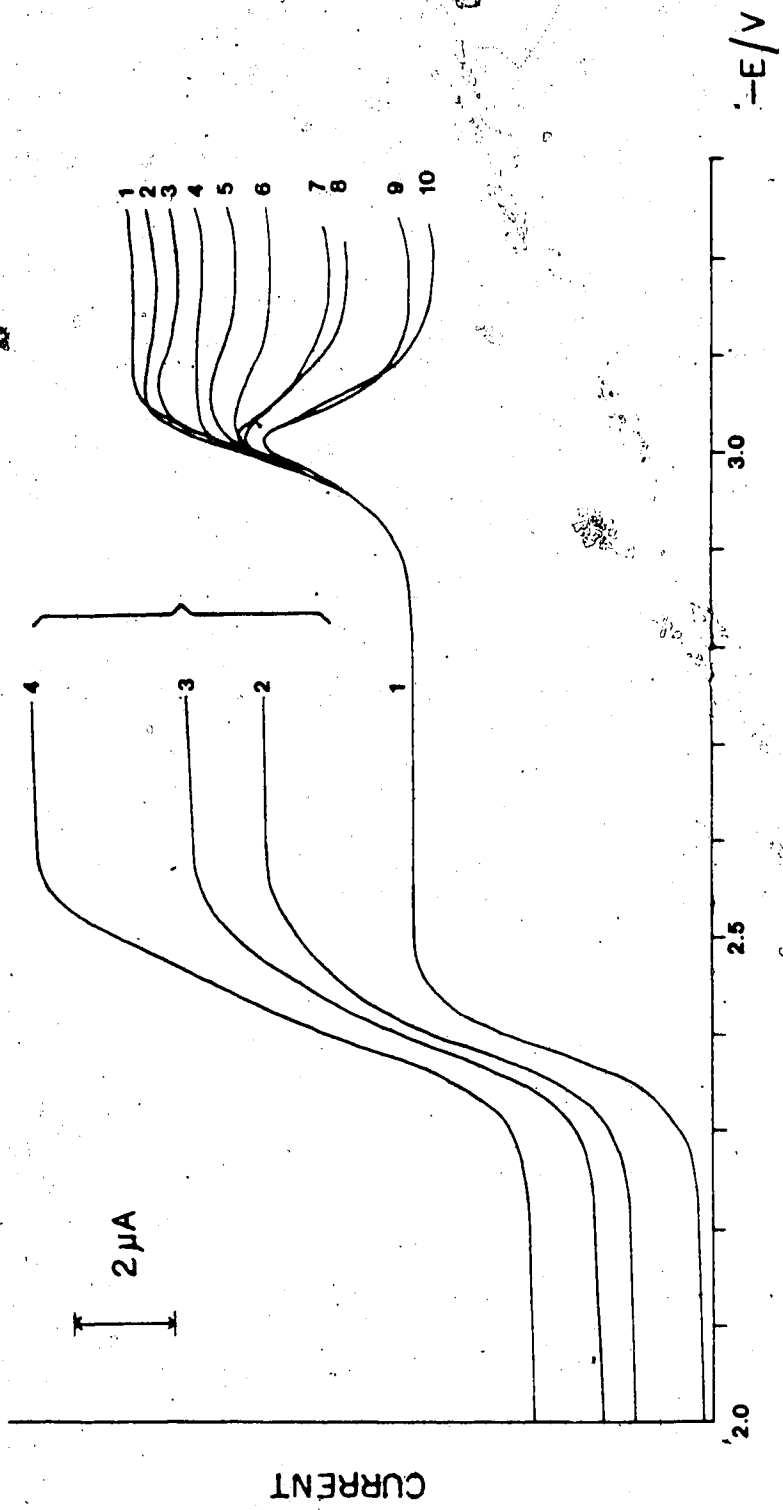
Figure 12. Polarograms of anthracene-potassium cation
mixtures in DMF at 25°C.
Anthracene concentration fixed at 1.00 mM.
Potassium cation concentrations are (in mM):
(1) 0.00, (2) 0.39, (3) 0.57, (4) 1.08,
(5) 1.24, (6) 1.54, (7) 2.20, (8) 2.67,
(9) 3.45, (10) 3.93.
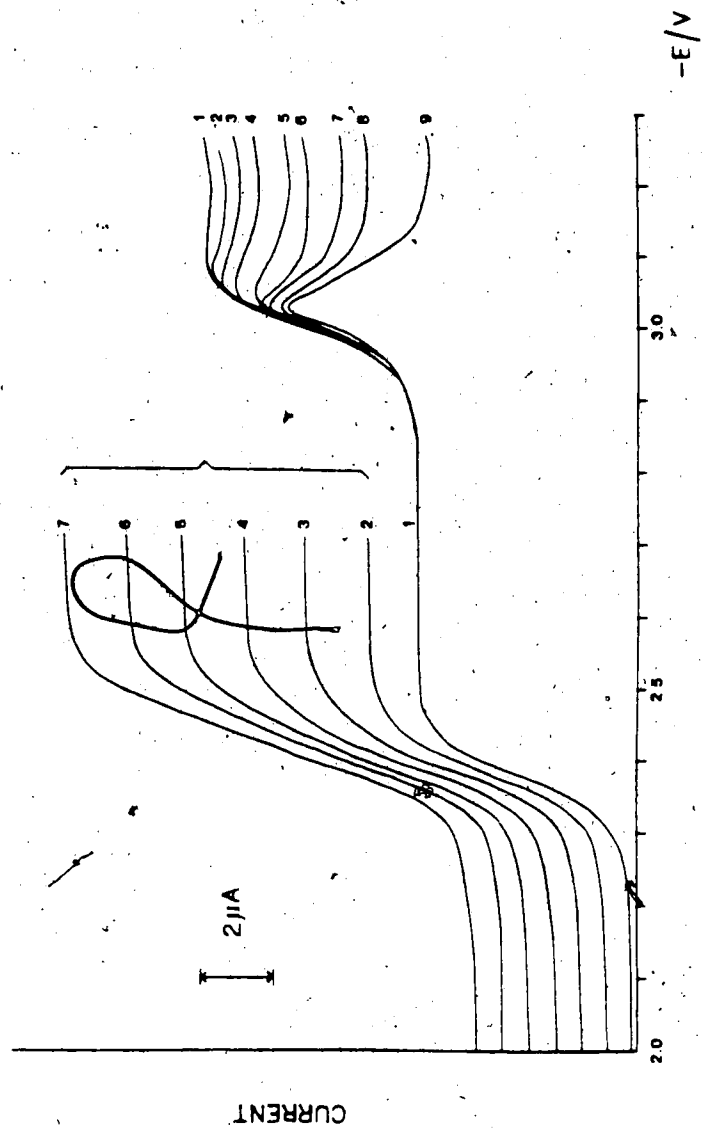
Figure 13. Polarograms of anthracene-rubidium cation
mixtures in DMF at 25°C.
Anthracene concentration fixed at 1.00 mM.
Rubidium cation concentrations are (in mM):
(1) 0.00, (2) 0.56, (3) 0.74, (4) 0.90,
(5) 1.22, (6) 1.52, (7) 1.93, (8) 2.84,
(9) 3.13.
Mercury column 57.0 cm.
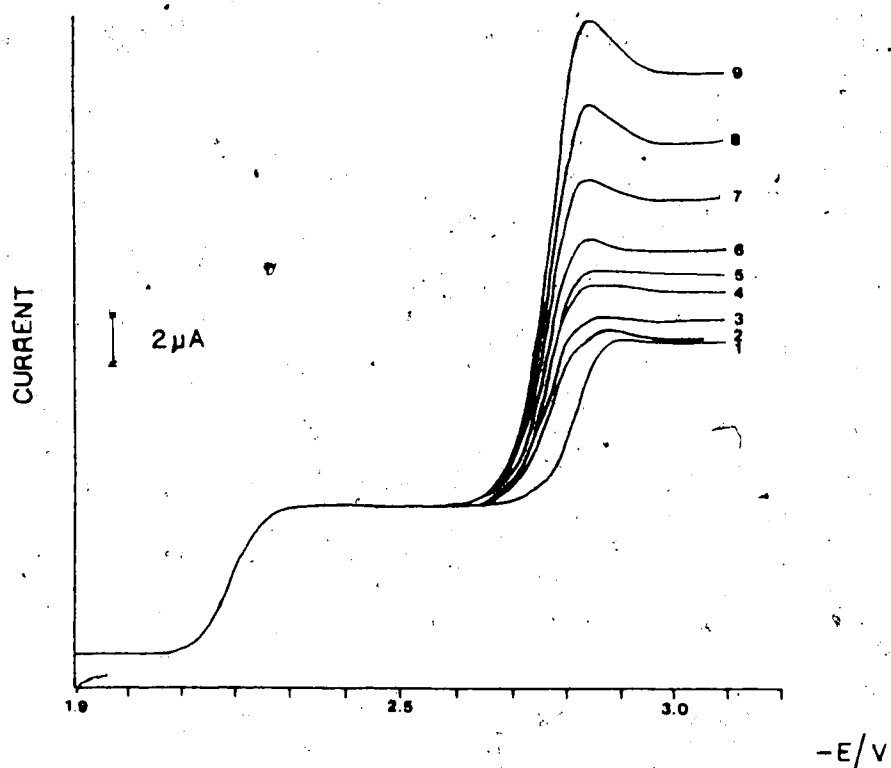
Figure 14.  Polarograms of fluoranthene-lithium cation
            mixtures in DMF at 25°C.
          - Fluoranthene concentration fixed at 1.00 mM.
            Lithium cation concentrations are (in mM):
            (1) 0.00, (2) 1.36, (3) 1.50, (4) 1.78,
            (5) 1.91, (6) 2.05, (7) 2.61, (8) 3.10
            (9) 3.69.
            Mercury column 57.0 cm.
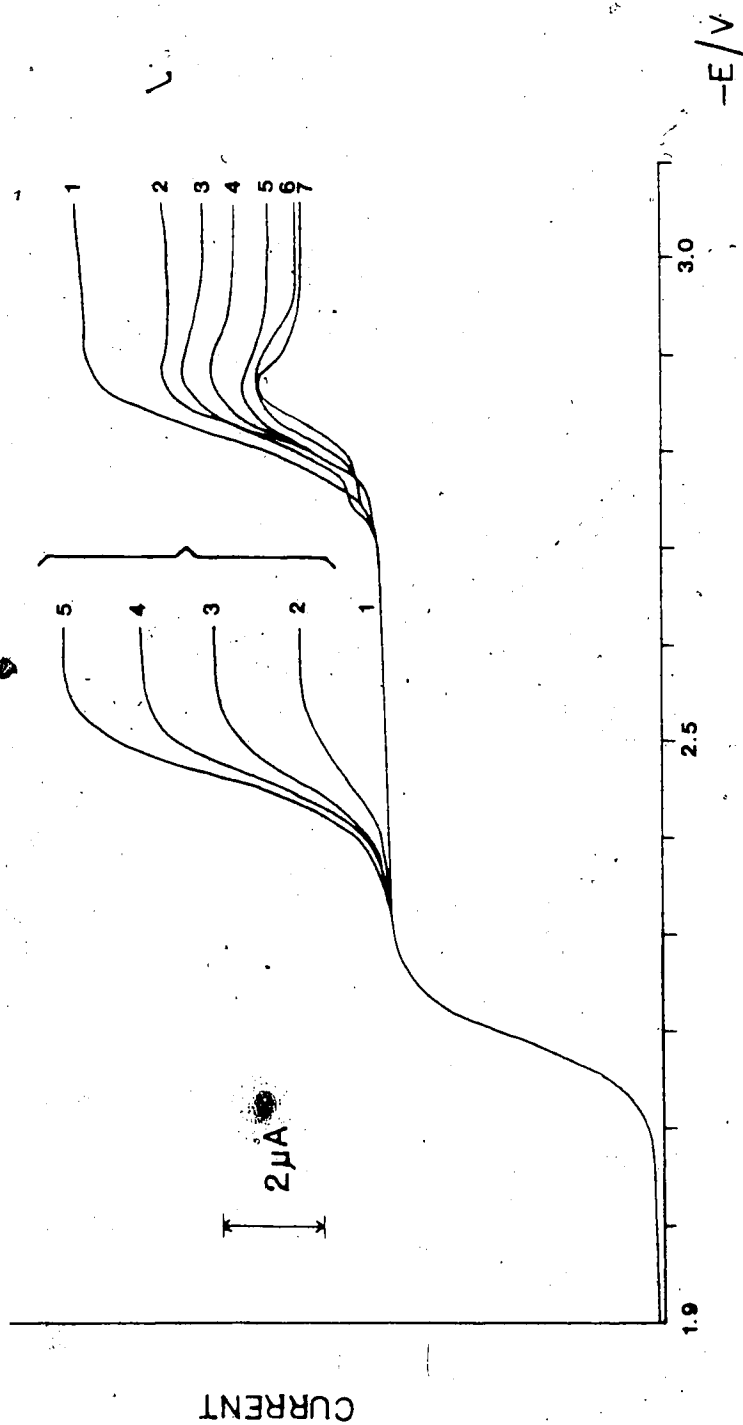
Figure 15. Polarograms of fluoranthene-sodium cation
mixtures in DMF at 25°C.
Fluoranthene concentration is fixed at 1.00 mM.
Sodium cation concentrations are (in mM):
(1) 0.00, (2) 0.38, (3) 0.73, (4) 1.06,
(5) 1.37, (6) 2.17, (7) 4.14.
Mercury column 57.0 cm.
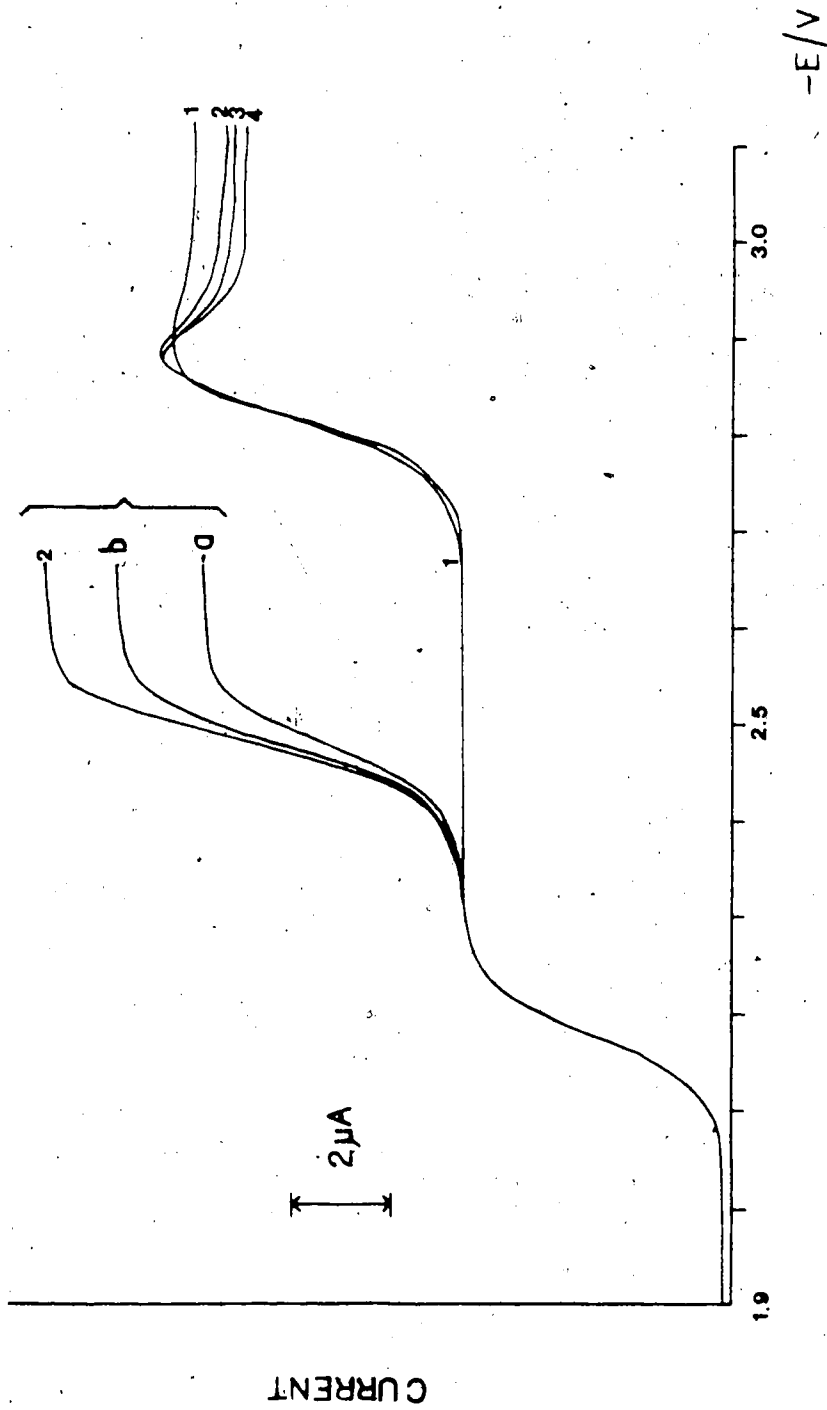
Figure 16. Polarograms of fluoranthene-potassium cation mixtures in DMF at 25°C. Fluoranthene concentration fixed at 1.00 mM. Sodium cation concentrations are (in mM): (1) 0.00, (a) 1.09, (b) 1.40, (2) 1.69, (3) 2.69, (4) 3.65.

103
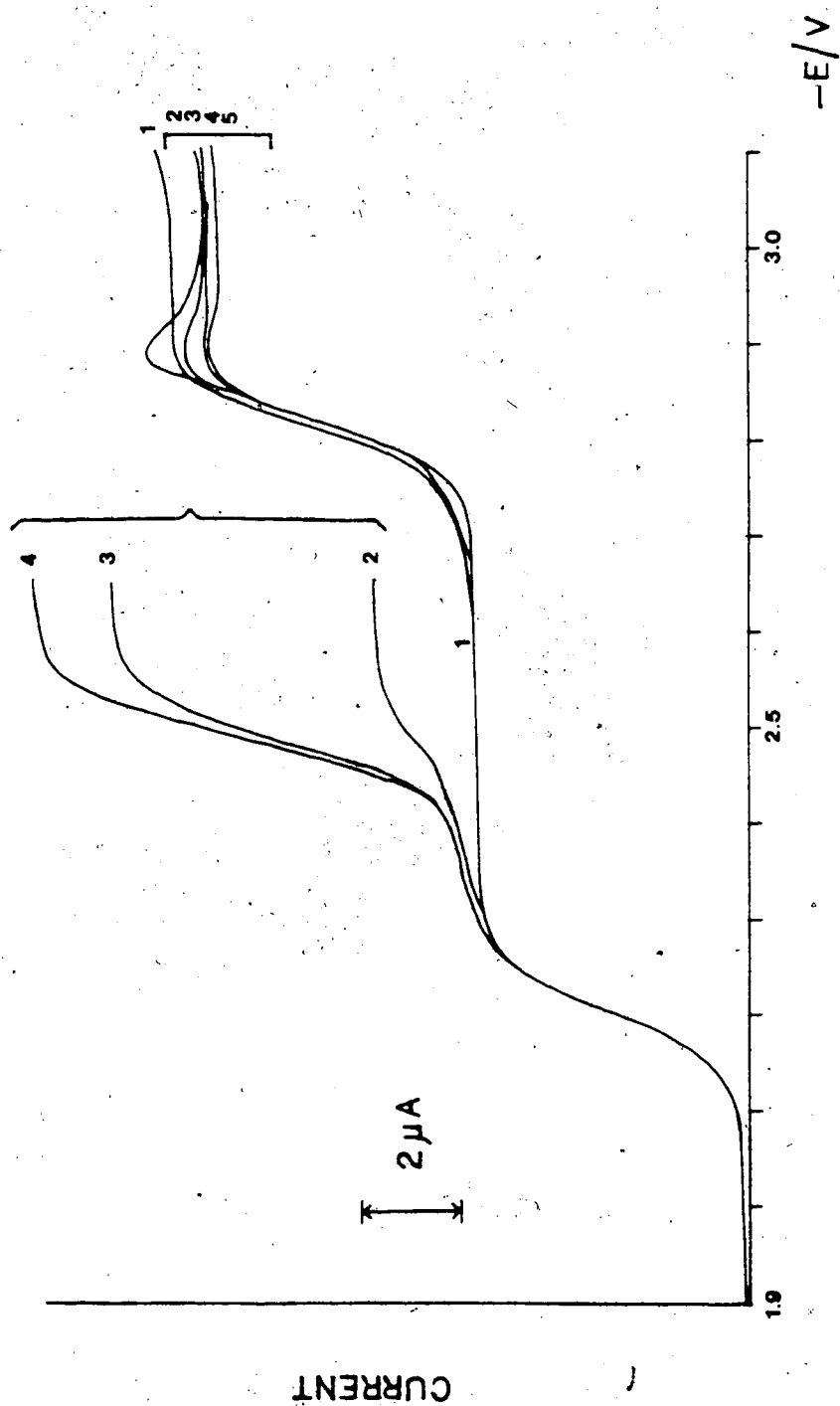


Figure 17. Polarograms of fluoranthene-rubidium cation mixtures in DMF at 25°C. Fluoranthene concentration fixed at 1.00 mM. Rubidium cation concentrations are (in mM): (1) 0.00, (2) 0.39, (3) 1.40, (4) 1.70, (5) 3.97. Mercury column 57.0 cm.
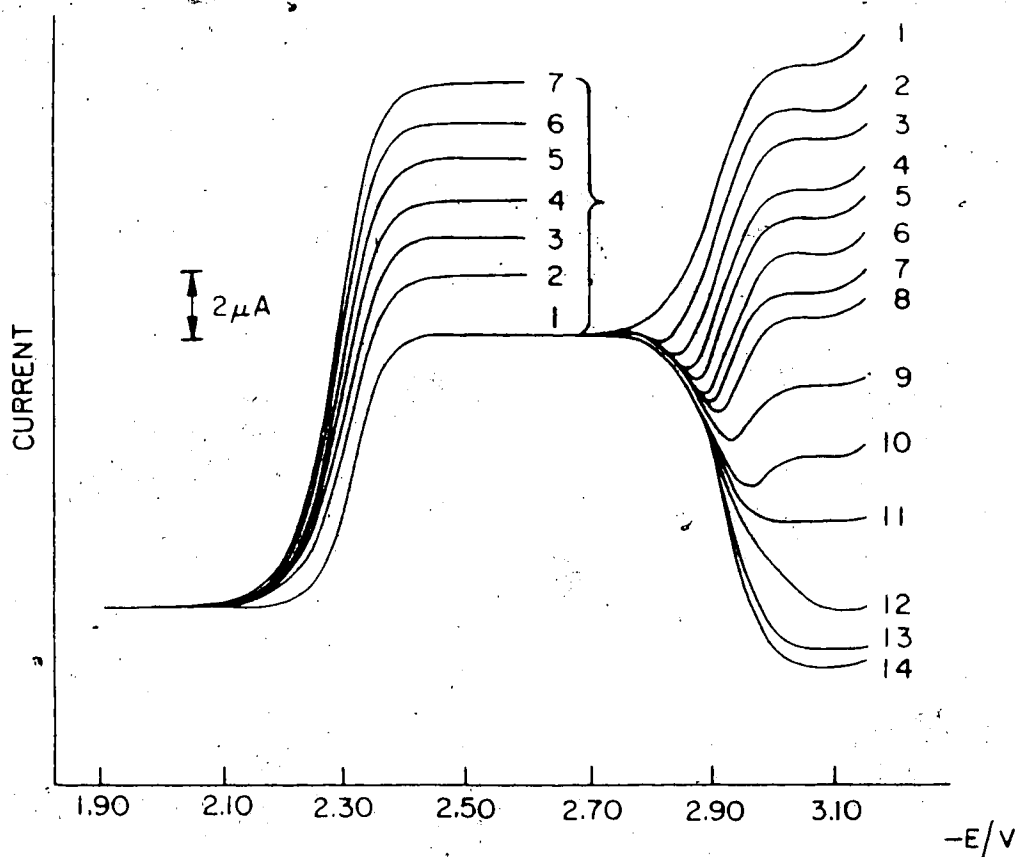
Figure 18.  Polarograms of anthracene-lithium cation
            mixtures in ACN at 25°C.
            Anthracene concentration fixed at 1.00 mM.
            Lithium cation concentrations are (in mM):
            (1) 0.00, (2) 0.38, (3) 0.57, (4) 0.74,
            (5) 0.91, (6) 1.07, (7) 1.23, (8)1.38,
            (9) 1.67, (10) 1.94, (11) 2.19, (12) 2.65,
            (13) 3.59, (14) 3.90.
            Mercury column 57.0 cm.
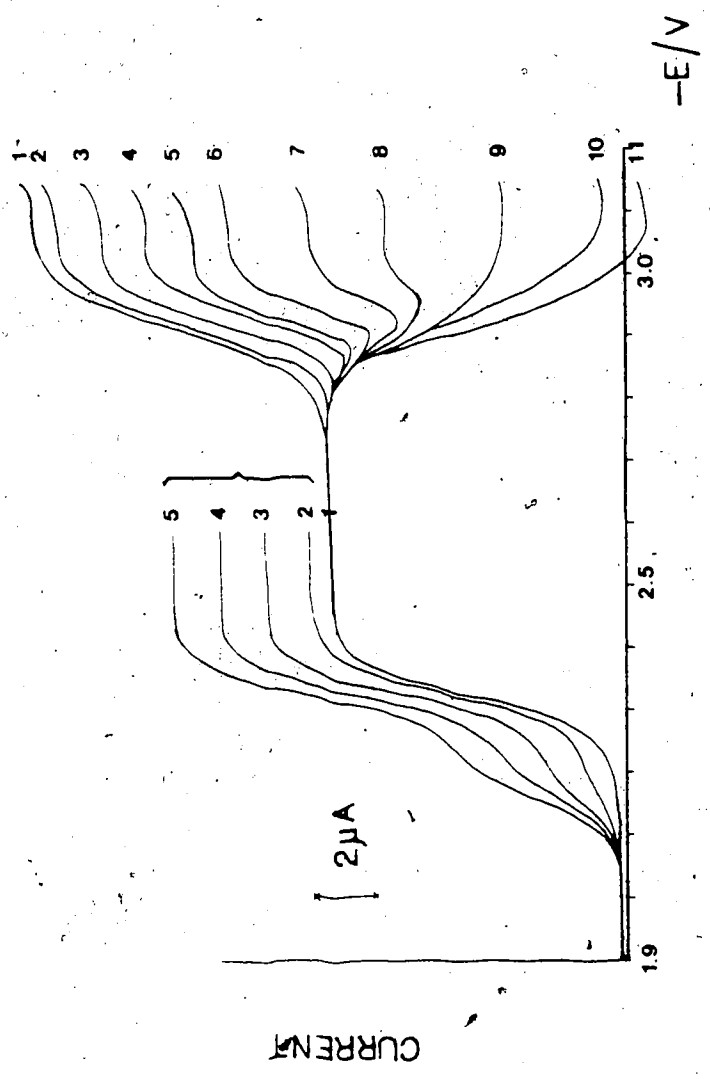
Figure 19.  Polarograms of anthracene-sodium cation
mixtures in ACN at 25°C.
Anthracene concentration fixed at 1.00 mM.
Sodium cation concentrations are (in mM):
(1) 0.00, (2) 0.20, (3) 0.39, (4) 0.57,
(5) 0.74, (6) 0.91, (7) 1.23, (8) 1.53,
(9) 1.94, (10) 2.54, (11) 3.43.
Mercury column 57.0 cm.
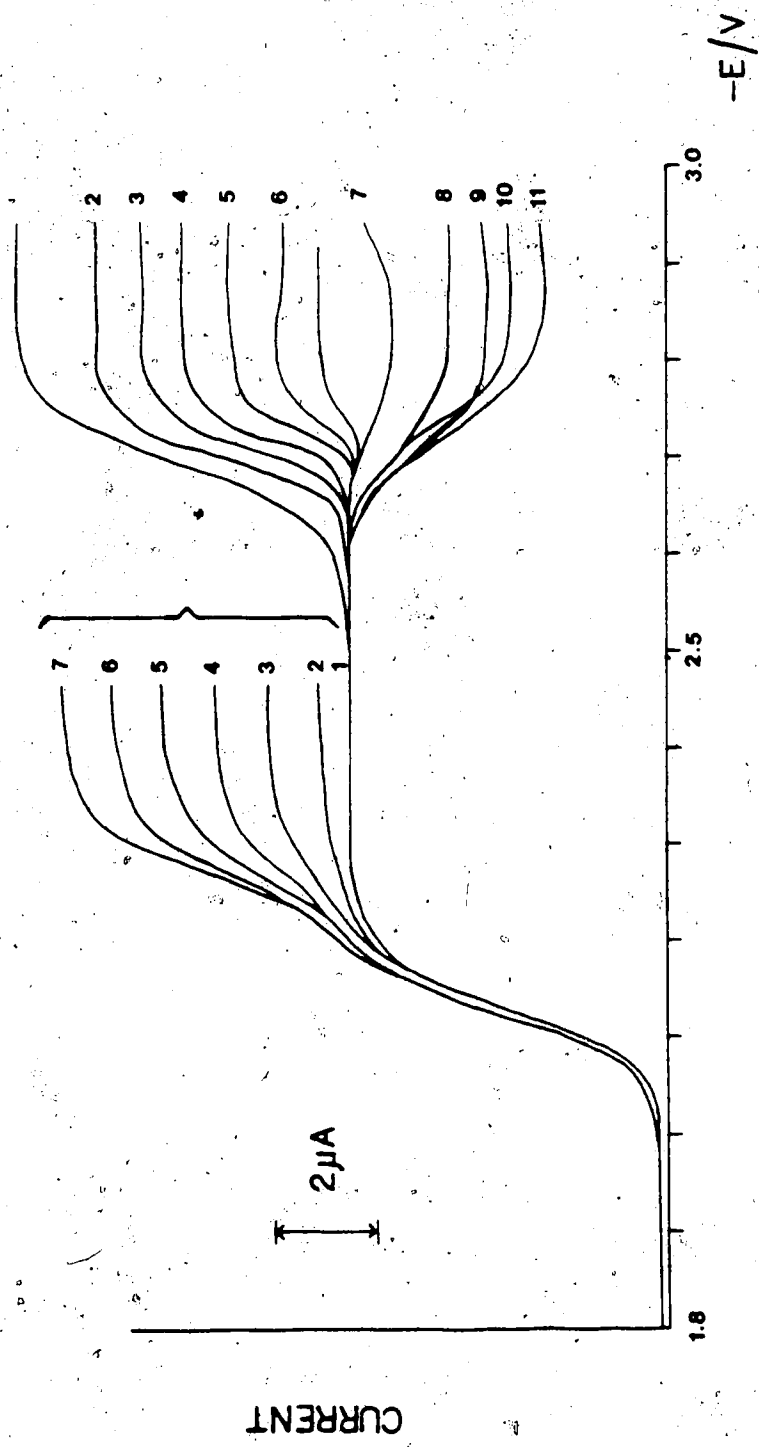
Figure 20. Polarograms of fluoranthene-lithium cation mixtures in ACN at 25°C. Fluoranthene concentration fixed at 1.00 mM. Lithium cation concentrations are (in mM): (1) 0.00, (2) 0.39, (3) 0.57, (4) 0.75, (5) 0.92, (6) 1.08, (7) 1.24, (8) 1.68, (9) 2.20, (10) 2.56, (11) 3.17. Mercury column 40.0 cm.
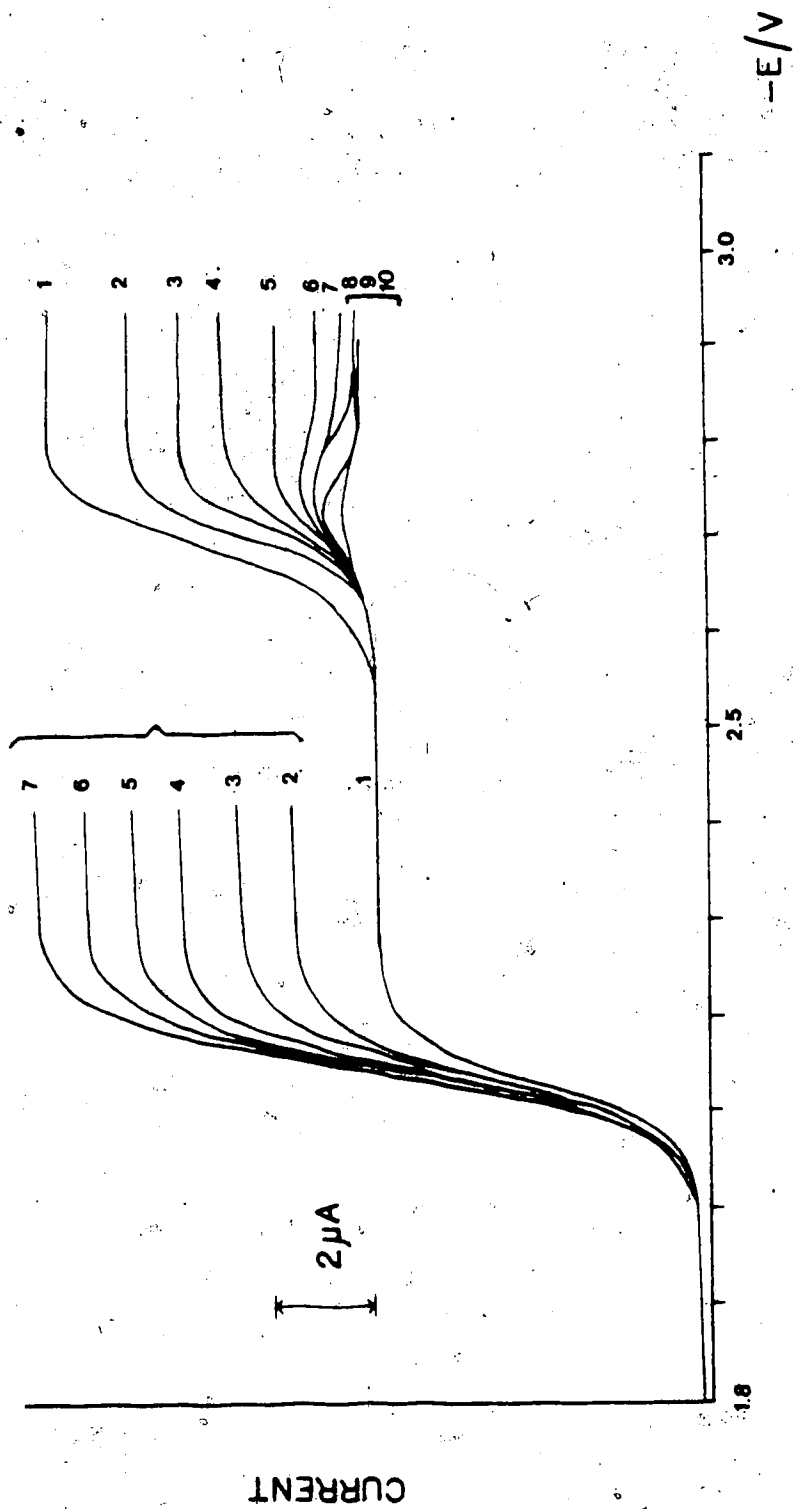
Figure 21.  Polarograms of fluoranthene-sodium cation
mixtures in ACN at 25°C.
Fluoranthene concentrations fixed at 1.00 mM.
Sodium cation concentrations are (in mM):
(1) 0.00, (2) 0.39, (3) 0.58, (4) 0.75,
(5) 0.93, (6) 1.09, (7) 1.25, (8) 1.41,
(9) 1.97, (10) 2.47.
Mercury column 40.0 cm.

since the Li+ and the anion radical reduction occurred

concomitantly. Fa solutions with the other three cations

exhibited three resolved waves (Figure 15-17).

As mentioned earlier, in acetonitrile, studies were

limited to Li+ and Na+, since the solubilities of K+ and

Rb+ were too low. In acetonitrile, in all cases, the

hydrocarbon reduction wave and that of the metal cation

were not resolved (Figures 18-21).

It is obvious from Figures 10-21, except in the case

of Fa:Li+ in DMF (Figure 14), that the addition of alkali

metal cations caused the reduction wave of the anion radi-

cal of the hydrocarbon to dianion to decrease in height.

The amount of height reduction is a function of metal

cation concentration, generally increasing with increasing

concentration. In some instances, especially where Li+

and Na+ were concerned, the current depressions were so

severe that the polarographic wave was reversed (i.e. the

current as measured from the plateau of the previous wave

is negative). It is believed these are the first reported

examples of "inverted" diffusion controlled polarograms.

There have been examples of current depression in polaro-

graphic waves due to adsorption processes. Two such

reports involved the polarographic reduction of hexaamine

cobalt (III) ion (215) and copper (II) acetate (216) in

the presence of alkali metal cations in ACN. In the first

case, a decrease in the current was noted as the hexaamine

cobalt (III) concentration was increased to 5 mM and above.

The decrease was attributed to the formation of a film of

cobaltous hydroxide at the mercury surface. The intensity

of the current decrease was independent of depolarizer

concentration. In the second case, a decrease in the

amount of the second polarographic wave of copper (II) in

the presence of Li+ and Na+ was attributed to the forma-

tion of an insoluble film of alkali metal acetate at the

electrode surface. Film formation was also implicated

by the abnormal behavior of the current time transients in

the potential region exhibiting the decrease.

However, in this work, the current-time transients

exhibited normal diffusion control characteristics at

potentials on the diffusion plateau and the current depres-

sion region. For example, in the case of anthracene in

the presence of Li+ in ACN, (Figure 22), current-time

transients at the diffusion plateau (potentials -2.500 and

-2.800 V) and at the current depression (potential -3.100

V) showed diffusion controlled behavior (Figure 22).

Further, by employing reverse pulse polarography, (i.e.

setting the initial potential at negative potentials

(-3.200 V) and scanning to more positive potentials) on a

solution of 1.00 mM anthracene and 3.83 mM Li+ in DMF, it

was noted that no desorption or film destruction currents

were observed. What was observed was the interesting fact
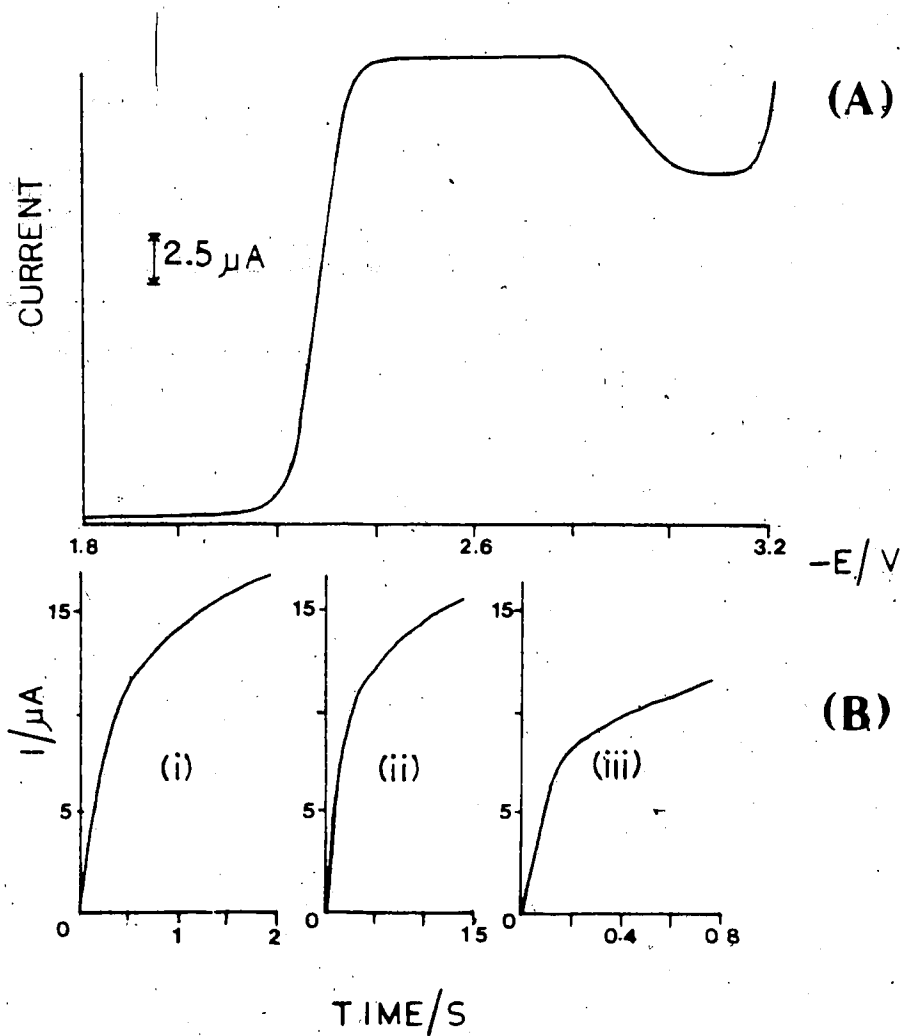
Figure 22. A. Polarogram of a solution mixture containing
1.00 mM anthracene and 3.53 mM lithium cation
in ACN (0.10 M TBAF) at 25°C.
B. Current-time transients for the same
solution at 25°C: (i) -2.5 V, (ii) -2.8 V,
(iii) -3.10 V.
In both cases, the mercury column was 40.0 cm.
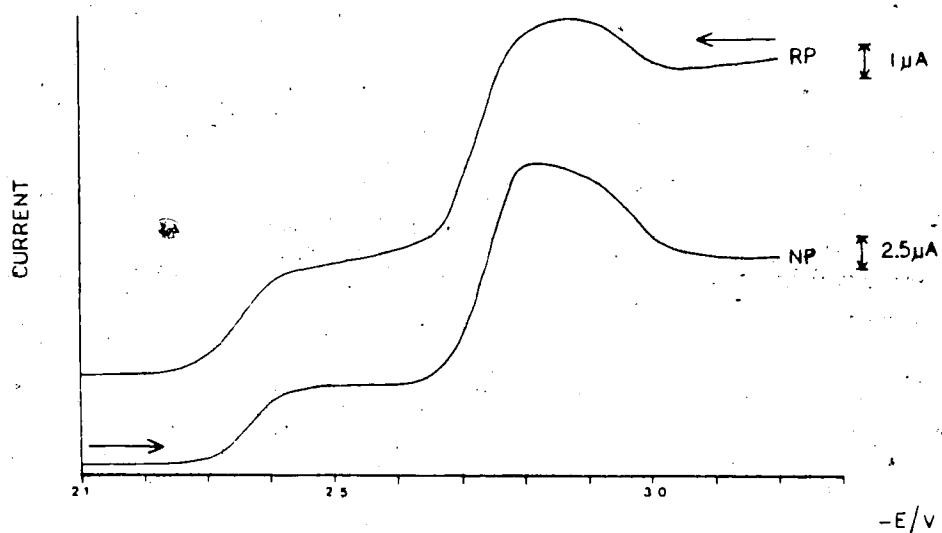
Figure 23. Normal pulse (NP) and reverse pulse (RP) polarograms of a solution mixture containing 1.00 mM anthracene and 3.83 mM lithium cation in DMF (0.10 M TBAF) at 25°C.
For NP, the initial potential was -2.1 V whereas for RP the initial potential was -3.2 V. Mercury column was 57.0 cm.

that the current, in the potential region of the Li+

reduction plateau just positive of the second reduction

wave of anthracene, moved to cathodic values; thus a

cathodic current was observed on a positive potential

scan (Figure 23).

The case of Fa:Li+ in DMF was a rather special one in

that this was the only system studied where the reduction

wave of Li+ and the fluoranthene anion radical (Fa$^-$) to

the dianion (Fa$^=$) were not resolved. Therefore only two

reduction waves were observed for this system. Here there

was no change in the height of the second wave with addition

of Li+ up to a concentration of 1.36 mM, after which the wave

increased in height with further Li+ addition (Figure 14).

It was noted in Figures 10 and 11 (An:Li+, Nat+ systems)

that a small peak appeared at the beginning of the wave

corresponding to the reduction of the anion radical of

anthracene (An$^-$), prior to current depression. This peak

was absent in ACN (Figures 18-19).

The magnitude of the decrease of the anion radical

reduction waves of the hydrocarbons in the presence of

alkali cations is a direct measure of the strength of the

interaction between metal cations and aromatic hydrocarbon

dianions (Fa$^=$, An$^=$). To facilitate further discussions,

the following notation will be used: in systems where

there were three resolved waves (An:Li+ in DMF, Fa:Na+,

K+, Rb+ in DMF), the limiting currents due to the aromatic

hydrocarbons reduction are denoted by i1 and i2 while that

of the metal cations reduction by im (m=Li+, Na+, K+, Rb+).

Where the reductions of the hydrocarbon and that cations

were not well resolved (An:Na+, K+, Rb+ in DMF, An:Li+,

Na+, Fa:Li+, Na+ in ACN), the limiting currents are

combined as i1 + im.    Finally, in the case of Fa:Li+ in

DMF, where only two waves were observed, the limiting current

of the combined Li+ reduction and An$^-$ reduction was denoted

by im + i2 . The plots of these currents for the various

systems are given in Figures 24-26.

For the system An:Li+ in DMF (Figures 24-25), the

value of il was unaffected by the addition of metal

cations. The Eh values for these reduction waves of

the hydrocarbons were also unchanged in the presence of

cations. In addition, the im vs metal ion concentration

plots are linear and the slopes (Figures 24-25) are

virtually identical to those of the calibration curves

for the metal cations (compare values in Figures 24-25

with those in Table 1). The Eh values for the metal

cation waves were also unchanged. In all the other

systems, where there were only two measurable limiting

currents, linear plots of il + im vs metal cation concen-

trations were observed, the slopes of which agree well

with the calibration curves for the metal cations.

Further, the intercepts of these plots with the current
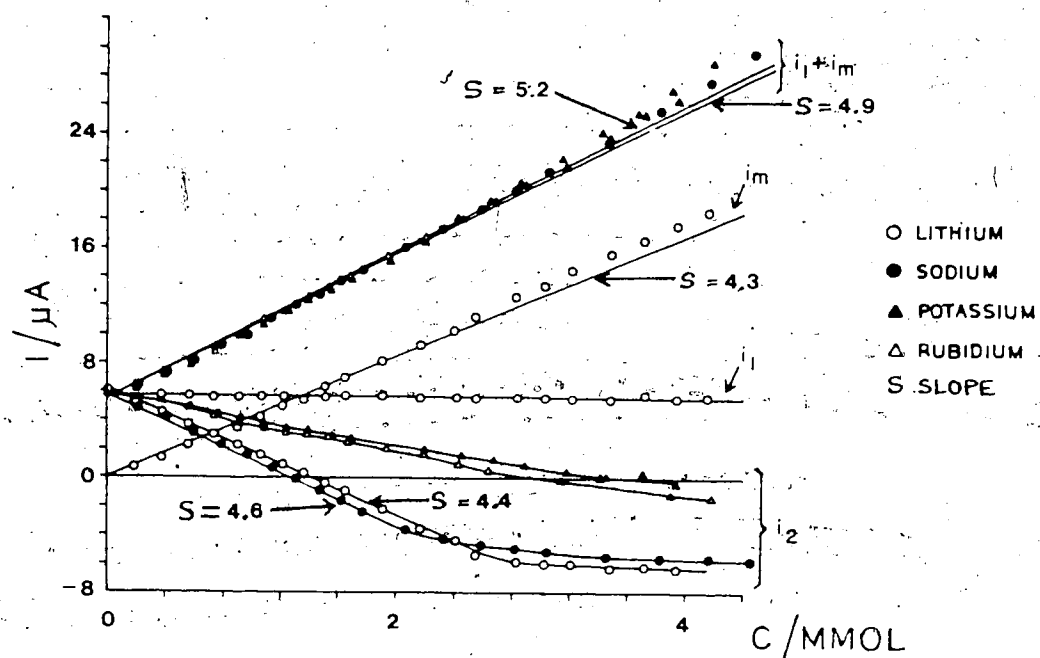
Figure 24. Plots of limiting currents versus concentration
of metal cations for anthracene-metal cation
mixtures in DMF at 25°C.
The anthracene concentration was fixed at 1.00
mM. Mercury column 57.0 cm.
i1: limiting current of anthracene reduction
i2: limiting current of anthracene anion
radical reduction
im: limiting current of cation reduction
i1 + im: combined limiting current of
anthracene and cation reductions
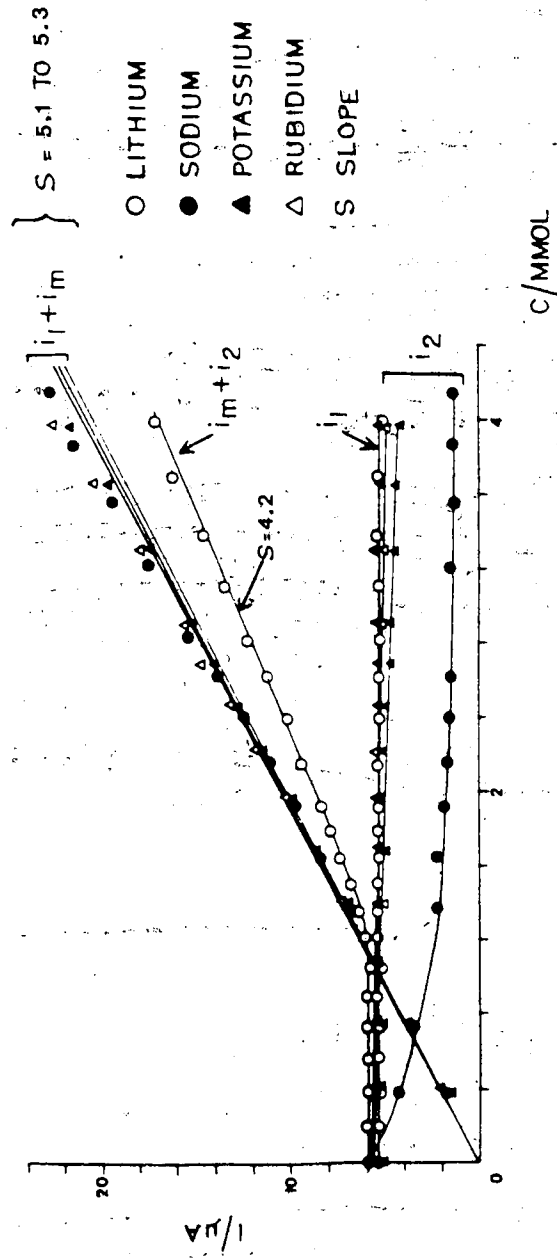
Figure 25. Plots of limiting currents versus concentration
of metal cations for fluoranthene-metal cation
mixtures in DMF at 25°C.
The fluoranthene concentration was fixed at
1.00 mM. Mercury column 57.0 cm.
i1: limiting current of fluoranthene reduction
i2: limiting current of fluoranthene anion
    radical reduction
i1 + im: combined limiting current of
         fluoranthene and cation reductions
im + i2: combined limiting current of metal
         cation and fluoranthene anion radical
         reductions

○ LITHIUM
● SODIUM
▲ POTASSIUM
△ RUBIDIUM
S SLOPE

S = 5.1 TO 5.3
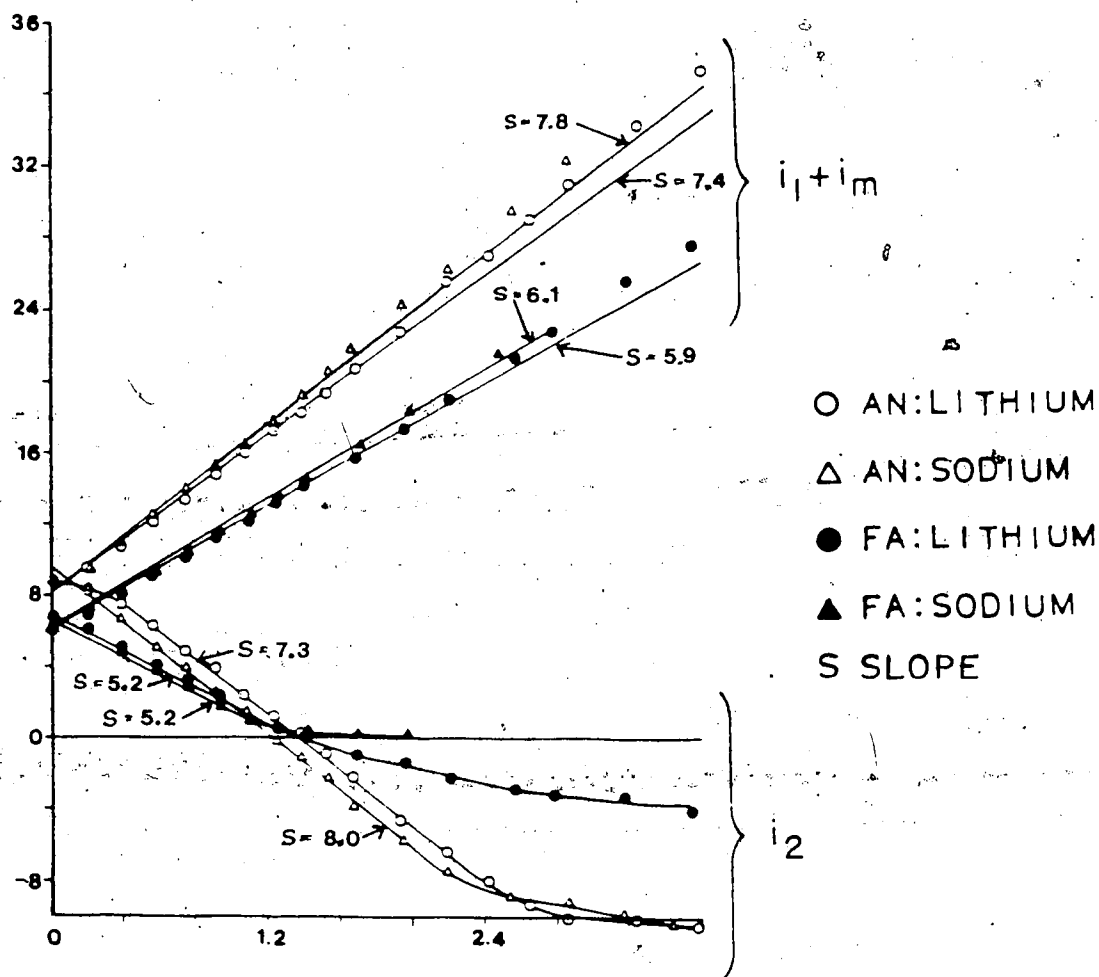
Figure 26. Plots of limiting currents versus concentration
of metal cations for anthracene-metal cations
and fluoranthene-metal cations mixtures in ACN
at 25°C.
The anthracene and fluoranthene concentrations
were fixed at 1.00 mM. The mercury column for
anthracene-cation systems was 57.0 cm while
that for the fluoranthene-cation systems was
40.0 cm.
il + im is the combined limiting current for
the first reduction wave of the hydrocarbon and
the cations. i2 is the limiting current for
the second reduction wave.

axis corresponded closely with the limiting current value

for the reduction of the hydrocarbon for the particular

system. However, it should be noted that both the im and

il+im plots gave significant positive deviations of the

points from linearity at the high end of the metal concen-

tration range. In the special case of Fa:Li+ in DMF system

il was again independent of Li+ concentration and the Eh

values remained constant (Figure 25). Further, im + i2

remained constant at a value equal to that of i2 for

fluoranthene in the absence of Li+, for Li+ concentrations

up to about 1.31 mM. At higher concentrations of Li+,

im + i2 increased and the slope of this increase was 4.2

uA/mM, close to that for Li+ calibration (4.0 uA/mM, see

Table 1).

Figures 24-26 also showed that the value of i2 is a

function of the system considered. For the Fa:K+, Rb+ in

DMF systems, only a slight decrease in the value of i2 was

observed even at high metal cation concentrations. At the

other extreme, large negative values of i2 were observed

for the An:Li+, Na+ systems in DMF and ACN, indicating

strong interactions of the dianion with Li+ and Na+ to form

species which were not reducible at these potentials. In

these latter systems, the slopes of the i2 vs metal con-

centration plots correspond closely to those of the im

or i1 + im plots for the respective systems. These

results are summarized in Table 2.

A clear way to graphically demonstrate the extent of

interaction dianion with metal cation M+ is to plot the

number of mmol of M+ reacted as a function of the concen-

tration of M+. The ordinate for such a plot may be

obtained for each polarogram (which represents one point)

from the relation

Table 2. Summary of the behavior of the various limiting
currents (uA)**

| System | Number of waves | DMF i1, im or i1 + im | i2 |
|---|---|---|---|
| An:Li+ | 3 | i2 constant at 5.6. im linear with slope 4.3 | i2 decreasing to negative values with slope -4.4 |
| An:Na+ | 2 | i1 + im linear with slope 5.0 | i2 decreased to negative values with slope -4.6 |
| An:K+ | 2 | i1 + im linear with slope 5.2 | slow decrease did not reach negative values |
| An:Rb+ | 2 | i1 + im linear with slope 5.3 | slow decrease did not reach negative values until high Rb+ concentration |
| Fa:Li+ | 2 | i1 constant at 5.4 *im + i2 constant until [Li+]=1.20 mM, then linear increase with slope 4.2 | --- |
| Fa:Na+ | 3 | i1 constant at 5.4. im linear with slope 5.1 | decreased but did not reach negative values |
| Fa:K+ | 3 | i1 constant at 5.4. im linear with slope 5.2 | very small decrease |
| Fa:Rb+ | 3 | i1 constant at 5.4. im linear with slope 5.3 | very small decrease |

**Continued next page.

Table 2 Continued

ACN

| System | Number of waves | i1, im or i1 + im | i2 |
|---|---|---|---|
| An:Li | 2 | i1 + im linear with slope 7.4 | decreased to negative values with slope -7.3 |
| An:Na+ | 2 | i1 + im linear with slope 7.8 | decrease to negative values with slope -8.0 |
| An:K+ | --- | --- | --- |
| An:Rb+ | --- | --- | --- |
| Fa:Li+ | 2 | i1 + im linear with slope 5.9 | decreased to negative values with slope -5.2 |
| Fa:Na+ | 2 | i1 + im linear with slope 6.1 | decreased to negative values with slope -5.2 |
| Fa:K+ | --- | --- | --- |
| Fa:Rb+ | --- | --- | --- |

mmol M+ reacted = [(i(absence of interaction) -

$$i(observed))](M+ mmol)]/im \qquad (3.2)$$

These results are shown in Figures 27-30. It is observed

that in DMF that the plots for the An:Li+ and An:Na+

(Figure 27) have slopes of unity on the linear portions of

the plots. For the An:Na+ system, the curve has a plateau

at 2 mM metal ion concentration whereas An:Li+ has a

plateau close to 3 mM Li+. In the An:K+ and An:Li+

solutions, the curves increase continuously up to the

highest concentration used.

Figure 28 shows the results for the Fa:M+ solutions

in DMF. Like the anthracene systems, the Fa:Li+ and

Fa:Na+ plots show an initial slope of 1 but the Fa:Na+

curve levels at 1 mM whereas the Fa:Li+ curve levels at

less than 2 mM. Similar trends are observed in the

acetonitrile solutions of both An:M+ and Fa:M+ (Figure 29
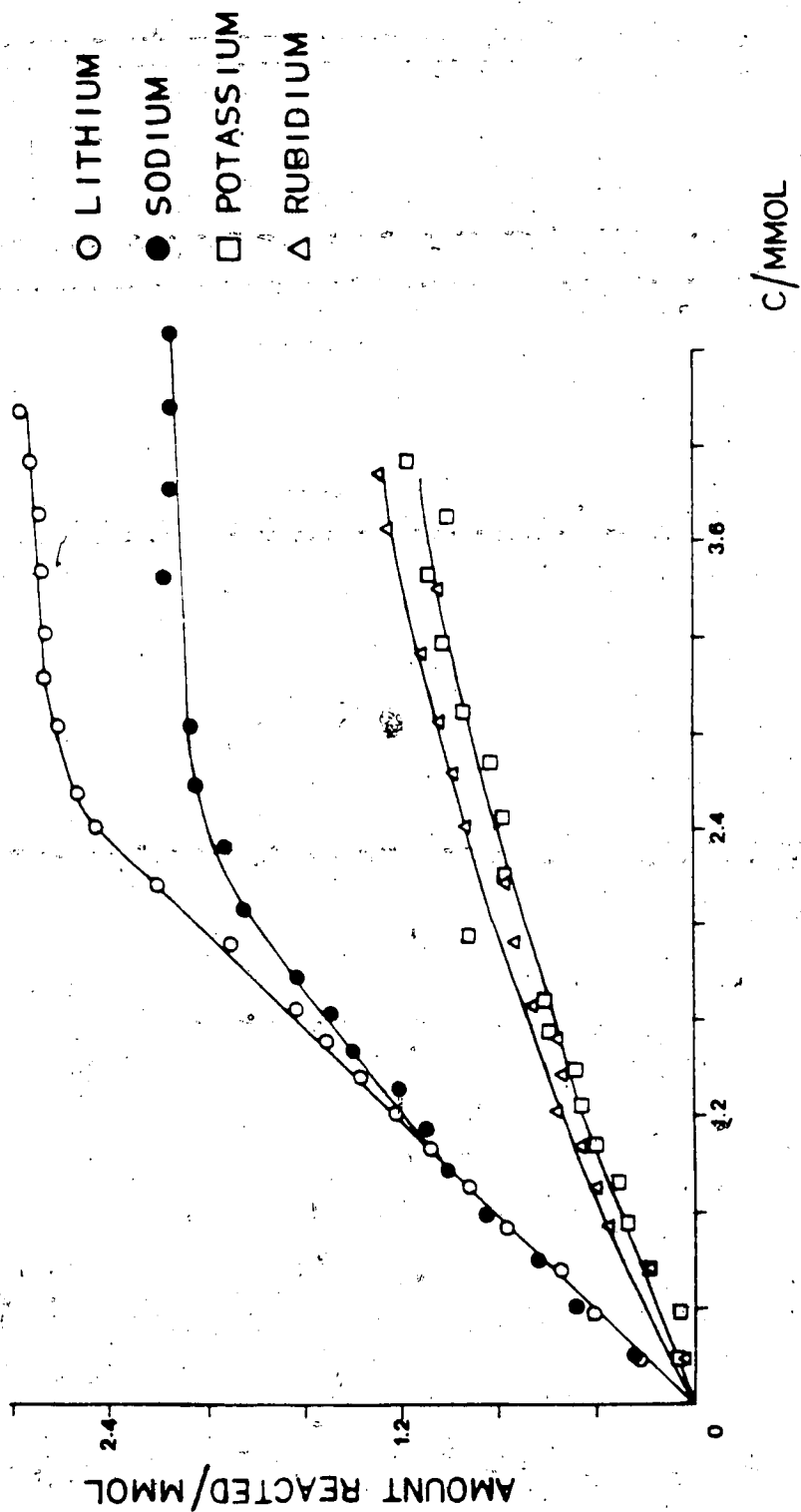
Figure 27. Plot of the amount of metal cation reacted versus cation concentration for the anthracene-metal cation system in DMF at 25°C. The concentration of anthracene is fixed at 1.00 mM.
Mercury column 57.0 cm.
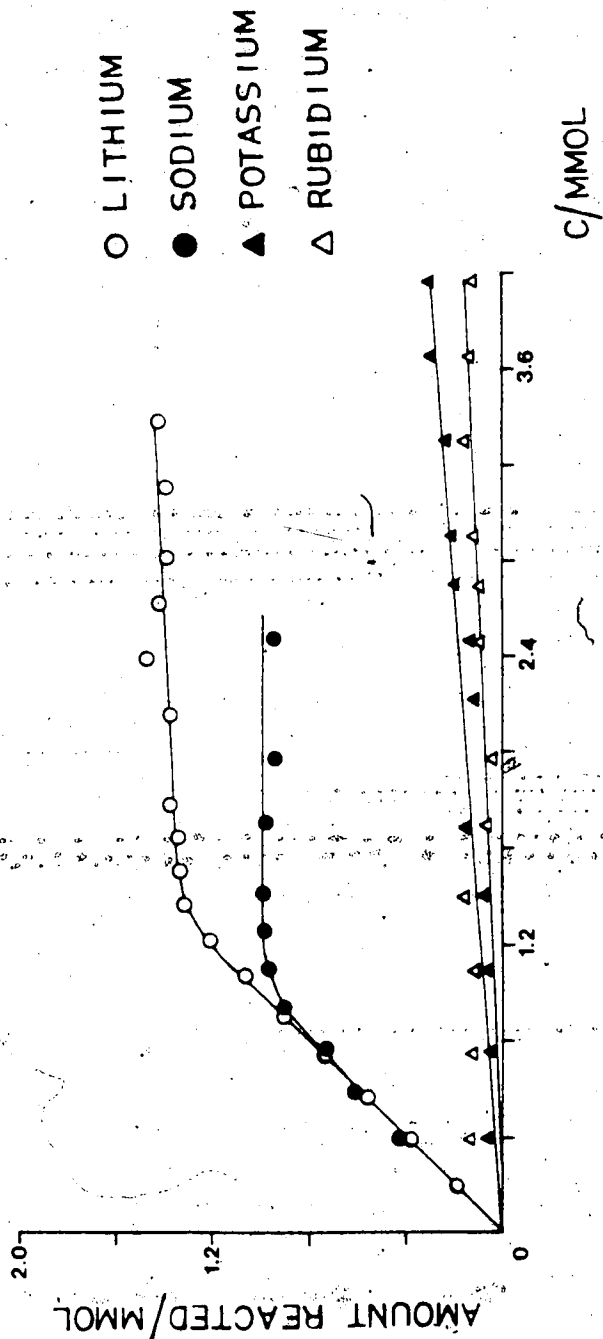
Figure 28. Plot of the amount of metal cation reacted versus cation concentration for the fluoranthene-metal cation system in DMF at 25°C.
The concentration of fluoranthene is fixed at 1.00 mM.
Mercury column 57.0 cm.
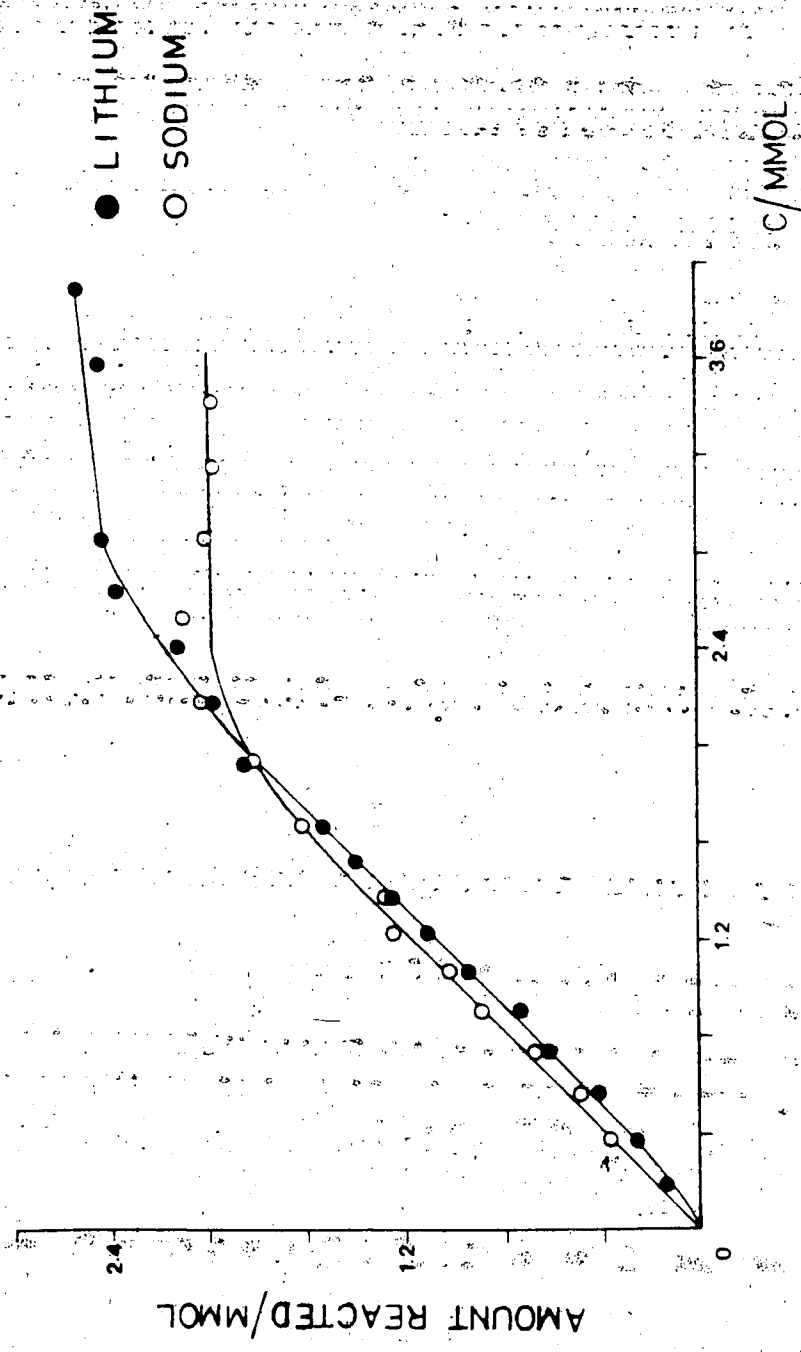
Figure 29. Plot of the amount of metal cation reacted versus cation concentration for the anthracene-metal cation system in ACN at 25°C. The concentration of anthracene is fixed at 1.00 mM. Mercury column 57.0 cm.

● LITHIUM
O SODIUM

C/MMOL

AMOUNT REACTED/MMOL
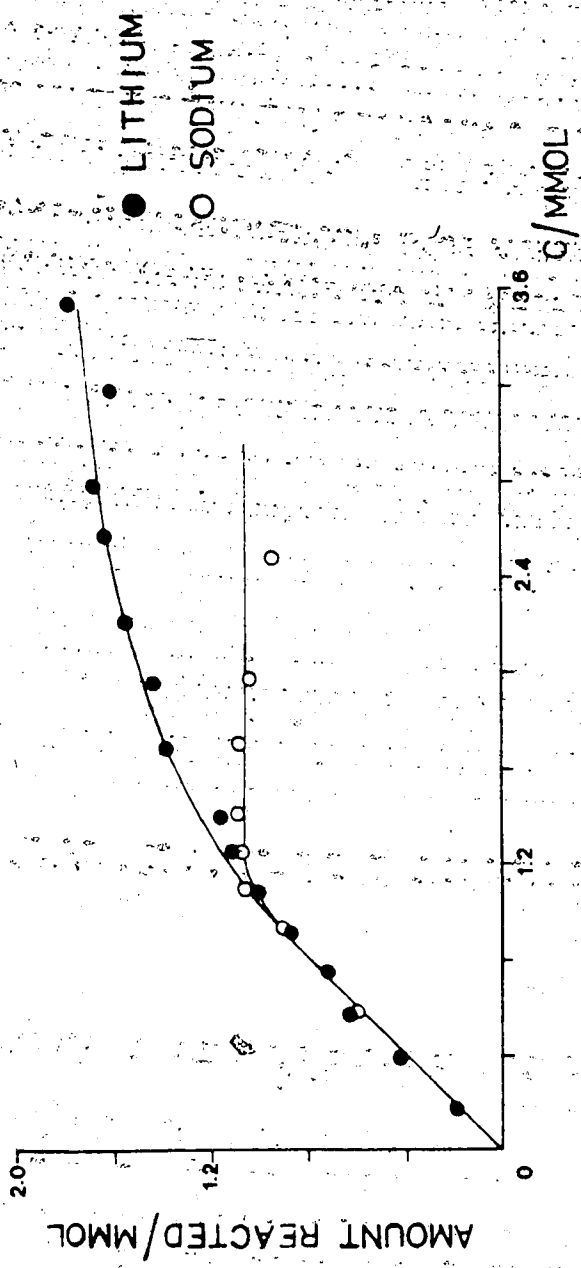
Figure 30. Plot of the amount of metal cation reacted versus cation concentration for the fluoranthene-metal cation system in ACN at 25°C.
The concentration of fluoranthene is fixed at 1.00 mM.
Mercury column 40.0 cm.

and 30).

Experiments were also carried out where the hydrocarbon concentration was varied while that of the cation remained fixed. This was done as a further check to ensure that the current depression observed was indeed due to the interaction between the metal cation and the dianion. If this was so, a similar behavior should be observed by performing the experiments in reverse, i.e. varying the concentrations of the hydrocarbon. Figure 31 shows the result of the experiment where the Li+ concentration was kept fixed at 1.50 mM and the anthracene concentration was varied in DMF. As can be seen, at low concentrations of An, i2 was negative but this was increased linearly with increased An concentration. The slope of this increase was approximately equal to that for il. Here, the Li+ reduction wave (im ) remained constant in height. Figure 31 also shows the plot of mmol Li+ reacted vs An concen-
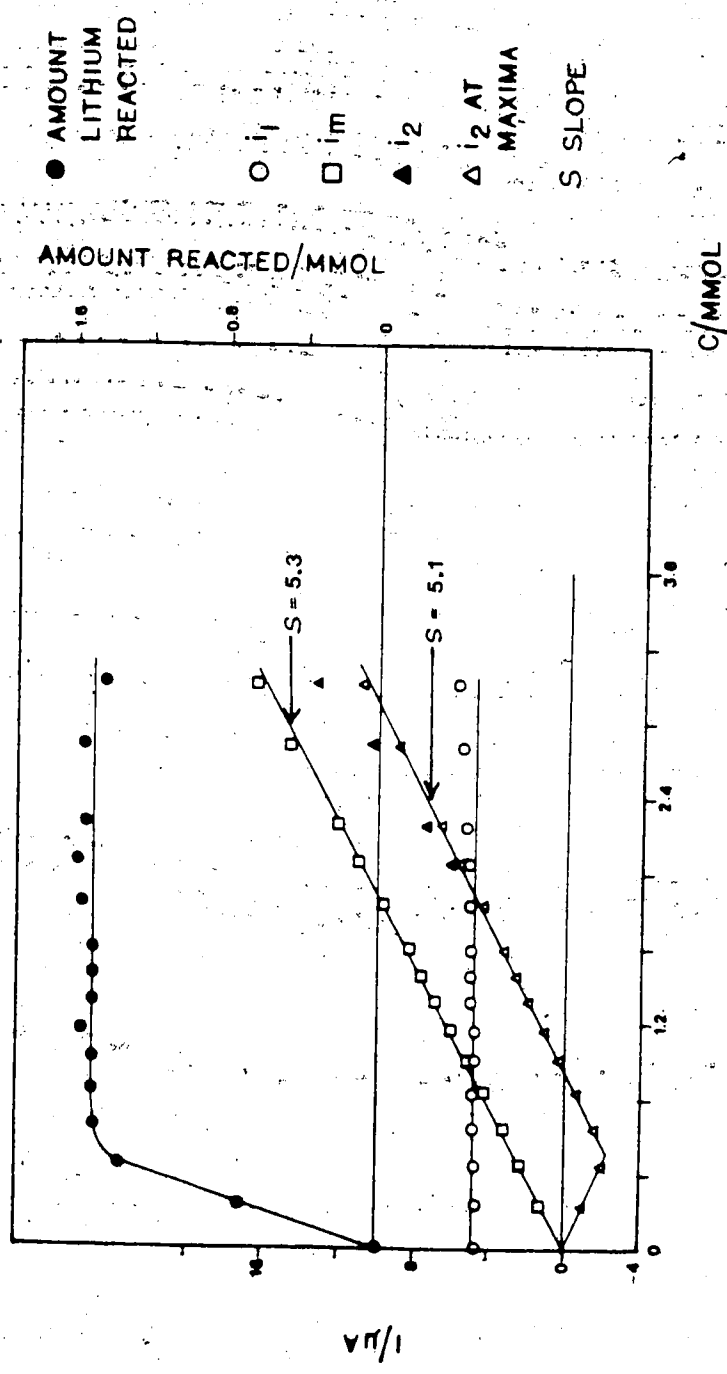
Figure 31. Plots of limiting currents and amount of
lithium cation reacted versus anthracene
concentration in DMF at 25°C.
Lithium cation concentration was fixed at
1.50 mM.
Mercury column 50.0 cm.
i1: limiting current for anthracene reduction
im: limiting current for lithium cation
reduction
i2: limiting current for anthracene anion
radical reduction

tration.  It can be seen that, at low concentration of

An, a linear portion with a slope of 3.0 was obtained and

the plot leveled out at 1.50 mM Li+.  It should also be

pointed out that the curve begins to level out when the

concentration of An is about 0.50 mM.

Figure 32 shows a similar experiment where the Na+

concentration was kept constant at 2.00 mM and the anthra-

cene concentration varied in DMF.  As mentioned earlier,

in the system only two waves were observed corresponding

to i1 + im  and i2.  Again, i2 was negative at low con-

centrations of An and starts to increase linearly with a

slope equal to that for the i1 +im  plot.  It is signifi-

cant that the intercept for the i1 +im  cuts the current

axis at the current value for 2.00 mM Na+ in the absence

of any anthracene.  Again the mmol Na+ vs An concentration

plot starts with a linear portion with a slope of 1.9 and

then starts to level at about 1.00 mM An.  The leveling
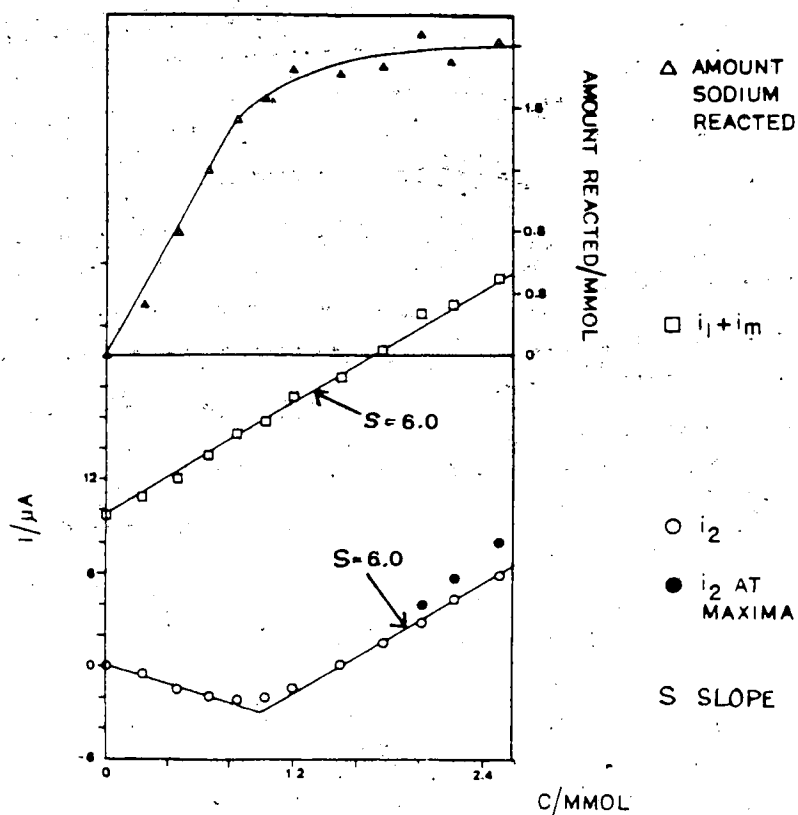
Figure 32. Plots of limiting currents and amount of sodium
cation reacted versus anthracene concentration
in DMF at 25°C.
Sodium cation concentration was fixed at
2.00 mM.
Mercury column 57.0 cm.
i1 + im: combined limiting current of
anthracene and sodium cation
reduction
i2: limiting current of anthracene anion
radical reduction

occurs at Na+ concentration of 2.00 mM.

It was observed in Figures 31 and 32 that for the

second wave of the hydrocarbon, i2, that polarographic

maxima were obtained. It was stated earlier that for

anthracene and fluoranthene, maxima appeared at concen-

trations of the hydrocarbon above about 2.00 mM.

However, as can be observed in Figures 31 and 32, current

measured at the diffusion plateau following the maxima

gave good results.

## 3.4 Discussion

The electrochemical behavior of the alkali metal

cations observed in aprotic solvents such as acetonitrile

and dimethylformamide were found to be in agreement with

those of many previous workers. Previous studies have

found that Na+, K+, and Rb+ were polarographically

reversible (59,60,63). Polarographic maxima have also

been observed previously (59) for Li+ and Na+ at concentrations greater than 3 mM and for Rb+ at even lower concentrations. However in this work, only small maxima were observed at higher concentrations for all cations (greater than 3 mM) and did not pose any serious problems.

From the slopes of the calibration plots (Table 1), it can be seen that Li+ has a much lower value than the other cations. This is due to the higher solvation of Li+. For example, Li+ has higher solvation numbers than those of the other cations in DMF:

| Cation | Solvation number in DMF (217) | Slope of calibration plot (uA/mmol) in DMF |
|--------|-------------------------------|--------------------------------------------|
| Li+ | 5.0 | 4.0 |
| Na+ | 3.0 | 4.9 |
| K+ | 2.6 | 5.0 |
| Rb+ | 2.5 | 5.2 |

Also, it has been found that the Stokes radii of the alkali metal cations in most solvents follows the order

Li+ > Na+ > K+ > Rb+ (217). Brown and Urfali (59) have found

that diffusion current constants for the alkali metal

cations in DMF are 60% to 70% of the values obtained in

acetonitrile. Table 1 shows that this can also be said

for the present study. The diffusion coefficients of the

ions are affected mainly by two factors; namely, solvation

and viscosity. Within the same solvent, it can be seen

that solvation determined the size of the ions and there-

fore the diffusion coefficients. However comparison in

different solvents has to involve viscosities. Certainly,

the solvation of the cations in DMF (Gutmann donor number

26.6) is higher than that in ACN (Gutmann donor number

14.1). However, the viscosity of DMF(0.802, 25°C) is also

larger than that of ACN (0.345 25°C). Therefore, these two

factors contribute to the much smaller diffusion currents

observed in DMF than in ACN. Eh values in Table 1 also

reflect the greater solvation of Li+ compared to the

other alkali metal cations and also the more basic char-

acter of DMF as compared to ACN. Although comparisons of

Eh values cannot be absolute where different reference

electrodes are used, relative inferences can be drawn.

Therefore, the relative case of reduction of the alkali

cations in this work was in accord with the results of

Brown and Urfali in DMF.

| Cation | This work V vs Ag/Ag+ | Brown and Urfali(59) V vs Hg pool |
|--------|------------------------|-----------------------------------|
| Li+ | -2.771 | -1.81 |
| Na+ | -2.463 | -1.53 |
| K+ | -2.492 | -1.55 |
| Rb+ | -2.481 | -1.52 |

The electroreduction of anthracene and fluoranthene

gave two waves of approximately equal height. This implies

that the diffusion coefficients for the hydrocarbon and

its anion radical are not greatly different. In tetrahydro-

furan, it was found that the diffusion coefficients of the

anion radicals of biphenyl and anthracene are equal to

those of the uncharged hydrocarbons (218). These results

are expected since the single negative charge in these

conjugated systems is well dispersed and solvation does not

increase. The reversibility of the first reduction waves

of anthracene and fluoranthene, in both aprotic solvents

are in agreement with results obtained for aromatic hydro-

carbons as discussed in the introduction of Chapter 1.

Also cyclic voltammetric data (not given here) have shown

that the anion radicals of both hydrocarbons are stable in

DMF and ACN for at least the time scale of the cyclic

voltammetric experiments (about 10 s). Cyclic voltam-

metry also showed the dianions to be unstable since no

reoxidation current was observed on the reversed scan.

Therefore the polarographic irreversibility as evidenced

by the slope of the E vs log((i(d)-i)/i) plots results from

chemical instability rather than slow rate of electron

137

transfer. The rate constant for electron transfer to the

anion radical of anthracene has been estimated to be 0.5

cm/s, which is fast and therefore electrochemical

reversibility should result if there were no chemical

complications (29). In DMF, the slopes for the second

waves of anthracene and fluoranthene were close to

reversibility (61-64 mV). Although the cyclic voltam-

metric data showed no reoxidation current, the pulse

polarogaphic time scale is much shorter, 57 ms    compared

to several seconds. Therefore, protonation of the dianions

in DMF possibly was only partial. Further, DMF is a more

"aprotic" solvent than ACN with respect to the presence of

small amounts of water. This arises out of the ability

of amide type solvents to form complexes with water (219).

As will be discussed later, the present work, and previous

investigations have shown that addition of water (< 5%

volume/volume) to DMF did not seem to affect the stability

of the anion radicals of the hydrocarbons (25). In constrast, the slope of E vs $\log((i(d)-i)/i)$ plots for the second waves in acetonitrile showed a higher degree of irreversibility; 67 mV for fluoranthene and 76 for anthracene. Acetonitrile does not have as good an ability as DMF to complex water and therefore water activity is much higher in the solvent. Also since the wave heights were approximately equal for both waves of the hydrocarbons, the protonation products of the dianion are not reducible at the potentials of the second wave.

The Eh values showed that fluoranthene is more easily reduced than anthracene. This is expected because the electron affinity of fluoranthene is 0.840 eV whereas that for anthracene is 0.653 eV but the energies of solvation of the hydrocarbon anion radical are not much different (4,220). This argument follows from the relation between the half-wave potential and electron

affinity as given by

$$Eh = EA + i* - delGsolv \ (m^{\pm}) \tag{3.3}$$

where EA = electron affinity

   i* = electric work function of the mercury

      electrode

   delGsolv $(m^{\pm})$ = free energy of solvation of the anion

         radical.

From the experimental evidence presented so far in

this work, the mechanism for the electroreduction of

aromatic hydrocarbons in aprotic media follows that of

Hoijtink et al (23). Therefore, if R is the hydrocarbon

$$
\begin{array}{llll}
R + e & = & R^{\pm} & E1 \\
R^{\pm} + e & = & R= & E2 \quad (E2<E1) \\
R= + HX & = & RH- + X- \\
RH- + HX & = & RH_2 + X-
\end{array}
$$
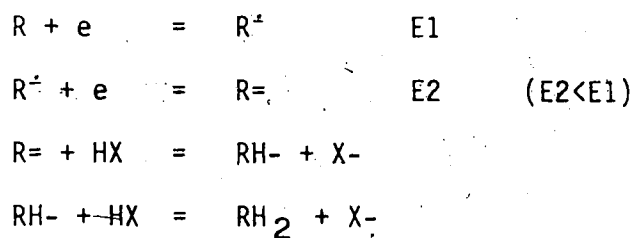
In the case of anthracene and fluoranthene in DMF and ACN,

it appears that $RH_2$ is not reducible at the potentials

investigated.

Before starting the actual investigations into the

interactions of the anions of anthracene and fluoranthene

with alkali metal cations, it was decided to check whether

the addition of Woelm supergrade neutral alumina to the

solutions could improve the stability of the dianions by

removing the trace water. However, it was found that

addition of alumina affected the reduction of the

alkali metal cations. For example, Li+ reduction waves

were found to be drastically reduced in the presence of

alumina, and even disappeared completely if enough

alumina was added. It is conjectured that Li+ ions are

adsorbed onto the active alumina surface sites although

no further work was done to confirm this.

Also, in the early phase of these studies, the results

were found to be irreproducible and seem to vary with the

deaeration time. This was attributed to the presence of

oxygen due to insufficient deaeration time. At the

negative potentials used, oxygen is reduced to the super-

oxide anion radical in aprotic media (221). The super-

oxide has been reported to tie up alkali metal ions,

causing low results for the electrolysis of these ions

(222). However, this problem was simply overcome by

longer deaeration times (at least 15 minutes) to reduce

the oxygen concentration to negligible values.

Prior studies in solvents of low dielectric constants

(223-225) have shown that ion pairs were formed between

anion radicals of polycyclic aromatic hydrocarbons and

alkali metal cations. The anion radicals could dispropor-

tionate to give the dianions which were also paired with

the cations. In this work no evidence of any ion pairing

interactions between $An^\pm$, $Fa^\pm$, and the alkali metal cations

was observed. This is not surprising since the dielectric

constants of acetonitrile (36.0) and dimethylformamide (37.0)

(226) are much higher than those of ethereal solvents and

also, the single negative charge in the conjugated hydro-

carbons is well dispersed.

Thus, the equilibrium

$$R: + M+ \quad = \quad R:,M+ \tag{3.4}$$

lies far to the left. The constancy of Eh values for the

first hydrocarbon wave with increasing cation concentration

provides the evidence for the lack of any significant

ion pairing. Further, il values were unchanged by

cations in all systems studied as opposed to i2 where

clearly dianion-cation interaction occurs. The linearity

of the im vs cation concentration plots is further proof

that no complications arise from any reaction between the

anion radicals and the cations. The slopes of these lines

coincided well with the calibration plots for the

individual metal cations. Where the wave of the metal

cation is not resolved from that of the hydrocarbon, the

linearity, slopes and intercepts of the $i1 + i_m$ vs metal

concentration plots imply that these combined waves are

simply additive with no chemical complications. The fact

that the slopes agree well with those for the calibration

plots of the metal cations and the intercepts are close to

the wave height of the hydrocarbon reduction strongly

support this deduction. Positive deviations from linearity

of the $i1$ and $i1 + i_m$ plots at high metal concentrations

are probably due to maxima observed at these high concen-

trations. However, these deviations are small and do not

detract from the results.

It is proposed that the current depression of the

dianion waves, $i2$, is due to the interaction between the

dianion and the metal cations. All the results observed

point in this direction. Adsorption and film formation

effects have been ruled out from the normal diffusion

controlled behavior of the current-time transients at the

potentials where current depression occurs. These effects

do not normally show the concentration dependence which

has been observed in these experiments. Reverse pulse

polarography does not show any desorption or film

destruction currents which will support the presence of

adsorption or film formation. Another possible explanation

for the current depression could be due to the presence

of trace water. Under the careful purification procedure

used in this work, the water concentration is probably

much less than 5 mM. However, in the presence of water,

the following reactions could conceivably occur:


$$R^= + H_2O = RH- + OH-$$

$$RH- + H_2O = RH_2 + OH-$$

$$M+ + OH- = MOH$$
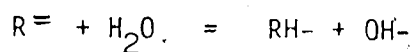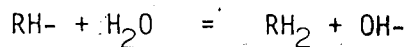
If this were the case, the addition of water should

increase the magnitude of the current depression. This

could happen if the presence of OH- results in the removal

of metal cations. However, alkali metal hydroxides are

relatively soluble in these solvents, and it is doubtful

that at such low concentration the solubility products

could be exceeded. However, what is more important is

that further experiments involving the addition of water,

which will be discussed in a later chapter, lifted the

depression of current i2 rather than reinforcing it.

Therefore, from the above discussion, the only

possible explanation for depression of current i2 is the

interaction of dianions with metal cations. The course of

events leading to the decrease in the magnitude of i2 is

viewed as follows: at the diffusion current plateau for

the metal ion reduction, the concentration of the metal

ion at the surface of the electrode is zero and a vir-

tually linear metal concentration gradient has been

established in the diffusion layer. As the potential scan

proceeds to more negative values, reduction of the hydro-

carbon anion radical to the dianion begins. The dianions

which are formed start to diffuse through the diffusion

layer out into solution. In this layer, encounters

between the dianions and the metal cations result in

interaction between the two. Interaction with the cations

effects their removal and thus reduces the number of

cations which can arrive at the electrode to be reduced.

This means that the diffusion current of the metal cation

which has been established prior to the formation of the

dianions can no longer be maintained. Since this phenome-

non occurs at the potential region of the reduction of the

anion radicals, it manifests itself as a drop in i2. The

reason for the observed cathodic current on an anodic scan

for the An:Li+ in DMF system is now clear (Figure 23). As

the potential is scanned positive, a potential is reached

where dianions are no longer formed and Li+ is no longer

being removed in the diffusion layer. Thus the arrival of

the Li+ to the electrode surface results in a cathodic

current.

It is therefore logical that the strength of inter-

action between the dianions and the metal cations is

reflected in the magnitude of the current depression.

Li+ and Na+ react strongly with An$^=$ in both ACN and DMF.

In Figures 24 and 26, the slopes for the i2 plots are

essentially equal to the slopes for the i1 and i1 + im

plots. This means that almost complete removal of Li+

and Na+ is effected. It is interesting to note, in the

An:Li+ system in DMF for example, that the point where

the i2 plot crosses the concentration axis occurs at

1.45 mM.  If complete removal of Li+ is the case, the

removal of 1.45 mM of Li+ would result in a loss in

current of 1.45 x 4.0 = 5.8 uA.  Since the current depres-

sion occurs at the i2 wave for anthracene and the diffusion

current for this wave for 1.00 mM An is 6.1 uA, this

would mean that the actual observed i2 is only 6.1-5.8 =

0.3 uA which is very close to zero.  The very strong

interaction of Li+ and Na+ with An$^{=}$ is obvious if Figure

27 is considered.  It can be seen that up to a concentra-

tion of 2.00 mM of Li+ added, the amount of Li+ reacted is

also 2.00 mM, resulting in a slope of 1 for the curve

given in Figure 27.  The same can be said for Na+ up to

1.00 mM.  With Na+, the curve levels off at 2.00 mM

whereas with Li+ it approaches 3 mM.  The interpretation

is therefore that a 1:3 stoichiometry of An:Li+ is

obtained in DMF whereas An:Na+ gives a 1:2 stoichiometry.

The same result is true for An: with Li+ and Na+ in ACN.

The formation of the 1:3 complex An,3Li+ is very inter-

esting from charge considerations since it gives rise to

an overall positive charge. However, this is not without

precedent since the same stoichiometry was found for the

interaction of anthraquinone dianion with Li+ (227).

In the case of K+ and Rb+, i2 did not reach large

negative values as can be seen from Figure 24. Figure

27 also shows that reactions between An= and these cations

are not as strong as for Li+ and Na+. The plots in

Figure 27 show continuous increase in the mmol of cation

reacted with increasing metal concentration. Reaction

for Rb+ appears to be slightly greater than K+. It is

proposed that for these two cations, both 1:1 and 1:2

complexes are present and these have small formation

constants.

Li+ with Fa= reacts strongly on a 1:1 basis in DMF.

There is some 1:2 complex formed but this does not appear
to be strong. This can be observed from Figure 25 where
the il + im plot remains constant up to about 1.2 mM Li+
and then increases linearly with a slope of 4.2 which is
approximately equal to that for Li+ calibration of 4.0
uA/mM. This is supported by Figure 28 where a slope of
1 was obtained and the mmol Li+ reacted starts to level
out at 1.2 mM Li+. In acetonitrile, similar results are
obtained (Figure 26) except that more of the 1:2 compex
Fa=,2Li+ is formed and the mmol Li+ reacted approaches
2.0 mM (Figure 30).

Na+ reacts very strongly with Fa= both in DMF and
ACN as can be seen from Figures 28 and 30 where slopes of
1 were obtained. However, only a 1:1 complex(Fa=,Na+) appears.
The reaction did not proceed to the 1:2 complex Fa=,2Na+
since the curves leveled off exactly at 1 mM of Na+. K+
and Rb+ reacted only very weakly with Fa= and from what

has been said for Li+ and Na+ with Fa=, it can be deduced

that only 1:1 complexes are formed with very small forma-

tion constants (Figure 28).

The results obtained from the experiments where the

hydrocarbon concentrations were varied confirm the

conclusions which were reached in the above discussion.

In the An:Li+ in DMF system (Figure 31), where the Li+

concentration was fixed at 1.50 mM, the constancy of the

Li+ reduction current with added anthracene concentration

and the fact that Eh values for the first anthracene

wave and the Li+ waves did not change significantly imply

that no interaction occurs between $An^-$ and Li+. The il

vs An concentration plot was linear. The i2 plot which

was linearly increasing beyond a concentration of 0.51 mM

for An, has the same slope as the il plot. This means

that no further reduction in the i2 current occurred after

0.51 mM of anthracene had been added. The mmol Li+

reacted vs An concentration plots is most informative.

The initial linear portion has a slope of 3.0 and it starts

to level off at an anthracene concentration of 0.5.  In

the level portion the mmol Li+ reacted was 1.50 mM.  All

this supports the argument that Li+ reacts very strongly

with An= to form the 1:3 complex An=,3Li+.  (Note:

Current values in this experiment (Figure 31) should not

be compared with calibration plots of other experiments

because for this particular experiment the Hg head was

changed to 50.0 cm instead of the usual 57.0 cm in DMF

throughout this work.)

The results for the experiment where the Na+ concen-

tration was fixed at 2.00 mM (Figure 32) again confirmed

earlier conclusions for this system.  The i1 + im plot

has a slope of 6.0 which agrees with the calibration

plots for An in DMF.  The i2 plot increased linearly with

An concentration beyond 1.00 mM and has a slope of 6.0.

The mmol Na+ reacted vs An concentration has a slope of 1.9 and levels at 2.00 mM Na+. Therefore Na+ forms a strong 1:2 complex with An= in DMF.

From the above discussion, it is clear that inter-action of dianions with alkali metal cations increases

1) with decreasing size of the cation;

2) with decreasing size of the hydrocarbon; and

3) from dimethylformamide to acetonitrile.

The nature of the interaction between the dianion and the alkali metal cation needs to be discussed. In the chemical reduction of aromatic hydrocarbons with alkali metals in ethereal solvents it is assumed that the dianions form ion pairs with the alkali metal cations. Here, the dianion-alkali metal cation interactions are also believed to be ion pairing. Since the extent of ion pairing increases with decreasing radius of the cations, contact ion pairs are formed. This is reason-

able since the larger the charge/radius ratio for the

cations (Li+ > Na+ > K+ > Rb+), the greater the strength of

interaction. The ionic radii of Li+, Na+, K+, and Rb+ are

0.68, 0.97, 1.33 and 1.47 Å respectively. Contact ion pairs

have also been found in interactions of ketone anions with

alkali metal cations (227). This trend is observed in this

work except for K+ and Rb+ with An in DMF where the two are

reversed (Figure 27). For these two cations, solvent sepa-

rated ion pairs may exist since stabilization by contact ion

pair formation may not be large enough to compensate for the

destabilization arising from desolvation. It is known that

increase in radius of countercation favors the solvent

separated ion pair because the gain in coulombic energy on

collapse to the contact ion pair is decreased (reference 217,

p. 356). The situation can arise, where both the solvent

separated and contact ion pair exist in equilibrium. For the

K+ and Rb+ case then, the solvent separated ion pair should

be more favored resulting in the reversal in trend as observed

above. This study however, does not provide enough informa-

tion to test this situation.

The dianions of the aromatic hydrocarbons had half-wave

potentials more negative than the alkali metal cations

(Table I). (Note: The hydrocarbon anion radicals reductions

to the dianions were not reversible, therefore the Eh values

do not have any thermodynamic significance. However,

for the sake of argument here, they will be assumed to be

reversible Eh values.) Examination of Table 1 shows that in

DMF, the second reduction wave of anthracene has the most

negative Eh, this value being -2.989 V and Na+ the most posi-

tive Eh, with value -2.463 V. The difference between these

two values is 526 mV. In acetonitrile, where K+ and Rb+ were

not studied, again the most negative and positive Eh values

belong to anthracene second wave (-2.904 V) and sodium cation

(-2.159 V) respectively, the difference being 745 mV. In

general, solvation effects in going from DMF to ACN are much

larger for the cations than for the hydrocarbons and therefore,

in terms of electron transfer, the cations are more acidic in

acetonitrile. Therefore considering the anthracene-cation

systems in ACN, it seems that the An= is a much stronger base

compared to the cations. As mentioned above, the difference in

Eh between the An$^-$/An= couple and Na+ is 745 mV. The differ-

ence between the same couple and Li+ is 639 mV. From these

views therefore, the argument can be made that the current

depression observed is due to electron transfer from An= to

the metal cations in the diffusion layer which would prevent

these cations from reaching the electrode.

However, careful examination shows that the above argu-

ment cannot be true. This is because polarographic half-wave

potentials obtained for alkali metal cations are not applica-

ble since reduction at the mercury electrode results in

amalgam formation whereas reduction by An=, if it were to

occur, would result in formation of the alkali metal in the

solution. This means that E(O) values for the alkali metal

cations must be used. The standard reduction potentials for

Na+ and Li+ in ACN are given below (see reference 172, p.400).

.Cation          E(O) (vs Standard Hydrogen Electrode (SHE))

Li+          -2.645 V

Na+          -2.421 V

Since the Eh value for the $An^-/An=$ couple was obtained

with reference to the Ag/Ag+ (0.01 M) reference electrode,

this can be converted to the hydrogen scale. The Ag/Ag+

electrode is +0.3 vs aqueous SCE which in turn is +0.246 vs

SHE and therefore the Eh value for $An^-/An=$ is -2.358 V vs

SHE which means that the solution reduction of the cations

without amalgam formation is negative of the $An^-/An=$

couple. Charge-transfer complexes (EDA type) have been

observed for contact ion pairs in solvents of low dielectric

constant (reference 217, p. 410). However, in view of the

above discussion and from the fact that no colored species

were observed at the surface of a hanging mercury drop

electrode, this type of complex is not thought to occur to

any extent in this case.

The increase in ion pairing in going from anthracene

to fluoranthene can be explained in terms of the larger

size of the fluoranthene molecule due to more fused rings.

Therefore, the two negative charges in fluoranthene

dianion are more diffuse compared to anthracene. This is

evident from the more positive reduction potential of

fluoranthene.

It is obvious that solvation must play an important

part in the dianion-cation interactions. The results of

the An:Li+ system in ACN and DMF serve to demonstrate this

point. A distinct peak appears at the beginning of the

dianion wave before depression occurs in DMF (Figure 10).

This peak is absent in ACN (Figure 18). It is well known

that Li+ is much more strongly solvated in DMF than in ACN.

It is expected that both the kinetics and the equilibrium

of ion pair formation is more favorable in ACN than in DMF.

The appearance of the peaks in DMF could mean that a small

amount of dianion has to be present before interaction

becomes favorable. The slopes of the calibration plots for

Na+, K+ and Rb+ are closely grouped in DMF. This means

that the solvated radii of these ions in DMF are not very

much different. However, Na+ interacts much more strongly

than K+ or Rb+ with dianions. This is another indication

of contact type of ion pairing in the case of Na+. Unfor-

tunately, no studies could be made for K+ and Rb+ in ACN so

that no comparison could be made for these two ions in

different solvents.

The observation of different stoichiometries for

different systems in this study is very interesting. In

many previous studies in ethereal solvents, not much

attention has been paid to these variations in stoichi-

ometries. In most cases, it has been implicitly assumed

that anion radicals pair with one cation whereas dianions

pair with two cations. However, electrochemical studies

of ion pairs of negative ions of ketones with alkali metal

cations in DMF and ACN have revealed that these different

stoichiometries exist (209-212). It is not very clear to

the author at this point why these different stoichi-

ometries occur for the aromatic hydrocarbons. Clearly

charge considerations alone are not enough since Li+ and

An= forms a 1:3 complex An,3Li+. Obviously, structural

factors and solvation of the ion pairs play important

roles in these interactions. Fast spectroscopic tech-

niques could provide valuable information on these aspects.

Spectroelectrochemical methods would be relevant in these

areas. However, difficulties arise in electrode fabrica-

tion. Mercury thin film electrodes have so far not been

very successful.  Further research in this area in these

laboratories is in progress.

Temperature studies have also been made.  Experiments

were carried out at 5°C and 45°C besides 25°C.  However,

over this temperature range, no measurable changes in the

interactions were detected.  So far, the discussion has

been qualitative in nature.  It is necessary to perform

some calculations to obtain the equilibrium constants

for the ion pairs.  However, the value of these calcula-

tions would be very doubtful due to the unstable nature

of the dianions.  However, it is felt that this present

study provides an important starting point for further

investigation.  To the best of the author's knowledge,

this is one of the few, if not the only, study of the

interactions between aromatic hydrocarbon dianions and

alkali metal cations in dipolar aprotic solvents.

From the results and discussion presented so far,

162

the following summary concerning the interaction of the

negative ions of anthracene and fluoranthene with alkali

metal cations in ACN and DMF can be made:

 i) No interaction of the anion radicals with alkali

    metal cations occurs in either solvent.

 ii) Ion pairs are formed between the dianions and alkali

    metal cations.  These ion pairs are of the contact

    type except for K+ and Rb+ with An= in DMF where

    solvent separated ion pairs may exist.

iii) The strength of interaction follows the trend

    Li+ > Na+ > K+ > Rb+.

 iv) Interactions are stronger in ACN compared to DMF.

  v) The stoichiometries of interactions do not depend on

    charge considerations alone.

    The following scheme for the reactions are postulated

where R represents the aromatic hydrocarbon and M+ the

alkali metal cation:

$$R^{\pm} + M+ \quad = \quad R^{\pm},M+ \quad (I) \qquad \text{equilibrium lies very} \\ \text{far to the left}$$

$$R= + M+ \quad = \quad R=,M+ \quad (II)$$

$$R=,M+ + M+ \quad = \quad R=,2M+ \quad (III)$$

$$R=,2M+ + M+ \quad = \quad R=,3M+ \quad (IV)$$
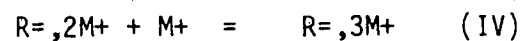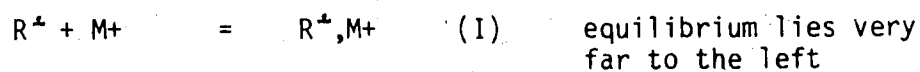
Step II occcurs very strongly for An:Li+,Na+, and

Fa:Li+,Na+ in both solvents, but only weakly for

An:K+,Rb+ and Fa:K+,Rb+ in DMF. Step III occurs very

strongly for An:Li+ in both solvents, An:Na+ in ACN but not

quite as strong for An:Na+ in DMF. It is of moderate

strength for Fa:Li+ in ACN but weak for Fa:Li+ in DMF

and An:K+,Rb+ in DMF. Step IV occurs strongly in An:Li+

in both solvents.

Chapter 4.  The Effect of Water on the Interactions
between Aromatic Negative Ions and Alkali
Metal Cations

4.1  Introduction

In Chapter 3, it was found that the second reduction

wave of anthracene and fluoranthene was irreversible due to

the reactive nature of the dianion with respect to protona-

tion by proton donors (such as water) present in the solvents

even after purification.  However, it has been established

that Li+ and Na+ interact strongly with the dianions.

Hence, under the experimental conditions described earlier,

the dianions-cation interactions take precedence over pro-

tonation in the diffusion layer.  Also, the possible

presence of the hydroxide ions was not thought to be the

cause for the observed current depression of the dianion

wave.  In this chapter, evidence will be presented that

shows this is indeed so.

From what has been discussed, it is reasonable to expect that there is a competition between the metal cations and the proton donors for the available dianions close to the electrode surface. If this is true, then conditions could be altered so that the protonation reaction proceeds faster compared to the dianion-cation reaction. One such alteration is then to drastically reduce the concentrations of the electroactive species and determine the effect on the limiting currents. Another is to have controlled addition of water to the system. The addition of water would also substantiate the proposal that hydroxyl ions are not the cause of current depression since if this were so, current depression will be increased or in the limit remain constant.

The following sections describe the experiments performed to test the above assumption.

4.2  Experimental

4.2.1  Instrumentation

The equipment used is exactly the same as that

described in Chapter 3.

4.2.2  Purification of Chemicals

The purification of anthracene, fluoranthene, alkali

metal perchlorates and the solvents acetonitrile and

dimethylformamide has already been described.  The water

used here was tap distilled water which had been deionized.

It was then made alkaline by adding sodium hydroxide.

Potassium permanganate was then added.  This mixture was

distilled and the distillate was taken through

another distillation stage.

4.2.3  Procedure

In all experiments, the supporting electrolyte used

was tetra-n-butylammonium tetrafluoroborate (TBAF) at

0.10 M. The deaeration procedure was the same as that
described in Chapter 3. Temperature was controlled at
25.0 ± 0.1°C.

In the dilution experiment, 25 ml of a solution
containing 2.00 mM anthracene and 3.00 mM lithium per-
chlorate in DMF was pipetted into the polarographic cell.
Into each solution, measured volumes of the background
solution (solvent at 0.10 M TBAF) equilibrated at 25°C was
transferred .

In water addition experiments, water was added to
separate solutions of the metal cations and the hydro-
carbons in DMF. Then water was added to mixtures of
solutions of the metal cations and the hydrocarbon. For
example, in the first case water was added separately to
1.00 mM anthracene and also to 3.83 mM Li+ solutions in
DMF. Then a mixture containing 1.00 mM anthracene and

3.83 mM Li+ was used to which water addition was performed.

Finally, a water concentration was chosen to be used in

kinetic studies.  In the case of the An:Li+ system this

concentration was 2.14 M in water.  25 ml of a 1.00 mM

solution of anthracene in DMF (0.10 M TBAF) which was

also 2.14 M in water was pipetted into the polarographic

cell.  After each run a known volume of a stock solution

of Li+ which was also 1.00 mM in anthracene and 2.14 M in

water was transferred into the cell.

Similar experiments were also carried out for the

An:Na+ system in DMF.  In this case water was added to a

mixture containing 1.00 mM anthracene and 3.92 mM Na+ in

DMF.  From this experiment a water concentration of 0.22 M

was chosen for further studies.

For fluoranthene, water was also added, using a micro-

syringe, to a 1.00 mM solution of fluoranthene in DMF.

Similar experiments as for anthracene were carried out with

water addition to Fa:Li+ and Fa:Na+ solution mixtures in

DMF. In the case of Li+, the concentration of fluoran-

thene was 1.00 mM and Li+ was 1.02 mM whereas for Na+, the

concentration of fluoranthene was 1.00 mM and Na+ was 2.45

mM. From these experiments a fixed water concentration of

1.72 M was chosen for kinetic studies of the Fa:Li+ system.

The limiting currents were corrected for dilution effects

due to the addition of water.


4.3  Results

Figure 33 shows the effect of dilution on a mixture

of 2.00 mM anthracene and 3.00 mM Li+ in DMF. It can be

seen that at the high concentration end, current depres-

sion of the third wave is obvious. As the solution was made

more and more dilute, the magnitude of the depression

became less until at a concentration of 0.09 mM anthra-

cene and 0.15 mM Li+, the current depression was completely
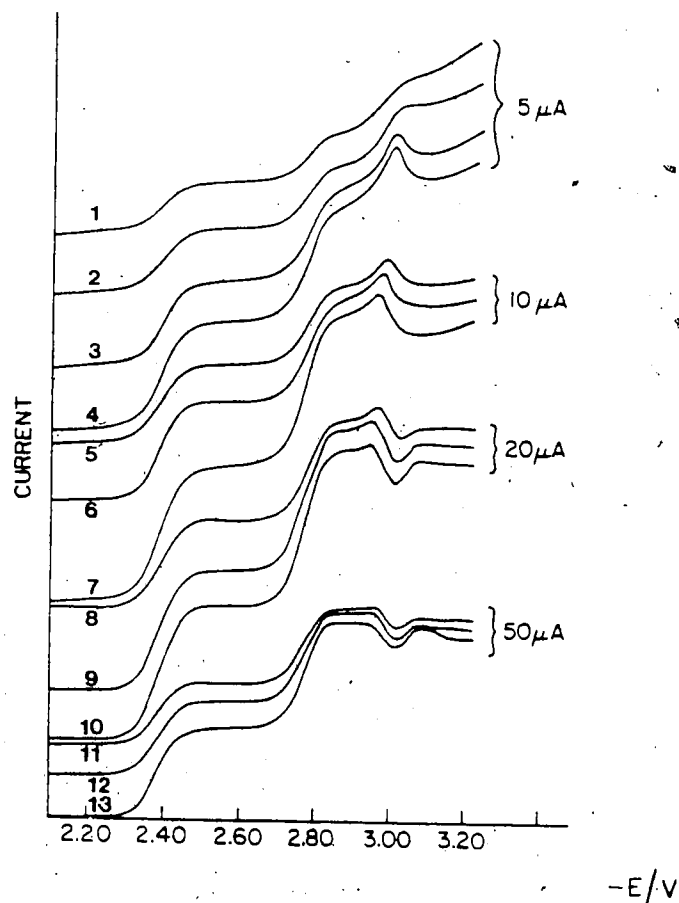
Figure 33. Dilution experiments: polarograms showing the
effect of dilution on mixtures of anthracene:
lithium cation in the concentration ratio 1:1.5
in DMF at 25°C.
Anthracene:Li+ concentrations are (in mM):
(1) 0.07:0.11, (2) 0.09:0.15, (3) 0.13:0.21,
(4) 0.24:0.37, (5) 0.34:0.52, (6) 0.44:0.66,
(7) 0.62:0.93, (8) 0.79:1.19, (9) 1.11:1.67,
(10) 1.25:1.88, (11)1.43:2.14, (12)1.67:2.50,
(13) 2.00:3.00.
Mercury column 57.0 cm.

lifted. At this concentration, the height of the third

wave which was due to the reduction of the anthracene anion

radical to the dianion, was equal to that of the first

wave, which is the expected result in the total absence of

any interaction between the dianion and Li+. Figure 34

shows the plots of the heights of the anthracene and

lithium reduction waves against concentration. It can be

seen that these plots are linear and the slopes agree well

with those of the calibration plots given in Table 1.

Further, the plot of percentage of Li+ reacted vs concen-

tration of Li+ shows that below about 0.90 mM Li+, the

An: Li+ interaction begins to be affected as the percen-

tage of Li+ reacted starts to decrease sharply from 100%.

It should also be pointed out that polarographic behavior

remained essentially unchanged with dilution within the

limits of experimental error. For example, the Eh values

of the anthracene and Li+ reduction waves remained con-
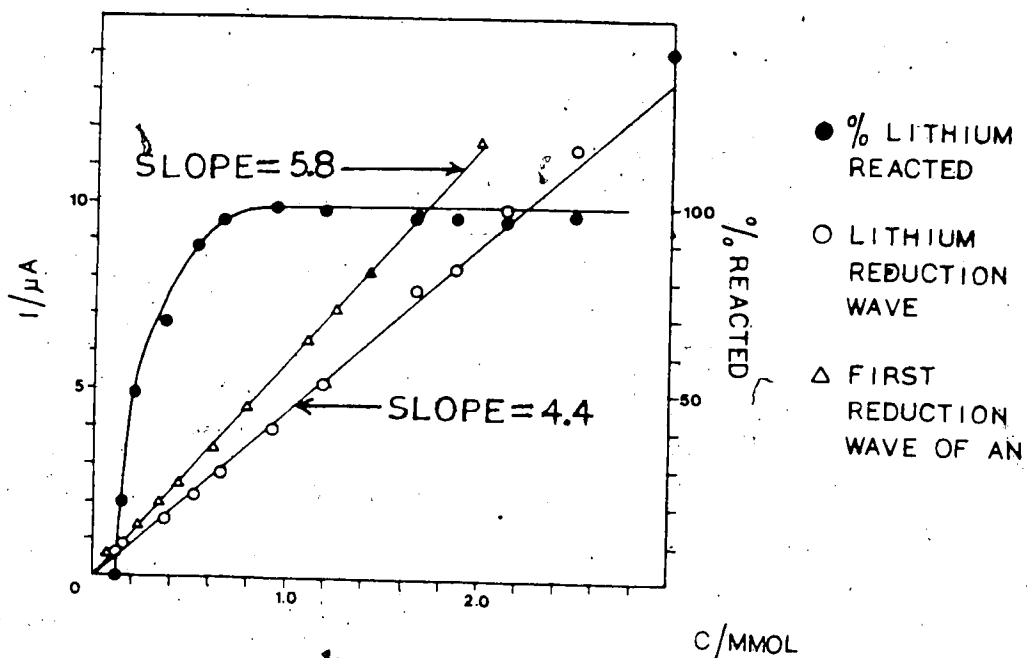
Figure 34. Dilution experiment: plots of limiting
currents and percentage of lithium cation
reacted versus lithium cation concentration
in DMF at 25°C.
An:Li+ concentration ratios kept at 1:1.5
Mercury column 57.0 cm.

stant.

Before the effect of water on mixtures of anthra-

cene and Li+ solution was examined, it was decided to

investigate the effect of water on separate solutions of

anthracene and Li+ in DMF. Figure 35 shows the effect of

water, up to 5.00 M, on the limiting currents of a 1.00 mM

solution of anthracene and a 3.83 mM solution of Li+ in

DMF. In the case of anthracene, both the limiting

currents of the first (i1) and second (i2) reduction

waves decreased linearly with water concentration. The

limiting currents were corrected for dilution effects due

to the addition of water. The decreases were approxi-

mately equal for both waves and amounted to about 17% at a

water concentration of 5.20 M. The Eh values for the

first wave were shifted negative by about 20 mV, but

those for the second wave were shifted positive by about

55 mV at 5.05 M water as compared to the dry solution.

Plots of E vs log((il -i)/i) showed that for the first

wave the slope was 60 mV for a reversible one-electron

transfer. This behavior did not change even up to addi-

tion of about 4.31 M water. For the second wave, the

slope was 66 mV in the absence of water but increased to

71 mV at 4.31 M water.

In the case of the 3.83 mM Li+ solution in DMF,

the limiting current decreases from 15.2 uA in the absence

of water to 12.6 uA in the presence of 5.05 M water,

again a decrease of 17% (see Figure 35). The Eh values

remained essentially constant( within 10 mV). Plots of

E vs log ((iA -i)/i) showed that the slopes did not change

very much, decreasing slightly from 65 mV with no water

to 63 mV at 4.31 M water.

The results of the addition of water to a mixture

of 1.00 mM anthracene and 3.83 mM Li+ in DMF are shown in

Figure 36. It can be seen that at low water concentra-
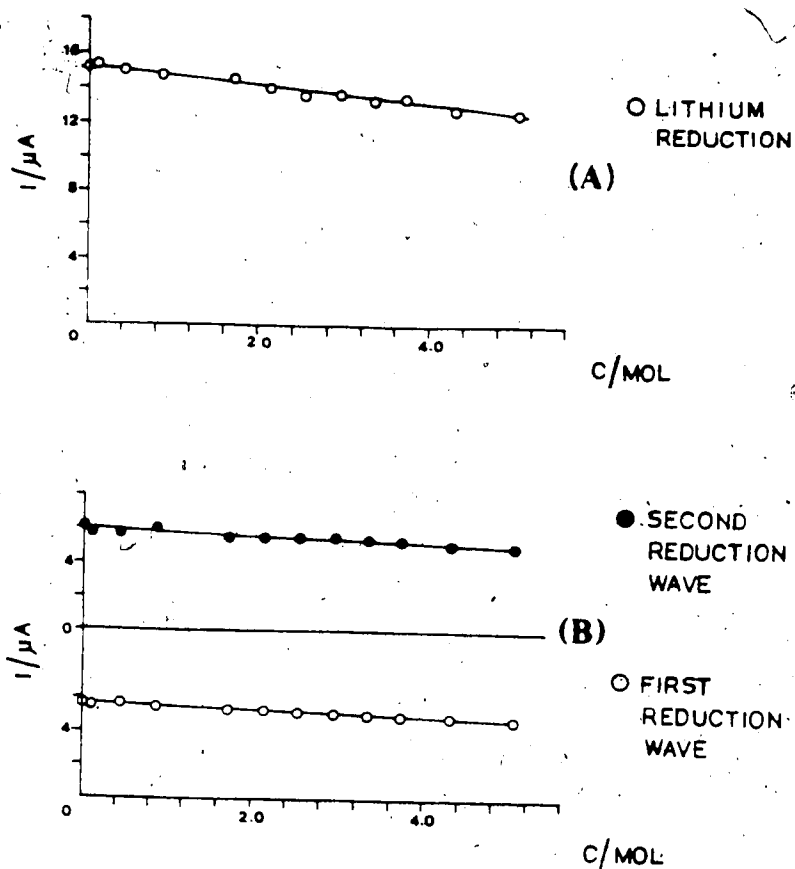
Figure 35. A. Effect of water on the limiting current of
a 3.83 mM lithium cation solution in DMF
at 25°C.

B. Effect of water on the limiting currents of
a 1.00 mM solution of anthracene in DMF
at 25 C.

Horizontal axis show concentration of water.
Mercury column 57.0 cm.
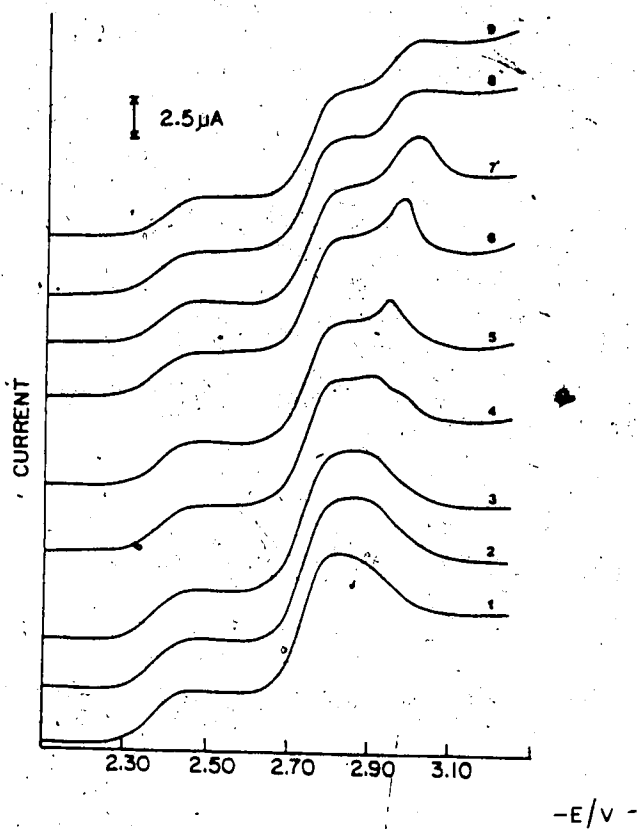
Figure 36. Polarograms showing the effect of water
addition on a mixture of 1.00 mM anthracene
and 3.83 mM lithium cation in DMF at 25 C.
Water concentrations are (in M):
(1) 0.00, (2) 0.11, (3) 0.44, (4) 1.72,
(5) 2.34, (6) 2.75, (7) 3.14, (8) 3.73,
(9) 4.31.
Mercury column 57.0 cm.

tions (up to about 0.11 M), there was not much effect on

the current depression of the third wave. As the concen-

tration of water was increased, the magnitude of the current

depression decreased until at about 3.73 M water, there

was no depression and the height of the third wave became

equal to the first. Figure 37 shows the plots of the

limiting currents vs water concentration. The currents

have been corrected for the dilution effects due to

water addition. The plots of anthracene ($i_l$) and Li+

($i_m$) reduction currents vs water concentration, show the

same trend as those of Figure 35. They decreased linearly

with increasing water concentration. However, the limiting

current for Li+ appeared to be slightly higher here. For

the anthracene and Li+ reduction waves, the same results

were obtained here concerning the Eh values and the E vs

log (($i_l$-i)/i) as for the separate solutions with respect

to water addition. The current due to the reduction of

Figure 37. Effect of water addition on the limiting
currents and amount of lithium cation reacted
.for a mixture of 1.00 mM anthracene and 3.83
mM lithium cation in DMF at 25°C.
Horizontal axis show water concentratons.
Mercury column 57.0 cm.
i1: limiting current for anthracene reduction
im: limiting current for lithium cation
    reduction.
i2: limiting current for anthracene anion
    radical reduction

—

the anthracene anion radical (i2) remained approximately

constant at its depressed value up to about 1.0 M water

and then increased at higher water concentrations. Above

3.4 M water, the height of the dianion wave became equal

to that for the first wave. The plot of mM Li+ reacted

vs water concentration is also shown in Figure 37.

When no water was added, the amount of Li+ reacted was

exactly 3.00 mM. Increasing the water concentration

about 1.70 M did not change this value much. However, at

higher water concentrations, the amount of Li+ reacted

decreased and approached zero at 3.35 M water. Figure 38

shows the results of the experiment where the water

concentration was fixed at 2.14 M and the concentration of

Li+ in a 1.00 mM anthracene solution was increased. As

expected the limiting current of the first wave (i1)

remained constant while the Li+ wave (im) showed a

linear increase with slope of 3.9 uA/mm, slightly lower

Figure 38. Plots of limiting currents and the amount of lithium cation reacted versus lithium cation concentration for mixtures of anthracene and lithium cations containing 2.14 M water in DMF at 25°C.

Anthracene concentration fixed at 1.00 mM. Mercury column 57.0 cm.

i1: limiting current for anthracene
im: limiting current for lithium cation reduction
i2: limiting current for anthracene anion radical reduction.

to that of the Li+ calibration slope of 4.0 uA/mm. The

depression of the third wave (i2), as can be seen from

Figure 38, was very much less as compared to that in the

absence of water. The plot of mM Li+ reacted showed an

induction region corresponding to about 0.40 mM Li+ before

any reaction occurred between An= and Li+.

Figure 39 shows the effect of water addition on a

solution containing 3.92 mM Na+ and 1.00 mM anthracene in

DMF. The first wave corresponding to the unresolved

reduction of anthracene and sodium (i1+im) decreased

linearly with increased water concentration. The

magnitude of the current depression (i2) decreased until

at concentrations of water above about 1.0 M, the value

of i2 was approximately equal to the first reduction of

anthracene. Figure 39 shows that initially when no water

was added the mM Na+ reacted was exactly 2.00 mM and

decreased quite sharply with water addition as
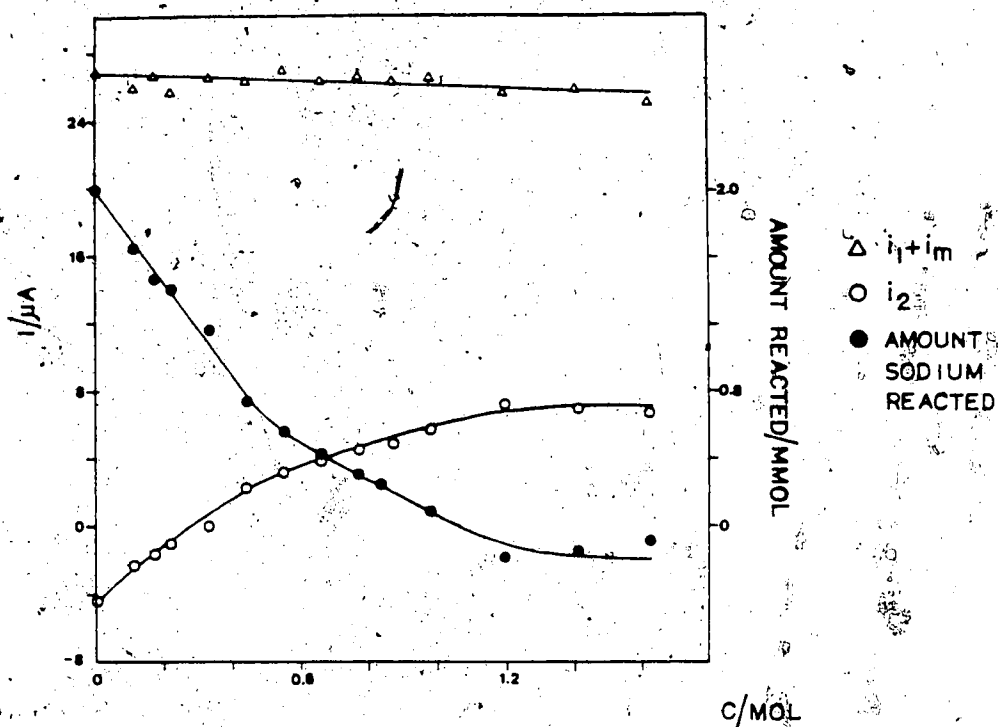
Figure 39. Effect of water addition on the limiting
currents and the amount of sodium cation
reacted for a mixture of 1.00 mM anthracene
and 3.92 mM sodium cation in DMF at 25°C.
Horizontal axis show water concentration.
Mercury column 57.0 cm.
i1 + im:  combined limiting current for
anthracene and sodium cation
reductions
i2:  limiting current for anthracene anion
radical reduction

compared to the case of Li+ (Figure 37) and approached

zero at 1.0 M water concentration. Figure 40 shows the

results of the experiment where the water concentration

was fixed at 0.22 M and the Na+ concentration in a

1.00 mM anthracene solution in DMF was increased. The

$i1+im$ plot was linear with slope of 5.1 uA/mM and intercept

of 5.7 uA. These values are in accord with the calibration

slopes of Na+ and the wave height for 1.00 mM anthracene.

Again, the current depression of the i2 wave was much

less as compared to that in the absence of water. As in the

case of An,Li+ system, the mM Na+ reacted vs Na+ concen-

tration plot showed an initial induction region, this

time up to about 0.20 mM Na+.

Figure 41 shows the effect of water on the first (i1)

and second (i2) reduction waves of fluoranthene. Similar

results were obtained for fluoranthene as for anthracene.

The limiting currents for both waves decreased linearly
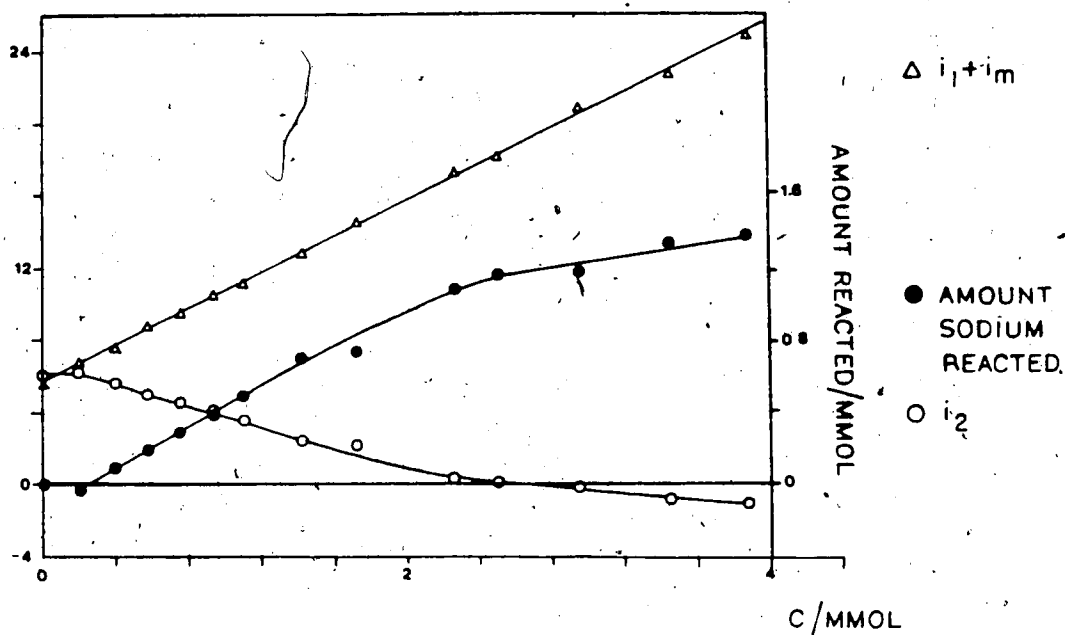
Figure 40.  Plots of limiting currents and amount of
sodium cation reacted versus sodium cation
concentration for mixtures of anthracene and
sodium cation containing 0.22 M water in DMF
at 25°C.
Anthracene concentration fixed at 1.00 mM.
Mercury column 57.0 cm.
il + im:  combined limiting current for
anthracene and sodium cation
reductions
i2:  limiting current for anthracene anion
radical reduction
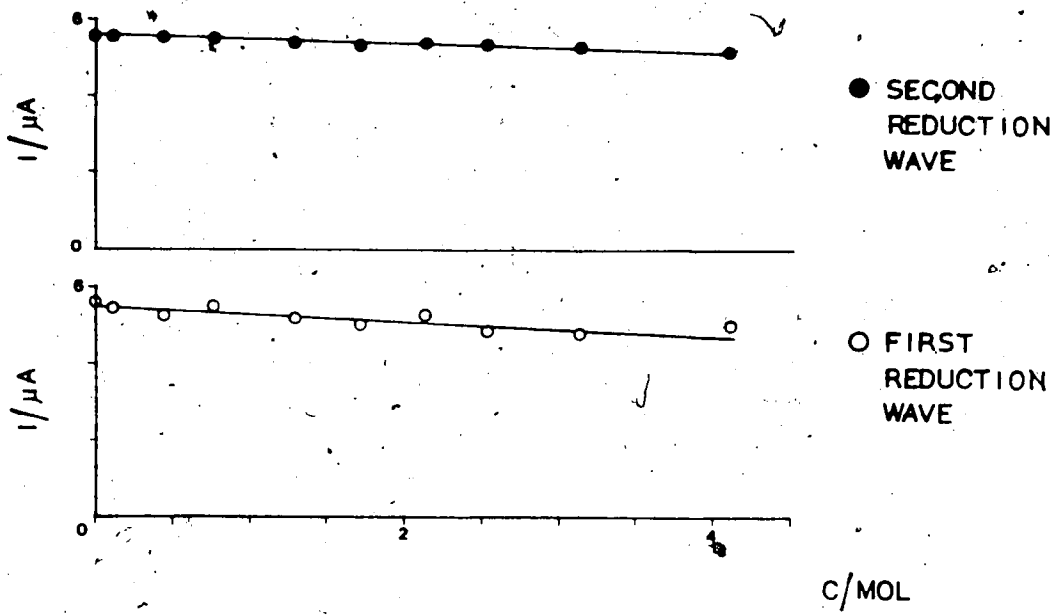
Figure 41. Effect of water addition on the limiting
currents of a 1.00 mM fluoranthene solution
in DMF at 25°C.
Horizontal axis show water concentration.
Mercury column 57.0 cm.

by about 10% at 4.1 M water. Eh values for the first wave

were approximately constant shifting in magnitude by about

18 mV for the water concentration range studied whereas

the Eh values for the second wave shifted positive by

about 90 mV. Slope of the E vs log ((id-i)/i) plots for

the first wave was unchanged and corresponded to 60 mV for

a one-electron reversible wave whereas for the second wave

the slope increased slightly from 63 mV to 68 mV for the

highest concentration of water used. /

The results of water addition to a solution con-

taining 1.00 mM fluoranthene and 1.02 mM Li+ in DMF are

presented in Figure 42. The limiting current for the

first wave (il), as expected, decreased linearly with

water concentration increase as was observed for the

addition of water to fluoranthene. The second wave

corresponding to im + i2, which was not resolved,

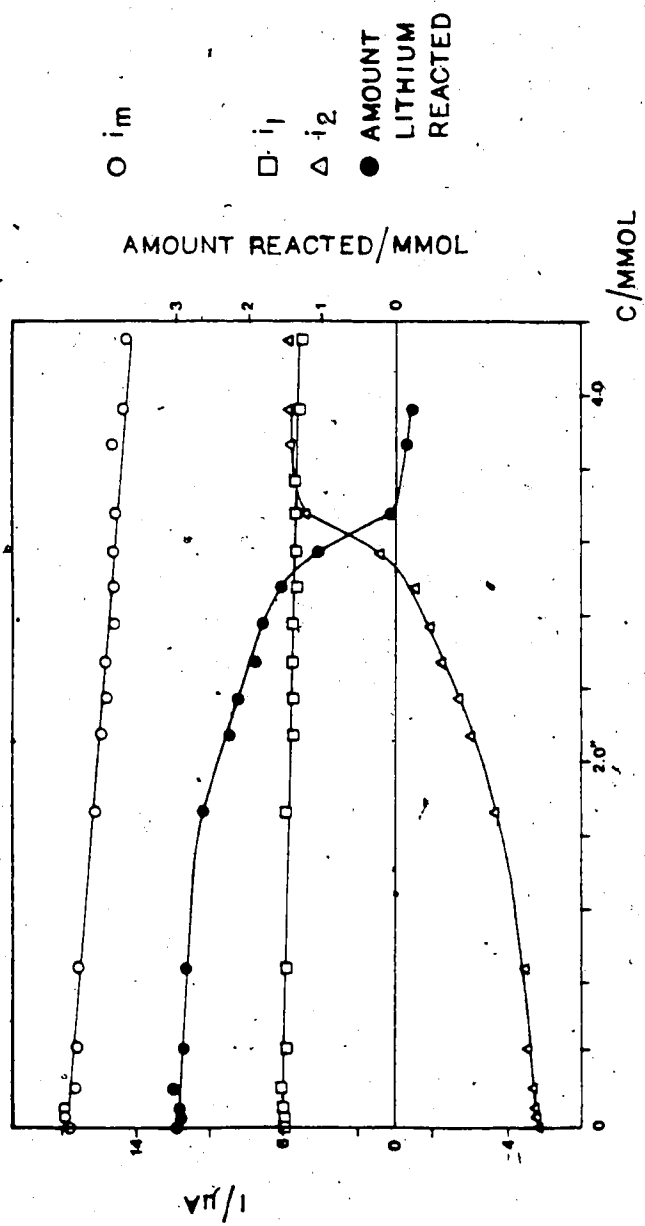remained approximately constant until about 1.0 M water
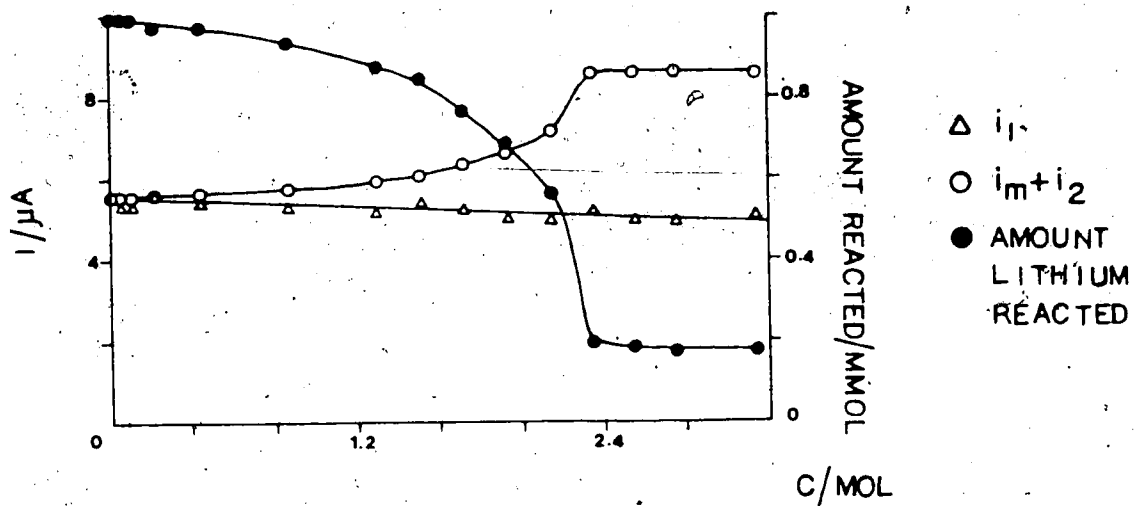
Figure 42. Effect of water addition on the limiting
currents and amount of lithium cation reacted
for a mixture of 1.00 mM fluoranthene and 1.02
mM lithium cation concentration in DMF at 25°C.
Horizontal axis show water concentration.
Mercury column 57.0 cm.
il:  limiting current for fluoranthene
     reduction
im + i2:  combined limiting current for lithium
          cation and fluoranthene anion radical
          reduction

and then increased before leveling out at a water con-
centration of 2.34 M. The value of im + i2 at the

final water concentration of 3.14 M was 8.6 uA. From

Figure 41, the limiting current i2 for the second wave

of fluoranthene at 3.14 M water was 5.3 uA. Also, from

Figure 35, it can be calculated that at 3.14 M water, the

limiting current for 1.02 mM Li+ is 3.6 uA. The sum of

these two waves at 3.14 M water therefore is 8.8 uA which

is close to the value of 8.6 uA for the mixture. The mM

Li+ reacted plot (Figure 42) shows that in the absence of

water, a value of 1.0 was obtained which decreased and

approached zero at high water concentrations.

Figure 43 shows the result for the experiment where

the water concentration was fixed at 1.72 M and Li+ was

added to a solution of 1.00 mM fluoranthene in DMF. The

value of the first wave (i1) was constant whereas the

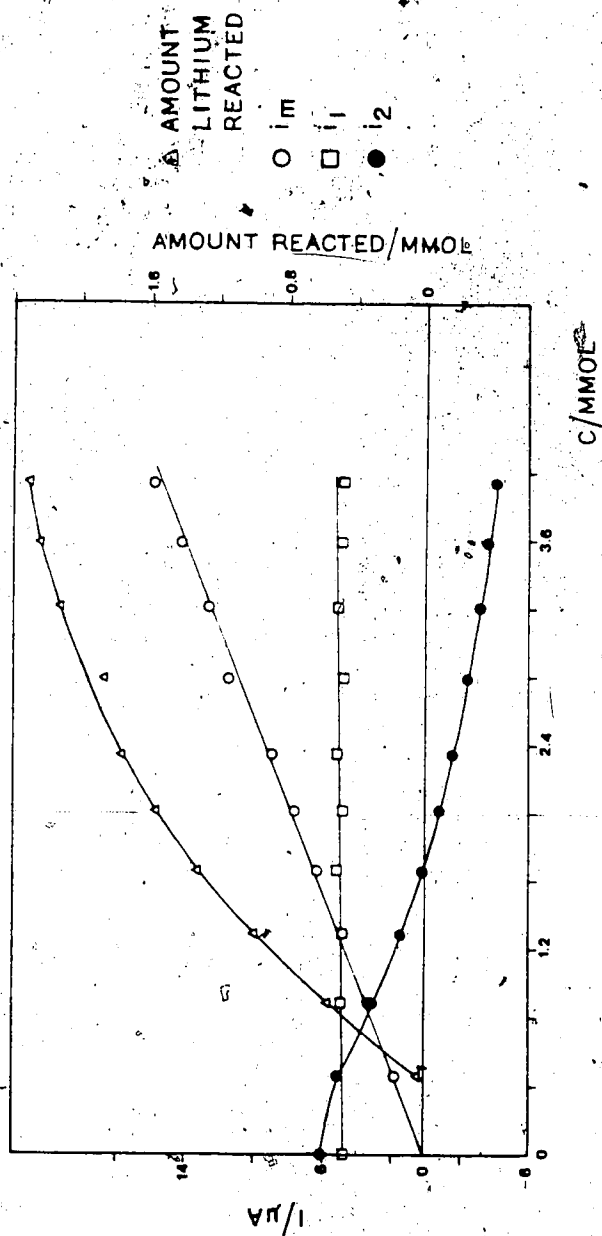im + i2 limiting current showed more complex behavior.
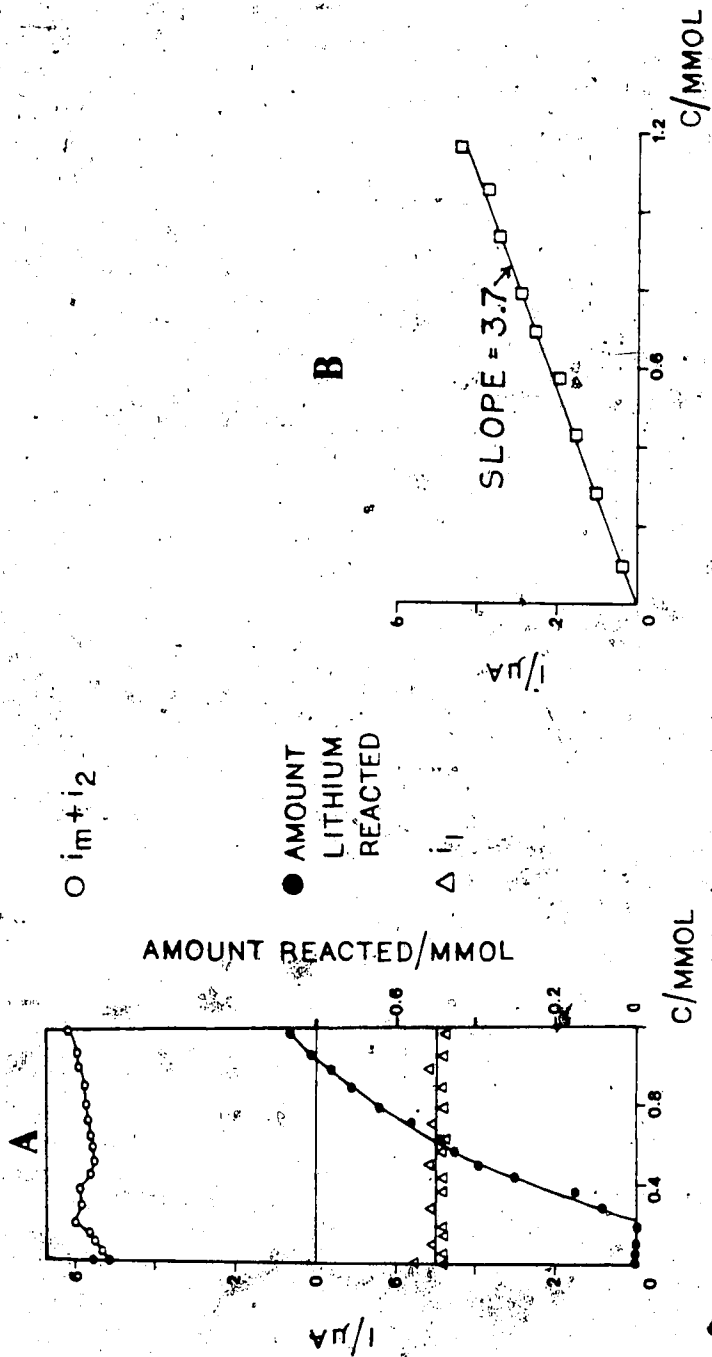
Figure 43. A. Plots of limiting currents and amount of lithium cation reacted versus lithium cation concentration for mixtures of fluoranthene and lithium cations containing 1.72 M water in DMF at 25°C.

B. Calibration plots for lithium cation in DMF solutions containing 1.72 M water. Fluoranthene concentration fixed at 1.00 mM. Mercury column 57.0 cm.

i1: limiting current for fluoranthene reduction

im + i2: combined limiting current for lithium cation and fluoranthene anion radical reductions

This result is best presented as the plot of mM Li+

reacted vs Li+ concentration. Since the Li+ reduction

wave and the dianion wave were not resolved, to perform

the calculations on the mM Li+ reacted, a calibration

plot for Li+ reduction at 1.72 mM water was obtained.

The limiting currents from this plot (Figure 43) were

then used in subsequent calculations. As in all the

other cases, there was an initial induction region

corresponding to about 0.20 mM Li+, before there was any

reaction between the fluoranthene dianion and Li+. After

the induction region, the mM Li+ reacted increased as

can be observed from Figure 43.

In Figure 44, the results of water addition to a

solution containing 1.00 mM fluoranthene and 2.45 mM

Na+ are presented. The limiting currents for the first

(il) and second (im) waves again show small decreases

due to water addition. In the absence of water, the
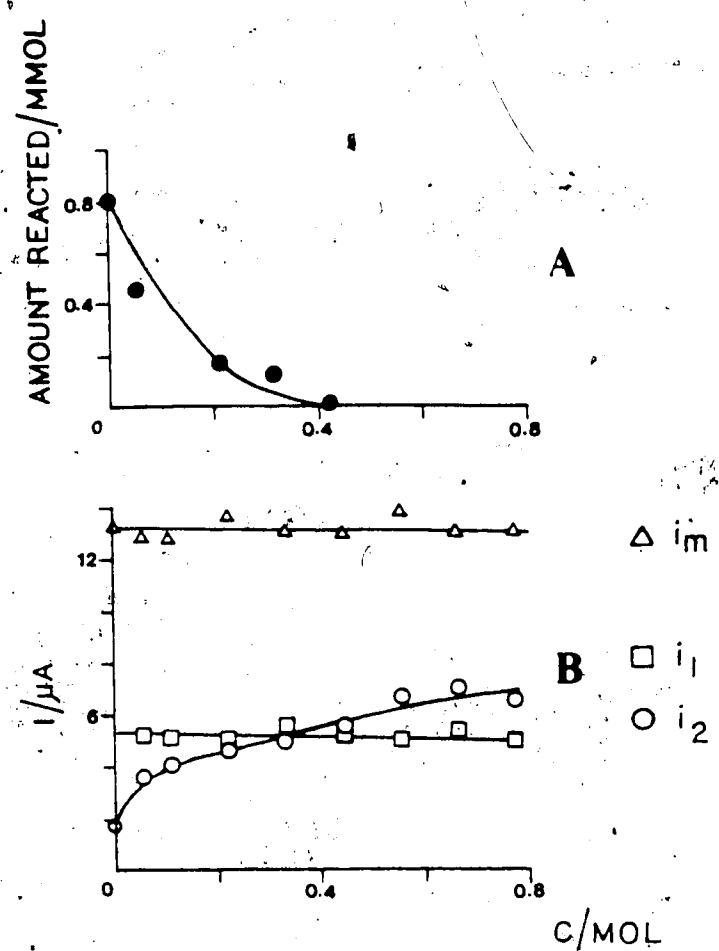
Figure 44.  A.  Effect of water addition on the amount of
               sodium cation reacted for a mixture of
               1.00 mM fluoranthene and 2.45 M sodium
               cation in DMF at 25°C.
           B.  Effect of water on the limiting currents
               for the same mixture above.
           Horizontal axis show water concentration.
           Mercury column 57.0 cm.
           i1:  limiting current for fluoranthene
                reduction
           im:  limiting current for sodium cation
                reduction
           i2:  limiting current for fluoranthene anion
                radical reduction

dianion wave gave a depressed current corresponding to

only 0.8 mM Na+ reacted. This is slightly lower than the

value of 1.0 mM expected with addition of water. Current

depression was again lifted with water addition.


4.4 Discussion

For the An,Li+ system in DMF at 2.00 mM anthracene

and 3.00 mM Li+ (Figure 34), it is again confirmed that

there is a strong interaction between An= and Li+. The data

show that at concentrations above 0.60 mM An and 0.90 mM

Li+ the amount of Li+ reacted with An= is 100%. A 100% reac-

tion is expected since it has been shown that An,Li+ reacts

in the ratio 1:3 whereas in this case the An,Li+ ratio is

only 1:1.5. The proposal that there is a competition bet-

ween trace proton donors and metal cations for An= was veri-

fied by the results obtained at low concentrations in the

dilution experiment. Obviously, at concentrations below

0.09 mM anthracene and 0.15 mM Li+, the rate of protona-

tion of An= is faster than An,Li+ interaction so that

the former predominates.  At concentrations in between

those mentioned, both processes occur to a varying degree.

The addition of water does not seem to affect the

electrochemical behavior of the aromatic hydrocarbons and

the alkali metal cations very much.  The stability of the

anion radicals is evidenced by the slopes of the E vs

log ((id-i)/i) plots. These plots show that there is no

deviation from one-electron reversible reduction behavior.

The small changes in Eh values of the first reduction wave

of the hydrocarbons and the decrease in the limiting

currents are attributed to changes in dielectric properties

of the solvent and diffusion constants of the species.  The

limiting current of the second wave is affected to the same

extent as the first wave and approximate equality of the

wave heights at all water concentrations used are main-

tained. However, the Eh values are affected more, shifting

positive by about 50 mV for anthracene and 90 mV for

fluoranthene. Further, the slopes of the E vs $\log((id-i)/i)$

plots tend to increase in the presence of water, indicating

the increasing irreversibility of the second wave arising

from increasing proton addition to the dianions. These

effects have been discussed in previous studies (4,25).

At concentrations of water in DMF in the region of 5% or

less, water is effectively solvated and is thus unable to

react with the anion radicals of both anthracene and

fluoranthene. Similar results have been obtained for aromatic

hydrocarbons in DMF and dioxane (4,25). Therefore, in the

concentration range used, the addition of water does not

affect the mechanism of reduction of anthracene and fluor-

anthene in DMF which involve two successive one-electron

transfers, the first of which forms a stable anion radical

and the second the unstable dianion.

The same can not be said of acetonitrile. Results

obtained for the reduction of anthracene and fluoranthene

in the presence of water in acetonitrile have indicated

that there is a change in the mechanism of hydrocarbon

reduction. As a result no further studies were conducted

in this solvent and the results were not presented in the

previous section. However, it was observed that in the

presence of water, the stability of the anion radicals is

affected. The first wave was observed to increase in height

at the expense of the second wave which suffers a reduction

in wave height. The same results have been observed in

dioxane-water mixtures with increasing water concentration

(23). Therefore the mechanism now becomes

$$R + e = R^{\overline{\cdot}} \qquad E1 \qquad (I)$$

$$R^{\overline{\cdot}} + H_2O = RH^{\cdot} + OH- \qquad (II)$$

$$RH^{\cdot} + e = RH- \qquad E2 \qquad (III)$$

$$RH- \ + \ H_2O \ = \ RH_2 + OH- \qquad (IV)$$

$$R^{\pm} \ + \ e \ = \ R= \qquad E3 \quad (V)$$

$$R= \ + \ H_2O \ = \ RH- + OH- \qquad (VI)$$

$$RH- \ + \ H_2O \ = \ RH_2 + OH- \qquad (VII)$$
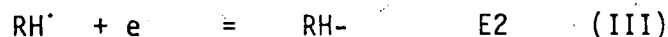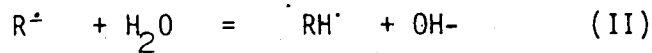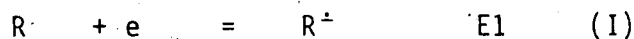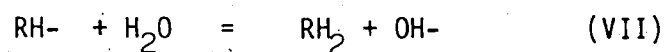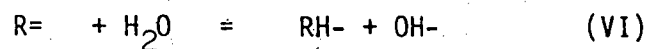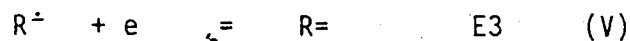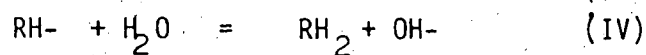
For alternant hydrocarbons e.g. anthracene, it is known

that E2 is positive of E1. At sufficiently high water

concentrations, the second wave is nonexistent and the

first wave doubled in height corresponding to a two-

electron wave. It is apparent that the ability of DMF to

complex water causes the water activity to be lower in DMF

than in acetonitrile, which has very low acidic and basic

properties.

The results obtained for the addition of water to the

An:Li+,Na+ and Fa:Li+,Na+ systems in DMF further substan-

tiates the conclusion made in Chapter 3 and the discussion at

the beginning of this chapter. For the solution mixture

studied, namely 1.00 mM An and 3.83 mM Li+, 1.00 mM An and

3.92 mM Na+, 1.00 mM Fa and 1.02 mM Li+, and 1.00 mM Fa and

2.45 mM Na+, the results (Figures 37, 39, 42, 44) in the

initial absence of water confirmed the stoichiometries of the

dianion-cation interaction obtained in Chapter 3. It is

important to note that in all the experiments with so many

variations in mixing, the stoichiometries have always remained

the same. Here, the An,Li+ stoichiometry was again found to

be 1:3, the An,Na+ gave 1:2 and both the Fa,Li+ and Fa,Na+

systems gave 1:1 stoichiometry.

The limiting currents of the dianion wave in all

cases behaved as expected in the presence of water. The

highly depressed values for An:Li+ and An,Na+ in the

absence of water began to increase on addition of water,

this indicative of decreased dianion-cation interaction.

At high enough water concentrations, the limiting currents

approached a value equal to that for the reduction of 1.00

mM An alone. This means that the protonation reaction

dominates the dianion-cation interaction. The same can be

said of the Fa,Na+ system except that the interaction in

the absence of water leads to a smaller depressed value for

the Fa,Li+ system. The calculation in the previous section

again showed that in the presence of enough water, the im +

i2 limiting current gave a value expected in the total

absence of Fa,Li+ reaction.

Clearly, the disappearance of current depression

in the presence of water gives evidence that hydroxyl

ions are not responsible for current depression. Further,

the results complement that obtained in the dilution

experiment. In the dilution experiment, the concentration

of the hydrocarbon and the metal ions are brought down to

a level where the trace proton donors can compete favorably

for the dianions whereas the addition of water brings the

concentration of proton donors up to a level for the same

effect.

For the above cases (Figures 37, 39, 42; 44) little

need be said concerning the variations of the il,

il+im and im limiting currents with the addition of

water because the values and the slopes found in all

cases were in agreement with what has been said in

Chapter 3 except for small differences due to changes in

diffusion constants arising from the addition of water.

However, the plots of amount of metal cation reacted vs.

water concentration show a very interesting difference

between Li+ and Na+. From Figures 37, 39, 42 and 44, it

can be seen that in the case of Li+ with both An and Fa,

the amount of Li+ reacted decreased only slowly at lower

concentrations of water whereas Na+ with both the aro-

matic hydrocarbons decreased sharply with the addition of

water. This points strongly to a faster dianion-Li+

reaction as compared to the dianion-Na+ reaction.

The establishment of a competitive reaction between water and metal cations for dianions provides the basis for kinetic studies of dianion-cation reaction. This can be done if conditions are controlled so that both interaction and protonation reactions can proceed. These conditions can be fulfilled with the proper choice of water concentration so that the protonation reaction does not far outrun the dianion-cation reactions for the range of metal cation concentrations used (up to 4 mM). Thus, from the results of water addition experiments (Figures 37, 39, 42, 44) the water concentration chosen for the An:Li+ system was 1.72 M and for the An:Na+ system was 2.14 M. The results for these experiments where the water concentration is fixed has been reported in the previous section (Figures 38, 40, 43). Again, the variation of the limiting currents il, il+im and im with metal concentration shows (except for small decreases in values due to changes in

diffusion constants as a result of the presence of water)

essentially the same behavior. The depression of the dianion

wave for the An,Li+ and An,Na+ systems, as expected,

was smaller as compared to the situation where no water was

added (Figures 38, 40). In the An,Li+ case, the current had

only small negative values at high Li+ concentrations.

In the An,Na+ system, no negative values were obtained at

all Na+ concentrations. However, the fact that current dep-

ression was observed shows that dianion-cation interaction

occurred.

Complex behavior was seen for the second wave of the

Fa,Li+ system in DMF. In the absence of water, this wave,

which corresponds to the combined $Fa^-$ and Li+ reductions,

remained constant with the addition of Li+ slightly past

1.00 mM Li+. However, in the presence of water, at small

Li+ concentration the im + i2 limiting current increased as

the protonation reaction is more favorable under these

conditions. At higher concentrations of Li+, the current

decreased since the Fa,Li+ reaction became more effective

and could compete favorably (Figure 43).

Induction regions were observed in all cases for

the amount of cation reaction vs cation concentration

plots (Figures 38, 40, 43). The explanation for these is

quite simple. Since considerable amounts of water are

present initially, protonation of the dianions proceeds

very fast. Introduction of small amounts of the metal

cations initially have negligible effects. However, with

continued addition of metal cations, a concentration of

the cations is reached where the dianion-cation reaction

is initiated, and at increasing metal cation concentra-

tion, the rate increases and becomes competitive with

protonation.

The kinetic treatment for the competitive reactions

is based on the following model and assumptions:

$$M+ \qquad\qquad M+ \qquad\qquad M+$$

$$\longrightarrow R=,M+ \longrightarrow R=,2M+ \longrightarrow \cdots$$

$$k1$$

$$R=$$

$$k2$$

$$H_2O \qquad\qquad H_2O$$

$$\longrightarrow RH- \longrightarrow RH_2$$
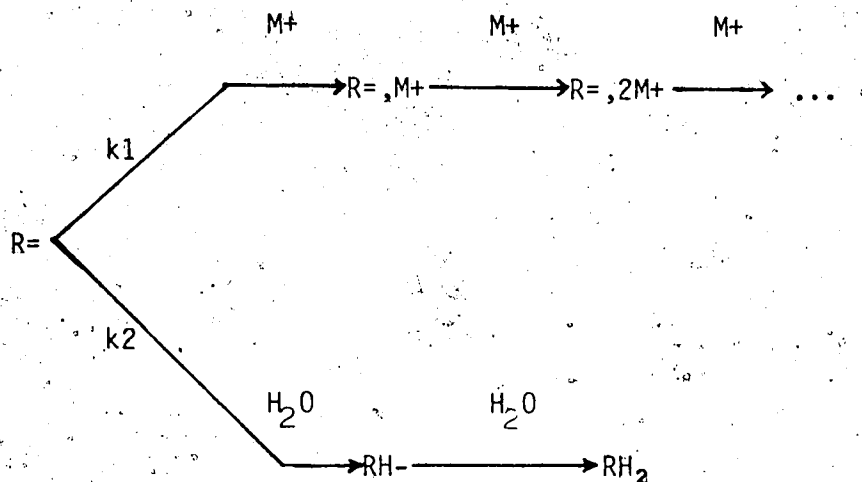
where R= represents the aromatic hydrocarbon dianions,

M+ the metal cations, and k1, k2 the rate constants for

the dianion-cation reaction and the protonation reaction

respectively.

It is assumed that the R= which are formed are rapidly

and completely destroyed through reaction with M+ and

water.  This is reasonable because of the very reactive

nature of the dianions and the well known fact that the

dianions are rapidly protonated even in aprotic solvents

without the addition of water.  Further, it is assumed

that the R:M+ reactions are strong and follow fixed

stoichiometries. These stoichiometries have been

established to be 1:3 for An,Li+, 1:2 for An,Na+,

1:1 for Fa,Li+ and Fa,Na+. Therefore, even though

the R,M+ reactions may be stepwise, after the initial

reaction of one M+, the complexation continues until the

stoichiometries are satisfied. For this reason, no

kinetic studies have been made for K+ and Rb+ since

results have shown that R:K+,Rb+ reactions are not

strong reactions and therefore the above assumptions will

not be true for those cations.

From the above discussion, it follows that

$$[R=]total = [R=]reacted\ with\ M+ + [R=]reacted\ with\ water \tag{4.1}$$

Also,

$$y = \frac{[R=]reacted\ with\ M+}{[R=]total} = \frac{k1[M+][R=]}{k1[M+][R=] + k2[H_2O][R=]} \tag{4.2}$$

and

$$x = \frac{[R=] \text{reacted with } H_2O}{[R=] \text{total}} = \frac{k2[(H_2O)[R=]}{k1[M+][R=] + k2[H_2O][R2=]} \quad (4.3)$$

Rearrangement gives

$$y = \frac{[R=] \text{reacted with } M+}{[R=] \text{total}} = \frac{[M+]}{[M+] + (k2/k1)[H_2O]} \quad (4.4)$$

and

$$x = \frac{[R=] \text{reacted with } H_2O}{[R=] \text{total}} = \frac{[H_2O]}{(k1/k2)[M+] + [H_2O]} \quad (4.5)$$

The above approach is similar to the common method of determining relative rates of competing reactions from analysis of reaction products. Both the values of x and y are experimentally available. For the present purpose the equation above involving y is used. Thus the parameter of y is calculated from the values of amount of cation reacted which were plotted in Figures 38, 40, and 43. For example, in the

case of An,Li+ system, y is obtained by dividing the amount

of Li+ reacted by 3 and then dividing by the bulk concen-

tration of anthracene, which is 1.00 mM.  Similarly, for

the An,Na+ system, the amount of Na+ reacted is divided by

2 and the Fa,Li+ system by 1.  It should be pointed out

that these divisors are merely the stoichiometries of the

dianion-cation complexes and follow from the assumptions

made earlier.  The y values so obtained are plotted against

metal concentration in Figures 45-47.  From these plots,

it can be seen that the initial induction regions occur in

all cases.  These are expected because the data are

calculated from those of Figues 38, 40 and 43 where the

induction region exists.  From equation (4.4), it can be

seen that when $(k2/k1)[H_2O] \gg [M+]$, then equation (4.4)

reduces to

$$y = \frac{[M+]}{(k2/k1)[H_2O]}$$  (4.6)
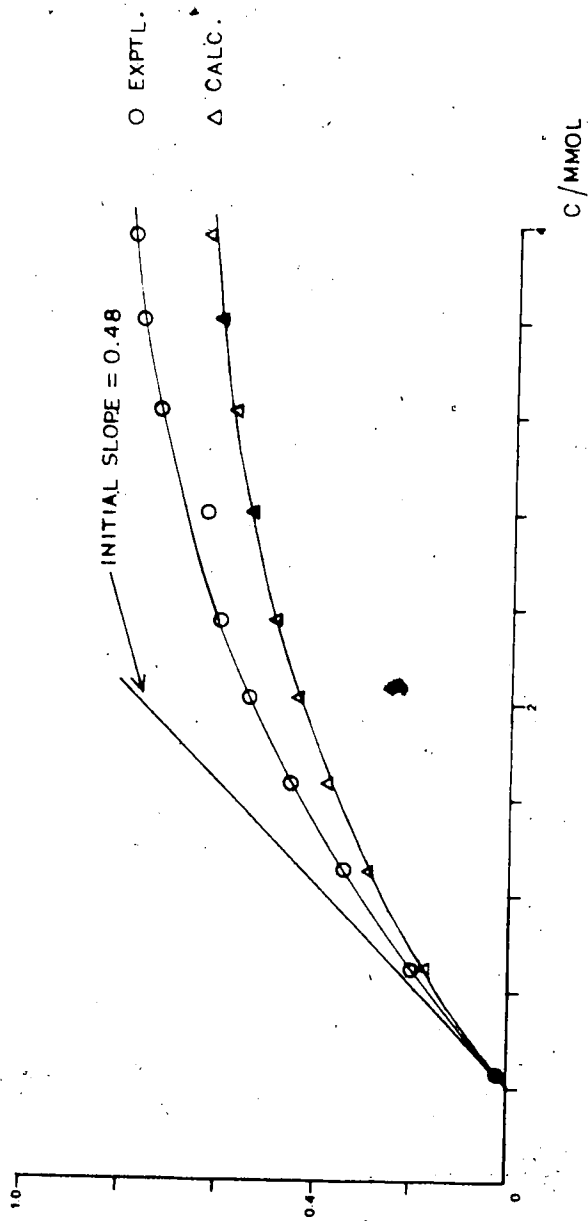
Figure 45. Plot of Y versus lithium cation concentration for mixtures of anthracene and lithium cation containing 2.14 M water in DMF at 25°C. Anthracene concentration fixed at 1.00 mM. Mercury column 57.0 cm.
Y = [An=]reacted/[An=]total
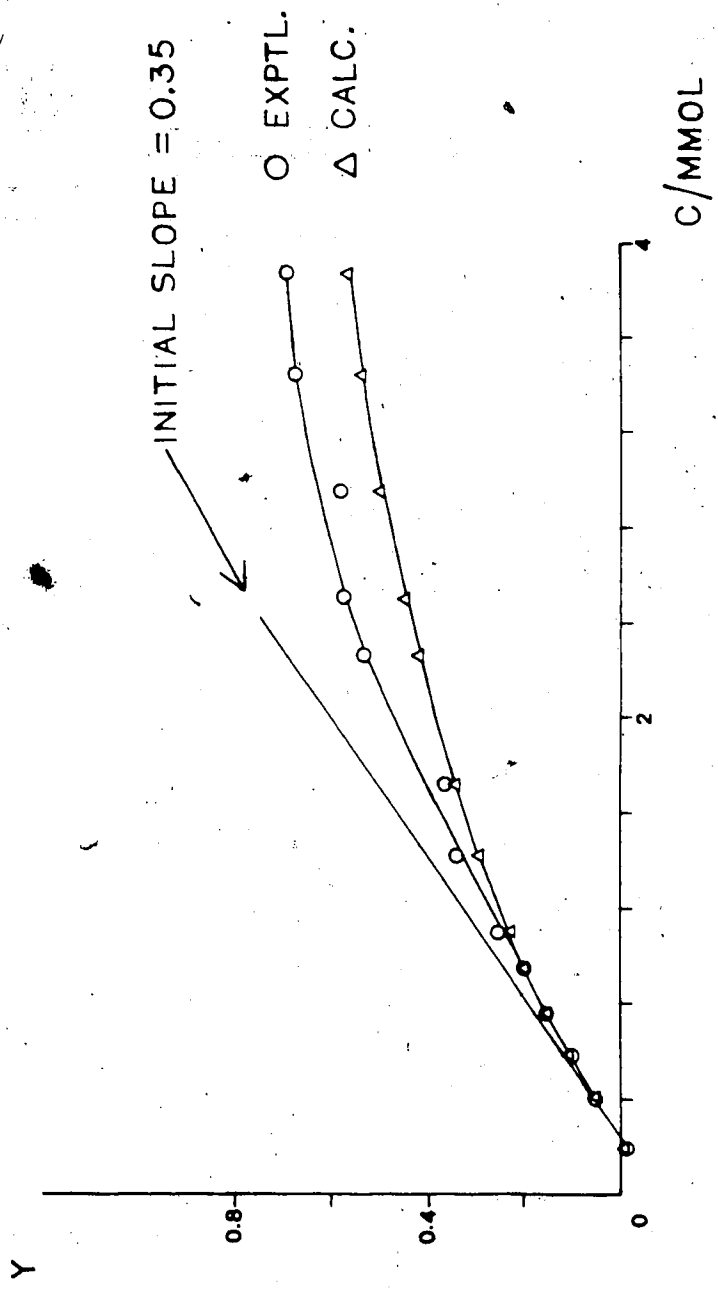
Figure 46. Plot of Y versus sodium cation concentration for mixtures of anthracene and sodium cations containing 0.22 M water in DMF at 25 C. Anthracene fixed at 1.00 mM. Mercury column 57.0 cm. $Y = [An=]reacted/[An=]total$
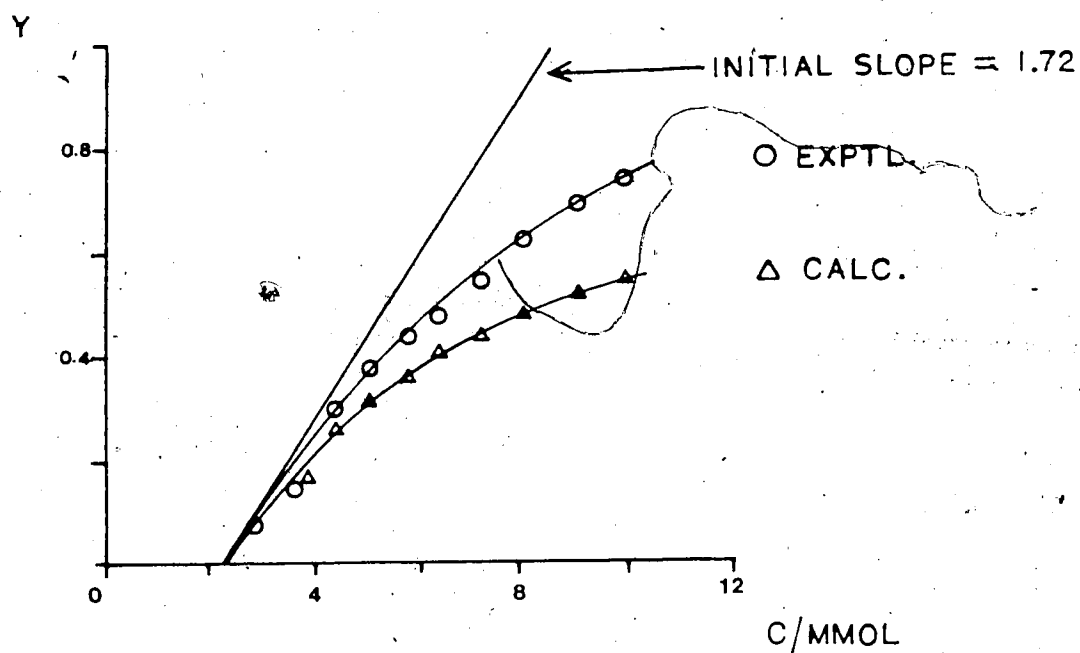
Figure 47. Plot of Y versus lithium cation concentration
for mixtures of fluoranthene and lithium cation
containing 1.72 M water in DMF at 25°C.
Fluoranthene fixed at 1.00 mM. Mercury column
57.0 cm. Y= [Fa⁼]reacted/[Fa=]total.

Therefore, at low cation concentrations, the plots

should be approximately linear with slope $(k1/k2)[H_2O]$. To

a first approximation, this is found to be so as can be

seen from Figures 45-47. The values of the slopes thus

obtained are tabulated in Table 3. From these slopes, the

ratios of the rate constants $k1/k2$ are calculated. These

ratios are 1.0e3, 80 and 2.8e3 for the An,Li+,

An,Na+ and Fa,Li+ systems respectively. If the rate

constants $k2$ for the protonation of the dianions are known

then the rate constants $k1$ for the dianion-cation inter-

actions can be calculated. There have been many studies

of the protonation of the anion radicals of aromatic

hydrocarbons by such proton donors as alcohols and water

(228-230). However, the protonation of dianions has not

been thoroughly studied. Values ranging from 1.0e8 to

1.0e10 /M s have been given (231,232). No data for the

protonation of fluoranthene dianion is available. Here

Table 3.  Estimated Rate Constants**

| System | $[H_2O]$ /M | $k1/k2[H_2O]$ | $k1/k2$ | $k2$ /M$^{-1}$s$^{-1}$ | $k1$ /M$^{-1}$s$^{-1}$ |
|---|---|---|---|---|---|
| An:Li+ in DMF | 2.14 | 0.48 | 1.0e3 | 1.0e9 | 1.0e12 |
| An:Na+ in DMF | 0.22 | 0.35 | 80 | 1.0e9 | 0.8e10 |
| Fa:Li+ in DMF | 1.72 | 1.62 | 2.8e3 | | - |
| Fa:Na+ in DMF | - | - | - | | |

**Continued next page.

Table 3 Continued

| System | $[D_2O]$ /M | k1/k2$[D_2O]$ | k1/k2 | k2 /$M^{-1}s^{-1}$ | k1 /$M^{-1}s^{-1}$ |
|---|---|---|---|---|---|
| An:Li+ in DMF | 2.14 | 0.45 | 0.9e3 | 1.1e9 | 1.0e12 |
| An:Na+ in DMF | 0.22 | 0.38 | 80 | 1.0e9 | 0.8e10 |
| Fa:Li+ in DMF | - | - | - | | |
| Fa:Na+ in DMF | - | - | - | | |

the rate constant for the protonation of anthracene

dianion will be taken to be 1.0e9 /M s.  The rate constants

for the An=,M+ interaction are 1.0e12 and 8.0e10 /M s

for Li+ and Na+ respectively.

The rate constants for the diffusion controlled

reactions between two ions is given by the Debye extension

of the Smoluchowski equation (233;234)

$$k(d) = [(8RT/3000n")] [O/(e^{O} -1)] \qquad (4.7)$$

$$where \quad O= Z(A)Z(B) \; e^{2}/\ell kTa \qquad (4.8)$$

a=distance of closest approach of ions

$\ell$=dielectric constant of solvent

n"=viscosity

e=electronic charge

Z(A),Z(B) are the charge numbers of the ions.

The other terms have their usual meaning.

For DMF the viscosity is 0.802 c.p.(25°C) and at 25°C the

term 8RT/3000n" has the value 1.0e10 /M s.  Since the

dianions and metal cations have charges -2 and +1

respectively and assuming that the distance of closest

approach is approximately 2.8 Å (using 2.1 Å for the An=,

estimated from covalent bond lengths, and 0.7 Å for ionic

radius of lithium).

Then

$$\phi = \frac{(-2)(+1)(4.8e-10)}{(3.7)(1.38e-16)(296)(2.8e-8)}$$

$$= -109$$

Therefore k(d) = 1.1e12/M s.

Based on a similar approach, k(d) for Na+, K+ and Rb+ (ionic

radii 1.0, 1.3, and 1.5 Å respectively) can be calculated to

be 9.8e11, 9.0e11, and 8.5e11/M s.  The experimental value

obtained for the An:Li+ system in DMF was 1.0e12/M s which

is in very good agreement with the calculated value above.

This value is over an order of magnitude larger than for Na+

which has an experimentally determined rate of 8.0e10/M s.

Therefore, the rate of ion pair formation obtained for

An=:Li+ in DMF is very close to the diffusion controlled

limit and that for An=:Na+ about 10 times less than diffusion

controlled. These are not too surprising because ion pair

formations have been consistently found to be very fast reac-

tions. For example, in tetrahydrofuran, the association of

benzophenone anion radical has a rate constant of 1.1e11 and

in carbon tetrachloride-nitrobenzene mixture, tetra-n-butyl-

ammonium bromide has an association rate constant of 1.3e11/

M s (see reference 217, p. 443). It was noted that these

rate constants are within a factor of 4 of the computed values

for diffusion control.

The experimentally determined rate constants are

expected to be a bit high because the actual activity of water

in DMF is in all probability lower than the added value. This

is because DMF molecules have the ability to complex water

and therefore decrease its activity.  Further, very

accurate values for the rate constant for protonation of

anthracene were not available.  The value of 1.0e9/M s

used in this study was an estimated figure.  Therefore an

error range of about half an order of magnitude is to be

expected for the determined rate constants, which would

occur on the high side from the discussion above.  Even so,

considering the approximate nature of the reactions, the

experimentally determined values are good estimates

considering what is known about the rate constants for ion

pair formation and taking the other factors into account.

The computed values for the rate constants, based on

the distance of closest approach being the sum of the radius

of the anthracene molecule and the ionic radius of the

cation, shows that the An=:Li+ system should be about 10

times faster than the An=:Na+ system.  However, experimentally,

An=:Li+ was found to be 100 times faster. For contact ion

pair formation, the solvent sheath has first to be removed.

The solvation of Li+ cation by DMF molecules is much stronger

than that of Na+. The fact that the formation of An=:Li+ ion

pair being 100 times faster than the An=:Na+ ion pair does

not reflect the differences in solvation. The possible

explanation is that the initial An:M+ reaction involves a

solvent separated ion pair which on formation expels the

solvent molecules to give the contact ion pair which is the

thermodynamically favored species.

Since no data for the rate constant for the protona-

tion of Fa= is available, the rate constant for Fa:Li+

reaction cannot be calculated. Polarographic data point

to the fact that Fa= is less basic than An= since the Eh

value for the Fa= wave is positive to that of the An= wave

by 170 mV. Therefore, it is expected that protonation of

Fa= is slower. The higher value of 2.8e3 obtained

for k1/k2 for this system as compared to 1.0e3 for

for the An,Li+ system is likely due, in major part, to

this lower basicity.

Figures 45-47 also show the plots of the computed

values of the y parameter in equation (4.4). In order to

obtain these computed values, the experimental slopes

which corresponded to $(k1/k2)[H_2O]$ are substituted into

equation (4.4). This equation is then transformed into

$$ycalc = \frac{([M+] - a)}{slope + ([M+] - a)} \qquad (4.9)$$

where the constant a refers to the concentration of M+

corresponding to the induction region. As can be seen

from the figures, the agreement at low M+ concentrations

is good but at higher M+ concentrations the computed values

are lower than the experimental values. However, since

the other constants are derived from data at the low

concentration end, these deviations are not of too much

concern.

As a further check of the model, experiments were

also carried out for the An:Li+ and An:Na+ systems

employing heavy water instead of water. The same concen-

trations of $D_2O$ as $H_2O$ were used and the results were

treated similarly. Table 3 shows that the ratios of

k1/k2 for the An:Li+ and An:Na+ systems are 9.0e4 and

80 respectively. Since the rate constants for

association of the dianion and cations are independent of

whether $H_2O$ or $D_2O$ are used and therefore should remain

unchanged, the values of k2 are calculated to be 1.1e9/

M s for the An:Li+ system and 1.0e9 for the An:Na+ system.

These values are essentially the same as the assumed value

of 1.0e9 /M s for the protonation of An=. Therefore, it is

concluded that the protonation of An= does not show any

kinetic isotope effect. Rainis and Szwarc(231) have observed,

that due to the high basicity of $An=$, the transition

state of its protonation resembles the final state and

therefore significant kinetic isotope effect is not

expected. The present results support this observation.

Chapter 5   Electrochemical Studies of Tetracyanoethylene (TCNE)
            and 7,7,8,8-Tetracyanoquinodimethane (TCNQ).
            The Effect of Countercations.

## 5.1   Introduction

As already mentioned in Chapter 1, there has been great

interest in TCNE and TCNQ since their discovery.  These

substances have exceptional properties.  In particular,

intense interest is generated in the organic conducting

salts and high conducting charge-transfer complexes formed

by those compounds (153,155).

The presence of the four electron-withdrawing cyano

groups means that the olefinic and quinoid functionalities

of TCNE and TCNQ respectively are electron deficient.  The

ease with which these molecules are reduced is quite

remarkable.  For example, they have been reported to

undergo a one-electron transfer to form the anion radicals

by metals (124,152), by UV light irradiation (133), by

CN- ion (124) and even by certain basic solvents such as

dimethylsulfoxide and dimethylformamide. Formation of

anion radicals in these solvents appears to be faster in

the presence of light (135-137). The anion radicals are

stable in solution in the absence of oxygen and water

(124,163).

Relatively few electrochemical studies have been made.

The determination of fundamental electrochemical parameters

such as the reduction potentials and standard rate con-

stants are useful for testing of theories and in many

applications. For example, electrode potentials can be

correlated to molecular orbital energies and electron affi-

nities. The conducting salts and complexes formed by TCNE

and TCNQ have been employed in batteries (235), photocells

(236), electrochromic systems (237) and potentiometric ion

selective sensors (238). Knowledge of electrochemical

parameters in general is necessary for better understanding

of these systems.

In general, the reduction of TCNE and TCNQ to their anion radicals has been found to be electrochemically reversible. Peover (128,129) found this to be so polarographically in dimethylformamide, acetonitrile, chloroform, and methylene chloride. He also found this to be so for the reduction of $TCNE^{-}$ to $TCNE^{=}$ in methylene chloride and $TCNQ^{-}$ to $TCNQ^{=}$ in chloroform and methylene chloride. The supporting electrolyte used was tetra-n-butylammonium perchlorate. Sharp studied the first reduction of TCNE and TCNQ at different electrodes and in different solvents (148,149). In acetonitrile, the standard rate constants for TCNE were found to be 0.159 cm/s at platinum, 0.390 cm/s at gold and 0.0019 cm/s at graphite. For TCNQ, the values were 0.260, 0.208 and 0.0035 for platinum, gold and graphite respectively. Rate constants were also determined in dimethylformamide, dimethylsulfoxide and propylene carbonate at platinum and gold electrodes.

Diffusion coefficients for TCNE were found to be 1.91e-5

and 2.8e-6 cm/s in acetonitrile and propylene carbon-

ate respectively. In the case of TCNQ these values were

1.45e-5 cm/s in acetonitrile, 6.7e-6 cm/s in

dimethylformamide, 2.7e-6 cm/s in dimethylsulfoxide and

2.8e-6 cm/s in propylene carbonate.

Although these studies invariably found the first

reduction to be reversible, there seems to be some

inconsistency in the reduction of TCNE$^-$ to TCNE=. For

example, Mulvaney et al (239) reported this reduction to

be reversible at 100 mV/s scan rate, using lithium

perchlorate as supporting electrolyte in acetonitrile at

a platinum electrode. Sharp noted that this wave was

irreversible in acetonitrile at a graphite electrode using

lithium perchlorate as supporting electrolyte under similar

conditions (148). Jeanmaire et al (138) found this wave to

be quasireversible in acetonitrile using a platinum elec-

trode. However, the supporting electrolyte used was tetra-

n-butylammonium perchorate. They proposed a change in

geometry in going from a planar TCNE$^-$ to a nonplanar

TCNE= as a possible explanation. Pons et al (139) reported

similar results using a platinum electrode in acetonitrite

with tetra-n-butylammonium tetrafluoroborate as supporting

electrolyte. According to them this behavior could be due

to one of several causes such as complexation of the anion

radical by the electrolyte, distortion of the TCNE$^-$ or

adsorption of electrolysis products. FTIR spectroelectro-

chemistry confirmed the existence of adsorption.

The causes of the discrepancies could be the result of

electrode material or supporting electrolyte. To date, no

study of the countercation effect has been undertaken.

In Chapter 3, the electrochemical behavior of aromatic

hydrocarbons has been found to be dependent on the counter-

cations used. It should be interesting to examine these

effects on a different class of compounds. The presence

of the four cyano groups in TCNE and TCNQ imparts high

electron affinity to these molecules and also higher

stability to the negative ions as compared to the hydro-

carbons. Therefore, the dianions are not as reactive as

their aromatic hydrocarbons counterparts. As a result,

they are reduced at more positive potentials which means

that the use of solid electrodes does not present any

problems.

This chapter describes the use of cyclic voltammetry

and chronoamperometry to study the reduction of TCNE and

TCNQ to their anion radicals and dianions at glassy carbon

and platinum electrodes. The effect of different counter-

cations is also studied. The species formed during

electrolysis are identified using modulated specular

reflectance spectroscopy.

## 5.2 Experimental

### 5.2.1 Instrumentation

The modulated specular reflectance (MSRS) tech-

nique was described in Chapter 1. A schematic

diagram of the instrumentation is given in Figure 48.

The lamp source was a 200 watt Hg-Xe arc lamp. Light

from the source passed through a GCA MacPherson 201

monochromator. The light reflected from the electrode

was detected by means of a RCA 31000M photomultiplier

(PMT). The signal from the PMT was taken through a

Kronheit filter operated in the band pass mode to pass the

modulation frequency of interest. The output was taken

into the lock-in-amplifier (LIA, Bentham 223). The output

from the LIA, after going through a current-to-voltage

conversion and amplification stage, yielded the spectrum

of interest.
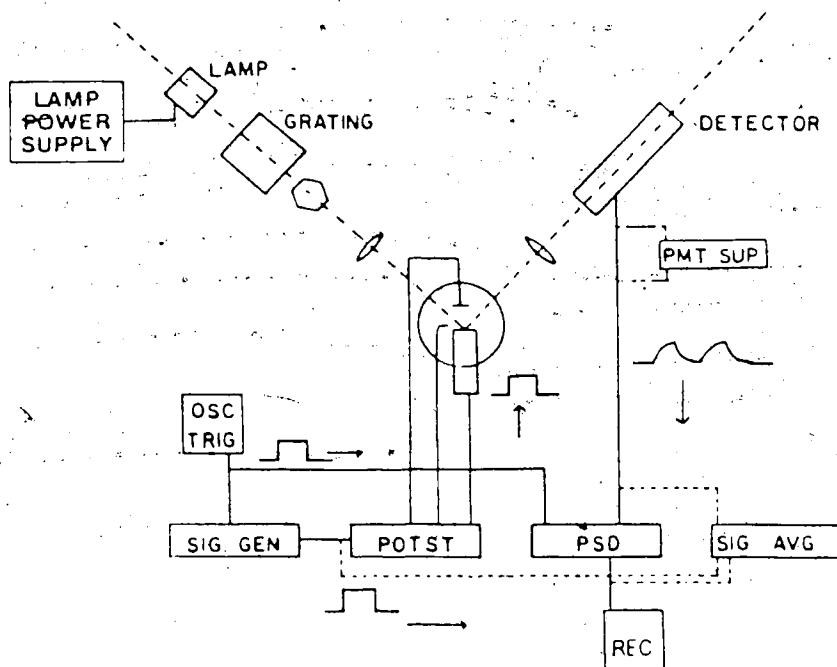
Figure 48.  Instrumentation for MSRS.
   POTST:      Potentiostat
   PSD:        Phase Sensitive Detector
   SIG AVG:    Signal Averager
   PMT SUP:    Photomultiplier Supply
   OSC TRIG:   Oscillator Trigger
   SIG GEN:    Signal Generator
   REC:        Recorder

The working electrode was a 7 mm diameter polished platinum button attached to the end of a brass rod which had been forced into a heated 9 mm (o.d.) Kel-F tube which shrunk on cooling to give a tight seal. The potential of this electrode was controlled by a HiTek DT 2101 potentiostat. Potential waveform pulses were supplied by a HiTek PPR1 waveform generator which was triggered by square wave pulses from a Global Associates function generator at the required frequency (40Hz). Normalized reflectance-time transients were signal averaged by a signal averager. The cell arrangement used for the MSRS experiment is shown in Figure 49. The quartz windows through which light passed in and out of the cell were positioned at 45 degrees each to the axis along the length of the electrode.

The electrochemical cell used in cyclic voltammetric and chronoamperometric experiments is shown in Figure 50. Two materials for the working electrodes were used. The

230



A — Secondary Electrode
B — Reference Electrode
C — Light Entry (Exit) Port
D — Working Electrode Mirror
E — $N_2$ Entry
F — $N_2$ Out
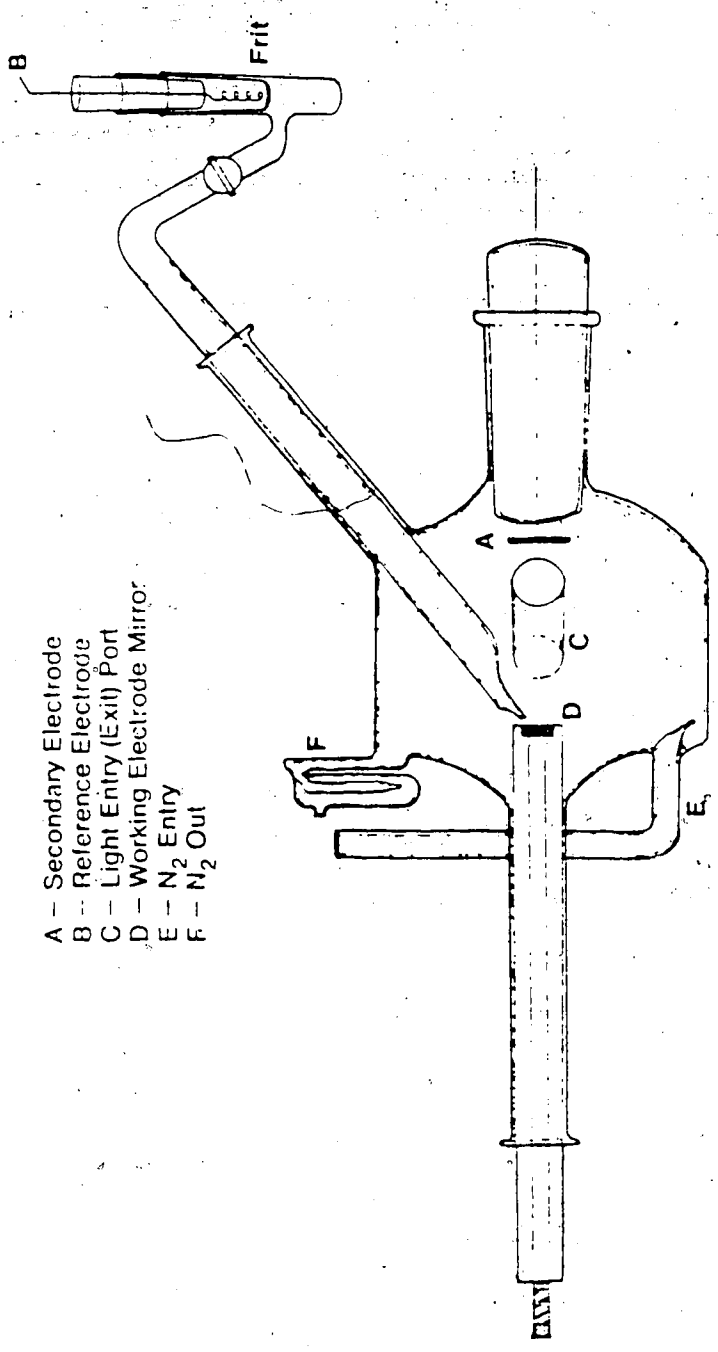
Figure 49. Optical cell for MSRS experiment.
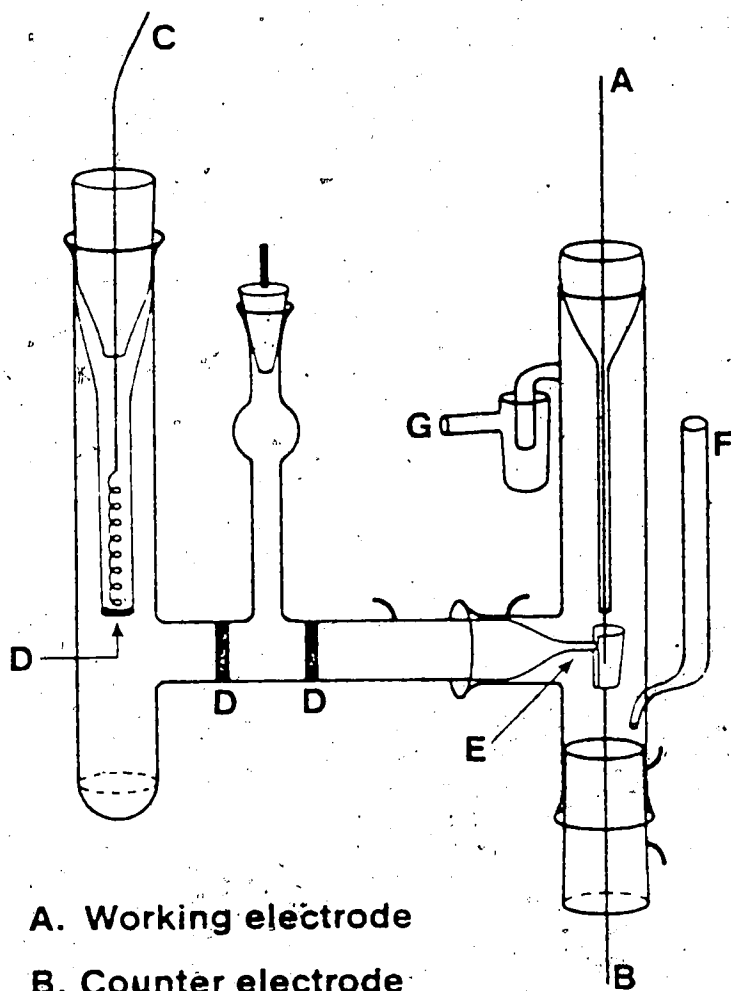
A. Working electrode

B. Counter electrode

C. Reference electrode

D. Frit

E. Luggin

F. Gas inlet

G. Gas Exit

Figure 50. Cell configuration for the voltammetric and chronoamperometric experiments.

platinum working electrode consisted of a platinum wire

sealed into glass and connected to the external circuit by

a copper lead soldered to the platinum wire. The carbon

electrode was made from a piece of glassy carbon rod (3 mm

diameter, Tokai) sealed into a glass tubing with epoxy.

The end of the carbon rod which was leveled with the end

of the glass tubing was polished to a mirror finish with

alumina on a polishing cloth. The result was a circular

planar glassy carbon electrode. Mercury was then put

into the glass tubing to contact the carbon rod. A piece

of copper wire was then dipped into the mercury and the

external contact was made to this copper wire. The

potentiostat used to control the potential of the working

electrode with respect to the reference electrode and the

waveform generator were the same instruments as those used

for the MSRS experiment. The potential ramp for the cyclic

voltammetric experiments and the potential steps for the

chronoamperometric experiments were introduced into the

adder input of the potentiostat. The reference electrode

(Ag/Ag+) was the same as that used for the polarographic

experiments (see Figure 3). The reference solution was

0.01 M AgNO3, 0.1 M in the supporting electrolyte in the

same solvent as that for the experiments. Recording of

experimental curves was made with a Linseis LX1000 recorder

which could be operated either in the x-y (voltage-current)

or y-t (current-time) mode.


5.2.2 Purification of Chemicals

Purification of lithium and sodium perchlorates,

tetra-n-butylammonium tetrafluoroborate and acetonitrile

has been described previously (see Chapter 3). Tetra-n-

ethyl perchlorate (TEAP) (Eastman, reagent grade) was

recrystallized twice from triply distilled water. It was

dried in vaccuo at 70°C. Commercial reagent grade TCNE

and TCNQ were obtained from Eastman. The TCNE was

recrystallized twice from chlorobenzene (148) and TCNQ

recrystallized twice from acetonitrile (240). The dried

crystals of TCNE melted at 200-201°C while those of

TCNQ melted at 294-295°C. These values agreed with those

reported in the literature (148).


5.2.3 Procedure

From Figure 50, it can be seen that the cell used

for cyclic voltammetric and chronoamperometric experiments

consisted of two separated parts. The part which included

the Luggin probe was filled with the background solution

i.e. the solvent containing 0.10 M of the supporting

electrolyte. The other compartment contained a solution

of the electroactive species of interest. Concentrations

of electroactive species used were in the millimolar range.

In all cases, experiments were performed at room tempera-

ture. This temperature was found to be $(23.0 \pm 0.5)°C$
throughout the period in which these experiments were
performed. Deaeration of solutions was carried out by
bubbling purified nitrogen through the cell.

The Luggin probe was placed as close as possible to
the working electrode to reduce iR loss. Further, positive
feedback was employed for the same purpose. It was
estimated that the iR loss under these circumstances was
not more than the error in reading potentials from the
recorded voltammograms $(\pm 5 mV)$. In all cyclic voltam-
metric experiments, the scan rate used was not more than
800 mV/s. For the chronoamperometric experiments, a
pulse time of 2 s was used.


5.3 Results

It is common practice in electrochemistry to use
"electrochemical area" rather than the "geometrical area"

of electrodes. This is because electrodes are not perfect-
ly smooth and therefore the actual area is always larger
than the geometrical area. One frequently used method in
determining electrochemical areas is by utilizing the
Cottrell equation (equation 2.12) which is given by


$$i = nFA\ D(0)^{\frac{1}{2}}\ C^{*}\ /(\pi t)^{\frac{1}{2}}$$


If a compound exhibiting well-behaved electrochemistry
and whose diffusion coefficient is known accurately is
used, then all the variables in the Cottrell equation can
either be measured or are known and therefore the area A
can be calculated. One such compound is anthracene. In
acetonitrile, the first reduction to the anion radical
shows a reversible one-electron wave. The diffusion
coefficient in acetonitrile (0.10 M TEAP)) at 25°C has
been found to be 2.55e-5 cm$^2$/s (241). Here the

concentration of anthracene used was 0.943 mM in acetoni-

trile (0.10 M TEAP). Figure 51 shows the cyclic voltam-

mogram for the first reduction of anthracene at a glassy

carbon electrode. From this cyclic voltammogram a poten-

tial of -2.500 V was chosen for the potential step so that

reduction is in the diffusion-controlled limit. The

chronoamperograms for the anthracene solution, as well as

for the background solution are also shown in Figure 51.

From these, the value of $(it)^{\frac{1}{2}}$ can be calculated with

correction for background current. Since the literature

value for the diffusion coefficients of anthracene was

quoted at 25°C and the experiment was conducted at 23°C, a

simple correction for this temperature difference can be

made by making use of the Stokes-Einstein equation.

$$D = kT/6\pi n''r \tag{5.1}$$

**(B)**



**(A)**
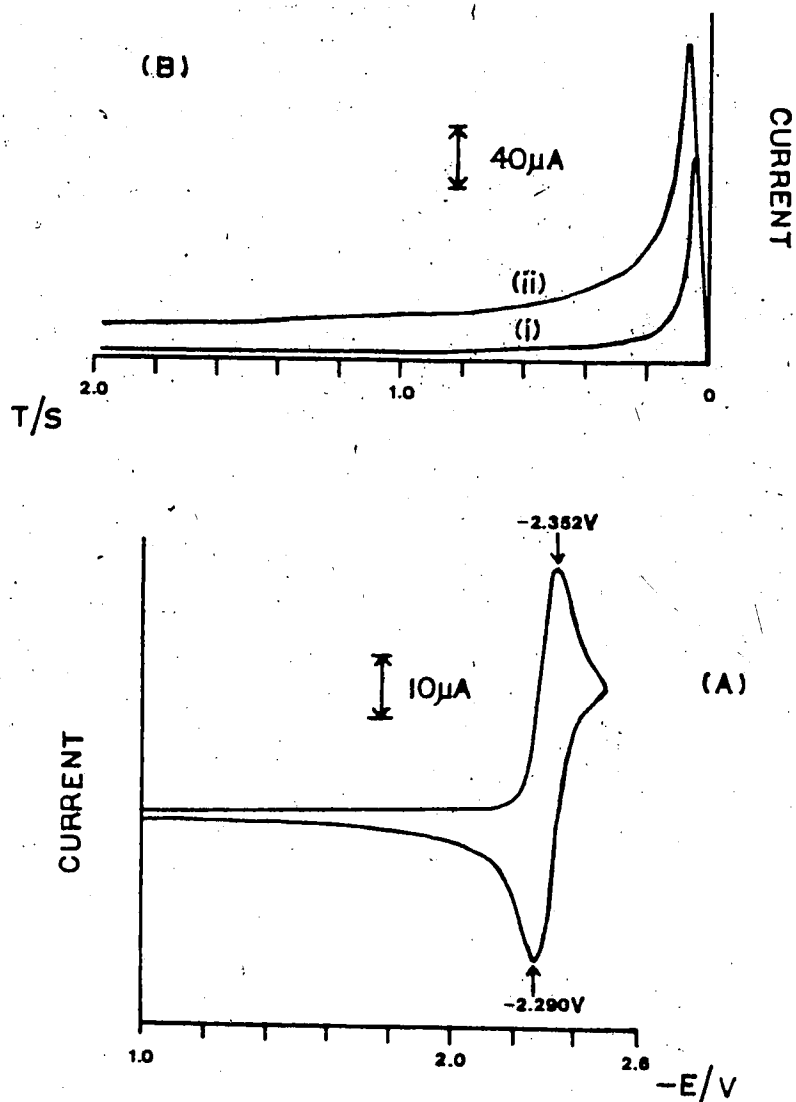


Figure 51. A. Cyclic voltammogram showing the reduction
of anthracene (0.943 mM in ACN, 0.1 M TEAP)
to its anion radical at platinum electrode.
100 mV/s    Peak reduction current is 38 uA.

B. Chronoamperograms for (i) 0.943 mM anthra-
cene in ACN (0.1 M TEAP) (ii) ACN background
(0.1 M TEAP).
Pulse -1.00 V to -2.500 V for 2 s.  Pt
electrode. it$^{\frac{1}{2}}$  (corrected for background)
= 22.7 uA s$^{\frac{1}{2}}$.

where n" = viscosity and r = radius of the molecule and

the other symbols have their usual meaning. Assuming that

the radius is independent of temperature, then

$$D1/D2 = (T1n"2)/(T2n"1) \qquad (5.2)$$

where n" (25°C) is 3.44 millipoise and n" (23°C) is 3.495

millipoise (242). Therefore

$$2.55/D2 = [298(3.495)]/[296(3.44)]$$

and D2 is 2.45 cm$^2$/s at 23°C.

From the results of four different experiments, the

area of the glassy carbon electrode was found to be 0.095

± 0.005 cm$^2$ and that of the platinum electrode was 0.229

± 0.016 cm$^2$.

Cyclic voltammograms of 1.00 mM solutions of TCNE

using different supporting electrolytes were obtained at

sweep rates ranging from 25 mV/s to 600 mV/s at

platinum and glassy carbon electrodes.  Figure 52 shows

some representative cyclic voltammograms.  The relevant

cyclic voltammetric parameters for the first reduction

wave at a scan rate of 100 mV/s are given in Table 4.

Table 4  Peak Potentials for the First Reduction of
TCNE (1.00 mM) at 100 mV/s

| | Glassy Carbon Electrode | | | Platinum Electrode | | |
|---|---|---|---|---|---|---|
| Supporting Electrolyte | E(p,c) (-V) | E(p,a) (-V) | delE(p) mV | E(p,c) (-V) | E(p,a) (-V) | delE(p) mV |
| TBAF | 0.091 | 0.020 | 71 | 0.110 | 0.038 | 72 |
| TEAP | 0.102 | 0.040 | 59 | 0.105 | 0.042 | 63 |
| NaClO4 | 0.102 | 0.041 | 61 | 0.110 | 0.042 | 68 |
| LiClO4 | 0.114 | 0.052 | 62 | 0.108 | 0.045 | 63 |

In all cases, delE(p) values did not change significantly

from the above values with variation of sweep rates

TEAP

−0.102

−1.092

−0.040

−0.988

LiClO₄

−0.114

−0.840

0.052

−0.753

20μA

TBAF

−0.091

−1.290

−0.890

−0.020

NAClO₄

−0.102

−0.981

−0.753

−0.041

+0.4    0.0    −0.4    −0.8    −1.2    −1.6

E/V

+0.4    0.0    −0.4    −0.8    −1.2

E/V
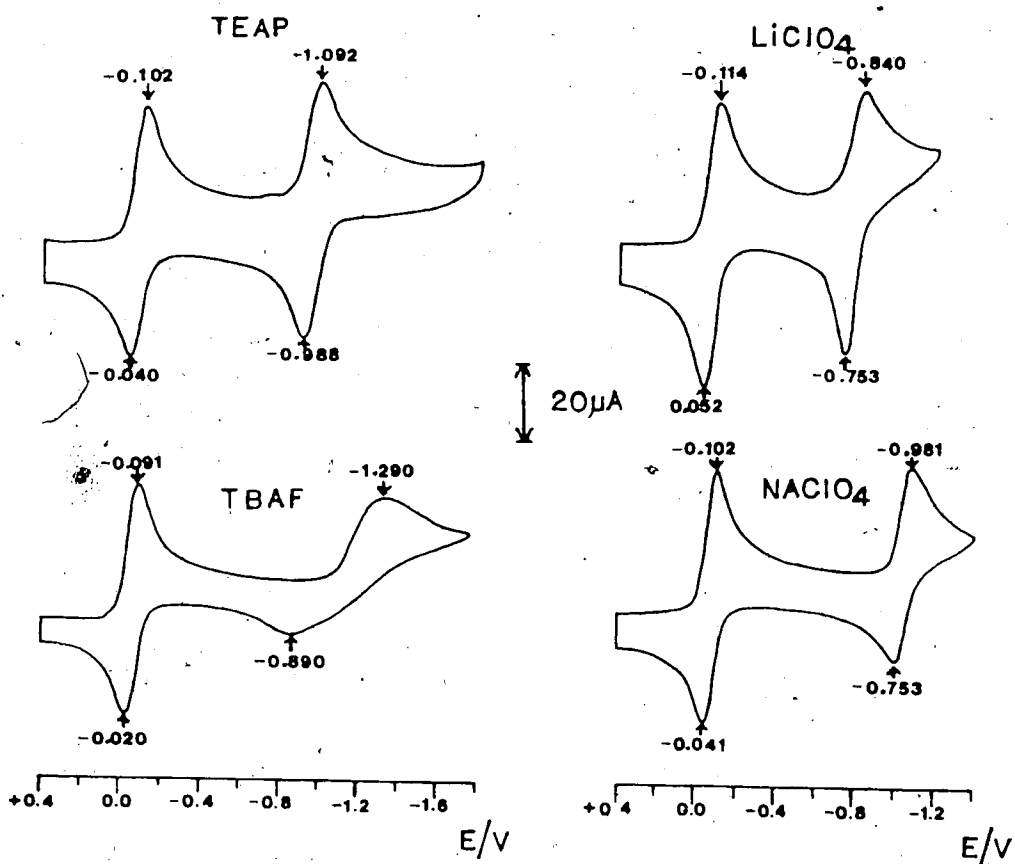
Figure 52.    Cyclic voltammograms showing the first and
second reduction of TCNE (1.00 mM in ACN,
0.1 M supporting electrolyte) at glassy carbon
with different supporting electrolytes at
100 mV/s.

ranging from 25 mV/sec to 600 mV/sec.

Values for the ratio of the anodic peak current to

the cathodic peak current i(pa)/i(pc) for the first wave were

obtained by recording cyclic voltammograms in the

current-time (y-t) mode. For all sweep rates and support-

ing electrolytes, the observed values were very close to

1.00 (for example see Figure 53). For the planar glassy

carbon electrode, the ratio of peak cathodic current to

square root of the sweep rate $i(pc)/v^{\frac{1}{2}}$ was constant for

all sweep rates studied and had approximately the same

values for the different electrolytes. They were 112,

111, 108 and 110 $uA/(v/s)^{\frac{1}{2}}$ for TBAF, TEAP, NaClO4 and

LiClO4 respectively. However, for the platinum wire

electrode, $i(pc)/(v)^{\frac{1}{2}}$ values appeared to be larger at

slower sweep rates. Figure 53 shows a plot of

$i(pc)/(v)^{\frac{1}{2}}$ for TBAF at glassy carbon and platinum wire

electrodes.
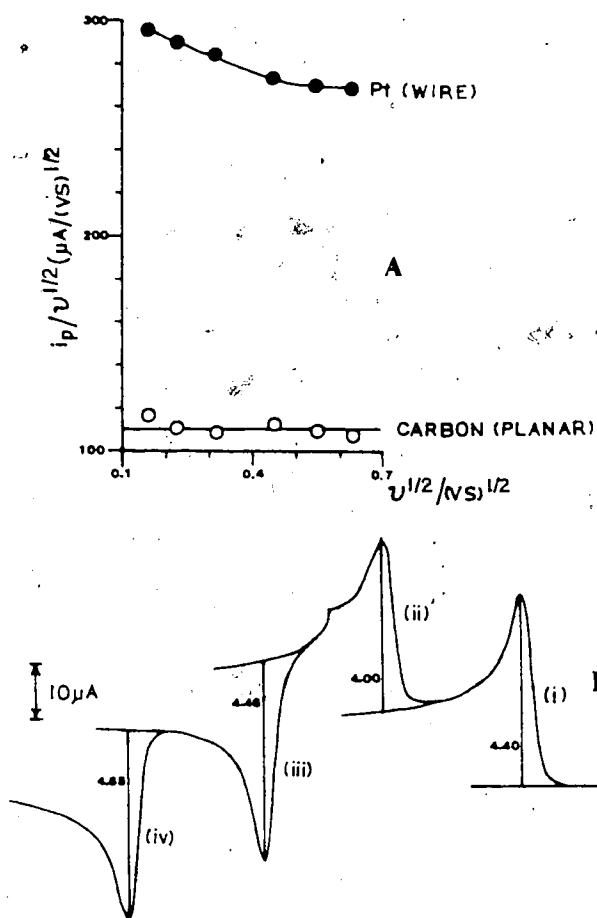
Figure 53. A. Plots of i(pc)/v$^{\frac{1}{2}}$ versus v$^{\frac{1}{2}}$ for the first
reduction wave of TCNE (1.00 mM in ACN,
0.1 M TBAF) at glassy carbon and platinum
electrodes.

B. Cyclic voltammogram of TCNE (1.00 mM in ACN,
0.1 M TBAF) at platinum electrode recorded
in y-t mode.

Scan +0.5 V to -1.10 V at 25 mV/s.

$$\frac{i(pa)1}{i(pc)1} = \frac{(iv)}{(i)} = 1.1 \qquad \frac{i(pa)2}{i(pc)2} = \frac{(iii)}{(ii)} = 1.1$$

Diffusion coefficients for TCNE, as determined by

chronoamperometry, were found to be independent of the

countercations used. The observed value was (2.20 ±

0.05)e-5 cm$^2$/s. For a reversible wave, the

peak current from the cyclic voltammograms and the

it$^{\frac{1}{2}}$ values for the chronoamperometric experiment

can be combined to give the value for the number of

electrons transferred. From the Randles-Sevcik equation

equation (2.16)

$$ip = 2.69e5 \ (n)^{3/2} \ A \ (D(0)v)^{\frac{1}{2}} \ C(0)$$

and the Cottrell equation (2.12)

$$it^{\frac{1}{2}} = nFA \ (D(0))^{\frac{1}{2}} \ C(0)$$

we obtain

$$ip/it^{\frac{1}{2}} = (2.69e5 \ n^{\frac{1}{2}} \ \pi^{\frac{1}{2}} v^{\frac{1}{2}} )/ \ F \qquad (5.3)$$

where ip is in uA, $it^{\frac{1}{2}}$ is in uA $s^{\frac{1}{2}}$ and v is in V/s.

Thus $n = [ (ip)F/((it^{\frac{1}{2}}) (2.69e5) (\pi^{\frac{1}{2}} v^{\frac{1}{2}}))]$      (5.4)

where n is the number of electrons transferred. This

method of obtaining n is known as Malachesky's method (120).

It is very convenient since no prior knowledge of the

electrode area is required and the concentration of the

solution need not be known as long as it is the same for

both techniques. One drawback is that it can only be

applied to a reversible electrode reaction with no chemical

complications. Malachesky's method was applied to study

the number of electrons transferred for the first reduc-

tion of TCNE. For both electrodes and all supporting

electrodes used, values of n ranging from 0.9 to 1.0 were

obtained.

It is observed in Figure 52 that the second

reduction wave for TCNE in acetonitrile shows remarkable

differences with different countercations. Similar

behavior was also observed at a platinum electrode. The

cyclic voltammetric parameters for this wave at 100 mV/s

scan rate are given in Table 5.

Table 5   Peak Potentials for Second Reduction Wave
of TCNE (1.00 mM) at 100 mV/s

| | Glassy Carbon | | | Platinum Wire | | |
|---|---|---|---|---|---|---|
| Supporting Electrolyte | E(p,c) (-V) | E(p,a) (-V) | delE(p) mV | E(p,c) (-V) | E(p,a) (-V) | delE(p) mV |
| TBAF | 1.290 | 0.890 | 400 | 1.625 | 1.100 | 525 |
| TEAP | 1.092 | 0.988 | 94 | 1.264 | 0.967 | 297 |
| NaClO4 | 0.981 | 0.909 | 72 | 0.980 | 0.907 | 73 |
| LiClO4 | 0.840 | 0.753 | 87 | 0.833 | 0.756 | 77 |

For the countercations TBA+ and TEA+, delE(p) values

increased with increasing sweep rates. This increase was

greater at platinum than at carbon and greater for TBA+

than for TEA+. For Na+ and Li+, delE(p) values did not

change very much with variation in sweep rates.   With both

NaClO4 and LiClO4 supporting electrolytes i(pa)/i(pc) values

for the second wave were close to 1.0 at a platinum

electrode.   For NaClO4, at a carbon electrode, the same

result was also obtained.   However, LiClO4 supporting

electrolyte at a carbon electrode gave values of i(pa)/i(pc)

which were significantly greater than 1.0.   These values

are given in Table 6 for different sweep rates.

Table 6.   Variation of i(pa)/i(pc) for Second Reduction of
           TCNE (1.00 mM) with LiClO4 Supporting Electrolyte
           at a Glassy Carbon Electrode

| v<br>mV/s | i(pa)/i(pc) |
|---|---|
| 50 | 1.29 |
| 100 | 1.39 |
| 200 | 1.41 |
| 300 | 1.52 |

The second reduction wave also gave approximately constant

values for $i(pc)/(v)^{\frac{1}{2}}$ at different sweep rates with Na+

and Li+ countercations. However, these values were 10-15%

lower compared to those for the first wave. In the cases

of TBAF and TEAP supporting electrolytes, this was also

true. Further, in all cases, chronoamperometry showed

that the total number of electrons transferred for the

sum of the first and second reduction waves were close to

2.0 (the values obtained ranged from 1.7 to 1.9).

It has been described in Chapter 2 that variation of

delE(p) values with sweep rates can be used to determine

heterogeneous rate constants for quasireversible electrode

reactions. For this to be applicable, delE(p) values should

be less than about 210 mV. For this reason, heterogeneous

rate constants with TBAF as supporting electrolyte at a

platinum electrode could not be determined by this method.

Equation (2.26) in Chapter 2 shows that the heterogeneous

rate constant is related to a certain parameter $\Delta$ by

$$\Delta = ((D(O)/D(R))^{\frac{1}{2}} ks)/(D(O)\pi v(nF/RT))^{\frac{1}{2}}$$

The values of $\Delta$ for different delE(p) values have been

theoretically calculated (54). These values are plotted

in Figure (54).

Assuming that $D(O) \approx D(R)$ at 23°C

$$\Delta = ks/[(2.20e\text{-}5)(\pi) v (39.206)]^{\frac{1}{2}} \qquad (5.5)$$

$$ks = 0.05505 \, \Delta \, (v)^{\frac{1}{2}} \qquad (5.6)$$

The calculated values for the apparent heterogeneous rate

constants for the second reduction of TCNE are given in

Tables 7-9.

Table 7. Apparent Heterogeneous Rate Constants for TCNE
(1.00 mM in ACN) Second Reduction at a Glassy
Carbon Electrode with TBAF Supporting Electrolyte

| v mV/s | delE(p) mV | $\Delta$ | ks cm/s |
|---|---|---|---|
| 10 | 132 | 0.28 | 1.5e-3 |
| 15 | 168 | 0.20 | 1.3e-3 |
| 20 | 171 | 0.19 | 1.5e-3 |
| 25 | 177 | 0.18 | 1.6e-3 |
| 35 | 205 | 0.13 | 1.3e-3 |

average (1.4±0.1)e-3 cm/s
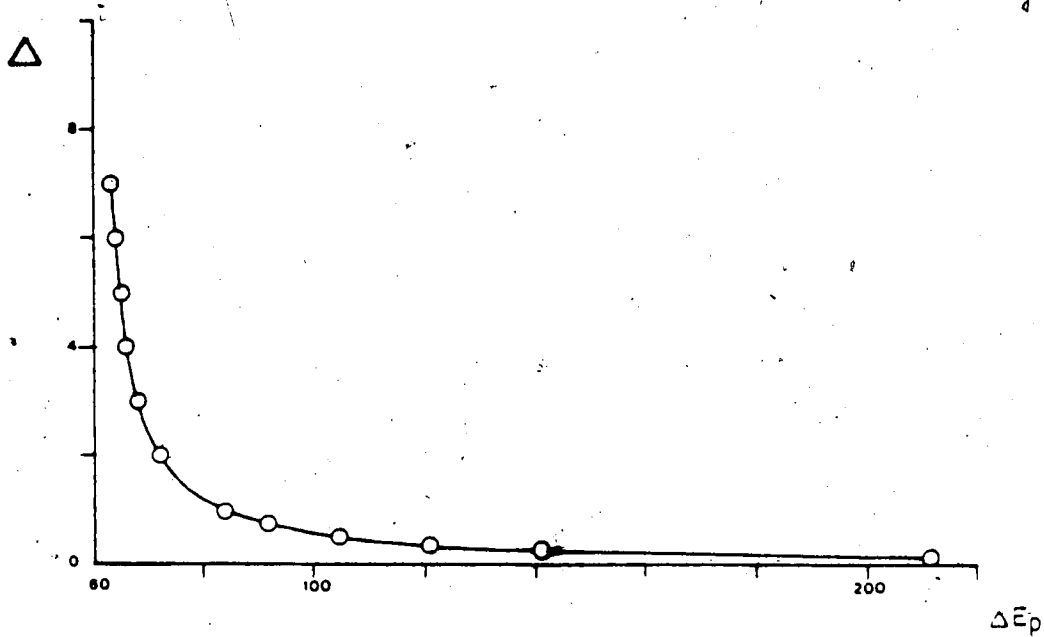
Figure 54. Plot of Δ function versus delE(p)
Assume α = 0.5

Table 8. Apparent Heterogeneous Rate Constants for TCNE
(1.00 mM in ACN) Second Reduction at a Glassy
Carbon Electrode with TEAP Supporting Electrolyte

| v mV/s | delE(p) mV | Δ | ks cm/s |
|---|---|---|---|
| 50 | 84 | 0.98 | 1.2e-2 |
| 100 | 94 | 0.71 | 1.2e-2 |
| 200 | 111 | 0.41 | 1.0e-2 |
| 400 | 122 | 0.34 | 1.2e-2 |
| | | average | (1.1±0.1)e-2 cm/s |

Table 9. Apparent Heterogeneous Rate Constants for TCNE
(1.00 mM in ACN) Second Reduction at a Platinum
Electrode with TEAP Supporting Electrolyte

| v mV/s | delE(p) mV | Δ | ks cm/s |
|---|---|---|---|
| 15 | 138 | 0.27 | 1.8e-3 |
| 20 | 144 | 0.25 | 1.9e-3 |
| 25 | 154 | 0.22 | 1.9e-3 |
| 30 | 184 | 0.17 | 1.6e-3 |
| | | average | (1.8+0.1)e-3 cm/s |

At a platinum electrode, the second reduction wave

of TCNE with TBAF as supporting electrolyte showed a slow

electron transfer. The method used for determination of

rate constant for quasi-reversible reactions could not be

applied in this case since delE(p) values were too large

at all sweep rates studied. Matsuda and Ayabe (180) and

Nicholson (194) have shown that, for the case of

irreversible charge transfer,

$$i(p) = 0.227 \ nF \ ks \ C(0) \ exp[(-\alpha nF/RT)(E(p)-E(0)] \quad (5.7)$$

where all the terms have their usual meaning.

However, values of E(0) are not always available and

Reinmuth (244) has derived a useful relationship where the

current at the foot of the reduction wave (i<10% i(p)) is

given by

$$i = nFAC(0) \ ks \ exp[(-\alpha nF/RT)(E-E(i))] \quad (5.8)$$

where E(i) is the initial potential. This equation has

provided the basis for determination of rate constants

for irreversible electrode reactions where E(0) is unknown

(62).

From equation (5.8)

$$\log i = \log(nFA\ C(0)\ ks) - 0.4343(-\alpha nF/RT)(E-E(i)) \qquad (5.9)$$

where i is in uA and C(0) in mM. At 23°C

$$\log i = 4.34 + \log ks - 17.02\ \alpha\ (E-E(i)) \qquad (5.10)$$

Therefore, if log i was plotted against E-E(i), the

slope would yield $\alpha$. Once $\alpha$ is known, the value of ks can

be calculated from equation (5.10) which on rearranging gives

$$\log ks = \log i + 17.02\alpha(E-E(i)) - 4.34. \qquad (5.11)$$

This was done for the reduction of TCNE anion radical to

the dianion at a platinum electrode with TBAF as supporting

electrolyte. The results are plotted in Figure 57. From

the slope of the straight line plot, α was found to be 0.8.

This value was substituted into equation (5.11) and ks

calculated (Table 10).

Table 10. Apparent Heterogeneous Rate Constants for the
Reduction of TCNE: to TCNE= at a Platinum
Electrode. Concentration of TCNE is 1.00 mM
in ACN (0.10 M TBAF).

| E-E(i) (Volts) | log i | log ks | kj cm/s |
|---|---|---|---|
| -0.06 | 0.75 | -4.41 | 3.9e-5 |
| -0.05 | 0.62 | -4.40 | 4.0e-5 |
| -0.04 | 0.45 | -4.43 | 3.7e-5 |
| -0.03 | 0.29 | -4.46 | 3.5e-5 |
| | | | (3.8±0.1)e-5 |

The value of 0.8 for α obtained from Figure 57 is in close

agreement with that obtained by another method. For an

irreversible electrode reaction, peak potentials and half-

peak potentials depend on the sweep rate. For two different
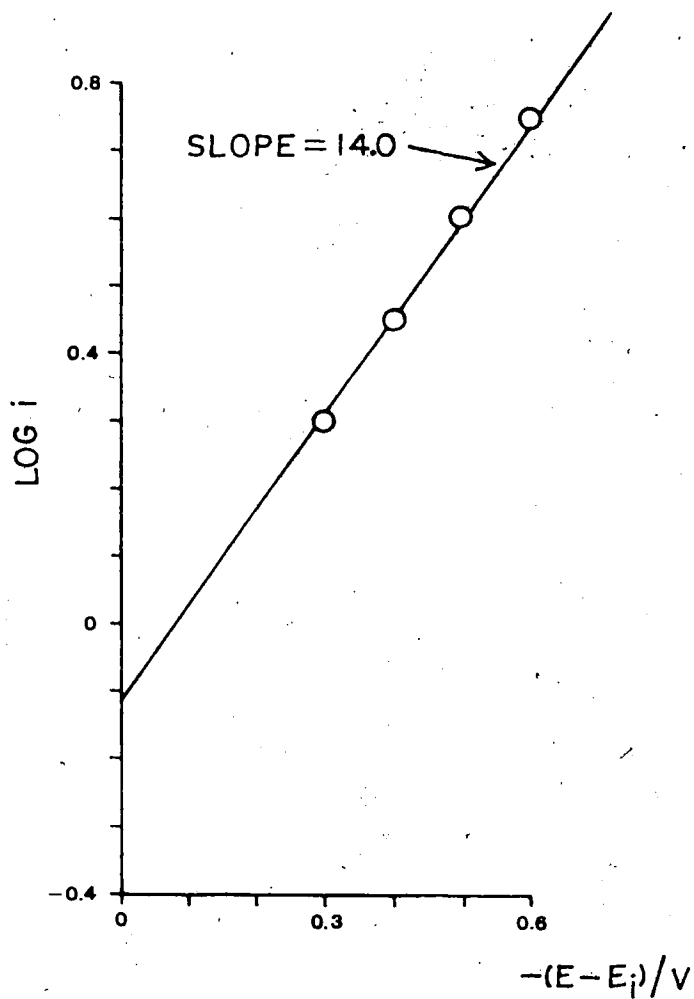
Figure 57.  Plot of log i versus E-Ei for the reduction
            of TCNE anion radical at platinum.

sweep rates, $\alpha$ is related to the peak potential $E(p)$, half-

peak potentials $E(p/2)$ and the sweep rates v by (62)

$$(E(p/2))2 - (E(p/2))1 = (E(p))2 - (E(p))1$$
$$= RT/nF \ln (v(1)/v(2))^{\frac{1}{2}} \qquad (5.12)$$

Since irreversible voltammetric waves are rather broad,

the measurement of peak potentials are less accurate than half-

peak potentials, and therefore $E(p/2)$ will be used.

$$(E(p/2))2 - (E(p/2))1 = (0.02551/\alpha) \ln (v1/v2) \qquad (5.13)$$

The results are shown in Table 11.

Table 11. Determination of $\alpha$ for TCNE$^{\pm}$ Reduction at a
Platinum Electrode using Equation (5.13).
Concentration of TCNE is 1.00 mM ACN (0.10 M TBAF)

| v mV/sec | E(p/2) (Volts) | $\alpha$ |
|---|---|---|
| 15 | -1.374 | |
| | | 0.71 |
| 50 | -1.418 | |
| | | 0.70 |
| 100 | -1.443 | |

Figure 55 shows some representative cyclic voltammograms for

1.00 mM TCNQ in acetonitrile at a glassy carbon electrode at

100 mV/sec. Peak potentials for the first and second reduction

waves are given in Tables 12 and 13 respectively.

Table 12. Peak Potentials for the First Reduction of
TCNQ (1.00 mM in acetonitrile) at 100 mV/sec
Scan Rate

|  | Glassy Carbon | | | Platinum | | |
|---|---|---|---|---|---|---|
| Supporting Electrolyte | E(p,c) (-V) | E(p,a) (-V) | delE(p) mV | E(p,c) (-V) | E(p,a) (-V) | delE(p) mV |
| TBAF | 0.140 | 0.072 | 68 | 0.140 | 0.077 | 63 |
| NaClO4 | 0.146 | 0.080 | 66 | 0.145 | 0.078 | 67 |
| LiClO4 | 0.146 | 0.082 | 64 | 0.140 | 0.072 | 68 |

Table 13. Peak Potentials for the Second Reduction of
TCNQ (1.00 mM in acetonitrile) at 100 mV/sec
Scan Rate

|  | Glassy Carbon | | | Platinum | | |
|---|---|---|---|---|---|---|
| Supporting Electrolyte | E(p,c) (-V) | E(p,a) (-V) | delE(p) mV | E(p,c) (-V) | E(p,a) (-V) | delE(p) mV |
| TBAF | 0.691 | 0.627 | 64 | 0.695 | 0.628 | 70 |
| NaClO4 | 0.659 | 0.597 | 62 | 0.660 | 0.592 | 68 |
| LiClO4 | 0.551 | 0.490 | 61 | 0.558 | 0.498 | 60 |
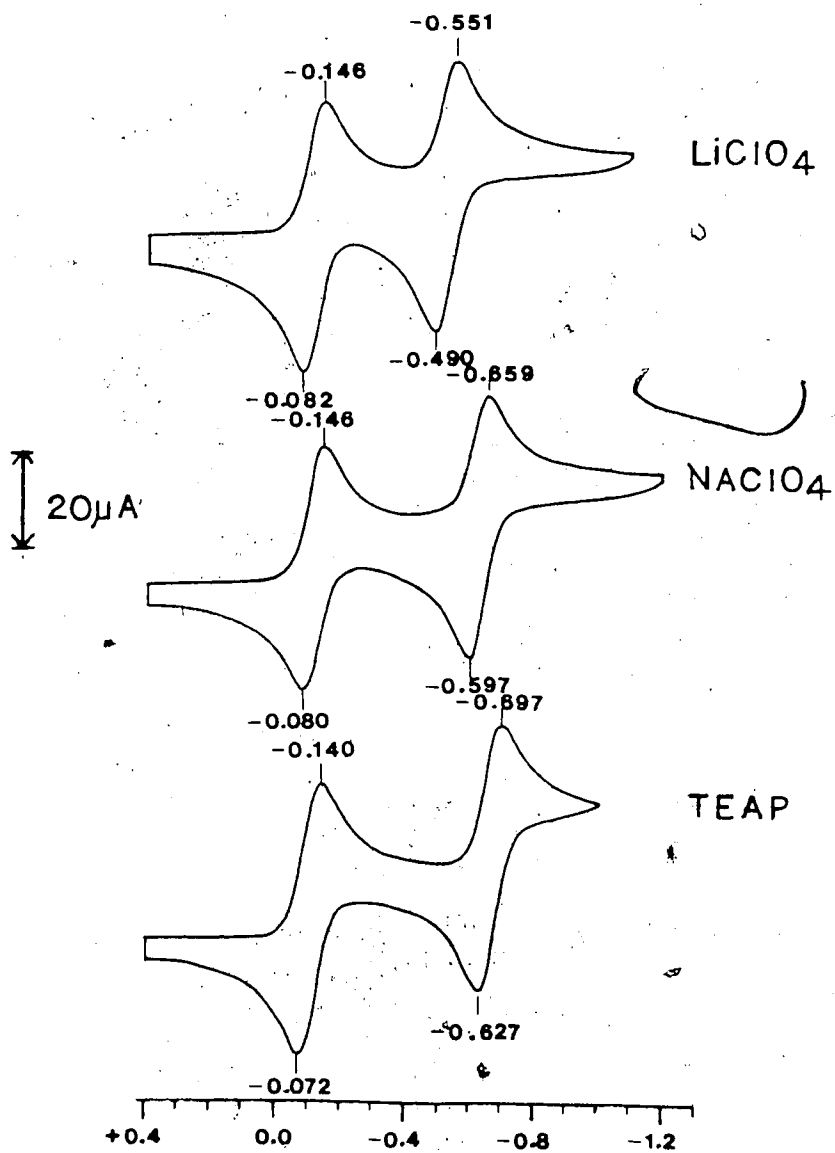
Figure 55. Cyclic voltammograms for reduction of TCNQ (1.00
mM in ACN, 0.1 M supporting electrolyte) at
glassy carbon with diferent supporting electrolytes.

Considering the first reduction wave of TCNQ in aceto-

nitrile, delE(p) values remained close to the theoretical

reversible value of 59 mV at sweep rates from 25 to

500 mV/s in all cases. The ratio i(pa)/i(pc) was found to

be 1.00 for all systems. Figure 56 shows a typical

y-t recording for the forward and reverse waves. Diffu-

sion coefficients determined from chronoamperometry did

not show any dependence on the supporting electrolyte

used. The value obtained was $(2.00 \pm 0.06)$e-5 cm$^2$/s.

The current constant $i(p)/v^{\frac{1}{2}}$ was approximately

constant with sweep rate variation and has an average

value of 100 uA/(V/s)$^{\frac{1}{2}}$ for the glassy carbon

and 244 for the platinum wire electrode. Malachesky's

method revealed that the number of electrons transferred

in the first wave was 1.0.

Similar results were obtained for the second wave.

As can be seen from Table 11, delE(p) values were close to
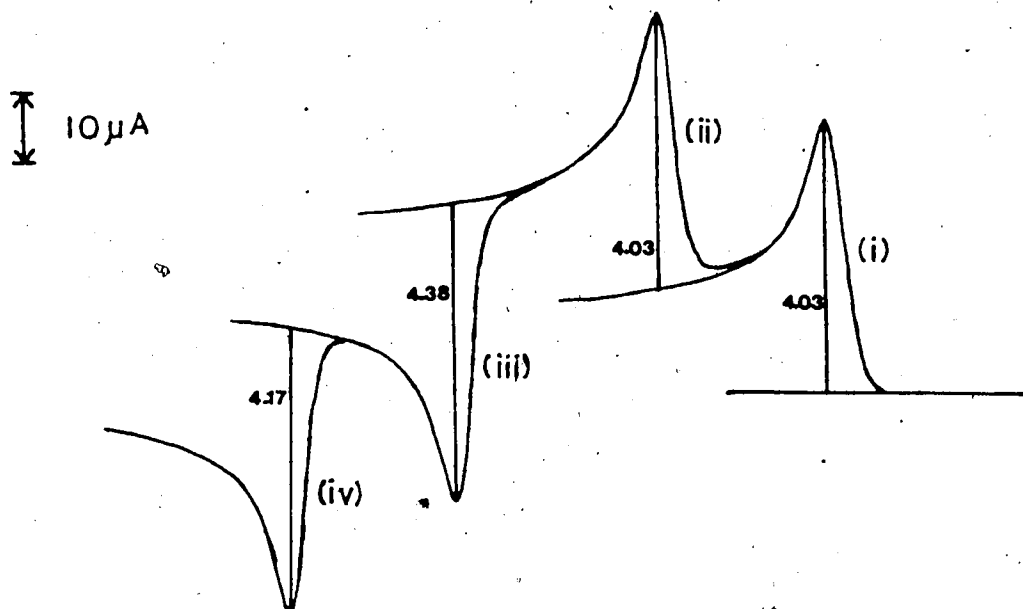
Figure 56. Cyclic voltammogram for reduction of TCNQ
(1.00 mM in ACN, 0.1 M TBAF) at platinum
electrode recorded in the y-t mode.
Scan from +0.50 V to -1.00 V at 25 mV/s.

$$\frac{i(pa)1}{I(pc)1} = \frac{(iv)}{(i)} = 1.03 \qquad \frac{i(pa)2}{i(pc)2} = \frac{(iii)}{(ii)} = 1.09$$

the reversible value in all cases. i(pa)/i(pc) gave a value

of 1.00 (see Figure 56) and $i(pc)/v^{\frac{1}{2}}$ did not vary

much with sweep rate. The average value obtained at the

carbon electrode was 92 and at the platinum electrode

229 $uA/(V/s)^{\frac{1}{2}}$. Chronoamperometry showed that the total

number of electrons transferred for the first and second

waves was 2.0.

The results from Tables 4 and 12 showed that the peak

potentials for the first reduction wave of TCNE and TCNQ

did not change significantly, with different electrode

materials or countercations. In contrast, the peak

potentials of the second reduction wave changed with

countercations (Tables 5 and 13). Further, in the case of

TCNE with TBA+ and TEA+, the peak potentials were more

negative at platinum compared to carbon. For Na+ and Li+

this did not occur. However, with TCNQ there were no

differences in peak potentials with different electrode

material. E(p) values for the second reduction wave of

both TCNE and TCNQ were found to shift to more positive

values according to the order TBA+ < TEA+ < Na+ < Li+.

Plots of Eh for the second reduction wave of TCNE and TCNQ

at a carbon electrode vs ionic radii of countercations are

shown in Figure 58. For TCNE, Eh values with TBA+ were

not obtainable due to irreversibility of the reduction but

for TEA+ the reduction at slow sweep rates (10 mV/sec)

was sufficiently close to reversibility (delE(p) 71 mV) for

the Eh value to be known. It can be seen from Figure 58

that for TCNE, positive shift of Eh in going from TEA+ to

Na+ countercations was 49 mV and from Na+ to Li+ was 77 mV.

For TCNQ, where TEA+ was not studied, positive shift of 30 mV

occurred from TBA+ to Na+ and 80 mV from Na+ to Li+.

It is well known that the presence of ion pairing of

electrolytically formed negative ions with countercations

causes positive shifts in the Eh values, the magnitude of
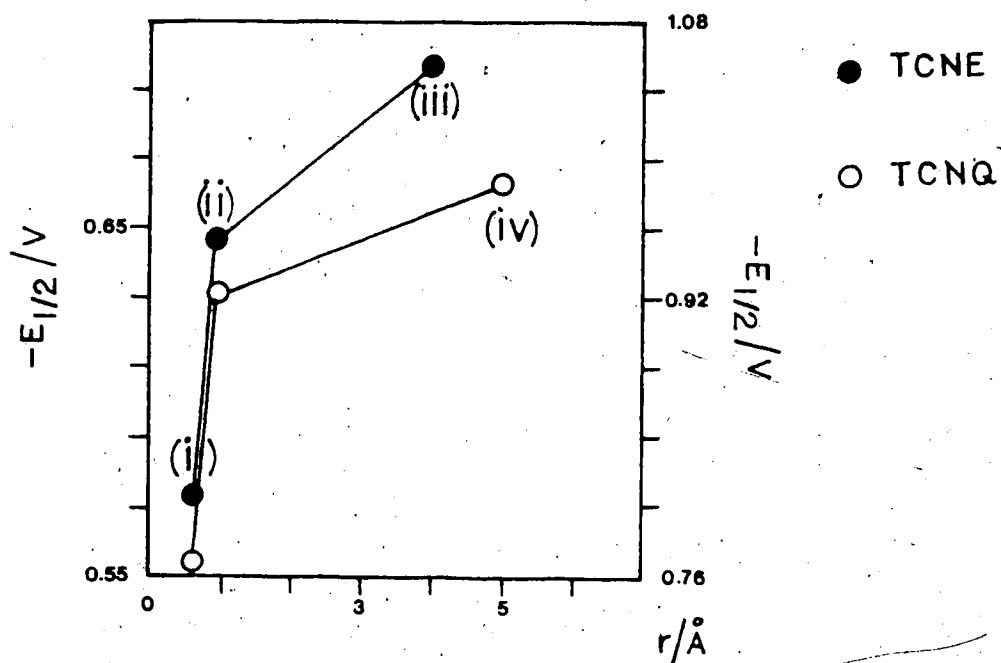
Figure 58. Plot of half-wave potential (Eh) versus
ionic radii of countercations for TCNE and
TCNQ second reduction wave at platinum and
glassy carbon.
i)Li+, ii)Na+, iii) TEA+, iv).TBA+
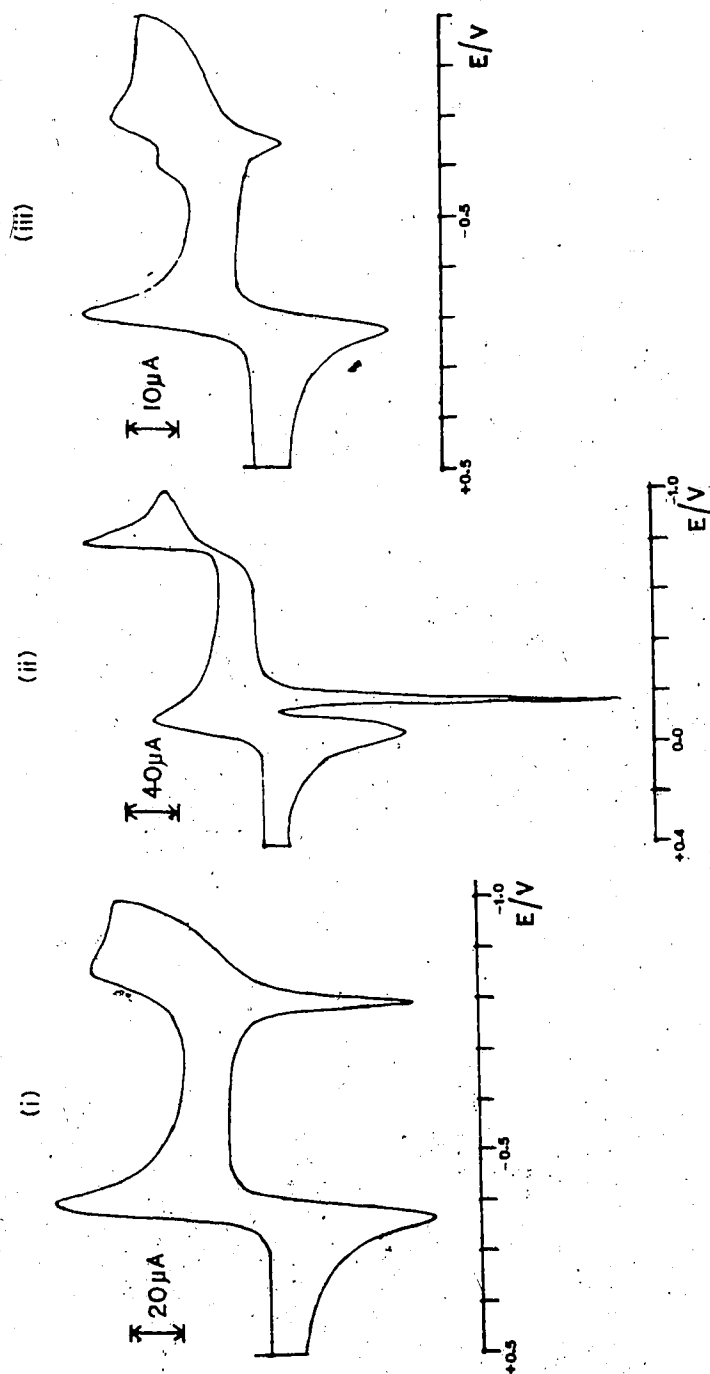
Figure 58A. Cyclic voltammogram of TCNE (1.00 M in ACN)
with mixtures of supporting electrolytes.
(i)   Pt electrode 0.095 M TBAF+0.005 M LiClO$_4$
(ii)  Pt electrode 0.05 M TEAP+ 0.05 M LiClO$_4$
(iii) Carbon electrode 0.05 M TBAF+0.05 M LiClO$_4$
All at 100 mV/s.

this shift depending on the strength of ion pairing and

the concentration of countercations, where the concentra-

tion of the electroactive species is kept constant (209-

212). Therefore it was decided to study the shifts in Eh

as a function of concentration of countercations. The

requirements for such a study are that the reduction wave

must be electrochemically reversible and the species

formed stable. Further, the ionic strength should be kept

constant preferably with the supporting electrolyte whose

countercation cation is assumed not to ion pair with the

species of interest. In the case of TCNE, it was found that

such a study could not be made since the dianion wave was

irreversible with TBAF as supporting electrolyte. Further,

it was observed that the reductions with mixtures of

supporting electrolytes TBAF-LiClO4, TEAClO4-LiClO4 gave

waves which exhibited adsorption characteristics at both

electrolytes (Figure 58A). As can be seen from this figure,

the reduction wave of TCNE was not affected with different

mixtures of supporting electrolytes and electrode materials.

The various criteria for electrochemical reversibility as

discussed earlier are still applicable. However, for mixed

electrolytes, TCNE⁻ reduction shows waves characteristic of

adsorption effects. For example, with 0.095 M TBAF and

0.005 M LiClO4 at a platinum electrode, the reverse wave is

very sharp and does not show $t^{\frac{1}{2}}$ decay for diffusion

control. For 0.05 M TEAP and 0.05 M LiClO4 at platinum, the

forward wave rose sharply and the reverse wave was not

observed. Instead, a very strong sharp current transient

was observed just prior to the reverse wave for the first

reduction. In the case of 0.05 M TBAF and 0.05 M LiClO4 at

carbon, a prepeak was observed for the forward wave and the

reverse wave was again quite sharp. For TCNQ, no

such problems arose. It was assumed that the TCNQ dianion

did not form any ion pair with TBA+ and therefore the

ionic strength was kept constant at 0.10 M with appropriate

additions of TBAF. This assumption was verified by

reducing TCNQ at different concentrations of TBAF. The

results are shown in Table 14.

Table 14. Peak Potentials for TCNQ Reduction (0.50 mM in
ACN) as a Function of TBAF Concentration. Scan
Rate 25 mV/s .

| [TBAF] M | E(pc)1 V | E(pa)1 V | delE(p)1 mV | E(pc)2 V | E(pa)2 V | delE(p)2 mV |
|---|---|---|---|---|---|---|
| 0.02 | -0.156 | -0.094 | 62 | -0.718 | -0.655 | 63 |
| 0.04 | -0.151 | -0.086 | 65 | -0.710 | -0.647 | 63 |
| 0.06 | -0.146 | -0.082 | 64 | -0.703 | -0.639 | 64 |
| 0.08 | -0.142 | -0.078 | 64 | -0.698 | -0.634 | 64 |
| 0.10 | -0.140 | -0.075 | 65 | -0.694 | -0.629 | 65 |

The calculated shifts in Eh with respect to the Eh in

0.10 M TBAF are given below.

Table 15. Half Wave Potential Shifts and Calculated Junction
Potentials for TCNQ Reductions as a Function of
TBAF Concentration.  0.05 mM TCNQ in ACN.  Scan
Rate 25 mV/s

| [TBAF] M | delEh(1) | delEh(2) | Ej |
|----------|----------|----------|-----|
| 0.02 | 14 | 24 | 11 |
| 0.04 | 11 | 16 | 6 |
| 0.06 | 6 | 9 | 4 |
| 0.08 | 2 | 4 | 2 |
| 0.10 | 0 | 0 | |

However, since the reference electrode used was Ag/AgNO3

(0.01M), 0.10 M TBAF in acetonitrile, junction potentials

are expected to exist at concentrations of TBAF other than

0.10 M.  These junction potentials can be estimated by

making use of the Henderson equation for a 1:1 electrolyte

$$P(x)-P(y) = [(\lambda(TBA+) -\lambda(BF4-))/(\lambda(TBA+) + \lambda(BF4-))] \quad (5.14)$$
$$\ln [(a\pm(y))/(a\pm(x))]$$

where the junction is given by

x M TBA BF4⁻‖ y M TBA BF4⁻
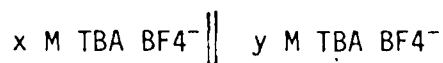
Since the activity coefficients for the various solutions

were not known, rational activity coefficients were

calculated using the extended Debye-Huckel equation

$$\log f\pm = -A\ u^{\frac{1}{2}} /(1+B\ u^{\frac{1}{2}} ) \qquad\qquad (5.15)$$

where f± is the rational activity coefficient, u is the

ionic strength, $A=1.8246e6/(\ell T)^{3/2}$, $B=50.29e8/(\ell T)^{\frac{1}{2}}$, $\ell$

being the dielectric constant.  The relevant parameters for

TBA+ and BF4- in acetonitrile, taken from the data of Coetzee

and Cunningham (245) are given in the table below.

Table 16. Conductance Data for Ions of TBAF in ACN.

| | $\lambda(0)$ $cm^2/\Omega$ equiv | Stokes radius ($\text{Å}$) |
|---|---|---|
| TBA+ | 61.9 | 3.83 |
| BF4- | 120.9 | 1.96 |

In Equation (5.15) above, the ion size parameters were taken to be the sum of the Stokes radii for the 1:1 electrolyte TBAF. Also, since the equivalent conductances were not known, ionic conductances at infinite dilution were used in equation (5.14). This is not expected to give any serious errors since only the ratio of the conductances are involved. The calculated junction potentials are given in Table 15. A similar approach to the calculation of junction potentials was used by Chauhan et al (246). Further, since the reference solution contained 0.10 M TBAF whereas the working electrode solution contained NaClO4 and LiClO4 up to 0.10 M, junction

potentials may be present. However this was checked

experimentally and found to be negligible (< 5 mV).

For the reduction of TCNQ, the following mechanism

applies:

$$TCNQ + e = TCNQ^{\pm} \tag{5.16}$$

$$TCNQ^{\pm} + e = TCNQ^{=} \tag{5.17}$$

Nagaoka and Okazaki (247) have shown that in the case where

ion pairing was present for both the anion radical and

the dianion.

$$TCNQ^{\pm} + M^+ = TCNQ^{\pm} M^+ \tag{5.18}$$

$$TCNQ^{\pm} M^+ + M^+ = TCNQ^{\pm} M2^+$$

$$\vdots$$

$$\vdots$$

$$TCNQ^{\pm} M^+(i-1) = TCNQ^{\pm} M^+(i)$$
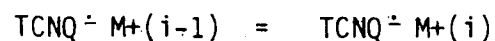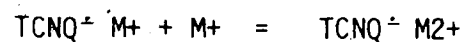
The shift in Eh for the first reduction wave is given by

$$delEh(1) = (RT/F) \ln(1 + C_{M+} K_{1,1} + C_{M+}^2 K_{1,2} \cdots + C_{M+}^i K_{1,i})$$

(5.19)

where the formation constant $K_{1,s}$ is given by

$$K_{1,s} = [TCNQ^- M_s^+]/[TCNQ^-] \ [M^+]^s$$

(5.20)

It is assumed that the concentration of the metal cation

is in large excess compared to the concentration of TCNQ.

Further, for the dianion

$$TCNQ^= + M+ = TCNQ^= M+$$

(5.21)

$$TCNQ^= M+ + M+ = TCNQ^= M+_2$$

$$\vdots$$

$$\vdots$$

$$TCNQ^= M+_{j-1} = TCNQ^= M+_j$$
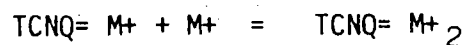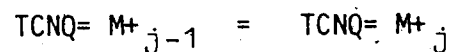
and the shift in Eh

$$delEh(2) = (RT/F)\ln \frac{1 + C_{M+}K_{2,1} + C_{M+}^2 K_{2,2} + \cdots + C_{M+}^j K_{2,j}}{1 + C_{M+}K_{1,1} + C_{M+}^2 K_{1,2} + \cdots + C_{M+}^i K_{1,i}}$$

(5.22)

where

$$K_{2,t} = \frac{[TCNQ= M_t^+]}{[TCNQ=][M^+]^t}$$

(5.23)

Equation (5.19) predicts that a plot of delEh(1) vs log

$C_{M+}$ would give a slope of 59 mV and 118 mV at 23°C for

quantitative formation of TCNQ: M+ and TCNQ: M2+. However,

the behavior of delEh(2) is more complicated. In the

presence of only TCNQ⁻ M+, (assuming that $C_{M+}$ $K_{1,1} \gg 1$), a

slope of 0 and 59 mV is expected for quantitative formation of

TCNQ=M+ and TCNQ=M+$_2$, respectively. In the absence of

any ion pairing between TCNQ⁻ and M+ then equation (5.22)

reduces to

$$delEh(2) = (RT/F)\ln(1 + C_{M+}K_{2,1} + C_{M+}^2 K_{2,2} + \cdots + C_{M+}^j K_{2,j})$$

(5.23A)

which is of the same form as equation(5.19). Therefore a

similar behavior would be expected for quantitative forma-

tion of TCNQ= M+ and TCNQ=. M2+, i.e. plots of delEh(2)

would give 59 and 118 mV respectively.

The results obtained for TCNQ with Na+ and Li+ in

ACN are shown in Figure 59. In all cases the concentra-

tion of TCNQ was 0.50 mM and the ionic strength was 0.10 M

The scan rate used was 25 mV/s. Both carbon and platinum

electrodes gave the same results. As can be seen from

Figure 59, both the plots of delEh vs log $C_{M+}$ for Na+ and

Li+ showed two linear sections. In the case of Na+ the

slopes were 27 and 80 mV while for Li+, these were 52

and 122 mV. It is clear from these results that two types

of ion pairs are formed between TCNQ= and the counter-

cations, namely those with stoichiometries 1:1 and 1:2.

The formation constants for both these ion pairs are

calculated from the data of Figure 59 by making use of
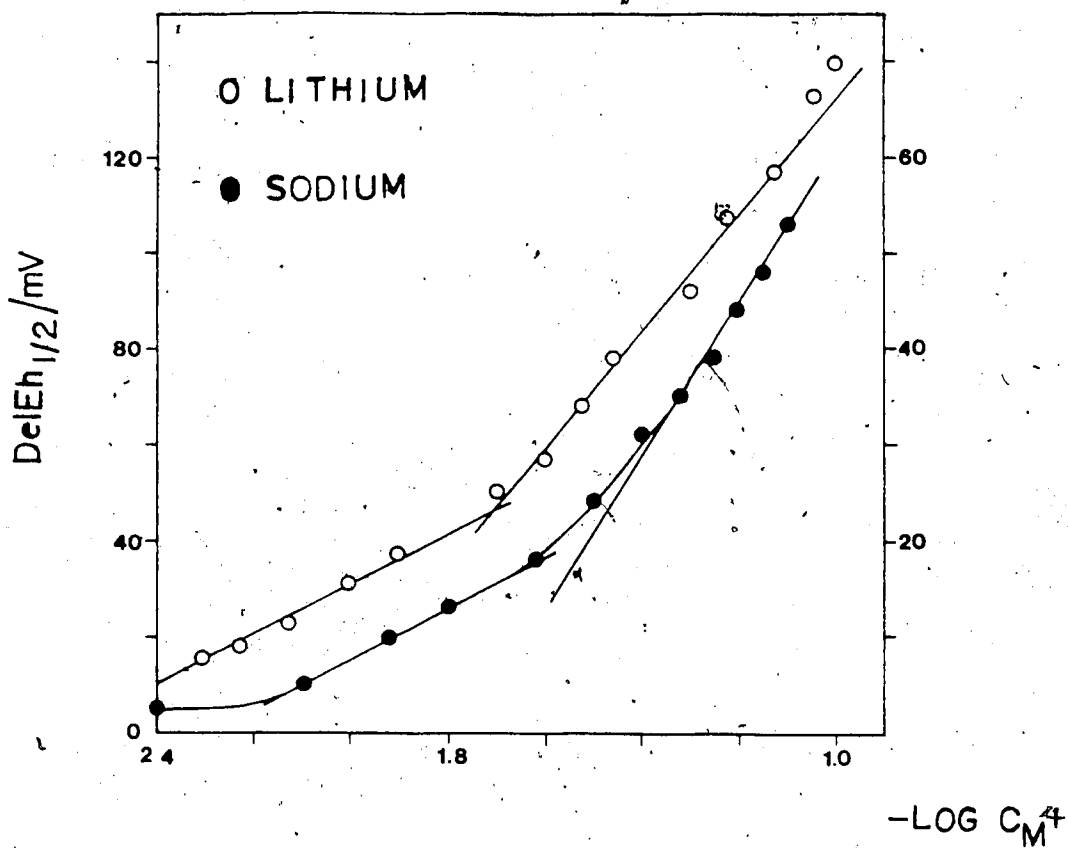
Figure 59.  Plot of half-wave potential change versus the negative logarithm of metal ion concentration

equation (5.23). It is assumed that at low concentrations,

only the 1:1 ion pair is formed whereas at the high.

concentration end both the 1:1 and 1:2 ion pairs are ,

formed. The results of these calculations are given in

Table 17.

Table 17. Formation Constants of TCNQ Ion Pairs

| Counter-cation | Stoichiometry | $K_{2,1}(M^+)$ | $K_{2,2}(M^+)$ |
|---|---|---|---|
| TCNQ=  Na+ | 1:1 | 33±1 | -- |
|  | 1:2 | -- | 394±47 |
| TCNQ=  Li+ | 1:1 | 176±14 | -- |
|  | 1:2 | | $(1.20\pm0.26)e4$ |

As was mentioned in the introductory section of this chapter, spectroscopic techniques were used to monitor the species formed during electrolysis. Figure 60 shows the UV absorption of a solution of TCNE and TCNQ in acetonitrile. Both TCNE and TCNQ did not absorb in the visible region in acetonitile. Further, the presence of 0.10 M TBAF or LiClO4 did not alter the spectra of fresh solutions of TCNE or TCNQ in any way. However, if the TCNE solutions were left standing for a few days the solution containing TBAF turned yellow and showed two additional absorption maxima at 3973 Å and 4159 Å which were much weaker than the UV absorption maxima at 2610 Å and 2708 Å. The solution containing LiClO4 did not show much color change for the same period of time. The spectrum of a solution of TCNE in water has a broad absorption maximum at 2969 Å and two weaker maxima at 3956 Å and 4125 Å (Figure 60).
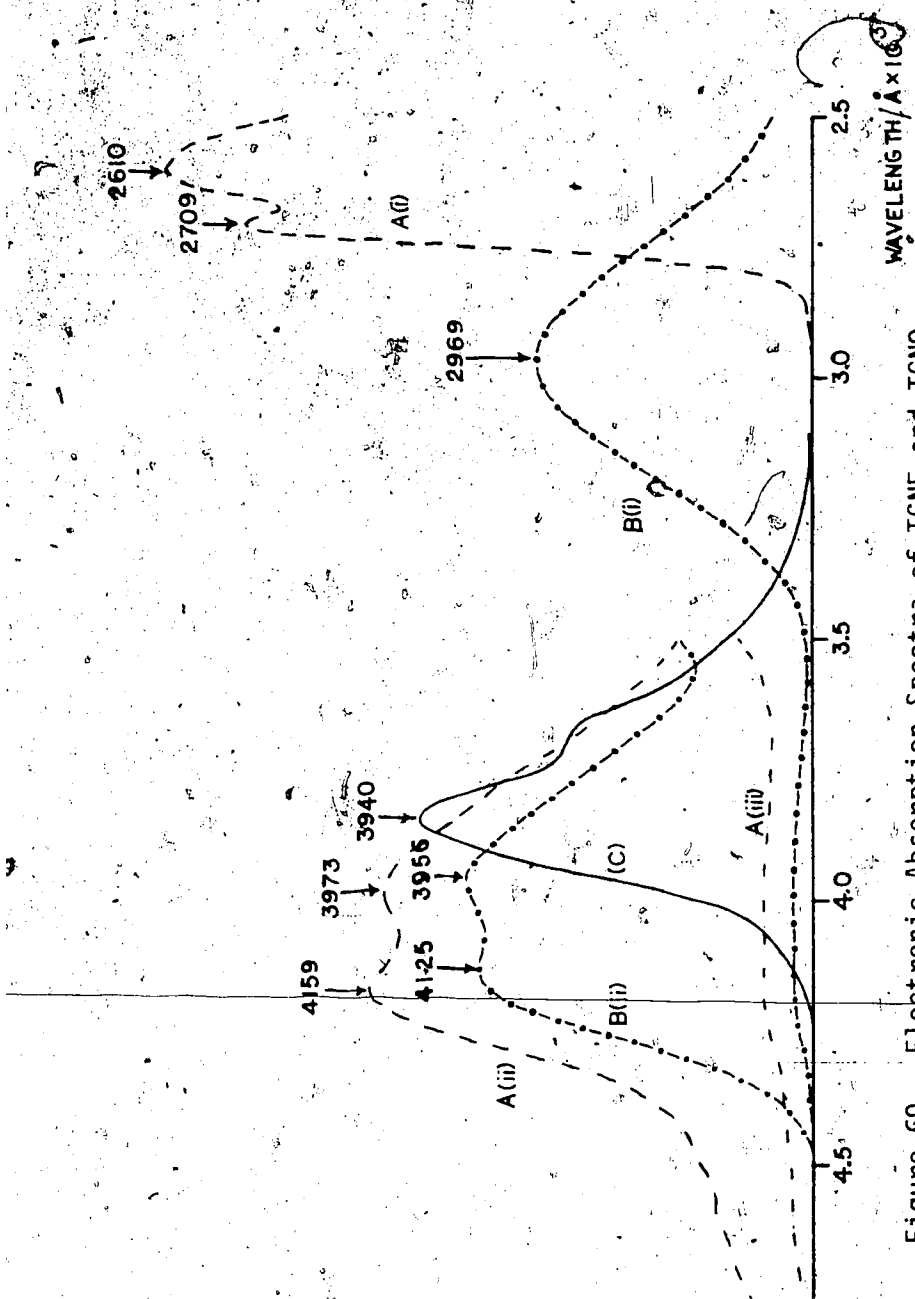
Figure 60. Electronic Absorption Spectra of TCNE and TCNQ in ACN.

A(i) 0.50 mM TCNE in ACN fresh solution (no electrolyte, with 0.1M TBA+, with 0.10 M Li+) Path length 1 mm.

A(ii) 10 mM TCNE in ACN (0.10M TBAF), solution five days old, pathlength 1 cm.

A(iii) as A(ii) in 0.10M lithium perchlorate.

B(i) as A(i), in water, no electrolyte.

B(ii) as B(i), 10 mM, 1 cm pathlength.

C As A(i) except TCNQ.

Figure 61 shows the MSRS spectra of TCNE and TCNQ

in acetonitrile where the potential of the electrode was

stepped to the diffusion controlled region of the first re-

duction wave. Wavelengths were scanned from 8000 Å to 2500

Å. For TCNE, the spectrum shows a broad absorption with

a series of fine structure bands. The center of the

absorption, which also corresponded to λ max was found

to be 4333 Å. This spectrum corresponded well with the

spectrum obtained for the anion radical of TCNE in

acetonitrile by Jeanmaire et al (138). Their spectrum

showed the same feature with λ max occurring at 4350 Å.

In the case of TCNQ, two absorptions were obtained;

a broad one in the wavelength range of 8000 to 6000 Å

consisting of several peaks and a narrow one with a single

peak with λ max 4426 Å. For the broad absorption, λ max

occurred at 7349 Å. The features of this spectrum agree

with those obtained by Melby et al (152) for the anion
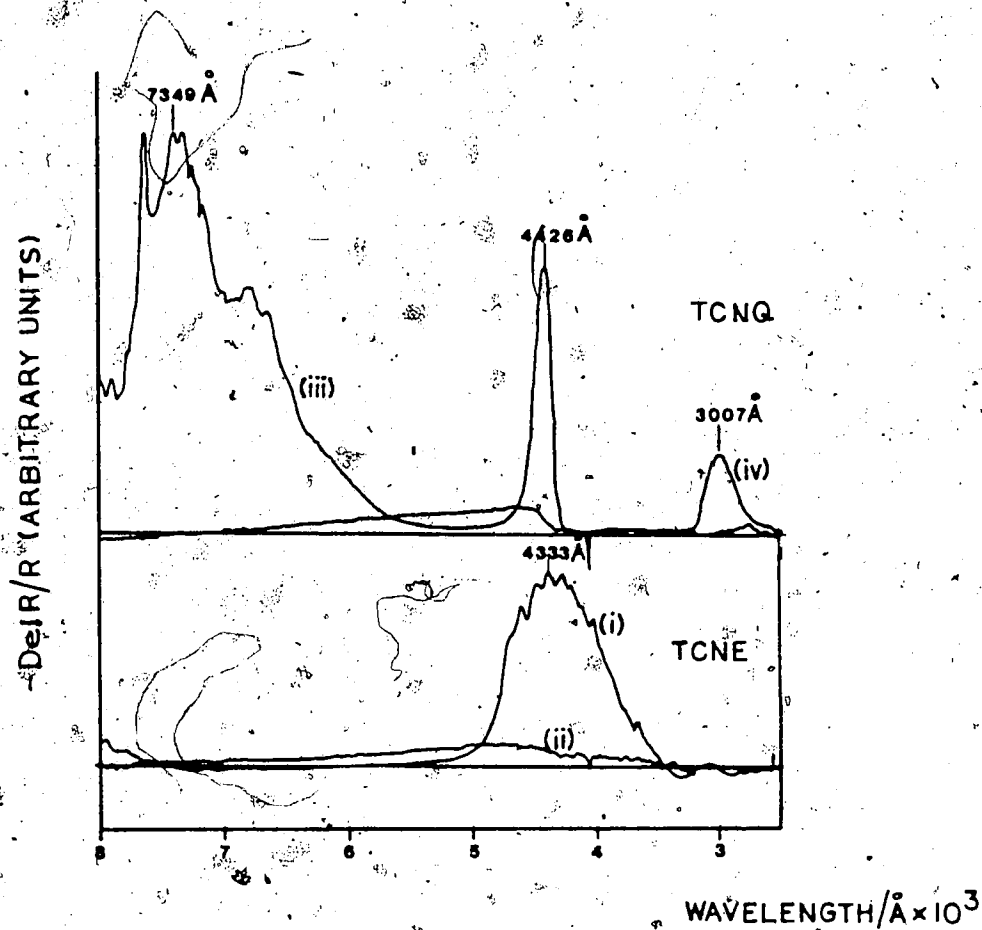
Figure 61. MSRS Spectra of anion radicals and dianions of
TCNE and TCNQ in ACN (0.10 M TBAF).
TCNE (i) Formation of TCNE⁻ Potential +0.40 to
-0.40 V.
(ii)Formation of TCNE= Potential +0.40 to
-2.20 V.
TCNQ(iii)Formation of TCNQ⁻ Potential +0.40 to
-0.30 V.
(iv)Formation of TCNQ= Potential +0.40 to
-0.80 V.

radical in acetonitrile. These workers obtained peaks at 420,

842, 744, 760, 680 and 615 nanometers. No major differences

were obtained for the spectra obtained here with different.

supporting electrolytes.

If the potential was stepped to the diffusion

controlled region of the second wave, TCNE did not show any

significant absorption peaks in the wavelength region

8000-2500 Å. TCNQ solutions had a weak absorption peak

with $\lambda$ max at 3007 Å (see Figure 61). Suchanski and

Van Duyne (163) observed the dianion absorption in aceto-

nitrile at 3300 Å. Again this absorption was found, in

this study, to be independent of supporting electrolyte.

It was shown in Chapter 2 that the normalized reflec-

tance is related to the integral of the current with

respect to time by equation (2.38)

$$-DelR/R = (4.606\ \ell)/(nFA\ \cos\theta)\int_0^t i(t)dt$$

The integral is the total amount of the absorbing species produced and is equal to q/nFA where q is the total amount of charge passed for the time interval considered. The value of q is determined by integrating the Cottrell equation with respect to time

$$\int_0^t i \, dt = \int_0^t (nFA(D)^{\frac{1}{2}} \, C)/(\pi \, t)^{\frac{1}{2}} \, dt \qquad (5.24)$$

$$= 2nFA(D\pi)^{\frac{1}{2}} \, C \, t^{\frac{1}{2}}$$

Substituting,

$$-DelR/R = \frac{4.606 \, \ell}{nFA \cos \theta} [2nFA(D\pi)^{\frac{1}{2}} \, C \, t^{\frac{1}{2}}] \qquad (5.25)$$

Therefore, if the absorbing species at the wavelength of interest is stable on the time scale of the experiment, a plot of -DelR/R vs $t^{\frac{1}{2}}$ should give a straight line through the origin.

However, if the absorbing species decay following

first order kinetics, it has been shown (198) that the

first order homogeneous rate constant is given by

$$k = \frac{[A(t)]_o - [A(t)]_k}{\int_0^t [A(t)]_k \, dt} \qquad (5.26)$$

where $[A(t)]_o$ is the absorbance which would be obtained

at time t if the absorbing species does not decay,

$[A(t)]_k$ the absorbance at time t where decay occurs with

first order rate constant k. The denominator in the above

equation represents the area under the actual absorbance-

time profile for the time interval 0 to t. Since for the

small values of DelR/R which are normally obtained (1.0e-3

or less), the time-dependent absorbance is directly

proportional to -DelR/R (see Chapter 2), then

$$k = \frac{[-DelR/R]_o - [-DelR/R]_k}{\int_0^t [-DelR/R]_k \, dt} \qquad (5.27)$$

Figure 62 shows the normalized reflectance-time pro-

files for 1.00 mM solutions of TCNE and TCNQ in acetoni-

trile. For these profiles, plots of -DelR/R vs $t^{\frac{1}{2}}$ show

a straight line through the origin (Figure 63). Normalized

reflectance time profiles were also obtained for TCNE and

TCNQ in the presence of water (Figure 62). From these,

-DelR/R were again plotted vs $t^{\frac{1}{2}}$, given in Figure 64.

These plots now show a marked difference in that at longer

times, -DelR/R values deviated, on the low side, from

linear behavior. Calculated k values are given in Table 18.

Table 18. Apparent First Order Rate Constants for Decay
of TCNE and TCNQ Anion Radicals

| Compound | $\lambda$ $\overset{\circ}{A}$ | $[H_2O]$ /M | $k_{-1}$ /s |
|---|---|---|---|
| TCNE | 4250 | 2.05 | 1.58 |
| TCNQ | 6450 | 3.64 | 1.20 |
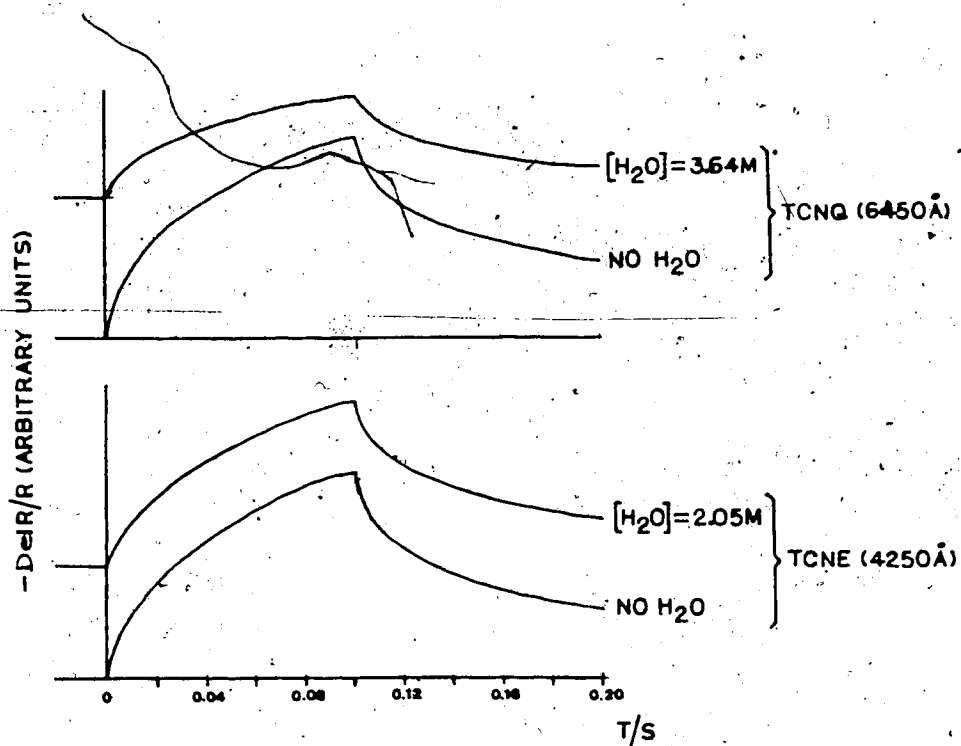
Figure 62. Normalized reflectance-time profiles for TCNE$^{\pm}$ and TCNQ$^{\pm}$, with and without water addition, in ACN (0.10 M TBAF).
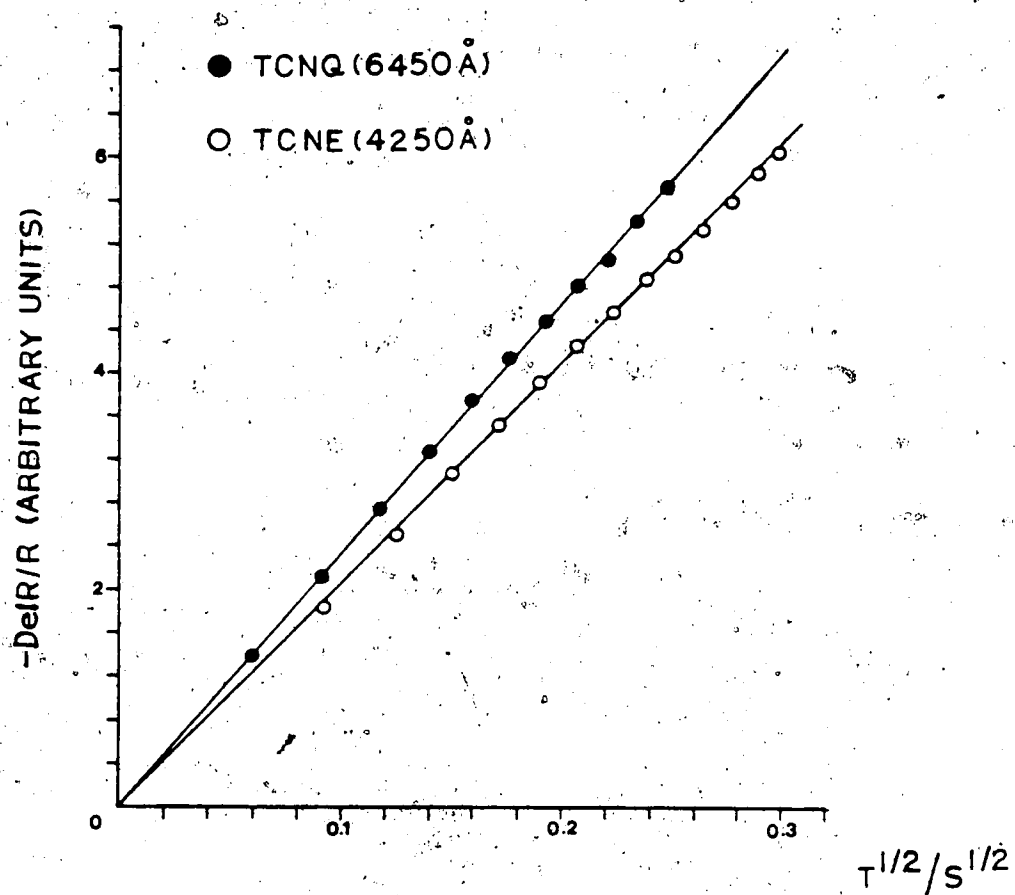
Figure 63. Plot of normalized reflectance (-delR/R) versus square root of time for 1.00 mM solutions of anion radicals of TCNE and TCNQ.
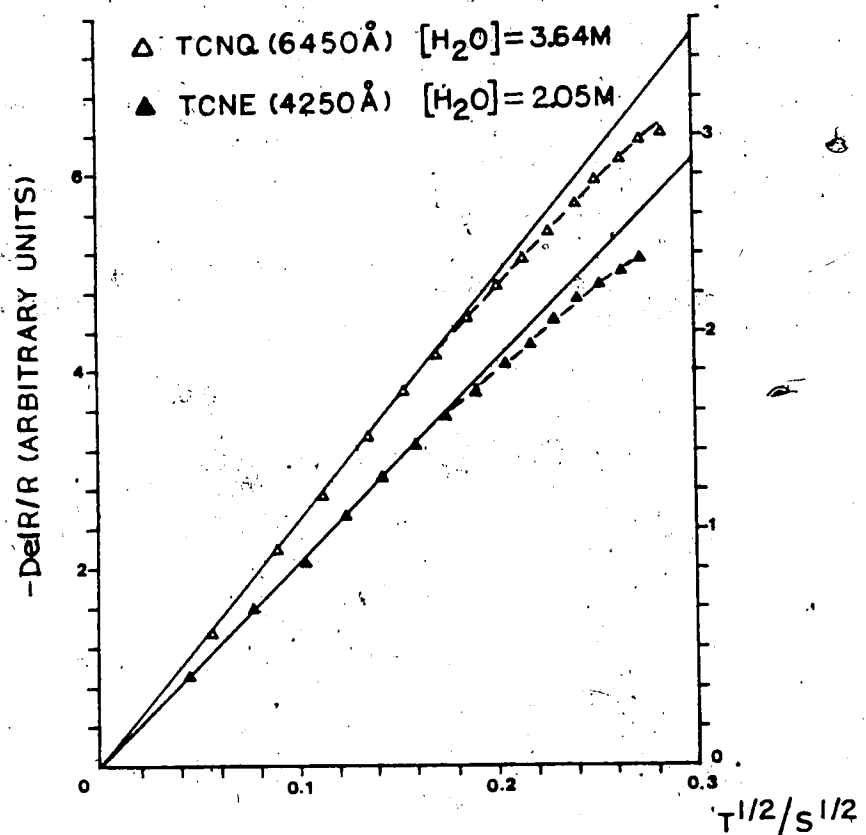
Figure 64. Plots of normalized reflectance versus square root of time for TCNE and TCNQ anion radical in ACN with water addition. Left hand scale for normalized reflectance refers to TCNE⁻ and right hand scale to TCNQ⁻.

## 5.4 Discussion

The cyclic voltammetric results gave overwhelming

evidence that the first reduction of TCNE and TCNQ in

acetonitrile at glassy carbon and platinum electrodes

corresponded to reversible behavior: the fact that

delE(p) values were close to the theoretical value of 59 mV

and did not vary with sweep rates supports this argument.

Also, i(pa)/i(pc) values close to 1.0 imply that the product

of the first reduction is a stable species on the time

scale of the experiments. Since the slowest sweep rate

was 25 mV/s, the species were stable for at least 40 s.

Previous investigations have established that these

products were stable for a much longer time (138,157). In

both cases, the first reduction waves involved one-electron

transfers. Therefore, the product formed must be the anion

radicals. Diffusion coefficients obtained for TCNE (2.20

e-5 cm$^2$ /sec) and TCNQ (2.00e-5 cm$^2$ /sec) were

slightly larger than those obtained by Sharp (148) who

found a value of 1.91e-5 cm$^2$/s for TCNE and 1.42e-5

cm$^2$/s for TCNQ. i(p)/(v)$^\frac{1}{2}$ values at the planar

glassy carbon electrode were constant at all sweep rates

but for the platinum wire electrode, the values increased

at low sweep rates. This is because, at low sweep rates,

cylindrical diffusion contributions must be considered.

Peak potentials were found to be invariable with

sweep rates. Also, examination of Table 4 and Table 10

reveals that different electrodes and supporting electro-

lytes do not affect these values. Therefore, there is

negligible ion pairing between the anion radicals of TCNE

and TCNQ and the countercations in acetonitrile. The

same conclusion was found for aromatic hydrocarbon anion

radicals studied earlier.

For reversible reduction the peak potentials and the

half peak potentials are related to polarographic Eh

values by the relation .

$$Eh = E(p) + 1.11 \; RT/nF \qquad (5.30)$$

$$Eh = E(p/2) - 1.09 \; RT/nF \qquad (5.31)$$

At 23°C, and for n=1, RT/nF=0.0255 volts and

$$Eh = E(p) + 0.028. \qquad (5.32)$$

or in terms of half peak potentials

$$Eh = E(p/2) - 0.028 \qquad (5.33)$$

The calculated Eh values are compared relatively to

literature values in Table 19.

Table 19. Comparison of Eh Values for the First
Reduction Wave of TCNE and TCNQ in Acetonitrile
(0.10 M LiClO4)

| Compound | Eh vs Ag/Ag+ This Work | Eh vs SCE Melby et al (152) |
|---|---|---|
| TCNE | -0.086 | +0.152 |
| TCNQ | -0.118 | +0.127 |

In both cases, the Eh value for TCNE is slightly

more positive that that for TCNQ. This means that TCNE

in acetonitrile is a slightly stronger π-acid than TCNQ.

Pons et al (139) have found, using a surface sensitive

FTIR technique, that in the presence of non-complexing

TBAF supporting electrolyte, that a monolayer of TCNE anion

radicals adsorbed flat on the surface of the platinum

electrode. This was attributed to the formation of an

electron-donor-acceptor complex between the platinum metal

and the TCNE molecules. This behavior was absent when

LiClO4 was used as supporting electrolyte. However, this

behavior was not detected in the cyclic voltammetric

studies of the first reduction wave. The presence of

adsorbed TCNE anion radical could affect the reversibility

of the first wave. i(pa)/i(pc) values could deviate from

unity values. If the adsorption was strong, prepeaks and

postpeaks could be observed. However, none of these

effects were observed. It is possible that the effect observed by Pons et al (139) was very small and since cyclic voltammetry is not as sensitive to surface species as the FTIR technique used, it was not observed in this work.

For the second reduction wave of TCNE, i.e. the reduction of the anion radical to the dianion (chronoamperometry showed that this reduction involved one electron) reversibility was only found for both platinum and carbon electrodes for Na+ countercation. With Li+, platinum electrode showed reversible reduction but the increase of i(pa)/i(pc) values was about the same as for the other case where no adsorption was present which means that the anion radical was not adsorbed. The behavior of the second wave with increase of i(pa)/i(pc) with increase in scan rate and the absence of prepeaks or postpeaks points toward weak product adsorption as discussed by Wopschall and Shain (243). Except for this

adsorption of the dianion at carbon, the electron transfer

rate for TCNE at both platinum and carbon electrodes with

Na+ and Li+ countercations appears to be fast enough so that

for the time scale of the voltammetric experiments (25 mV/s

to 500 mV/s scan rates), Nernstian behavior was observed.

However this cannot be said for TBA+ and TEA+ countercations

as shown by the results for these two countercations. Not

only was cation effect apparent but there was also dependence

on electrode materials. With TBA+ countercation the peak

cathodic potential for the second wave at glassy carbon

electrode was 335 mV more positive compared to that at plati-

num (Table 5). This value was 172 mV with TEA+ countercation.

Further, the apparent heterogeneous rate constants at glassy

carbon with TEA+ countercation was (1.2 ± 0.1)e-2 cm/s

compared to 1.8e-3 cm/s at platinum, which was 7 times

slower. The same trend was observed with TBA+ (3.8e-5 cm/s)

being 37 times slower than that at glassy carbon (1.4e-3 cm/s).

In addition, it was noted that the rate was faster with TEA+ than TBA+ countercation. The large shifts in E(pc) values, for the case of Na+ and Li+, where electrode reaction was fast points toward the existence of ion pairing. Further, the plot of Eh vs ionic radius given in Figure 58 showed that the smaller the ionic radius of the cation, the larger the positive shift. This indicates that contact ion pairs (172,210) were formed as opposed to solvent separated ion pairs. For contact ion pairs it would be expected that the strength of ion pairing increased in the order of decreasing ionic radius this being TBA+ < TEA+ < Na+ < Li+ as was shown here.

At a glassy carbon electrode, there was no evidence of adsorption of TCNE$^{\pm}$ with both electrodes and all cations, and except for the differences in heterogeneous rate constants with different countercations points toward the ion pairing abilities of the cations. TBA+ is not expected to ion pair to

TCNE= to any appreciable extent as confirmed by the results

obtained for TCNQ= (Table 15). Chauhan et al (246) have found

that TEA+ formed weak ion pairs with nitromesitylene anion .

radicals in ACN and this may well occur for TCNE=. However,

Na+ and Li+ ion paired strongly with TCNE= as shown by the

positive shifts in Eh. Therefore strong ion pairing tends to

increase the rate of electron transfer for TCNE$^{\pm}$ reduction.

The present results seem to confirm the proposal by Jeanmaire

et al (138): a change in geometry from planarity for TCNE$^{\pm}$ to

nonplanarity for TCNE= causes irreversibility for the reduction

of TCNE$^{\pm}$. Also no evidence was given in that study. In the

presence of the strong ion pairing Na+ and Li+ countercations,

the irreversibility of the reduction was lifted because ion

pairing tends to localize the negative charges at the ethylene

carbons and therefore maintain the planarity of the dianion.

For TEA+, only weak ion pairing may be present, and therefore

a compromised position is reached and the rate constant is

between the two extreme cases.  Huebert and Smith (2) have

observed a large stereochemical effect for the reduction of

the nonplanar cyclooctatetracene to its planar anion radical.

The electron transfer was found to be slow for this system.

The results obtained at a platinum electrode are more

difficult to explain.  Certainly, the ion pairing effect is

present since the TCNE$^-$ reduction showed Nernstian behavior

in the presence of Na+ and Li+ but not with TEA+ and TBA+.

For the latter two cations, rate constants were much slower

compared to those at a glassy carbon electrode.  Strong

adsorption of TCNE$^-$ at platinum was not observed since this

would result in postpeaks and prepeaks.  Further, anion

radical would show up in the first reduction wave.  However,

this was not so because the first wave gave Nernstian behavior

in all cases.  Also, adsorption of the dianion will cause the

reverse peaks to occur at more positive values but this was not

the case as can be seen from the data of Table 5.  However,

the fact that the reduction peak potentials were more negative

than those observed at carbon indicate the presence of

adsorption. Also, Pons et al (139) have shown that adsorption

of the anion radical of TCNE was present at platinum with TBA+

as countercation. It is possible that, as was mentioned

earlier, cyclic voltammetry was not sensitive enough to

detect adsorption in this case and further the presence of

weak adsorption would be masked by the irreversibility of the

wave due to geometry change. However, the cathodic peak

potential shifts at platinum compared to carbon (335 mV for

TBA+, 172 mV for TEA+) appear to be rather large to be

explained by weak adsorption. Therefore, the only firm conclu-

sion which can be reached here is that geometry change caused

the irreversibility of TCNE$^-$ reduction with TBA+ and TEA+

cations. The smaller rate constants found at a platinum

electrode compared to a carbon electrode, together with the

negative shift in cathodic peak potential, could only be

tentatively attributed to adsorption of the TCNE$^+$ assigned based on the results of Pons et al (139).

In passing, the method of the variation of delE(p) with scan rate used in the determination of rate constants deserves a little discussion. The $\Delta$ values for different delE(p) values, as calculatd by Nicholson (84), assumes that the transfer coefficient $\alpha$ is 0.5. The error expected in the calculated rate constant with this assumption is small, approximately 5%, if the reduction is sufficiently close to Nernstian behavior;  i.e. if $\alpha$ does not deviate too much from 0.5.  This means that delE(p) values should be between 60/n and 120/n mV.  At higher values of delE(p), deviations of $\alpha$ from 0.5 become larger.  For example for delE(p) having a value of 200/n mV, an error of 20% in the determined rate constants is expected (61).  However, at delE(p) values close to the reversible value of 59/n mV, small changes in delE(p) give rise to large variations in the values of $\Delta$, as can be

seen from Figure 54. Therefore the best accuracy can be

obtained if delE(p) values are kept between about 75 mV and

120 mV, if possible.

For the reduction of TCNQ, diagnostic criteria for the

cyclic voltammetric technique confirms the Nernstian behavior

of both the first and second wave at both electrodes and all

supporting electrolytes used. These include the constancy of

peak potentials at all sweep rates, the value of 1.0 obtained

for i(pa)/i(pc) values, and delE(p) values close to 59 mV for

reversible one-electron waves at all sweep rates. The number

of electrons transferred for the first wave was found to be

approximately 2.0 for the sum of the first and second wave.

This implies the formation of the anion radical and the

dianion. $i(pc)/v^{\frac{1}{2}}$ value for the second wave was found about

10% lower than that for the first wave, as was the case for

TCNE. This is attributed to a small decrease in diffusion

coefficient for the anion radicals. The peak potentials, for

the TCNQ potentials did not show any dependence on counter-

cations or electrode materials. Therefore no ion pairing was

present between $TCNQ^-$ and TBA+, Na+, or Li+, the cations used

in this investigation. The second reduction, $TCNQ^-$ to $TCNQ=$,

gave peak potential which were dependent on countercations

although not electrode material. The $E\bar{h}$ values, from Figure

58, increased with decreasing size of ionic radius according

to TBA+ > Na+ > Li+. These large shifts with ionic radius

were again attributed to the formation of contact ion pairs.

For the $TCNQ^-$ reduction no decrease in heterogeneous rate

constant was observed for TBA+ because there was no change in

planar geometry in going from $TCNQ^-$ to $TCNQ=$. The presence of

the quinoid functionality assures planarity whereas the

ethylenic group in TCNE could not.

In the presence of mixed electrolytes, the reduction of

$TCNE^-$ showed adsorption effects as was mentioned earlier

(Figure 58A). However, the reversible nature of TCNE reduction

was not affected. In general the adsorption characteristics

are typical of product adsorption, namely the adsorption of

TCNE= or its ion pairs. For example, with 0.095 M TBAF and

0.005 M LiClO4, at a platinum electrode, the sharpness of the

anodic peak is indicative of product adsorption. Wtih 0.05 M

TBAF and 0.05 M LiClO4 at carbon a prepeak was observed for

the cathodic scan as well as the sharp anodic peak. This is

the criterion for strong product adsortion, as given by

Wopschall and Shain (243). The change in cyclic voltammograms

for TCNE with 0.05 M TEAF and 0.05 M LiClO4 at platinum was

even more dramatic. Not only was a sharp cathodic peak for

TCNE⁻ reduction observed but no reverse peak was seen.

Instead a very large, sharp peak was observed just anodic of

the peak for TCNE⁻ oxidation. This is highly indicative of

formation of an insoluble mixed salt of TCNE= deposited on the

electrode which is not oxidized in the potential region of the

simple TCNE= oxidation and therefore no oxidation current was

seen. However at far more positive potential, destruction of

the insoluble film occurred-giving rise to the large, sharp

peak. The occurrence of this type of peak, which was much

larger than that caused by usual adsorption behavior, was

found by Nagaoka and Okazaki (247) for the sparingly soluble

anthranthrone anion radical / Ba++ salt in DMF. However, in

their case, the peak occurred in the region of the oxidation

of anion radical.

For TCNQ, mixed electrolytes did not change the reversible

behavior of both the first and second reduction. This means

that variation of Eh with cation concentrations could be

studied at constant ionic strength without the deleterious

effect of adsorption. Initially, it was established that TBA+

did not ion pair significantly with TCNQ=. This was shown by

the fact that Eh did not shift appreciably with TBA+ concen-

tration after correction for liquid junction potential. From

Table 15 it can be seen that for the concentrations of TBA+

used, the largest shift in Eh after correction for Ej was only

10 mV, certainly not much larger than experimental errors such

as errors in reading and in locating E(p/2) values used for

obtaining Eh (about 5 mV). For the variation of Eh with metal

cations Na+ and Li+, the condition of the metal cations being

in large excess of the TCNQ concentration for the validity of

equations (5.19) and (5.22) is satisfied by keeping the TCNQ

concentration at 5.00 mM or greater. Since TCNQ= did not form

any ion pairs with the cations studied, only equation (5.23)

applies to the present study. It was shown in Figure 59 the

plots for delEh vs log Cm+ exhibited two linear segments for

both Na+ and Li+. This is indicative of the formation of ion

pairs with two different stoichiometries. In the case of Li+,

the slopes of 52 and 122 mV for the two segments are very

close to those of 59 and 118 mV for the theoretical quantita-

tive formation of TCNQ=,Li+ ion pairs with 1:1 and 1:2 stoichi-

ometries. The formation constants were then calculated from

equation (5.23) using the data from the segment where the

respective ion-pair was formed. In the case of sodium the

slopes for the linear segments were smaller than the theoreti-

cal values, being only 27 and 80 mV. This means that formation

of the 1:1 and 1:2 ion pairs was not quantitative and therefore

less strong than for Li+. The same method was used for calcu-

lation of the formation constants for the TCNQ=,Na+ ion pairs.

However, in this case, care was taken to avoid points in the

crossover region for the two line segments where curvature of

the plot arose. Values of formation constants obtained in this

manner were found to be reasonably constant for different

points in the same linear segment, in all cases exhibiting a

standard deviation of about 10% of the calculated values. The

values for the formation constants given in Table 17 show that

the strength of ion pair formation for Li+ was about 100 times

greater than that for Na+ for both species formed.

The presence of ion pairing between TCNQ= and Na+ and Li+

cations has been confirmed by shifts in vibrational absorptions

of the C=N stretch mode observed in the authors laboratory

(172). The results are shown in Table 20.

Table 20. Vibrational Absorption (C=N stretch) for TCNQ: and
TCNQ= with Different Supporting Electrolytes (0.10M).
C=N Absorption Bands (cm ).

| Species | TBAF | NaClO4 | LiClO4 |
|---------|------|--------|--------|
| TCNQ: | 2181.5 | no change | no change |
| | 2154.5 | no change | no change |
| TCNQ= | 2150.6 | 2156.4 | 2116.1 |
| | 2104.3 | 2110.1 | 2117.8 |

For TCNQ: no ion pairing was present and no shift in the

absorption bands was observed. However, the TCNQ= absorption

bands shifted to higher energy with increased strength of ion

pairing (TBA+ > Na+ > Li+). This is consistent with the view

that ion pairing localizes the negative charges on the dicyano

carbon and reduces delocalization through the C=N bond which

tends to reduce the triple bond character.

As mentioned in the results section, freshly prepared solutions of TCNE in acetonitrile were colorless but upon standing turned yellow. If supporting electrolyte was present the color change was obvious for TBAF but not so much for LiClO4. The fact that the solution containing TBAF showed two additional absorption peaks at 3973 Å and 4159 Å (Figure 60) offers a simple explanation since these two peaks correspond to the absorption maxima of TCNE in water at 3956 A and 4125 Å (Figure 60). These two absorptions are probably due to the formation of weak charge-transfer complexes between water and TCNE. In the presence of LiClO4, these absorptions were not observed because at the low concentration level of water in purified acetonitrile (probably 1-2 mM), most of the water present was tied up by Li+ ions, which were present at 0.1M.

The MSRS spectrum obtained when the potential was

stepped to the diffusion controlled region of the first

wave corresponded to the spectra of the anion radicals of

TCNE and TCNQ obtained by other workers. The dianion of TCNE

did not show any absorption in the wavelength region studied

(8000 Å to 2000 Å) whereas, for TCNQ only a weak absorption

was observed with $\lambda$ max at 3007 Å. This is in agreement

with results by other investigators (163). The determination

of rate constant for the protonation of TCNE and TCNQ anion

radicals is based on the assumption of first order decay of

these species. Since the concentrations of water were 2.05 M

and 3.64 M for TCNE (1.00 mM) and TCNQ (1.00 mM) respectively,

pseudo first order conditions existed and the assumption is

valid.

Sharp (148) studied the first order decay of TCNE

and TCNQ anion radicals in acetonitrile by observing changes

in i(pa)/i(pc) with scan rates. No water was added to the

solutions and decay was assumed to be due to trace

impurities present in the solvent. The rate constant for

TCNE: decay was found to be about 20 times greater than

that for TCNQ:. However, in this work, this value was

found to be 2.

It is concluded that simple electrochemical techniques

can be effectively utilized to study ion association reactions

in solutions of high dielectric constant. Coupled with

standard spectrophotometry and spectroelectrochemistry, these

methods allow fast and accurate determination of stoichiome-

tries, mechanisms, and kinetic parameters of these reactions.

# LITERATURE REFERENCES

1.  M.E. Peover, J.S. Powell, J. Electroanal. Chem.,
    20 (1969) 427.

2.  B.J. Huebert, D.E. Smith, J. Electroanal. Chem.,
    31 (1971) 333.

3.  J.P. Stradins, Electrochim. Acta, 9 (1964) 711.

4.  G.J. Hoijtink in P. Delahay and C.W. Tobias, Eds.,"The
    Electrochemical Reduction of Aromatic Hydrocarbons,"
    in "Advances in Electrochemistry and Electrochemical
    Engineering," Vol. 7, Interscience, New York, 1970,
    p. 221.

5.  V.D. Parker, J. Am. Chem. Soc., 98 (1978) 98.

6.  P.H. Rieger, C.K. Fraenkel, J. Chem. Phys., 37 (1962)
    2795.

7.  A. Macoll, Nature, 163 (1949) 178.

8.  T.J. Katz, W.H. Reinmuth, D.E. Smith, J. Am. Chem.
    Soc., 84 (1962) 802.

9.  E. Itabashi, J. Electroanal. Chem., 36 (1972) 179.

10. W.J.M. van Tilborg, L.J.G. Dekker, C.J. Smit, Rec. Trav.
    Chim, Pays-Bas, 97, (1978) 321.

11. W.J.M. Van Tilborg. C.J. Smit, R.A. van Santen,
    Rec. Trav. Chim. Pays-Bas, 98 (1979) 526.

12. M.T. Watts, M.L. Lu, R.C. Chen, M.P. Eastman, J.
    Phys. Chem., 77 (1973) 2959.

13. M. Ogasawara, H. Takaoka, K. Hayashi, Bull. Chem.
    Soc. Japan, 46 (1973) 36.

14. Ions and Ion Pairs in Organic Reactions, M. Szwarc, Ed.,
    Vol. 1, Interscience, New York, 1972.

15. Ions and Ion Pairs in Organic Reactions, M. Szwarc, Ed.,
    Vol. 2, Interscience, New York, 1972.

16. B. Bockrath, L.M. Dorfman, J. Phys. Chem., 77 (1973)
    2618.

17. A. Rainis, M. Szwarc, Int. J. Chem. Kinetics, 7 (1975) 919.

18. E.J. Panck, T.J. Rodgers, J. Am. Chem. Soc., 96 (1974) 6921.

19. H.A. Laitinen, S. Wawzonek, J. Am. Chem. Soc., 64 (1942) 1765.

20. S. Wawzonek, H.A. Laitinen, J. Am. Chem. Soc., 64 (1942) 2365.

21. S. Wawzonek, J.W. Fan, J. Am. Chem. 68 (1946) 2541.

22. L.H. Chopard-dit-Jean, E. Heilbronner, Helv. Chim. Acta, 36 (1953) 144.

23. G.J. Hoijtink, J. van Schooten, E. de Boer, W.I. Aalsberg, Rec. Trav. Chim. Pays-Bas, 73 (1954) 355.

24. S. Wawzonek, E.W. Blaka, R. Berkey, M.E. Runner, J. Electrochem. Soc., 102 (1955) 235.

25. A.C. Aten, C. Buthker, G.J. Hoijtink, Trans Faraday Soc., 55 (1959) 324.

26. P.H. Given, M.E. Peover, J. Chem. Soc., (1960) 385.

27. P.H. Given, M.E. Peover, J. Schoen, J. Chem. Soc., (1958) 2674.

28. A.J. Bard, L.R. Faulkner, Electrochemical Methods: Fundamentals and Applications, John Wiley and Sons, New York, 1980, p. 96.

29. A.C. Aten, G.J. Hoijtink, Advances in Polarography, Pergamon Press, Oxford, 1961, p. 777.

30. H. Kojima, A.J. Bard, J. Electroanal. Chem., 63 (1975) 117.

31. D.E.G. Austen, P.H. Given, J.E. Ingram, M.E. Peover, Nature, 182 (1968) 1784.

32. B.S. Jensen, V.D. Parker, J. Am. Chem. Soc., 97 (1975) 5211.

33. S.V. Laszczynski, Z Elektrochem., 2 (1895) 55.

34. A. Brenner, "Electrolysis in Nonaqueous Systems," in P. Delahay and C.W. Tobias, Eds., "Advances in Electrochemistry and Electrochemical Engineering," Vol. 5, Interscience, New York, 1967, p. 205.

35. R. Jasinski, High-Energy Batteries, Plenum Pres, New York, 1967.

36. Lithium Batteries, The Electrochemical Society Soft-bound Series, H.V. Venkatasetty, Ed., 1981.

37. D.J. Astley, J.A. Harrison, H.R. Thirsk, Trans Faraday Soc., 64 (1968) 192.

38. R.F. Scarr, J. Electrochem. Soc., 117 (1970) 295.

39. S.G. Meibuhr, J. Electrochem. Soc., 117 (1970) 56.

40. J.N. Butler, D.R. Cogley, J.C. Synott, J. Phys. Chem., 73 (1969) 4026.

41. J.N. Butler, J. Electroanal. Chem., 14 (1967) 89.

42. B. Burrows, S. Kirkland, J. Electrochem. Soc., 115, (1968) 1164.

43. B.N. Kabanov, I.I. Astakhov, I.G. Kiseleva, Russian Chem. Rev., 34 (1965) 775.

44. J. Heyrovsky, Chem. Listy, 16 (1922) 256.

45. E.S. Peracchio, V.W. Meloche, J. Am. Chem. Soc., 60 (1938) 1770.

46. I. Zlotowsky, I.M. Kolthoff, Ind. Eng. Chem. Anal. Ed., 14 (1942) 473.

47. I. Zlotowsky, I.M. Kolthoff, J. Am. Chem. Soc., 64 (1942) 1297.

48. A.A. Vlcek, Coll. Czech. Chem. Commun., 20 (1955) 413.

49. V. Gutman, E. Nedbalek, Mh. Chem., 89 (1958) 203.

50. R.C. Larson, R.T. Iwamoto, J. Am. Chem. Soc., 82 (1960) 3239, 3526.

51. J.F. Coetzee, J.L. Hedrick, J. Physik. Chem., 67 (1963) 221.

52. V. Gutman, G. Schober, Z. Anal Chem., 171 (1959) 339.

53. G. Schober, V. Gutman, "Advances in Polarography,"
    I.S. Longmuir, Ed., Pergamon Press, London, 1960,
    p. 940.

54. J.F. Coetzee, W.S. Siao, J. Inorg. Chem., 2 (1963) 14.

55. G. Schober, V. Gutman, Mh. Chem., 89 (1958) 401.

56. H.A. Laitinen, C.E. Shoemaker, J. Am. Chem. Soc.,
    72 (1950) 4975.

57. L.A. Knecht, I.M. Kolthoff, J. Inorg. Chem., 1 (1962)
    195.

58. I.M. Kolthoff, J.F. Coetzee, J. Am. Chem. Soc., 79
    (1957) 870.

59. G.H. Brown, R.A. Urfali, J. Am Chem. Soc., 80 (1958)
    2113.

60. D.L. McMasters, R.B. Dunlap, J.R. Kuempel, L.W.
    Kreider, T.R. Shearer, Anal. Chem., 39 (1967) 103.

61. J.W. Diggle, A.J. Parker, D.A. Owensby, Aust. J.
    Chem., 28 (1975) 237.

62. G.J. Hills, L.M. Peter, J. Electroanal. Chem., 50
    (1974) 175.

63. V. Gutmann, M. Michlmayr, G. Peychal-Heiling, Anal.
    Chem., 40 (1968) 619.

64. R.R. Besette, D.F. Harwood, Anal. Chim. Acta, 66
    (1973) 105.

65. A. Baranski, W.R. Fawcett, J. Electroanal. Chem..
    94 (1978) 237.

66. A. Baranski, W.R. Fawcett, J. Chem. Soc. Faraday
    Trans. 1, 78 (1982) 1279.

67. W.R. Fawcett, J.S. Jaworski, J. Chem. Soc. Faraday
    Trans. 1, 78 (1982) 1971.

68. H. Berthelot, Ann., 143 (1867) 98.

69. W. Schlenk, J. Appenrodt, A. Michael, A. Tahl, Ber, 47 (1914) 479.

70. W. Schlenk, J. Bergmann, Ann., 463 (1928) 91.

71. C.B. Wooster, F.B. Smith, J. Am. Chem. Soc., 53 (1931) 179.

72. N.D. Scott, J.F. Walker, V.L. Hansley, J. Am. Chem. Soc., 58 (1936) 2442.

73. A. Jeannes, R. Adams, J. Am. Chem. Soc., 59 (1937) 2608.

74. V.L. Hansley, Ind. Eng. Chem., 43 (1951) 1759.

75. D. Lipkin, D.E. Paul, J. Townshend, S.I. Weissman, Science, 117 (1953) 534.

76. T.L. Chu, S.C. Yu, J. Am. Chem. Soc., 76 (1954) 3367.

77. G.J Hoijtink, E. de Boer, P.H. Van der Meij, W.P. Weijland, Rec. Trav. Chim. Pays-Bas 74 (1955) 277.

78. G.J. Hoijtink, E. de Boer, P.H. Van der Meijj, W.P. Weijland, Rec. Trav Chim. Pays-Bas, 75 (1956) 487.

79. G.J. Hoijtink, Rec. Trav. Chim. Pays-Bas, 74 (1955) 1525.

80. D.E. Paul, D. Lipkin, S.I. Weissman, J. Am. Chem. Soc., 78 (1956) 116.

81. P. Balk, G.J. Hoijtink, J.W.H. Schreurs. Rec. Trav. Chim. Pays-Bas, 76 (1957) 813.

82. P. Balk. S. de Bruijn, G.J. Hoijtink, Mol. Phys., 1 (1958) 151.

83. P. Balk, S. de Bruijn, G.J. Hoijtink, Rec. Trav. Chim. Pays-Bas, 76 (1957) 860.

84. G.J. Hoijtink, Rec. Trav. Chim. Pays-Bas, 76 (1957) 869.

85. G.J. Hoijtink, Rec. Trav. Chim. Pays-Bas, 76 ((1957) 885.

86. P. Balk, S. de Bruijn, G.J. Hoijtink, Rec. Trav. Chim. Pays-Bas, 76 (1957) 907.

87. P. Balk, S. de Bruijn, G.J. Hoijtink, Mol. Phys., 2 (1957) 151.

88. J. Jagur-Grodzinski, M. Feld, S.L. Yang, M. Szwarc, J. Phys. Chem., 69 (1965) 628.

89. S.I. Weissman, J. Townsend. D.E. Paul, G.E. Pake, J. Chem. Phys., 21 (1953) 2227.

90. S. Winstein, E. Clippinger, A.H. Fainberg. G.C. Robinson, J. Am. Chem. Soc., 76 (1954) 2597.

91. E. Grunwald, Anal. Chem., 26 (1954) 1696.

92. M. Szwarc, Carbanions, Living Polymers and Electron Transfer Processs, Interscience, New York, 1968.

93. S. Miertus, O. Kysel, J. Danciger, Coll. Czech. Chem. Commun., 45 (1980) 360.

94. R.N. Adams, J. Electroanal. Chem., 8 (1964) 151.

95. P.H. Rieger, I. Bernal, W.H. Reinmuth, G.K. Fraenkel, J. Am. Chem. Soc., 85 (1963) 683.

96. K.H.J. Buschow, J. Dieleman, G.. Hoijtink, J. Chem. Phys., 42 (1965) 1993.

97. J. Smid in "Ions and Ion Pairs in Org. Reactions," Vol. 1, M. Szwarc Ed., Wiley-Interscience, New York 1972, p. 85.

98. A. Streitwieser, G.J. Chang, W.B. Hollyhead, J.R. Murdoch, J. Am. Chem. Soc., 94 (1972) 5288.

99. A.J. Popov, Pure Appl. Chem., 41 (1975) 275.

100. S. Konishi, Y. Morioka, I Nakagawa, Chem. Phys. Lett., 55 (1978) 428.

101. J.C. Evans, G.Y.-S Lo, J. Phys. Chem., 69 (1965) 3223.

102. B. Herold, J. Catal. Rev., (1978) 17.

103. T.L. Cairns, R.A. Carboni, D.D. Coffman, V.A. Engel-
     hardt, R.E. Heckert, E.L. Little, E.G. McGeer, B.C.
     McKusick, W.J. Middleton, J. Am. Chem. Soc., 80
     (1957) 2340.

104. F.J. Brockman, Can. J. Chem., 33 (1955) 507.

105. T.L. Cairns, R.A. Carboni, D.D. Coffman, V.A.
     Engelhardt, R.E. Heckert, E.L. Little, E.G. McGeer,
     B.C. McKusick, W.J. Middleton, R.M. Scriber, G.W.
     Theobald, H.E. Weinberg, J. Am. Chem. Soc., 80
     (1958) 2775.

106. W.J. Middleton, R.E. Heckert, E.L. Little, C.G.
     Krespan, J. Am. Chem. Soc., 80 (1958) 2378.

107. W.J. Middleton, V.A. Engelhardt, J. Am. Chem. Soc.,
     80 (1958) 2788.

108. W.J. Middleton, V.A. Engelhardt, J. Am. Chem. Soc.,
     80 (1958) 2829.

109. B.C. McKusick, R.E. Heckert, T.L. Cairns, D.D.
     Coffman, H.F. Mower, J. Am. Chem. Soc., 80 (1958) 2806.

110. G. Briegleb, Electronen-Donator-Acceptor Komplexe,
     Springer 1961.

111. S.A. Berger, Spectrochim. Acta, 23A (1967) 2213.

112. Y. Matsunaga, Bull. Chem. Soc. Japan, 42 (1969) 2170.

113. L.E. Lyons, L.D. Palmer, Aust. J. Chem., 29 (1976)
     19.

114. E.C.M. Chen, W.E. Wentworth, J. Chem. Phys., 63
     (1975) 3183.

115. M.J.S. Dewar, H.S. Rzepa, J. Am. Chem. Soc., 100
     (1978) 784.

116. C.E. Looney, J.R. Downing, J. Am. Chem. Soc., 80
     (1958) 2840.

117. D.A. Long, W.O. George, Spectrochim. Acta, 19 (1963)
     1717.

118. T. Takenaka, S. Hayashi, Bull. Chem. Soc. Japan, 37
     (1964) 1216.

119. F.A. Miller, O. Sala, P. Devlin, J. Overend,
     E. Liipert, W. Luder, H. Moser, J. Varchmin,
     Spectrochim. Acta, 20 (1964) 1233.

120. P.A. Malachesky, Anal. Chem., 41 (1969) 1493.

121. S. Pons, T. Davidson, A. Bewick, J. Am. Chem. Soc.,
     105 (1983) 1802.

122. Y. Lida, Bull. Chem. Soc. Japan, 46 (1973) 423.

123. M. Itoh, J. Am. Chem. Soc., 92 (1970) 886.

124. O.W. Webster, W. Mahler, R.E. Benson, J. Am. Chem.
     Soc., 84 (1962) 3678.

125. J. Halper, W.D. Closson, H.B. Gray, Theoret. Chim.
     Acta, 4 (1966) 174.

126. M.D. Gordon, Tetrahedron, 36 (1980) 2113.

127. R.E. Merrifield, W.D. Phillips, J. Am. Chem. Soc.,
     80 (1958) 2778.

128. M.E. Peover, Trans. Faraday Soc., 60 (1964) 417.

129. M.E. Peover, Trans. Faraday Soc., 58 (1962) 2370.

130. A.R. Lepley, C.C. Thompson, Jr., J. Am. Chem. Soc.,
     89 (1967) 5523.

131. O. Webster, W. Mahler, R.E. Benson, J. Org. Chem.,
     25 (1960) 1470.

132. S.I. Weissman, J. Chem. Phys., 33 (1960) 626.

133. T. Sato, E. Yamada, Y. Okamura, J. Amada, K. Hata,
     Bull. Chem. Soc. Japan, 38 (1965) 1048.

134. D.F. Ilten, M. Calvin, J. Chem. Phys., 42 (1965) 3760.

135. F.E. Stewart, M. Eisner, W.R. Carper, J. Chem. Phys.,
     44 (1966) 2866.

136. F.E. Stewart, M. Eisner, Mol. Phys., 12 (1967) 173.

137. R.N. Butler, J. Oakes, M.C.R. Symons, J. Chem. Soc.
     A, (1968) 1134.

138. D.L. Jeanmaire, M.R. Suchanski, R.P. Van Duyne,
J. Am. Chem. Soc., 97 (1975) 1699.

139. S. Pons, S.B. Khoo, A. Bewick, M. Datta, J.J. Smith,
A. S. Hinman, G. Zachmann, J.Phys. Chem., in press.

140. J.C. Moore, D. Smith, Y. Youchne, J.P. Devlin,
J. Phys. Chem., 75 (1971) 325.

141. J.E. Pemberton, R.P. Buck, Appl. Spectroscopy, 35
(1981) 571.

142. M. Itoh, Bull. Chem. Soc. Japan, 45 (1972) 1947.

143. M.T. Watts, M.L. Lu, R.C. Chen, M.P. Eastman,
J. Phys. Chem., (1973) 2959.

144. E. Samuel, D. Vivien, J. Livage, Inorg. Chim. Acta,
21 (1977) 179.

145. M. Ogasawara, H. Takaoka, K. Hayashi, Bull. Chem.
Soc. Japan, 46 (1973) 35.

146. J.E. Bloor, B.R. Gilson, D.D. Shillady, J. Phys.
Chem., 71 (1967) 1238.

147. M.L. Kaplan, R.C. Haddon, F.B. Bramwell, F. Wudl,
J.H. Marshall, D.O. Cowan, S. Gronowitz, J. Phys.
Chem., 84 (1980) 427.

148. M. Sharp, Electrochim. Acta, 21 (1976) 973.

149. M. Sharp, J. Electroanal. Chem., 88 (1978) 193.

150. T.L. Cairns, B.C. McKusick, Agnew. Chem., 73 (1961)
520.

151. D.S. Acker, W.R. Hertler, J. Am. Chem. Soc., 84
(1962) 3370.

152. L.R. Melby, R.T. Harder, W.R. Hertler, W. Mahler,
R.E. Benson, W.E. Mochel, J. Am. Chem. Soc., 84
(1962) 3374.

153. L.B. Coleman, M.T. Cohen, D.J. Sandman, F.G. Yamagishi,
A. Garito, A.J. Heeger, Solid State Commun., 12
(1973) 1125.

154. R.C. Wheland, J.L. Gilson, J. Am. Chem. Soc., 98
(1976) 3916.

155. J.T. Devreuse, R.P. Evrard, V.E. van Doren, Highly
Conducting One-Dimensional Solids, Plenum, New York,
1979.

156. W.R. Hertler, H.D. Hartzler, D.S. Acker, R.E. Benson,
J. Am. Chem. Soc., 84 (1962) 3387.

157. D.L. Jeanmaire, R.P. van Duyne, J. Am. Chem. Soc., 98
(1976) 4129.

158. E. Ezumi, H. Miyasaki, T. Kubota, J. Phys. Chem.,
74 (1970) 2397.

159. I.N. Juchnovski, I.G. Biner, Chem. Phys. Lett.,
12 (1971) 40.

160. R. Bozio, A. Girlando, C. Pecille, J. Chem. Soc.
Faraday Trans. 2, 71 (1975) 1237.

161. G.R. Anderson, J.P. Devlin, J. Phys. Chem.,
79 (1975) 1100.

162. M.S. Khatkale, J.P. Devlin, J. Chem. Phys.,
70 (1979) 1851.

163. M.R. Suchanski, R.P. van Duyne, J. Am. Chem. Soc.,
98 (1976) 250.

164. K.K. Jespersen, Theoret. Chim. Acta, 47 (1978) 283.

165. M.A. Komanynsky, A.C. Wahl, J. Phys. Chem.,
7 (1975) 695.

166. P.H.H. Fischer, C.A. McDowell, J. Am. Chem. Soc.,
85 (1963) 2694.

167. P.H. Rieger, G.F. Fraenkel, J. Chem. Phys., 37
(1962) 2795.

168. A.W. Addison, N.S. Dalal, Y. Huyano, S. Huizinaga,
L. Weiter, Can. J. Chem., 55 (1979) 4191.

169. A. Yamagishi, Bull. Chem. Soc. Japan, 49 (1976) 1417.

170. A. Yamagishi, M. Sakamoto, Bull. Chem. Soc. Japan,
47 (1974) 2152.

171. R.H. Boyd, W.D. Phillips, J. Chem. Phys., 43 (1965)
2927.

172. J. Foley, private communication.

173. R.N. Adams, Electrochemistry at Solid Electrodes, Marcel Dekker, New York, 1969.

174. A.M. Bond, Modern Polarographic Methods in Analytical Chemistry, Marcel Dekker, New York 1980.

175. J.A. Plambeck, Electroanalytical Chemistry: Basic Principles and Applications, Wiley, New York, 1982.

176. Louis Meites, Polarographic Techniques, Interscience, New York, 1955.

177. G.F. Cottrell, Z. Physik. Chem., 42 (1902) 385.

178. J.E.B. Randles, Trans. Faraday Soc., 44 (1948) 327.

179. A. Sevcik, Coll. Czech. Chem. Commun., 13 (1948) 349.

180. H. Matsuda, Y. Ayabe, Z. Elektrochem., 59 (1957) 494.

181. H. Matsuda, Z. Elektrochem., 61 (1957) 489.

182. Y.P. Gokhstein, Doklady Akad. Nauk. SSSR, 126 (1959) 598.

183. J. Koutecky, Coll. Czech. Chem. Commun., 21 (1956) 433.

184. R.S. Nicholson, Anal. Chem., 37 (1965) 1351.

185. P. Delahay, J. Am. Chem. Soc., 75 (1953) 1190.

186. J.M. Saveant, E. Vianello, in "Advances in Polarography," I.S. Longmuir, Ed., Vol 1 Pergamon Press, New York, 1960, p. 367.

187. J.M. Saveant, E. Vianello, Electrochim. Acta, 8 (1963) 905.

188. J.M. Saveant, E. Vianello, Compdt. Rend., 256 (1963) 2597.

189. W.H. Reinmuth, Anal. Chem., 33 (1961) 1793.

190. J. Weber, Coll. Czech. Chem. Commun., 24 (1959) 1770.

191. R.S. Nicholson, I. Shain, Anal. Chem., 36 (1964) 706.

192. T. Kuwana, R.K. Darlington, D.W. Leedy, Anal. Chem., 36 (1964) 2023.

193. S. Pons, J.S. Mattson, L.O. Winstrom, H.B. Mark, Jr., Anal. Chem., 39 (1967) 685.

194. A. Bewick, K. Kunimatsu, S. Pons, Electrochim. Acta, 25 (1980) 465.

195. A. Bewick, A.M. Tuxford, Symp. Faraday Soc., 4 (1970)

196. E. Yeager, Surf. Sci., 101 (1980) 1.

197. M. Fleischmann, I.R. Hill, in "Modern Aspects of Electrochemistry," J. O'M. Bockris, B.E. Conway, Eds., Plenum Press, New York, 1983.

198. A. Bewick, J.M. Mellor, S. Pons, Electrochim. Acta, 25 (1980) 931.

199. N. Winograd, T. Kuwana, J. Electroanal. Chem., 23 (1969) 333.

200. A.W.B. Aylmer-Kelly, A. Bewick, P.R. Cantrill, A.M. Tuxford, Disc. Faraday Soc., 56 (1973) 96.

201. T. Davidson, S. Pons, A. Bewick, P.P. Schmidt, J. Electroanal. Chem., 132 (1982) 329.

202. S. Pons, S.B. Khoo, J. Am. Chem. Soc., 104, (1982) 3045.

203. N. Winograd, T. Kuwana, J. Electroanal. Chem., 7 (1974) 1.

204. W.N. Hansen in P. Delahay and C.W. Tobias, Eds., "Advances in Electrochemistry and Electrochemical Engineering," Vol. 9, Interscience, New York, 1973 p. 1.

205. J.D.E. McIntyre in P. Delahay and C.W. Tobias, Eds., "Advances in Electrochemistry and Electrochemical Engineering," Vol. 9, Interscience, New York, 1973, p. 227.

206. J. Heyrovsky, Chem. Listy, 16 (1922) 256.

207. D. Ilkovic, Collect. Czech. Chem. Commun., 6 (1934) 498.

208. D. Ilkovic, J. Chem. Phys., 35 (1938) 129.

209. T. Nagaoka, S. Okazaki, T. Fujinaga, J. Electroanal. Chem., 133 (1982) 89.

210. M.E. Peover, J.D. Davies, J. Electroanal. Chem., 6 (1963) 46.

211. J.S. Jaworski, M.K. Kalinowski, J. Electroanal. Chem., 76 (1977) 301.

212. A. Lasia, M.K. Kalinowski, J. Electroanal. Chem., 36 (1972) 511.

213. H. Lund, P. Iverson, in "Organic Electrochemistry," M. Baizer, Ed., Marcel Dekker, New York, 1973.

214. C.K. Mann, "Nonaqueous Solvents for ELectrochemical Uses," in Electroanalytical Chemistry, A.J. Bard, Ed., Marcel Dekker, New York, 1969, p. 57.

215. H.A. Laitinen. A.J. Frank. P. Kivalo, J. Am. Chem. Soc., 75 (1953) 2865.

216. E. Itabashi, J. Electroanal. Chem., 36 (1972) 179.

217. J.E. Gordon, The Organic Chemistry of Electrolyte Solutions, Wiley Interscience, Wiley and Sons, New York, 1975, p. 216-217.

218. R.B. Slates, M. Szwarc, J. Phys. Chem., 69 (1965) 4124.

219. J. Janata, R.D. Holtby-Brown, J. Chem. Soc. Perkin II, (1973) 991.

220. V.D. Parker, J. Am. Chem. Soc., 98 (1978) 98.

221. D.L. Marille, W.G. Hodgson, J. Chem. Phys. 37 (1965) 1562.

222. R.R. Bessette, I.W. Olver, J. ELectroanal. Chem., 17 (1968) 327.

223. F. Jachinowicz, H.C. Wang. G. Levin. M. Szwarc, J. Phys. Chem., 82 (1978) 1371.

224. H.C. Wang, G. Levin, M. Szwarc, J. Am. Chem. Soc., 99 (1977) 5056.

225. A. Rainis, M. Szwarc, J. Am. Chem. Soc., 96 (1974) 3008.

226. O. Popovych, R.P.T. Tomkins, Nonaqueous Solution Chemistry, Wiley-Interscience, New York, 1981, p 27.

227. M.E. Peover, J.D. Davies, J. Electroanal. Chem., 6 (1963) 46.

228. G. Levin, C. Sutphen, M. Szwarc, J. Am. Chem. Soc., 94 (1972) 2652.

229. S. Arai, L.M. Dorfman, J. Chem. Phys., 41 (1964) 2190.

230. S. Arai, E.L. Tremba, J.R. Brandon, L.M. Dorfman, Can. J. Chem., 45 (1967) 119.

231. A. Rainis, M. Szwarc, Int. J. Chem. Kinetics, 7 (1975) 919.

232. A. Rainis, R. Tung, M. Szwarc, J. Am. Chem. Soc., 95 (1973) 659.

233. A. Smolucowski, Z. Phys. Chem., 92 (1917) 129.

234. P. Debye, Trans. Electrochem. Soc., 82 (1942) 265.

235. F. Gutman, A.M. Herman, A. Rambaum, J. Electrochem. Soc., 114 (1967) 325.

236. O.K. Kolnikov. V.M. Vozzbeunikov, Z.V. Zvonkova, V.P. Glushkova, E.E. Shapiro, Dokl. Akad. Nauk. SSSR, 189 (1969) 353.

237. E.P. Goodings, Endeavour, 34 (1975) 129.

238. M. Sharp, G. Johansson, Anal. Chim. Acta, 54 (1971) 31.

239. J.E. Mulvaney, R.J. Cramer, H.K. Hall, Jr., J. Polymer Sci., 21 (1983) 309.

240. A.R. Siedle, G.A. Candela, J.F. Finnegan, Inorg. Chim. Acta, 35 (1979) 125.

241. A.J. Fry, Synthetic Organic Electrochemistry, Harper and Row, New York, 1972, p. 72.

242. G.J. Janz, R.P.T. Tomkins, Nonaqueous Electrolyte Handbook Vol. 1, Academic Press, New York, 1972.

243. R.H. Wopshall, I. Shain, Anal. Chem., 39 (1967) 1514.

244. W.H. Reinmuth, Anal. Chem., 32 (1983) 139.

245. J.F. Coetzee, G.P. Cunningham, J. Am. Chem. Soc.,
     87 (1965) 2529.

246. B.G. Chauhan, W.R. Fawcett, A. Lasia, J. Phys. Chem.,
     81 (1977) 476.

247. T. Nagaoka, S. Okazaki, J. Electroanal. Chem.,
     158 (1983) 139.